



**Carina Isabel Correia Crucho**

*Mestre em Bioorgânica*

# **Synthesis of Polymeric Nanoparticles for biomedical delivery applications**

Dissertação para obtenção do Grau de Doutor em  
Química

Orientador: Professora Doutora Maria Teresa Barros, Professor  
Associado com Agregação, FCT-UNL

Júri:

Presidente: Professora Doutora Maria João Lobo de Reis Madeira Crispim Romão

Arguentes: Professor Doutor Christopher David Maycock  
Professora Doutora Maria de Lurdes dos Santos Cristiano

Vogais: Professora Doutora Ana Paula da Assunção Esteves  
Professor Doutor Marco Diogo Richter Gomes da Silva  
Professor Doutor António Gil de Oliveira Santos  
Professor Doutor Alcino Jorge Lopes Leitão  
Doutora Maria Rita Mendes Bordalo Ventura Centeno Lima  
Doutora Krasimira Todorova Markova-Petrova



FACULDADE DE  
CIÊNCIAS E TECNOLOGIA  
UNIVERSIDADE NOVA DE LISBOA

Abril de 2015



**Carina Isabel Correia Crucho**

*Mestre em Bioorgânica*

# **Synthesis of Polymeric Nanoparticles for biomedical delivery applications**

Dissertação para obtenção do Grau de Doutor em  
Química

Orientador: Professora Doutora Maria Teresa Barros, Professor  
Associado com Agregação, FCT-UNL



*“Begin at the beginning and go on until you come to the end; then stop.”*

*— Lewis Carroll in Alice in the Wonderland*



## **Copyright**

A Faculdade de Ciências e Tecnologia e a Universidade Nova de Lisboa têm o direito, perpétuo e sem limites geográficos, de arquivar e publicar esta dissertação através de exemplares impressos reproduzidos em papel ou de forma digital, ou por qualquer outro meio conhecido ou que venha a ser inventado, e de divulgar através de repositórios científicos e de admitir a sua cópia e distribuição com objectivos educacionais ou de investigação, não comerciais, desde que seja dado crédito ao autor e editor.



## Acknowledgments

This thesis was a very lonely work! Although, many people gave me generous help and support for which I am extremely thankful.

I wish to express my gratitude to my supervisor, Professor Maria Teresa Barros, who has taught me the value of carbohydrate research. I am also grateful to her for granting me the freedom to choose my research direction. This experience will serve me well in future activities for which I will always be indebted.

I also thank Professor Christopher Maycock for sharing his experience and knowledge. His diligence, erudition and sympathy were a vital part for the completion of my research. Along the same lines, all committee members were very helpful.

I am very thankful to Photochemistry and Supramolecular Chemistry research group from Department of Chemistry, FCT-UNL, for an invaluable source of cooperation and for giving me the opportunity to use their DLS instrument for size characterization.

I would like to thank Professor Jorge Caldeira for his valuable scientific support in the introduction and use of AFM.

A special word of gratitude goes to my friend and colleague Dr. Paula Correia-da-Silva for valuable advice, kindness and friendship.

I am very thankful to my mother and sister for their support, which were very important to inspire me to continue and finish this thesis. Finally, I want to thank João Avó for bringing love and happiness to my life and some physical chemistry too! I would extend my thanks to all João family members.



## Abstract

Polymeric nanoparticles (PNPs) have attracted considerable interest over the last few years due to their unique properties and behaviors provided by their small size. Such materials could be used in a wide range of applications such as diagnostics and drug delivery. Advantages of PNPs include controlled release, protection of drug molecules and its specific targeting, with concomitant increasing of the therapeutic index.

In this work, novel sucrose and cholic acid based PNPs were prepared from different polymers, namely polyethylene glycol (PEG), poly(D,L-lactic-*co*-glycolic acid) (PLGA) and PLGA-*co*-PEG copolymer. In these PNP carriers, cholic acid will act as a drug incorporation site and the carbohydrate as targeting moiety.

The uptake of nanoparticles into cells usually involves endocytotic processes, which depend primarily on their size and surface characteristics. These properties can be tuned by the nanoparticle preparation method. Therefore, the nanoprecipitation and the emulsion-solvent evaporation method were applied to prepare the PNPs. The influence of various parameters, such as concentration of the starting solution, evaporation method and solvent properties on the nanoparticle size, size distribution and morphology were studied.

The PNPs were characterized by using atomic force microscopy (AFM), scanning electron microscopy (SEM) and dynamic light scattering (DLS) to assess their size distribution and morphology. The PNPs obtained by nanoprecipitation ranged in size between 90 nm and 130 nm with a very low polydispersity index ( $PDI < 0.3$ ). On the other hand, the PNPs produced by the emulsion-solvent evaporation method revealed particle sizes around 300 nm with a high PDI value. More detailed information was found in AFM and SEM images, which demonstrated that all these PNPs were regularly spherical.  $\zeta$ -potential measurements were satisfactory and evidenced the importance of sucrose moiety on the polymeric system, which was responsible for the obtained negative surface charge, providing colloidal stability.

The results of this study show that sucrose and cholic acid based polymeric conjugates can be successfully used to prepare PNPs with tunable physicochemical characteristics. In addition, it provides novel information about the materials used and the methods applied. It is hoped that this work will be useful for the development of novel carbohydrate based nanoparticles for biomedical applications, specifically for targeted drug delivery.

**Keywords:** *Carbohydrates, Drug delivery, Nanomedicine, Polymeric nanoparticles*



## Resumo

Nanopartículas poliméricas (NPPs) têm atraído um considerável interesse nos últimos anos devido às suas propriedades únicas e comportamentos proporcionados pelo seu pequeno tamanho. Estes materiais podem ser utilizados numa vasta gama de aplicações, tais como em diagnóstico e na veiculação de fármacos. As vantagens das NPPs incluem a libertação controlada, protecção do fármaco e o seu direccionamento a um alvo específico, com concomitante aumento do índice terapêutico.

Neste trabalho, novas NPPs baseadas em unidades de sacarose e de ácido cólico foram preparadas a partir de diferentes polímeros, nomeadamente polietileno glicol (PEG), poli(ácido láctico-co-ácido glicólico) (PLGA) e do copolímero PLGA-co-PEG. Nestas NPPs a unidade de ácido cólico irá actuar como o local de incorporação do fármaco e o açúcar como a unidade de direccionamento.

A incorporação das nanopartículas pelas células envolve geralmente processos de endocitose, que dependem primariamente do seu tamanho e superfície. Estas propriedades podem ser ajustadas de acordo com o método de preparação das nanopartículas. Deste modo, o método de nanoprecipitação e a técnica de emulsificação-evaporação do solvente foram utilizados para preparar as NPPs. A influência de vários parâmetros, tais como a concentração da solução inicial, o método de evaporação e as propriedades do solvente no tamanho médio das nanopartículas, na distribuição de tamanhos e na morfologia foram estudados.

As NPPs foram caracterizadas por microscopia de força atómica (AFM), microscopia electrónica de varrimento (SEM) e dispersão dinâmica de luz (DLS) para avaliar a distribuição de tamanhos e a morfologia. O tamanho das NPPs obtidas pelo método de nanoprecipitação variou entre 90 nm a 130 nm, com um baixo índice de polidispersão ( $PDI < 0,3$ ). Por outro lado, as NPPs obtidas pelo método de emulsificação-evaporação do solvente revelou partículas com um tamanho de cerca de 300 nm e com elevado valor de PDI. Informação mais detalhada foi encontrada nas imagens obtidas por AFM e SEM, que demonstraram que todas as NPPs eram regularmente esféricas. As medidas de potencial- $\zeta$  foram satisfatórias e evidenciaram a importância da unidade de sacarose no sistema polimérico, que foi responsável pela carga superficial negativa obtida, proporcionando maior estabilidade coloidal.

Os resultados deste estudo mostram que os conjugados poliméricos baseados em unidades de sacarose e ácido cólico, podem ser utilizados com sucesso na preparação de NPPs com características físico-químicas ajustáveis. Além disso, fornecem novas informações sobre os materiais utilizados e os métodos aplicados. Espera-se que este trabalho seja útil para o desenvolvimento de novas NPPs à base de glúcidos para aplicações biomédicas, especificamente para sistemas de veiculação direccionada de fármacos.

**Palavras-Chave:** *Glúcidos, Nanomedicina, Nanopartículas poliméricas, Veiculação de fármacos.*



# List of Contents

<b>CHAPTER I: SYNTHESIS OF POLYMERIC NANOPARTICLES: AN OVERVIEW OF THE PREPARATION AND CHARACTERIZATION METHODS</b>	<b>1</b>
<b>I.1 Introduction</b>	<b>3</b>
<b>I.2 Preparation of Polymeric Nanoparticles</b>	<b>5</b>
I.2.1 Two-step procedures based on Emulsification	6
I.2.1.1 Emulsification-solvent evaporation	7
I.2.1.2 Emulsification-solvent diffusion	10
I.2.1.3 Emulsification–reverse salting-out	12
I.2.2 One-step procedures	14
I.2.2.1 Nanoprecipitation or solvent displacement method	14
I.2.2.2 Dialysis	17
I.2.2.3 Supercritical fluid technology	19
<b>I.3 Characterization methods of Polymeric Nanoparticles</b>	<b>20</b>
I.3.1 Size, shape, surface properties and stability	22
I.3.2 Drug-polymer interactions	25
<b>I.4 Concept of this thesis</b>	<b>27</b>
<b>CHAPTER II: SYNTHESIS OF PEG-BASED POLYMERIC NANOPARTICLES</b>	<b>29</b>
<b>II.1 Introduction</b>	<b>31</b>
<b>II.2 Results and Discussion</b>	<b>32</b>
II.2.1 Synthesis and characterization of PEG-based polymer conjugates	32
II.2.1.1 Chemoselective derivatization of 6'-hydroxyl group of sucrose	33
II.2.1.2 Chemoselective derivatization at the 3' position of cholic acid	37
II.2.1.3 Synthesis of Suc-PEG-Chol polymer conjugates	39
II.2.1.4 Physicochemical characterization of Suc-PEG-Chol polymer conjugates	41
II.2.1.5 Synthesis of Cholic-PEG polymer conjugates	43
II.2.2 Preparation and physicochemical characterization of PNPs	44
II.2.2.1 PNPs prepared from Suc-PEG-Chol polymer conjugates	44
II.2.2.2 PNPs prepared from Cholic-PEG polymer conjugates	51
<b>II.3 Conclusion</b>	<b>53</b>

<b>CHAPTER III: SYNTHESIS OF PLGA-BASED POLYMERIC NANOPARTICLES</b>	<b>57</b>
III.1 Introduction	59
III.2 Results and Discussion	60
III.2.1 Synthesis and characterization of PLGA-based polymer conjugates	60
III.2.2 Preparation and physicochemical characterization of PNPs	63
III.2.2.1 PNPs prepared by the emulsion-solvent evaporation method	63
III.2.2.2 PNPs prepared by nanoprecipitation	65
III.3 Conclusion	71
<b>CHAPTER IV: SYNTHESIS OF PLGA-PEG-BASED POLYMERIC NANOPARTICLES</b>	<b>73</b>
IV.1 Introduction	75
IV.2 Results and Discussion	76
IV.2.1 One-pot synthesis of PLGA-co-PEG-based polymer conjugates	76
IV.2.2 Preparation and physicochemical characterization of PNPs	78
IV.3 Conclusion	80
<b>CHAPTER V: CONCLUSIONS AND FUTURE PERSPECTIVES</b>	<b>83</b>
<b>CHAPTER VI: EXPERIMENTAL PART</b>	<b>89</b>
VI.1 Materials and Instruments	91
VI.2 Synthesis and characterization of polymer conjugates	92
VI.2.1 Chemoselective derivatization of the 6' position of the sucrose	92
VI.2.1.1 6'- <i>O</i> - <i>tert</i> -butyldiphenylsilyl-sucrose (2)	92
VI. 2.1.2 1',2,3,3',4,4',6-Hepta- <i>O</i> -benzyl-6'- <i>O</i> - <i>tert</i> -butyldiphenylsilyl sucrose (4)	93
VI. 2.1.3 1',2,3,3',4,4',6-Hepta- <i>O</i> -benzyl-sucrose (5)	94
VI. 2.1.4 1',2,3,3',4,4',6-Hepta- <i>O</i> -benzyl-6'- <i>O</i> -succinyl-sucrose (6)	95
VI. 2.2 Chemoselective derivatization at the 3' position of cholic acid	95
VI. 2.2.1 Methyl 3 $\alpha$ ,7 $\alpha$ ,12 $\alpha$ -trihydroxy-5 $\beta$ -cholan-24-ate (8)	95
VI. 2.2.2 Methyl 3 $\alpha$ - <i>O</i> -benzyl, 7 $\alpha$ , 12 $\alpha$ -dihydroxy-5 $\beta$ -cholan-24-oate (9)	96
VI. 2.2.3 3 $\alpha$ - <i>O</i> -benzyl, 7 $\alpha$ , 12 $\alpha$ -dihydroxy-5 $\beta$ -cholic acid (10)	97
VI.2.3 General procedure 1 for DCC-mediated coupling reactions	97
VI.2.4 Synthesis of PEG-based conjugates	98

VI.2.4.1 Benzylated Suc-PEG2000-OH (11)	98
VI.2.4.2 Benzylated Suc-PEG4000-OH (12)	98
VI.2.4.3 Benzylated Suc-PEG6000-OH (13)	99
VI.2.4.4 Benzylated Suc-PEG2000-Chol (14)	100
VI.2.4.5 Benzylated Suc-PEG4000-Chol (15)	101
VI.2.4.6 Benzylated Suc-PEG6000-Chol (16)	102
VI.2.4 General procedure 2 for hydrogenation reactions	103
VI.2.5 Deprotection of PEG-based conjugates	103
VI.2.5.1 Suc-PEG2000-Chol (17)	103
VI.2.5.2 Suc-PEG4000-Chol (18)	104
VI.2.5.3 Suc-PEG6000-Chol (19)	105
VI.2.6 General procedure 3 for the synthesis of Cholic-PEG conjugates	107
VI.2.6.1 Cholic-PEG2000 (20)	107
VI.2.6.2 Cholic-PEG4000 (21)	108
VI.2.6.3 Cholic-PEG6000 (22)	109
VI.2.7 Synthesis of PLGA-based conjugates	111
VI.2.7.1 Benzylated Suc-PLGA-OH (23)	111
VI.2.7.2 Benzylated Suc-PLGA-Chol (24)	111
VI.2.7.3 Suc-PLGA-Chol (25)	112
VI.2.8 Synthesis of PLGA-PEG based conjugates	112
VI.2.8.1 One-pot synthesis of benzylated Suc/Chol-PLGA-PEG-Chol/Suc (26)	112
VI.2.8.2 Benzyl deprotection of Suc/Chol-PLGA-PEG-Chol/Suc 26 (27)	113
VI.2.9 Measurement of fluorescence spectroscopy (pyrene)	113
<b>VI.3 Preparation of polymeric nanoparticles</b>	<b>114</b>
VI.3.1 Emulsion-solvent evaporation method	114
VI.3.2 Nanoprecipitation method	114
<b>VI.4 Characterization of polymeric nanoparticles</b>	<b>115</b>
VI.4.1 Particle size and zeta potential	115
VI.4.2 Surface morphology – scanning electron microscopy (SEM) and atomic force microscopy (AFM)	115
<b>CHAPTER VII: REFERENCES</b>	<b>117</b>



## List of Figures

FIGURE 1 TYPES OF NANOCARRIERS FOR DRUG DELIVERY SYSTEMS. POLYMERIC NANOPARTICLES: A, NANOCAPSULES AND B, NANOSPHERES. C, LIPOSOMES. D, POLYMERIC MICELLES. E, DENDRIMERS. F, CARBON NANOTUBES. ....	4
FIGURE 2 SCHEMATIC REPRESENTATION OF SEVERAL TECHNIQUES FOR THE PREPARATION OF PNPS. ....	5
FIGURE 3 SCHEMATIC DIAGRAM OF EMULSIONS FABRICATED FROM OIL, WATER AND SURFACTANT.....	6
FIGURE 4 SCHEMATIC REPRESENTATION OF THE EMULSIFICATION-SOLVENT EVAPORATION METHOD FOR THE PRODUCTION OF NANOSPHERES. ....	7
FIGURE 5 NANOCAPSULES WITH DIFFERENT MORPHOLOGIES PREPARED BY ASHJARI <i>ET AL.</i> CORE-SHELL OR HALF-MOON MORPHOLOGY WAS OBSERVED WHEN SLOW EVAPORATION WAS USED COMPARED TO FAST EVAPORATION. [ADAPTED FROM REF. 31].....	8
FIGURE 6 SEM IMAGES OF PARTICLES OBTAINED FROM A POLYESTER (PCL) AND A POLYACRYLATE POLYMER (POLY(MMA-AA)). THE SOLVENT USED FOR POLYMER SOLUBILIZATION INFLUENCED THE PARTICLE SIZE AND MORPHOLOGY. [ADAPTED FROM REF. 34] .....	9
FIGURE 7 SCHEMATIC REPRESENTATION OF THE EMULSIFICATION-SOLVENT DIFFUSION METHOD FOR THE PREPARATION OF NANOCAPSULES. ....	10
FIGURE 8 SEM IMAGES OF THE PLA NANOPARTICLES PREPARED BY TRIMAILLE <i>ET AL.</i> A) 2% PLA; B) 10% PLA. [ADAPTED FROM REF. 39] .....	11
FIGURE 9 SCHEMATIC REPRESENTATION OF THE EMULSIFICATION-REVERSE SALTING-OUT TECHNIQUE. ....	13
FIGURE 10 SCHEMATIC ILLUSTRATION OF THE NANOPRECIPITATION METHOD FOR THE PREPARATION OF NANOSPHERES. FOR THE PREPARATION OF NANOCAPSULES AN OIL IS INTRODUCED IN THE ORGANIC PHASE. ....	14
FIGURE 11 INFLUENCE OF POLYMER CONCENTRATION IN THE ORGANIC PHASE ON THE MEAN DIAMETER OF PNPS. ABBREVIATION: BNZ, BENZYLAMINE; FITC, FLUORESCIEIN ISOTHIOCYANATE. [ADAPTED FROM REF. 63] .....	16
FIGURE 12 FESEM MICROGRAPHS OF POLYSTYRENE PNPS PREPARED BY NANOPRECIPITATION. POLYMER SOLVENT: TETRAHYDROFURAN. NON-SOLVENT: C, ACETONE; D, WATER AND PLURONIC-F68. [ADAPTED FROM REF. 65].....	17
FIGURE 13 SCHEMATIC REPRESENTATION OF THE DIALYSIS METHOD FOR THE PREPARATION OF NANOSPHERES. ....	17
FIGURE 14 SEM IMAGES OF PLGA 50:50 NANOPARTICLES PREPARED BY JEONG <i>ET AL.</i> A) DMAC OR B) ACETONE AS THE POLYMER SOLVENT. [ADAPTED FROM REF. 72].....	18
FIGURE 15 SEM IMAGES OF DIFFERENT MORPHOLOGIES OBTAINED FOR HYALURONIC ACID BASED NANOSTRUCTURES. EXPERIMENTAL CONDITIONS: $T = 4\text{ }^{\circ}\text{C}$ ; CONC. [MG/ML] = 0.5; SOLVENT PAIR: H, $\text{H}_2\text{O}/\text{ETOH}$ ; I, $\text{H}_2\text{O}/\text{MEOH}$ ; L, $\text{DMSO}/\text{MEOH}$ ; M, $\text{H}_2\text{O}/\text{ACETONE}$ . MORPHOLOGY: H, FLOWERLIKE; I AND L, SPHERES AND M, DANDELION-LIKE. [ADAPTED FROM REF. 70] .....	19
FIGURE 16 A RATIONAL CHARACTERIZATION STRATEGY FOR NANOPARTICLES. ....	20

FIGURE 17 SCANNING ELECTRON MICROGRAPHS OF A CANTILEVER TIP (A) AND SCHEMATIC OF AFM OPERATION (B).....	23
FIGURE 18 FESEM IMAGE (LEFT) AND AFM IMAGES (MIDDLE (2D IMAGE) AND RIGHT (ZOOM IN 3D IMAGE)) OF PLA-TWEEN 80-10 PNPS.....	23
FIGURE 19 SURFACE MORPHOLOGY OF PEG-G-PLA PNPS BY AFM. SCALE X-AXIS: 0.200 $\mu$ M/DIV.....	24
FIGURE 20 DSC RESULTS OF A) KETOPROFEN LOADED PLGA NANOPARTICLES, B) DRUG FREE PLGA NANOPARTICLES, C) PHYSICAL MIXTURE OF PLGA AND KETOPROFEN AND D) PURE PLGA POLYMER [ADAPTED FROM REF. 103]. .....	26
FIGURE 21 TYPICAL END-GROUPS IN POLYETHYLENE GLYCOL MODIFICATIONS.....	31
FIGURE 22 SYNTHETIC STRATEGY FOR PREPARING THE SUC-PEG-CHOL POLYMER CONJUGATES.....	32
FIGURE 23 DIFFERENT REACTIVITY OF PRIMARY/SECONDARY HYDROXYLS OF SUCROSE.....	33
FIGURE 24 HMQC SPECTRUM EXPANSION OF 6'-O-TERT-BUTYLDIPHENYLSILYL-SUCROSE 2 IN DMSO- <i>D</i> <sub>6</sub> , FOCUSED ON SUCROSE PROTONS.....	35
FIGURE 25 HMQC SPECTRUM EXPANSION OF 1',2,3,3',4,4',6-HEPTA-O-BENZYL-6'-O-TERT-BUTYLDIPHENYLSILYL SUCROSE 5 IN DMSO- <i>D</i> <sub>6</sub> , FOCUSED ON SUCROSE PROTONS.....	36
FIGURE 26 HMQC SPECTRUM EXPANSION OF 3A-O-BENZYL, 7A, 12A-DIHYDROXY-5B-CHOLIC ACID 10 IN CDCl <sub>3</sub> , FOCUSED ON THE STEROID SKELETON.....	39
FIGURE 27 A) FLUORESCENCE EMISSION SPECTRA OF PYRENE/SUC-PEG2000-CHOL AGAINST CONCENTRATION OF SUC-PEG2000-CHOL IN DISTILLED WATER. B) PLOTS OF THE OVERALL INTENSITY OF THE PYRENE EMISSIONS SPECTRA VS. POLYMER CONCENTRATIONS.....	42
FIGURE 28 <sup>1</sup> H-NMR SPECTRUM OF SUC-PEG4000-CHOL 18 IN D <sub>2</sub> O. ....	43
FIGURE 29 PARTICLE SIZE DISTRIBUTIONS OF SUC-PEG-CHOL PNPS PREPARED BY THE EMULSION-SOLVENT EVAPORATION METHOD. ....	45
FIGURE 30 AFM HEIGHT IMAGE OF SUC-PEG4000-CHOL PNPS PREPARED BY O/W EMULSION-SOLVENT EVAPORATION METHOD WITH THE EMULSION FORMULATED BY VORTEX MIXING. THE SAMPLE WAS PREPARED FROM A PNP SOLUTION OF 0.1 MG/ML.....	46
FIGURE 31 PARTICLE SIZE DISTRIBUTIONS OF SUC-PEG-CHOL PNPS PREPARED BY NANOPRECIPITATION.....	47
FIGURE 32 A) CONCENTRATION DEPENDENT PARTICLE SIZES OF SUC-PEG-CHOL PNPS AT ROOM TEMPERATURE PREPARED BY NANOPRECIPITATION. B) STUDY ON THE SUC-PEG4000-CHOL PNPS STABILITY, STORED AT 5°C OVER ONE MONTH. ....	48
FIGURE 33 AFM HEIGHT IMAGE OF SUC-PEG-CHOL PNPS FROM A PNP SOLUTION OF 0.1MG/ML DRIED AT 5 °C. A) SUC-PEG2000-CHOL PNPS. B) SUC-PEG4000-CHOL PNPS. C) SUC-PEG6000-CHOL PNPS. ....	49
FIGURE 34 AFM HEIGHT IMAGE OF LYOPHILIZED SUC-PEG-CHOL PNPS FROM A PNP SOLUTION OF 0.1MG/ML DRIED AT 5 °C. A) SUC-PEG4000-CHOL PNPS. B) SUC-PEG6000-CHOL PNPS. ....	50
FIGURE 35 AFM PHASE IMAGE OF LYOPHILIZED SUC-PEG2000-CHOL NANOPARTICLES FROM A PNP SOLUTION OF 0.1MG/ML DRIED BY FREEZE-DRYING.....	50
FIGURE 36 AFM PHASE IMAGE OF LYOPHILIZED SUC-PEG2000-CHOL NANOPARTICLES FROM A PNP SOLUTION OF 0.1MG/ML DRIED UNDER PHOSPHORUS PENTOXIDE. ....	51

FIGURE 37 AFM PHASE IMAGE OF LYOPHILIZED SUC-PEG4000-CHOL NANOPARTICLES FROM A PNP SOLUTION OF 0.1MG/ML DRIED UNDER PHOSPHORUS PENTOXIDE. VISUALIZATION OF NANOMETRIC CRYSTALLITES OF PEG. ....	51
FIGURE 38 SEM IMAGE OF A) SUC-PEG4000-CHOL PNPS AND B) SUC-PEG6000-CHOL PNPS. ....	52
FIGURE 39 PARTICLE SIZE DISTRIBUTIONS OF CHOLIC-PEG CONJUGATES PNPS PREPARED BY THE EMULSION-SOLVENT EVAPORATION METHOD. ....	53
FIGURE 40 AFM PHASE IMAGE OF LYOPHILIZED CHOLIC-PEG2000 NANOPARTICLES FROM A PNP SOLUTION OF 0.1MG/ML PREPARED BY THE EMULSION-SOLVENT EVAPORATION METHOD. ....	53
FIGURE 41 CHEMICAL STRUCTURE OF POLY(D,L-LACTIC-CO-GLYCOLIC ACID) AND ITS MONOMERS. ....	59
FIGURE 42 SYNTHETIC STRATEGY FOR PREPARING THE SUC-PLGA-CHOL POLYMER CONJUGATE. ....	61
FIGURE 43 <sup>1</sup> H-NMR SPECTRUM OF BENZYLATED SUC-PLGA-OH 23. ....	62
FIGURE 44 <sup>1</sup> H-NMR SPECTRUM OF BENZYLATED SUC-PLGA-CHOL 24. ....	63
FIGURE 45 PARTICLE SIZE DISTRIBUTIONS OF PLGA AND SUC-PLGA-CHOL PNPS PREPARED BY THE EMULSION-SOLVENT EVAPORATION. METHOD. ....	64
FIGURE 46 SEM MICROGRAPHS OF LYOPHILIZED PLGA PNPS PREPARED BY THE EMULSION SOLVENT EVAPORATION METHOD. ....	65
FIGURE 47 SEM MICROGRAPHS OF LYOPHILIZED SUC-PLGA-CHOL PNPS PREPARED BY THE EMULSION SOLVENT EVAPORATION METHOD. ....	65
FIGURE 48 EFFECT OF VARYING THE ORGANIC SOLVENT IN THE PARTICLE SIZE (GREY BAR) AND PDI (STRIPED BAR) OF SUC-PLGA-CHOL PNPS OBTAINED BY NANOPRECIPITATION. ....	66
FIGURE 49 INFLUENCE OF THE EVAPORATION RATE ON THE PARTICLE SIZE DISTRIBUTION OF PLGA AND SUC-PLGA-CHOL PNPS. SOLVENT EVAPORATION METHOD: A) AND C) EVAPORATION UNDER REDUCE-PRESSURE; B) AND D) ATM. PRESSURE EVAPORATION. ....	67
FIGURE 50 CORRELATION OF PNP MEAN PARTICLE SIZE WITH SUC-PLGA-CHOL POLYMER CONCENTRATION OBTAINED BY NANOPRECIPITATION. ALL THE SAMPLES WERE BROUGHT TO THE SAME CONCENTRATION BEFORE ANALYZED BY DLS. ....	68
FIGURE 51 SEM MICROGRAPHS OF LYOPHILIZED PLGA PNPS PREPARED BY NANOPRECIPITATION. ....	68
FIGURE 52 SEM MICROGRAPHS OF LYOPHILIZED SUC-PLGA-CHOL PNPS PREPARED BY NANOPRECIPITATION. .	69
FIGURE 53 SEM MICROGRAPHS OF LYOPHILIZED SUC-PLGA-CHOL PNPS PREPARED BY NANOPRECIPITATION LOADED WITH 0.25% RHODAMINE B. ....	69
FIGURE 54 SEM MICROGRAPHS OF LYOPHILIZED PLGA PNPS PREPARED BY NANOPRECIPITATION. THE SAMPLE WAS FREEZE-DRIED IN THE PRESENCE OF 10% (W/W) GLUCOSE AS A CRYOPROTECTOR. ....	70
FIGURE 55 SEM MICROGRAPHS OF LYOPHILIZED SUC-PLGA-CHOL PNPS PREPARED BY NANOPRECIPITATION AND DRIED UNDER VACUUM OVER PHOSPHORUS PENTOXIDE AS AN ALTERNATIVE TO FREEZE-DRYING. 70	
FIGURE 56 SEM MICROGRAPHS OF LYOPHILIZED SUC-PLGA-CHOL PNPS PREPARED BY NANOPRECIPITATION WITHOUT PURIFICATION BY CENTRIFUGATION. ....	71
FIGURE 57 SYNTHETIC STRATEGY FOR PREPARING THE SUC-PLGA-CO-PEG-CHOL POLYMER CONJUGATES. ....	76
FIGURE 58 <sup>1</sup> H-NMR SPECTRUM OF SUC-PLGA-CO-PEG-CHOL 27 POLYMER CONJUGATES. ....	77

FIGURE 59 EFFECT OF VARYING THE ORGANIC SOLVENT IN THE PARTICLE SIZE (GREY BAR) AND PDI (STRIPED BAR) OF SUC-PLGA-CO-PEG-CHOL PNPS OBTAINED BY NANOPRECIPITATION. ....	78
FIGURE 60 PARTICLE SIZE DISTRIBUTIONS OF PLGA-CO-PEG AND SUC-PLGA-CO-PEG-CHOL PNPS PREPARED BY NANOPRECIPITATION. ....	79
FIGURE 61 CORRELATION OF PNP MEAN PARTICLE SIZE WITH SUC-PLGA-CO-PEG-CHOL POLYMER CONCENTRATION, OBTAINED BY NANOPRECIPITATION. ALL THE SAMPLES WERE BROUGHT TO THE SAME CONCENTRATION BEFORE MEASURED BY DLS. ....	79
FIGURE 62 SEM MICROGRAPHS OF LYOPHILIZED SUC-PLGA-CO-PEG-CHOL PNPS PREPARED BY NANOPRECIPITATION. ....	80
FIGURE 63 SEM MICROGRAPHS OF LYOPHILIZED PLGA-CO-PEG PNPS PREPARED BY NANOPRECIPITATION. ....	80

## List of Schemes

SCHEME 1 PROTECTION/DEPROTECTION SEQUENCE FROM SUCROSE.	33
SCHEME 2 MECHANISM OF THE SILYLATION OF SUCROSE WITH TBDPSCL.	34
SCHEME 3 PENTACOORDINATE INTERMEDIATE INVOLVED IN THE DEPROTECTION OF TBDPS PROMOTED BY TBAF.	35
SCHEME 4 CHEMOSELECTIVE DE- <i>O</i> -BENZYLATION OF OCTABENZYLATED SUCROSE PROPOSED BY YIN <i>ET AL</i> .	36
SCHEME 5 SYNTHESIS OF THE SUCROSE SUCCINATE DERIVATIVE 1',2,3,3',4,4',6-HEPTA- <i>O</i> -BENZYL-6'- <i>O</i> -SUCCINYL-SUCROSE 6.	37
SCHEME 6 PROPOSED MECHANISM FOR THE ESTERIFICATION REACTION OF 1',2,3,3',4,4',6-HEPTA- <i>O</i> -BENZYL-6'- <i>O</i> - <i>TERT</i> -BUTYLDIPHENYLSILYL SUCROSE 5 WITH SUCCINIC ANHYDRIDE.	37
SCHEME 7 SYNTHETIC STRATEGY FOR PREPARING THE SELECTIVELY 3A-OH PROTECTED CHOLIC ACID DERIVATIVE 10.	38
SCHEME 8 SYNTHESIS OF THE BENZYLATED SUC-PEG-OH CONJUGATES BY A STEGLICH ESTERIFICATION.	39
SCHEME 9 THE REACTION MECHANISM OF STEGLICH ESTERIFICATION.	40
SCHEME 10 SYNTHESIS OF THE BENZYLATED SUC-PEG-CHOLIC CONJUGATES BY A STEGLICH ESTERIFICATION.	41
SCHEME 11 SYNTHESIS OF THE SUC-PEG-CHOL CONJUGATES BY PD/C CATALYZED HYDROGENOLYSIS.	41
SCHEME 12 SYNTHESIS OF THE CHOLIC-PEG POLYMER CONJUGATES BY A STEGLICH ESTERIFICATION.	43
SCHEME 13 SYNTHESIS OF THE BENZYLATED SUC-PLGA-OH CONJUGATES BY ESTERIFICATION REACTION THROUGH A PLGA-NHS INTERMEDIATE.	61
SCHEME 14 SYNTHESIS OF THE BENZYLATED SUC-PLGA-CHOL CONJUGATES BY ESTERIFICATION REACTION.	61



## LIST OF TABLES

TABLE 1 EFFECT OF STABILIZER TYPE ON PARTICLE SIZE, POLYDISPERSITY INDEX (PDI) AND ENTRAPMENT EFFICIENCY, FOR PLGA NANOPARTICLES PREPARED BY JAIN <i>ET AL.</i>	12
TABLE 2 PRINCIPAL TECHNIQUES FOR EVALUATION OF THE PHYSICOCHEMICAL CHARACTERISTICS OF PNPS.	21
TABLE 3 INFLUENCE OF THE PEG CHAIN LENGTH ON THE MELTING TEMPERATURE ( $T_M$ ) AND ON THE CRITICAL ASSOCIATION CONCENTRATION (CAC) OF THE SUC-PEG-CHOL CONJUGATES.	42
TABLE 4 INFLUENCE OF THE PEG CHAIN LENGTH ON THE MELTING TEMPERATURE ( $T_M$ ) OF THE CHOLIC-PEG POLYMER CONJUGATES.	44
TABLE 5 MEAN PARTICLE SIZE AND Z-POTENTIAL OF THE SUC-PEG-CHOL PNPS PREPARED BY O/W EMULSION-SOLVENT EVAPORATION METHOD WITH THE EMULSION FORMULATED BY VORTEX MIXING.	44
TABLE 6 MEAN PARTICLE SIZE OF THE SUC-PEG-CHOL PNPS PREPARED BY O/W EMULSION-SOLVENT EVAPORATION METHOD WITH THE EMULSION FORMULATED BY SONICATION.	46
TABLE 7 SIZE DISTRIBUTION AND Z-POTENTIAL OF THE SUC-PEG-CHOL PNPS PREPARED BY NANOPRECIPITATION.	47
TABLE 8 SIZE DISTRIBUTION OF LYOPHILIZED SUC-PEG-CHOL PNPS PREPARED BY NANOPRECIPITATION AFTER VORTEXING FOR 5 MIN.	48
TABLE 9 MEAN PARTICLE SIZE OF THE CHOLIC-PEG PNPS PREPARED BY O/W EMULSION-SOLVENT EVAPORATION METHOD WITH THE EMULSION FORMULATED BY SONICATION.	52
TABLE 10 PHYSICOCHEMICAL CHARACTERISTICS OF THE SUC-PEG-CHOL PNPS OBTAINED BY NANOPRECIPITATION AND EMULSION-SOLVENT EVAPORATION TECHNIQUE.	54
TABLE 11 GLASS TRANSITION TEMPERATURES ( $T_g$ ) OF PLGA AND PLGA-BASED CONJUGATES.	63
TABLE 12 MEAN PARTICLE SIZE AND POLYDISPERSITY INDEX (PDI) OF PLGA AND SUC-PLGA-CHOL PNPS PREPARED BY O/W EMULSION-SOLVENT EVAPORATION METHOD WITH THE EMULSION FORMULATED BY VORTEX MIXING.	64
TABLE 13 EFFECT OF EVAPORATION METHOD IN THE MEAN PARTICLE SIZE AND PDI OF PLGA AND SUC-PLGA-CHOL PNPS OBTAINED BY NANOPRECIPITATION.	67
TABLE 14 PHYSICOCHEMICAL CHARACTERISTICS OF THE PLGA AND SUC-PLGA-CHOL PNPS OBTAINED BY NANOPRECIPITATION AND EMULSION-SOLVENT EVAPORATION TECHNIQUE.	71
TABLE 15 SIZE DISTRIBUTION AND Z-POTENTIAL OF THE PLGA-CO-PEG AND SUC-PLGA-CO-PEG-CHOL PNPS PREPARED BY NANOPRECIPITATION.	79



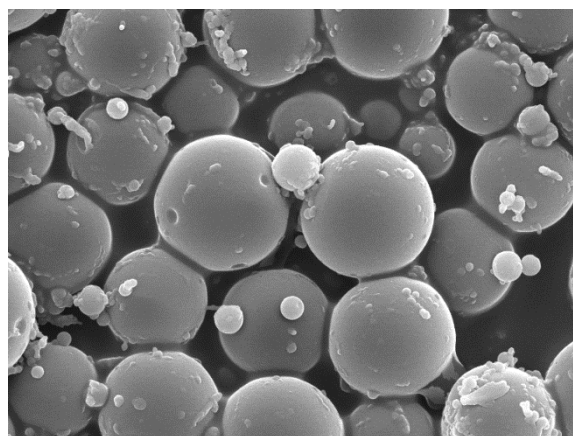
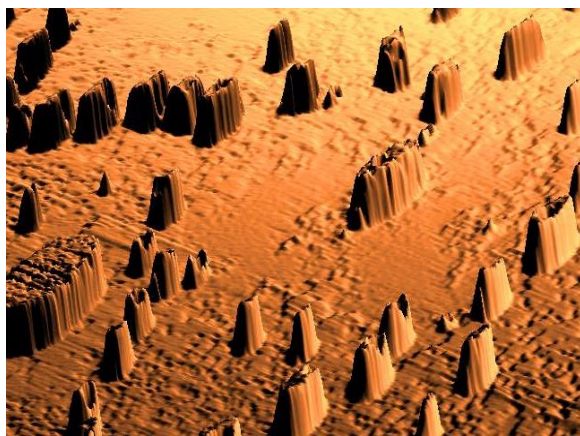
## List of Symbols and Abbreviations

ADME	Absorption, distribution, metabolism and excretion
AFM	Atomic force microscopy
atm	Atmospheric pressure
Bn	Benzyl
Bnz	Benzylamine
CAC	Critical aggregation concentration
Cisplatin	<i>cis</i> -Diamminedichloroplatinum (II)
CMC	Critical micelle concentration
COSY	Correlation spectroscopy
CTAB	Cetyltrimethylammonium bromide
D <sub>h</sub>	Hydrodynamic diameter
DCM	Dichloromethane
DCC	<i>N,N</i> -dicyclohexylcarbodiimide
DCU	Dicyclohexylurea
DDS	Drug delivery systems
DLS	Dynamic light scattering
DMAB	Didodecyldimethylammonium bromide
DMAc	Dimethylacetamide
DMAP	4-(Dimethylamino)pyridine
DMF	Dimethylformamide
DMSO	Dimethylsulfoxide
DSC	Differential scanning calorimetry
D <sub>t</sub>	Diffusion coefficient
EC	Ethyl cellulose
EO	Ethylene oxide
EPR	Enhanced permeability and retention effect
FDA	Food and Drug Administration
FESEM	Field Emission Scanning Electron Microscope
FITC	Fluorescein isothiocyanate
GAS	Gas antisolvent process
HMBC	Heteronuclear multiple-bond correlation spectroscopy
HMQC	Heteronuclear multiple quantum correlation spectroscopy
HPLC	High performance liquid chromatography
HOBt	1-Hydroxybenzotriazole

HOMO	Highest occupied molecular orbital
IR	Infrared spectroscopy
LED	Light-emitting diode
LUMO	Lowest unoccupied molecular orbital
MALDI-TOF	Matrix-assisted laser desorption ionization time-of-flight
m.p.	Melting point
MPS	Mononuclear phagocyte system
MS	Mass spectrometry
MWCO	Molecular weight cut-off
NMPy	<i>N</i> -methyl-2-pyrrolidinone
NMR	Nuclear magnetic resonance
NSOM	Near-field scanning optical microscopy
o/w	Oil-in-water
P20	Polysorbate 20
PBA	Polybutyladipate
PBLG	Poly( $\gamma$ -benzyl-L-glutamate)
PCL	Poly( $\epsilon$ -caprolactone)
PCS	Photon correlation spectroscopy
PDI	Polydispersity index
PDLLA	Poly(D,L-lactic acid)
PEG	Polyethylene glycol
PGA	Poly(glycolic acid)
PGGA	Poly( $\gamma$ -glutamic acid)
PGSS	Particles from gas-saturated solution
PLA	Poly(lactic acid)
PLC	Poly(D,L-lactide- <i>co</i> -caprolactone)
PLGA	Poly(D,L-lactic- <i>co</i> -glycolic acid)
PLLA	Poly(L-lactic acid)
PMMA	Poly(methyl methacrylate)
PNPs	Polymeric Nanoparticles
Poly(MMA-AA)	Poly(methylmethacrylate-acrylic acid)
PPA	Poly(phenyl acetylene)
PS	Polystyrene
PVA	Poly (vinyl alcohol)
RESS	Rapid expansion of supercritical solutions
r.t.	Room temperature

$R_f$	Ratio to solvent front
SAS	Supercritical antisolvent process
SC	Sodium cholate
scCO <sub>2</sub>	Supercritical carbon dioxide
SCF	Supercritical fluids
SDS	Sodium dodecyl sulfate
SEM	Scanning electron microscopy
S <sub>N</sub> 2	Bimolecular nucleophilic substitution
SPM	Scanning probe microscopy
STM	Scanning tunneling microscopy
T	Temperature
TBAI	Tetra- <i>n</i> -butylammonium iodide
TBAF	Tetra- <i>n</i> -butylammonium fluoride
TBDPSCI	<i>Tert</i> -butyldiphenylsilyl chloride
$T_c$	Critical temperature
TEM	Transmission electron microscopy
$T_g$	Glass transition temperature
$T_m$	Melting temperature
$P_c$	Critical pressure
THF	Tetrahydrofuran
TLC	Thin layer chromatography
TOF	Time of flight
w/o	Water-in-oil
w/o/w	(water-in-oil)-in-water
XPS	X-ray photoelectron spectroscopy
$\lambda$	Wavelength
4-HCCA	$\alpha$ -cyano-4-hydroxycinnamic acid





# Chapter I

## Synthesis of Polymeric Nanoparticles: An overview of the preparation and characterization methods\*

---

*Since the emergence of Nanotechnology in the past decades, the development and design of nanomaterials has become an important field of research. An emerging component in this field is nanomedicine, wherein nanoscale materials are being developed for use as imaging agents or for drug delivery applications. Much work is currently focused in the preparation of well-defined nanomaterials in terms of size and shape. These factors play a significantly role in the nanomaterial behavior in vivo. In this context, the first part of this chapter gives a general but non-exhaustive overview of the preparation methods of nanoparticles, while in the second part the characterization methods are discussed. In particular atomic force microscopy, dynamic light scattering and scanning electron microscopy will be discussed in detail.*

---

\* Part of this Chapter has been published in: Crucho, C.I.C.\*, *ChemMedChem*, 2015, 10, 24.



## I.1 Introduction

Nanotechnology has generated a significant impact in nearly every aspect of science. It deals with the characterization, synthesis and application of materials with new properties due to their small size: scales at which unique phenomena enable novel applications.<sup>1</sup>

Nature continues to be the ultimate in nanotechnology, where polymeric nanometer-scale architectures play a central role in biological systems.<sup>2</sup> Inspired by the way nature forms functional supramolecular assemblies, researchers are trying to make nanostructures and to incorporate these into macrostructures as nature does.<sup>2</sup>

Recent advances and progress in nanoscience have demonstrated the great potential that nanomaterials have for applications in healthcare.<sup>3</sup> In the realm of drug delivery, targeted nano-encapsulated medicinal drugs (nanomedicines)<sup>4</sup> have captured the attention of many scientists who have tried to realize the concept of the “magic bullet”, proposed by Paul Ehrlich almost a century ago.<sup>5</sup> Complications arise because drugs have to overcome natural biological hurdles and most infections are localized. Nevertheless, by delivering pharmacologically active agents more effectively and more selectively, nanomedicines aim to improve the pharmacokinetic and pharmacodynamic properties of therapeutic molecules, enhancing efficacy while reducing toxicity.<sup>6</sup> Many different nanostructures such as quantum dots, nanoparticles, cyclodextrin, dendrimers, liposomes and lipid-based nanocarriers, nanofibers, nanowires and carbon nanotubes have been developed and demonstrated increasing potential in diagnostics and therapeutics.<sup>7</sup> However, high tissue accumulation of non-biodegradable nanocarriers as rendered some of them as not-so-popular therapeutic and diagnostic systems due to toxicity problems.<sup>8</sup>

Polymeric nanoparticles (PNPs) also play an important role in the “Room at the Bottom” and this family may be considered amongst the most well studied nanomedicines to date.<sup>9</sup> These are solid colloidal particles generally varying in size from 10 to 1000 nm, although there is some degree of ambiguity regarding the upper size limit. In medical applications well-defined sizes are of great importance, as they play a crucial role in mediating biological effects and *in vivo* fate of the drug delivery system.<sup>10</sup> Therefore to assure the highest potential for *in vivo* applications, PNPs of intermediate size (20 - 100 nm) have the highest potential, given their ability to circulate in the bloodstream for long periods of time as well as their biodistribution patterns.<sup>11</sup>

Drugs or biomolecules can be either incorporated into PNPs by entrapment or adsorbed at their surface; depending upon the method of preparation, nanocapsules (Fig. 1A) or nanospheres (Fig. 1B) can be obtained.<sup>9a</sup> A nanocapsule particle consists of a liquid core (either oil or water<sup>12</sup>) in which the

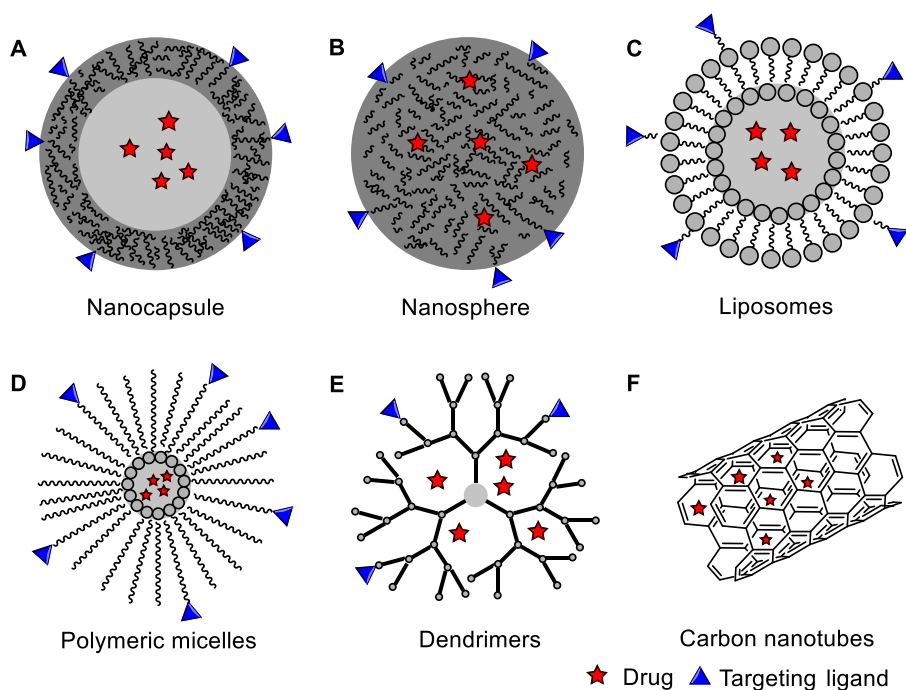


**Figure 1** Types of nanocarriers for drug delivery systems. Polymeric nanoparticles: A, Nanocapsules and B, Nanospheres. C, Liposomes. D, Polymeric micelles. E, Dendrimers. F, Carbon nanotubes.

drug is confined and surrounded by a polymer membrane. A nanosphere, however, has a matrix-like structure consisting of the drug and the polymer uniformly dispersed.

Surface functionality is another critical parameter in the development of ideal PNPs for drug delivery systems (DDS). PNPs can be conjugated to a bio-specific ligand or coupled to macromolecules that could target the PNPs to the desired site of action.<sup>8,13</sup> This allows efficient delivery of small-molecular-weight drugs, as well as macromolecules to target sites.<sup>14</sup> Targeting the desired site of action not only increases the therapeutic efficiency of a drug, but also increases its cellular uptake through receptor-mediated endocytosis. The surface of PNPs can also be suitably modified to avoid uptake by the body's mononuclear phagocyte system (MPS) after opsonization, thereby increasing their circulation half-life in the body.<sup>15</sup>

The main advantages of nanomedicines are enhanced stability, controlled release, improved bioavailability, significant decreased toxicity, as well as improved therapeutic effects due to a greater drug fraction able to reach the target site.<sup>8</sup> In addition, expensive potentially active substances could be applied efficiently in small amounts. In general, molecules susceptible to enzymatic (nuclease and protease) degradation, particularly protein, peptide and nucleic acid drugs, are better preserved when they are entrapped in nanocarriers.<sup>16</sup>

In drug delivery, the biodegradability and biocompatibility of the polymers are among the most important properties. A variety of materials have been used for the preparation of PNPs, such as proteins or other natural macromolecules, biodegradable polymers and non-biodegradable, but pharmaceutically acceptable polymers.<sup>17</sup> To self-assemble these materials into PNPs, a variety of preparation techniques has been successfully developed.<sup>18</sup>

## I.2 Preparation of Polymeric Nanoparticles

Polymeric nanoparticles have been synthesized by various methods depending on the needs of application and the physicochemical characteristics of the drug. The choice of the most suitable method plays a vital role in order to obtain PNPs with the desired properties for a particular application.<sup>19</sup>

Several preparation methods have been developed and can be divided into two groups, namely, those based on polymerization of monomers and those taking advantage of preformed polymers (Fig. 2).<sup>18</sup> These methods can be further classified into two categories: two-step procedures involving the preparation of an emulsification system followed by formation of nanoparticles in the second step of the process and one-step procedures where emulsification is not required previous to the formation of nanoparticles.

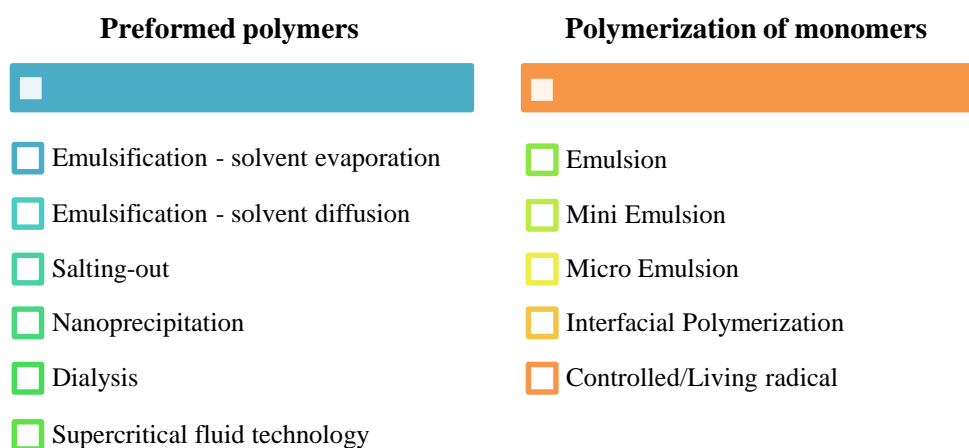


**Figure 2** Schematic representation of several techniques for the preparation of PNPs.

In polymerization methods, the monomers are polymerized to form the encapsulating polymer. This process can be carried out in two ways, either as emulsion polymerization techniques or interfacial polymerization.<sup>9</sup> Some drawbacks have been reported which have limited the use of polymerization methods for the synthesis of PNPs.<sup>9</sup> Not only are most PNPs formed from slowly biodegradable or nonbiodegradable monomers, but also non-biocompatible byproducts may be generated with these methods. Toxic residues such as monomers and initiators may persist which require extensive purification work to result in a pharmaceutically acceptable product. Another challenge is the requirement for free-radical polymerization or UV light to trigger polymerization, which prevents the addition of proteins or peptides during polymerization. Considering the limitations of polymerization techniques, attention is focused on describing the methods involving preformed polymers, as many of the problems involved in the former method can be avoided.

## I.2.1 Two-step procedures based on Emulsification

Colloidal delivery systems based on emulsions are widely used in food and pharmaceutical industries to encapsulate, protect, and deliver bioactive components.

The term emulsion is defined basically as a mixing of one liquid phase into another totally or partially immiscible, through the use of amphiphilic surface-active molecules (surfactants), which reduce the interfacial tension between the two liquids in order to achieve stability.

Emulsions can also be classified based on composition (oil, water, surfactants) or morphology.<sup>20</sup> Generally, emulsions may be of the oil-in-water (o/w) or water-in-oil (w/o) types depending on whether the oil is dispersed as droplets in water, or *vice versa*. In addition, more complex systems such as (water-in-oil)-in-water (w/o/w) can also be obtained. Depending on the droplet size, the emulsion formed can be classified into three main categories: nanoemulsions, miniemulsions and macroemulsions (Fig. 3).<sup>20</sup> In contrast to more common microscale emulsions, nanoemulsions have some interesting physical properties. For instance, nanoemulsions exhibit optical transparency, while microscale emulsions typically exhibit strong multiple scattering of visible light, and, as a result, have a white appearance.<sup>20</sup>

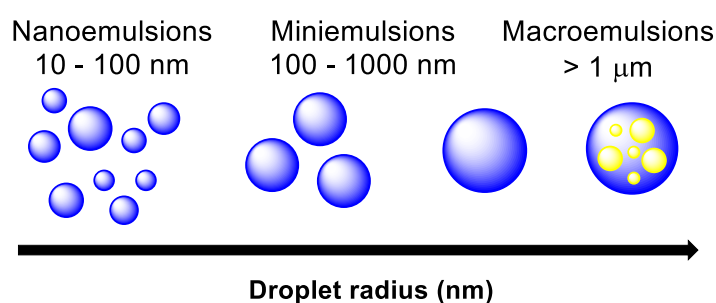


**Figure 3** Schematic diagram of emulsions fabricated from oil, water and surfactant.

A common mistake reported in the scientific literature is to describe nanoemulsions as “microemulsions”, thereby confusing an emulsion system with a thermodynamic phase.<sup>21</sup> Microemulsions are not emulsions in the classical sense, but rather nanoscale self-assembled equilibrium phases (lyotropic phases). In contrast, nanoemulsions do not form spontaneously, as an external shear must be applied to rupture larger droplets into smaller ones. Although these two kinds of colloidal dispersion can be comprised of three simple components (oil, water and surfactants) and have many structural similarities, the distinguishing difference is not one of composition, but rather one of thermodynamics: microemulsions are thermodynamically stable, whereas nanoemulsions are not.<sup>21</sup>

In two-step emulsification/solvent removal methods the polymer organic solution is emulsified in an aqueous phase. Low- and high-energy emulsification techniques can be used to produce nanodroplets and consequently nanoparticles.<sup>18</sup> In emulsion method the droplet formation step is fundamental because it determines the size and size distributions of the resulting PNPs. Polymer precipitation on preformed nanodroplets is achieved by removing the organic solvent by different

methods such as solvent evaporation, fast diffusion after dilution or salting out. A similarity between these techniques is the drug encapsulation process in which the drug is generally added in the polymer solution.<sup>9b</sup>

### I.2.1.1 Emulsification-solvent evaporation

Solvent evaporation was the first method developed to prepare PNPs from a preformed polymer.<sup>22</sup> In a pioneer work, Gurny *et al.* applied it successfully in the preparation of drug carriers from biocompatible polymers.<sup>23</sup> In this method, the polymer is first dissolved in a volatile solvent (see Fig. 4). Dichloromethane and chloroform have been widely used in the past. However, due to their toxicity they have been replaced by ethyl acetate which displays a better toxicological profile and therefore more suitable for biomedical applications.<sup>24</sup> The resulting organic solution is emulsified in the aqueous phase and the mixture is typically processed using a surfactant and high-speed homogenization or ultrasonication, yielding a dispersion of nanodroplets. Afterwards, a suspension of nanoparticles is formed by evaporation of the polymer solvent, which is allowed to diffuse through the continuous phase of the emulsion.<sup>24</sup> The solvent is evaporated either by continuous magnetic stirring at room temperature or under reduced pressure, which is a slow process. After the solvent has evaporated, the solidified nanoparticles can be washed and collected by centrifugation, followed by freeze-drying for long term storage.<sup>25</sup>

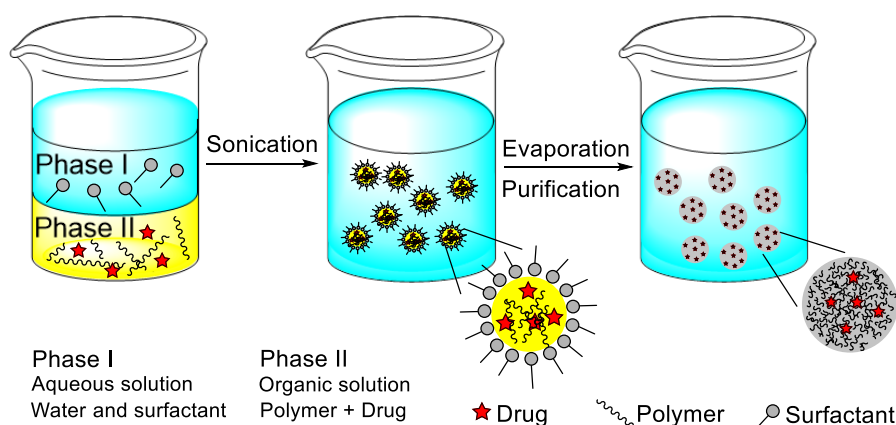


**Figure 4** Schematic representation of the emulsification-solvent evaporation method for the production of nanospheres.

The emulsification-solvent evaporation method has been widely applied to prepare PNPs with the desired characteristics by adjusting different experimental parameters. For example, poly(lactic acid) (PLA) PNPs with an average size around 200 nm were prepared by Zambaux *et al.* using dichloromethane and polyvinyl alcohol (PVA) as the solvent and stabilizing agent, respectively.<sup>26</sup> The authors adopted the double-emulsion method (w/o/w) to prepare the PNPs and studied the influence of experimental parameters such as the preparation temperature, solvent evaporation method, internal aqueous phase volume, surfactant concentration and polymer molecular weight on the physicochemical

properties of the obtained PNPs. In another report, Bilati *et al.* studied the effect of the sonication process on the characteristics of poly(D,L-lactic-co-glycolic acid) (PLGA) nanocapsules prepared by the w/o/w solvent evaporation method.<sup>27</sup> They concluded from their study that the duration of the second mixing step (leading to the w/o/w emulsion), had a greater influence on the final mean particle size than the first step (w/o emulsion). In order to study the effect of the polymer solvent on the PNP properties, Mainardes *et al.* prepared PLGA nanoparticles applying either of two organic solvents (dichloromethane and ethyl acetate) as the dispersed phase.<sup>28</sup> They demonstrated that the size of the PNPs prepared with dichloromethane was larger than those prepared with ethyl acetate. Manchanda and coworkers formulated PLGA nanoparticles using methanol and dichloromethane (1:2 v/v) as the solvent system and PVA as the stabilizing agent.<sup>29</sup> It was evidenced that an increase in polymer amount leads to larger nanoparticles. This was attributed to an increase in the viscous resistance of the emulsion mixture, thereby absorbing the agitation energy which in turn leads to reduction in shear stress resulting in droplets with larger size. When the concentration of PVA was taken into account, the particle size decreased from 159 nm (1 % PVA) to 113 nm (5 % PVA) due to an improvement in the emulsification process. PLGA and PLA nanoparticles were prepared by Budhian *et al.* by employing dichloromethane as the solvent and PVA as the stabilizing agent.<sup>30</sup> It was shown that decreasing the organic solvent volume resulted generally in a decrease in particle size. The method used to remove the organic solvent can also affect the final properties of the PNPs prepared by the solvent evaporation method. This effect was studied by Ashjari *et al.* who prepared magnetic/*cis*-Diamminedichloroplatinum (II) (cisplatin) - loaded PLGA nanocapsules through a w/o/w double emulsion-solvent evaporation technique.<sup>31</sup> They observed a change in the morphology and a decrease in the particle size of nanocapsules when slow evaporation at room temperature was used in comparison with evaporation at reduced pressure (Fig. 5). An extensive study was reported by Khoee *et al.* on the physicochemical properties of cisplatin loaded polybutyladipate (PBA) nanoparticles prepared from w/o/w emulsion.<sup>32</sup> The obtained PNPs showed a size dependence on polymer concentration, decreasing when the polymer concentration decreases. The size of PNPs was also influenced by other process parameters such as volume of oil phase, power of sonication and drug concentration in the internal water phase. Ethyl cellulose (EC) nanospheres were prepared by Wachsmann *et al.* to study the influence of surface properties on the accumulation

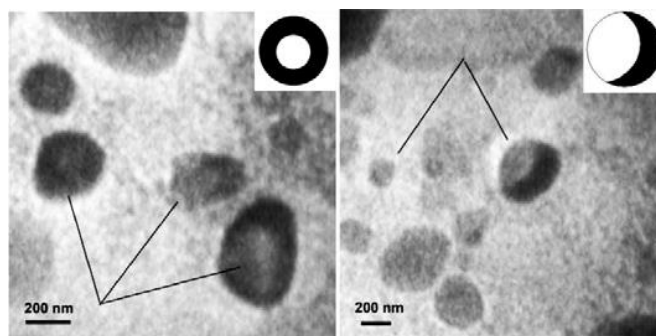


**Figure 5** Nanocapsules with different morphologies prepared by Ashjari *et al.* Core-shell or half-moon morphology was observed when slow evaporation was used compared to fast evaporation. [Adapted from ref. 31]

selectivity of nanoparticles in murine experimental colitis.<sup>33</sup> For this purpose, PNPs of similar sizes (212 - 258 nm) were prepared using different surfactants (polysorbate 20 (P20), SDS, sodium cholate (SC), cetyltrimethylammonium bromide (CTAB) and PVA). It was shown that the accumulation of PNPs in the inflamed areas as well as in the healthy tissue was dependent on surfactant type. The targeting pattern for P20 and CTAB particles showed a distinctly increased accumulation in the inflamed tissue compared to SDS particles with slightly higher values for P20. However, as CTAB particles also exhibited a significantly higher accumulation in healthy tissue compared to the other two preparations, the highest selectivity was obtained with P20 particles. More recently, Barba and coworkers developed a preparation technique based on multiple emulsion system to produce polymeric nano and microparticles.<sup>34</sup> Different polymers, such as polyesters (PCL, PLA and poly(D,L-lactide-*co*-caprolactone) 70:30 (PLC)) and poly(methylmethacrylate-acrylic acid) (Poly(MMA-AA)) 73/27, loaded with different model molecules, were explored. Depending on type of polymer and, consequently, on solvent used for solubilization (dichloromethane), polyester-based nanoparticles with round shape and smooth surface were obtained (Fig. 6). Conversely, polyacrylates yielded microparticles with high porosity and lower yield of encapsulation, due to the presence of hydrophilic co-solvents (ethanol and isopropyl alcohol) that caused an easy coalescence between the oil and the water phases (Fig. 6).

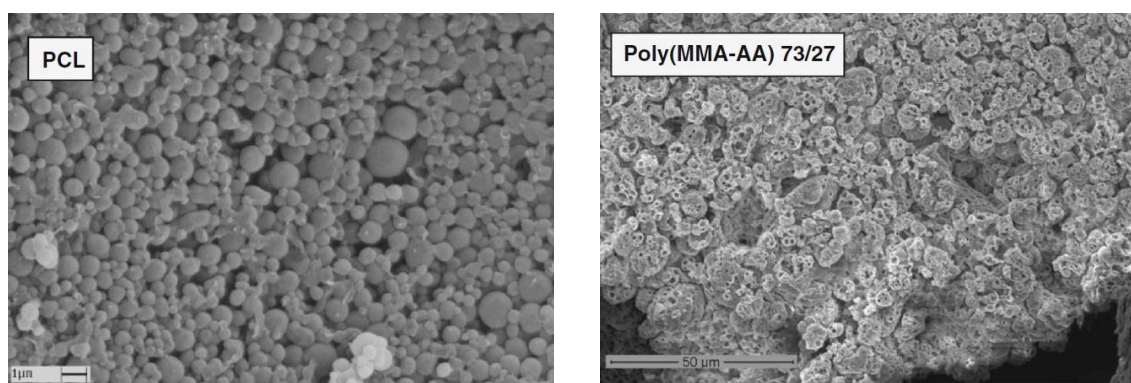


**Figure 6** SEM images of particles obtained from a polyester (PCL) and a polyacrylate polymer (poly(MMA-AA)). The solvent used for polymer solubilization influenced the particle size and morphology. [Adapted from ref. 34]

Over the past decade, methods for emulsion preparation with nanoscale droplets have been considerably developed due to the technological improvement of emulsification devices, which has prompted the development of the solvent evaporation technique. Although, this method is simple and versatile, it can only be applied mainly to liposoluble drugs, it is time consuming and there is also the possibility of nanoparticle coalescence during evaporation. In addition, for scale-up production alternative methods using low-energy requirements in homogenization are preferred.

### I.2.1.2 Emulsification-solvent diffusion

The emulsification-solvent diffusion method was first introduced by Leroux *et al.*<sup>35</sup> It consists in the formation of a conventional o/w emulsion between a partially water-miscible solvent containing the polymer and the drug, and an aqueous solution, containing a surfactant (Fig. 7). For the success of this method, the polymer solvent and water are mutually saturated at room temperature to ensure the initial thermodynamic equilibrium of both liquids. The subsequent dilution with an extensive amount of water, induces solvent diffusion from the dispersed droplets into the external phase, resulting in the formation of colloidal particles. Such diffusion process is milder than the direct evaporation of the organic solvent from the nanodroplets. In contrast with methods based on solvent evaporation, in this technique the droplet size decreases suddenly in a millisecond time scale during solvent diffusion.<sup>36</sup> Generally, nanospheres are produced by this method but nanocapsules can be obtained just by adding a small amount of oil, for example miglyol, in the organic phase. Finally, depending on its boiling point, the solvent can be eliminated by evaporation or filtration.

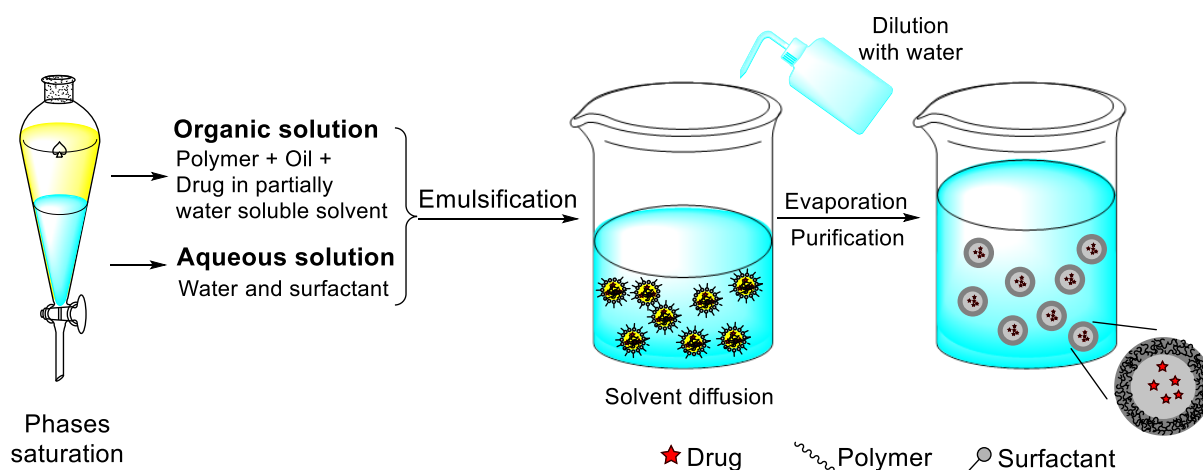


**Figure 7** Schematic representation of the emulsification-solvent diffusion method for the preparation of nanocapsules.

Several formulation parameters can affect the size of the obtained PNPs by solvent diffusion. For example, it has been shown that most properties of nanocapsules are determined at the emulsification step.<sup>36</sup> Guinebretière *et al.* prepared PCL nanocapsules using ethyl acetate and PVA as the solvent and stabilizing agent, respectively. They observed that the final size of the nanocapsules was influenced by the concentration of oil in the organic phase, volume of the solvent in the emulsion and nature and concentration of the surfactant.<sup>37</sup> Also, the thickness of the nanocapsule was linked to the polymer concentration in the organic phase. In another study, PLA nanospheres were prepared by Quintanar-Guerrero *et al.* by employing propylene carbonate as the solvent and PVA or Pluronic F68 as surfactants.<sup>38</sup> It was evidenced that high concentrations of polymer leads to larger particle sizes with an increase in the polydispersity index. On the other hand, an increase in stirring rate and in the surfactant concentration were found to reduce moderately the size of the PNPs. Similar results were obtained by

Trimaille *et al.* who prepared PLA nanoparticles using ethyl acetate and Pluronic F68 as the solvent and stabilizing agent, respectively.<sup>39</sup> It was shown that increasing the PLA concentration resulted in an increase of the mean particle size from approximately 260 to 530 nm (Fig. 8). The same experimental parameters were applied by Surassmo *et al.* for the preparation PCL nanocapsules.<sup>40</sup> The authors observed that an increase of the surfactant amount resulted in a decrease of the mean particle size. Although, it seems that above some level further significant size reduction is no longer possible as the excess surfactant remains in the continuous phase, and does not play any significantly role in the emulsification. In a different approach, Colombo and coworkers designed with chemical engineering equipment, a pilot plant to study the process of emulsification-diffusion.<sup>41</sup> It was demonstrated that the agitation time, stirrer type and rotational speed were the most important parameters in the emulsification

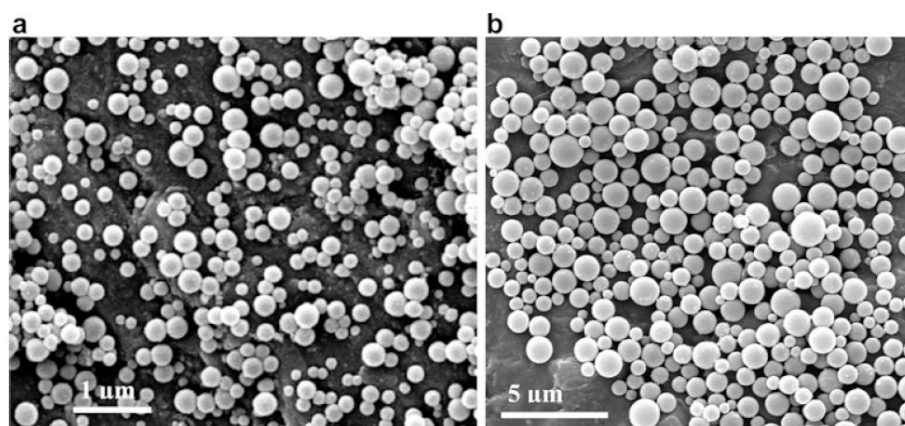


**Figure 8** SEM images of the PLA nanoparticles prepared by Trimaille *et al.* a) 2% PLA; b) 10% PLA. [Adapted from ref. 39]

step. In contrast, during the dilution step, the agitation has no influence on the final size distribution. Only sufficient mixing is needed in order to homogenize the mixture. In another report, Sahana and coworkers used a modified emulsification-diffusion method by using a non-saturated organic solvent and water. In their work they studied the influence of the type of solvent and surfactant on particle size distribution and entrapment efficiency of PLGA nanoparticles.<sup>42</sup> When didodecyldimethylammonium bromide (DMAB) and PVA were compared, the former gave the smallest particles but with the lowest encapsulation efficiency, regardless of the type of organic solvent. For both stabilizers, dichloromethane in combination with ethyl acetate yielded the highest entrapment efficiency. Similar results were obtained by Jain *et al.* who compared the influence of different stabilizers (Pluronic F68, DMAB and PVA) in the preparation of PLGA PNPs from ethyl acetate organic solutions.<sup>43</sup> DMAB, when used as surfactant, led to smaller particle sizes as compared to PVA, but on the other hand, PVA produced particles with higher entrapment efficiency (Table 1). The authors also studied the effect of droplet size reduction by using both homogenization and sonication. It was demonstrated that sonication resulted in smaller particles (165 nm) as compared to homogenization (around 225 nm). Hallouard *et al.* studied the oil nature on the physicochemical characteristics of nanocapsules.<sup>44</sup> For PCL-mPEG diblock copolymer, it was shown that the nature of the oil had no influence on the encapsulation rate. Though, it influenced the particle size and polydispersity, with macroglycerides, appearing to be the lipid

structure best suited to obtain the smallest monodisperse nanocapsules. More recently, Musazzi and coworkers prepared PNPs by a modified solvent-diffusion method without surfactant from a combination of PLGA and PCL-PEG copolymer.<sup>45</sup> The latter was used due to its amphiphilic nature, which stabilizes the nanodroplets surface in the emulsification step.

**Table 1** Effect of stabilizer type on particle size, polydispersity index (PDI) and entrapment efficiency, for PLGA nanoparticles prepared by Jain *et al.*<sup>43</sup>

Surfactants	Size (nm)	Polydispersity Index (PDI)	Entrapment efficiency (%)
2% PVA	165.6	0.085	86.20
1% DMAB	120.0	0.015	15.30
Pluronic F68	130.0	0.136	38.56

The experimental parameters related to the solvent diffusion step do not seem to affect particle size.<sup>46</sup> Free solvent diffusion is guaranteed as long as the organic solvent solubility condition is satisfied. This could explain some contradictory results reported by Song *et al.* in which the highest particle size was obtained at the lowest volume of water for dilution.<sup>47</sup> In their study, the lowest volumes of water used did not lead to complete solubility of the organic solvent. In addition, difficult solvent diffusion can be expected due to the barrier effect of the stabilizing agent on the emulsion droplet. This could also explain the results reported by Kwon *et al.* where the size of submicron particles prepared using PVA as a stabilizing agent is influenced by the temperature of the dilution water.<sup>48</sup> It was shown that the particle size decreased as the temperature of dilution water increases. In this case, reducing the viscosity of the external phase promoted solvent diffusion, and consequently a decrease in particle size.

The emulsification-diffusion technique presents clear advantages such as high yields, easy in scaling-up, no need for high-pressure homogenizers or ultrasonication, batch-to-batch reproducibility and generally good encapsulation efficiencies.<sup>49</sup> However, there are also disadvantages. For instance, high volumes of water to be eliminated from the suspension and possible leakage of water soluble drugs into the external phase throughout emulsification step.<sup>9b</sup>

### I.2.1.3 Emulsification–reverse salting-out

The emulsification-solvent diffusion procedure previously described can be considered as a modification of the emulsification-reverse salting-out method.<sup>50</sup> The main difference comes from the composition of the emulsion which is formulated from a water-miscible polymer solvent like acetone and an aqueous gel containing the salting-out agent and a colloidal stabilizer (Fig. 9). Examples of suitable salting-out agents include electrolytes such as magnesium chloride, calcium chloride or magnesium acetate, and non-electrolytes such as sucrose. The emulsification is achieved due to an Ouzo-

effect<sup>51</sup>, without employing any high-shear forces. The miscibility of acetone and water is reduced by saturating the aqueous phase, which allows the formation of an o/w emulsion from the otherwise miscible phases. A reverse salting-out effect is obtained by dilution of the formed o/w emulsion with an excess of water to promote the diffusion of acetone into the aqueous phase, which leads to the precipitation of the polymer dissolved in the emulsified nanodroplets. The remaining polymer solvent and salting-out agent are eliminated by cross-flow filtration.<sup>52</sup> The condition of complete miscibility between the organic solvent and water is not essential, but simplifies the execution process.<sup>50</sup> If it is not the case, there is a need for a greater water/solvent volume ratio during the formation of the nanoparticles.

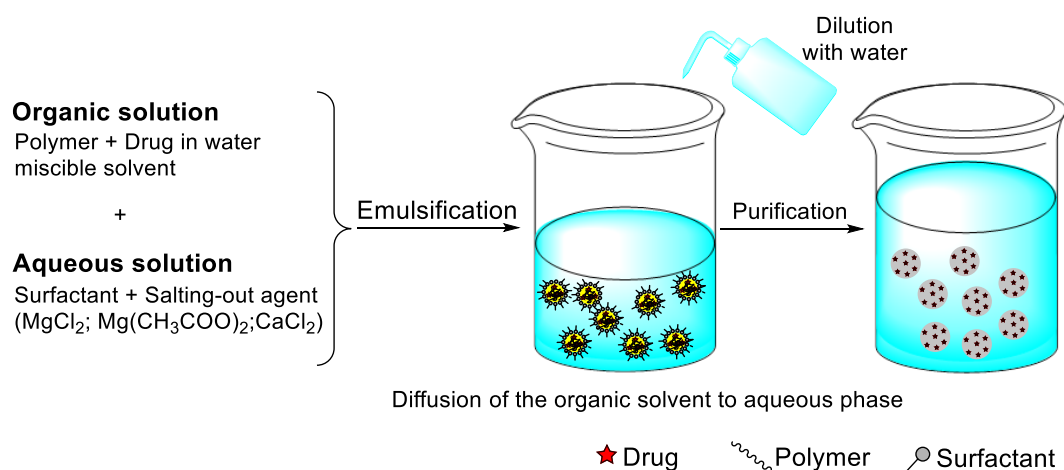


**Figure 9** Schematic representation of the emulsification-reverse salting-out technique.

PNPs have been prepared successfully by employing the emulsification-reverse salting-out method with several polymers, solvents and salting-out agents. The only condition which should be met is the need for a two-phase system in the presence of the salting-out agent. In a typical process carried out by Allémann *et al.* the influence of several process parameters on particle size was studied.<sup>53</sup> Eudragit® S PNPs were first prepared using acetone and magnesium chloride as the solvent and salting-out agent, respectively. In addition, PVA was also added to the aqueous phase as a viscosity-increasing agent and emulsion stabilizer. It was shown that by changing the molecular weight and concentration of PVA in the external phase, the size of the PNPs could be controlled within a wide range (186 – 1130 nm). Additionally, an increase in stirring rate also allowed a slight decrease in particle size. PNPs with a particle size of 200 to 500 nm were obtained by varying the polymer concentration or the internal/external phase ratio. When Eudragit® E was studied, magnesium acetate was selected as salting-out agent due to the solubility of the polymer in acidic medium. For PLA PNPs when an acidic aqueous phase (magnesium chloride) was changed to a basic one (magnesium acetate), a slight increase on the particle size was observed (228 to 247 nm). Zweers and coworkers also concluded in their studies that the particle size can be best controlled by adjusting the polymer concentration in the external phase.<sup>54</sup> In another report, Song *et al.* prepared PLGA nanoparticles by employing sodium chloride as the salting-

out agent instead of magnesium chloride or magnesium acetate.<sup>55</sup> Although acetone is the most commonly used organic solvent, other solvents have been reported. For example, Konan *et al.* prepared PLGA and PLA nanoparticles with a mean particle size below 200 nm using tetrahydrofuran (THF) as the polymer solvent.<sup>52</sup>

The main advantages of the salting-out method are the avoidance of chlorinated solvents, which are hazardous to the environment as well as to the physiological systems. The greatest disadvantages are the exclusive application in encapsulating lipophilic drugs and the need for intensive purification steps due to the use of salts. The latter can be responsible for the few reports that have been published in the recent years quoting the salting-out method.

## I.2.2 One-step procedures

### I.2.2.1 Nanoprecipitation or solvent displacement method

The nanoprecipitation method, also called solvent displacement, was firstly developed by Fessi *et al.*<sup>56</sup> The basic principle of this technique is based on the interfacial deposition of a polymer after displacement of the organic solvent from a lipophilic solution to the aqueous phase (Fig. 10).<sup>9</sup> The polymer is dissolved in a water-miscible solvent of intermediate polarity and this solution is added into a stirred aqueous solution in one shot, stepwise, dropwise or by controlled addition rate.<sup>46</sup> Due to the

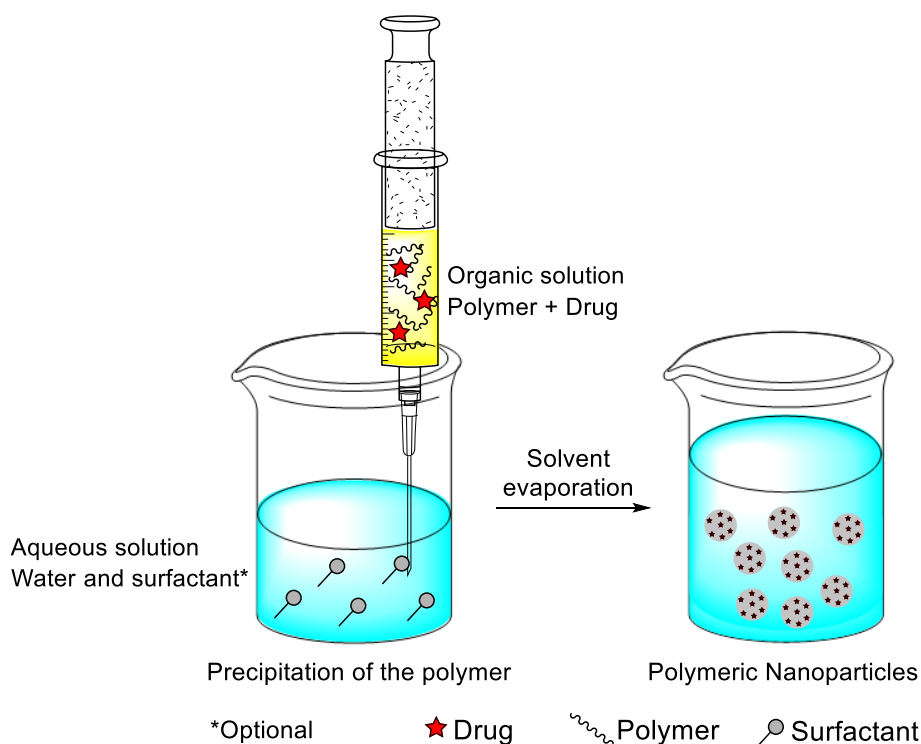


**Figure 10** Schematic illustration of the nanoprecipitation method for the preparation of nanospheres. For the preparation of nanocapsules an oil is introduced in the organic phase.

fast spontaneous diffusion of the polymer solution into the aqueous phase, the nanoparticles form instantaneously in an attempt to avoid the water molecules. This process appears to be governed by the Marangoni effect<sup>57</sup>, wherein a decrease in the interfacial tension between the two phases, increases the surface area due to the rapid diffusion and leads to formation of small droplets of organic solvent. As the solvent diffuses out from the nanodroplets, the polymer precipitates in the form of nanocapsules or nanospheres. In general, the organic phase is added to the aqueous phase but the protocol could also be reversed without compromising the nanoparticle formation. The most common used organic solvent is acetone, because it is miscible with water and easy to remove by evaporation. Though, ethanol and binary solvent blends, such as acetone with a small amount of water, ethanol or methanol can also be used.<sup>58</sup> It is also possible to use either two organic phases or two aqueous phases as long as solubility, insolubility and miscibility conditions are satisfied.<sup>46</sup> Usually, surfactants could be included in the process to guarantee the stability of the colloidal suspension, but their presence is not required to ensure formation of nanoparticles. The obtained nanoparticles are typically characterized by a well-defined size (around 200 nm in diameter) and a narrow size distribution, which is better than those produced by the emulsification solvent evaporation procedure.

The key variables that are conditioning the final nanoparticle properties are those related with the experimental design. By carefully adjusting the nature and concentration of the components, organic phase/aqueous phase ratio, organic phase injection rate, fluid dynamics and mixing speed, it is possible to control the PNP physicochemical properties. For example, increasing the polymer concentration or the polymer molecular weight generally results in an increase on particle size. These findings are explained by a higher organic phase viscosity, which hinders solvent diffusion and results in larger nanodroplets.<sup>59</sup> In a typical process carried out by Chancón *et al.* the polymer concentration, organic phase injection rate and needle gauge, were identified as the principal size determinants on the preparation of PLGA nanoparticles.<sup>60</sup> The smallest particles (46 nm) were obtained by using the lowest polymer concentration, the highest injection rate and the lowest needle gauge. Similar results were obtained by Simsek and coworkers in the preparation of PLGA-*b*-PEG nanoparticles.<sup>61</sup> The average hydrodynamic diameter of these particles could be controlled between 30 to 172 nm by the choice of polymer concentration and PEG content. Chorny *et al.* prepared nanospheres of PLA by employing acetone and dichloromethane (39:1 v/v) as the solvent system and Pluronic F-68 as the stabilizing agent.<sup>59</sup> It was demonstrated that replacing acetone in the organic phase by equal volumes of ethanol resulted in particle size reduction from 115 to 70 nm. The authors also observed that the organic solvent evaporation rate and an increase of aqueous phase volume had no influence on the nanosphere size. In another report, Dong *et al.* prepared PEG-PLA nanoparticles by using acetonitrile as the solvent and Pluronic F-68 as the surfactant.<sup>62</sup> They found that the surfactant concentration slightly influenced the nanoparticle size. Likewise, a slight smaller size were obtained by increasing the organic phase volume. PNPs were prepared by Özcan and coworkers by a modified nanoprecipitation method using several poly( $\gamma$ -benzyl-L-glutamate) (PBLG) derivatives.<sup>63</sup> Briefly, the polymers were dissolved in

tetrahydrofuran at 30 °C and this solution was added to an aqueous phase by dripping without the presence of any surfactant. As shown in Figure 11, the polymer concentration in the organic phase strongly influenced the mean diameter of the nonpegylated nanoparticles. In contrast, very small PNPs were obtained for the PBLG-PEG copolymer and almost no influence of the concentration was observed

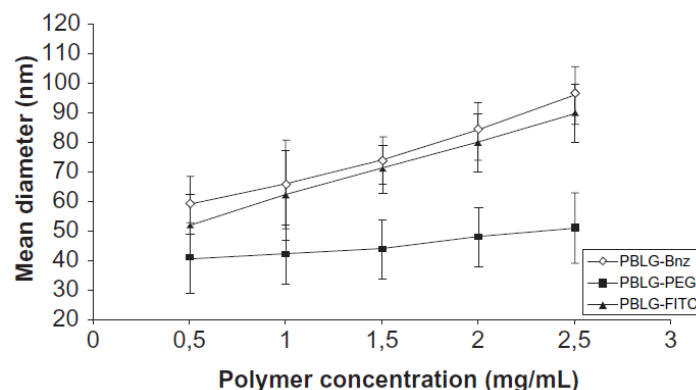


**Figure 11** Influence of polymer concentration in the organic phase on the mean diameter of PNPs. Abbreviation: Bnz, benzylamine; FITC, fluorescein isothiocyanate. [Adapted from ref. 63]

due to the amphiphilic nature of this copolymer. The mixing rate is also important in the preparation of PNPs by nanoprecipitation. Asadi *et al.* prepared nanoparticles from PLA-PEG-PLA tri-block copolymer.<sup>64</sup> It was shown that increasing the mixing rate led to a decrease in particle size. Furthermore, smaller particles were also obtained by decreasing organic/aqueous phase ratio due to a better dispersion of the solvent and faster diffusion rate. This is a conflicting result to that obtained by Dong *et al.*<sup>62</sup> Nevertheless, the polymer nature and the experimental parameters are different and could have influenced the results. More recently, Bukhari *et al.* studied the effect of solvent/non-solvent dispersion medium on the preparation of polystyrene (PS) nanoparticles.<sup>65</sup> Chloroform and tetrahydrofuran were explored as solvents for polystyrene and several dispersion phases (methanol, chloroform, acetone and water) were investigated. The results revealed that the combination of tetrahydrofuran with acetone and water, as well as chloroform with methanol and acetone leads to the formation of nanoparticles. They concluded from their study that the dielectric constant difference plus the affinity of the solvent for the non-solvent were responsible for nanoprecipitation. In addition, the morphology was remarkably dependent on the nature of the dispersion phase (Fig. 12).

Overall, the challenge in nanoprecipitation is to find a suitable drug/polymer/solvent/non-solvent system, which allows successful nanoparticle production and drug encapsulation. Though, this method is widely used due to its simplicity, rapidity and reproducibility. One of the difficulties is the mixing process during nanoprecipitation. A microfluidic platform<sup>66</sup> could be a promising tool for the controlled synthesis of PNPs, where the hydrodynamic flow ensures a fast and tunable mixing of solvent/non-solvent in the microfluidic channels. Other recent development is the advent of automation to nanoprecipitation with high throughput experimentation (pipetting robot, inkjet printing).<sup>67</sup> Another drawback is the poor encapsulation efficacy of hydrophilic drugs, because the drug can diffuse to the

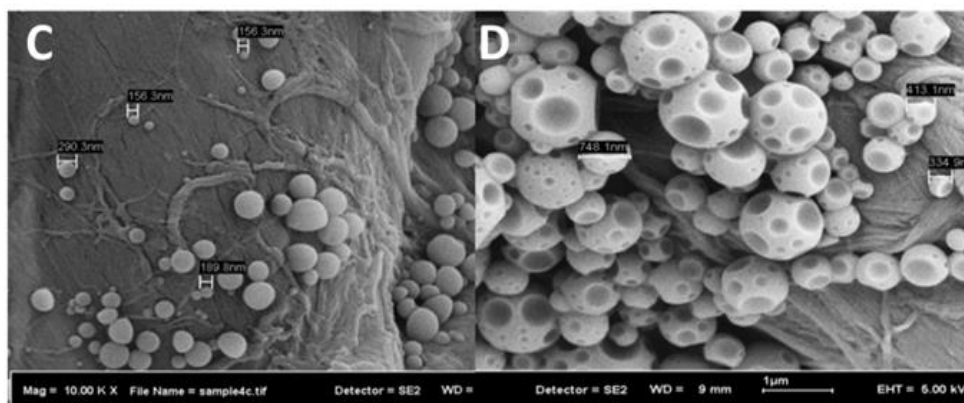


**Figure 12** FESEM micrographs of polystyrene PNPs prepared by nanoprecipitation. Polymer solvent: tetrahydrofuran. Non-solvent: C, Acetone; D, water and Pluronic-F68. [Adapted from ref. 65]

aqueous phase during polymer precipitation. By modifying the solubility of the drug through changes in the pH or varying the solvent composition are among other means to improve encapsulation efficiency.<sup>68</sup>

### I.2.2.2 Dialysis

The dialysis method has been applied successfully in the preparation of small PNPs with narrow size distribution.<sup>69</sup> It is governed by a mechanism resembling that previously described for the nanoprecipitation technique, but with a slightly different experimental setup. In this method, dialysis tubes or semipermeable membranes with a suitable molecular weight cut-off (MWCO) are used as a physical barrier for the polymer.<sup>9a</sup> Generally, the polymer is dissolved in an organic solvent, placed inside the dialysis membrane and dialyzed against a non-solvent (Fig. 13). Basic prerequisites are the miscibility of the solvents and the existence of dilute polymer solutions. The displacement of the solvent inside the membrane causes the mixture to be progressively less able to dissolve the polymer. In addition, an increase in interfacial tension results in polymer aggregation and leads to the formation of a colloidal suspension of nanoparticles. Although dialysis is a simple and common method, the large

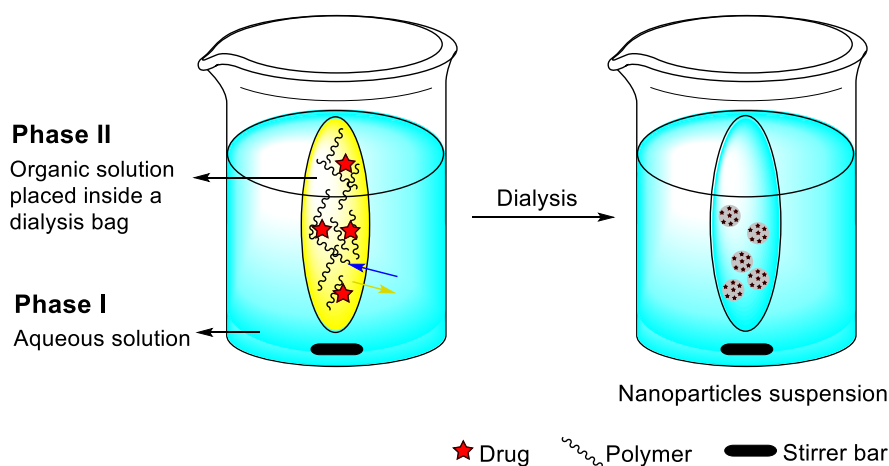


**Figure 13** Schematic representation of the dialysis method for the preparation of nanospheres.

volume of counter dialyzing medium could arouse a premature release of the nanoparticle payload due to the long duration of the process.

The morphology and particle size distribution of the obtained PNPs can be modulated by several experimental parameters, such as solvent/non-solvent pair, dialysis MWCO, the temperature at which the procedure is carried out, polymer concentration and speed of solvent mixing.<sup>70</sup> The influence of the solvent was examined in a work of Akagi *et al.* in which either of four organic solvents (dimethylsulfoxide (DMSO), dimethylformamide (DMF), dimethylacetamide (DMAc), *N*-methyl-2-pyrrolidinone (NMPy)) were applied as the polymer solvent to prepare PNPs based on poly( $\gamma$ -glutamic acid) (PGGA).<sup>71</sup> They concluded that the particles prepared with DMSO were smaller, with a narrower size distribution than those prepared with NMPy. A similar approach was used by Jeong *et al.* to prepare PLGA nanoparticles from DMAc, DMF, DMSO and acetone as the polymer solvent.<sup>72</sup> The size of the PNPs prepared from DMAc, DMF and DMSO were in the range of 200 – 300 nm and not significantly different. On the other hand, acetone yielded larger particles with a mean size of 642 nm (Fig. 14). This change in particle size could be explained by the difference in solvent viscosity, miscibility with water and in the solubility behavior of the polymer. In another report, Chronopoulou *et al.* studied the influence

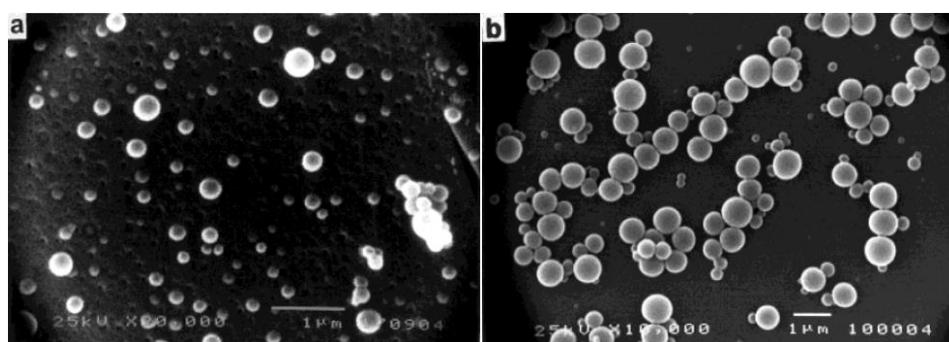


**Figure 14** SEM images of PLGA 50:50 nanoparticles prepared by Jeong *et al.* a) DMAc or b) acetone as the polymer solvent. [Adapted from ref. 72]

of several experimental parameters on the size and morphology of nanoparticles prepared from natural and synthetic polymers.<sup>70</sup> For poly(methyl methacrylate) (PMMA) nanoparticles, a linear correlation between polymer concentration and the size of the nanospheres was determined. The same behavior was observed for poly(phenyl acetylene) (PPA) nanospheres. In addition, at low concentrations, PPA nanoparticles with smaller diameters were obtained at low temperature than those obtained at room temperature. The influence of the MWCO was also studied for this synthetic polymer. It was shown, that reducing the membrane MWCO induces a decrease of the mean particle size. The biopolymers under study also followed the same trend. This is due to a decrease in the mixing rate of the solvents, thus favoring thermodynamic factors over kinetic ones. Different morphologies were observed for hyaluronic acid based nanostructures by changing the chemical properties of the solvent/nonsolvent pair (Fig. 15).

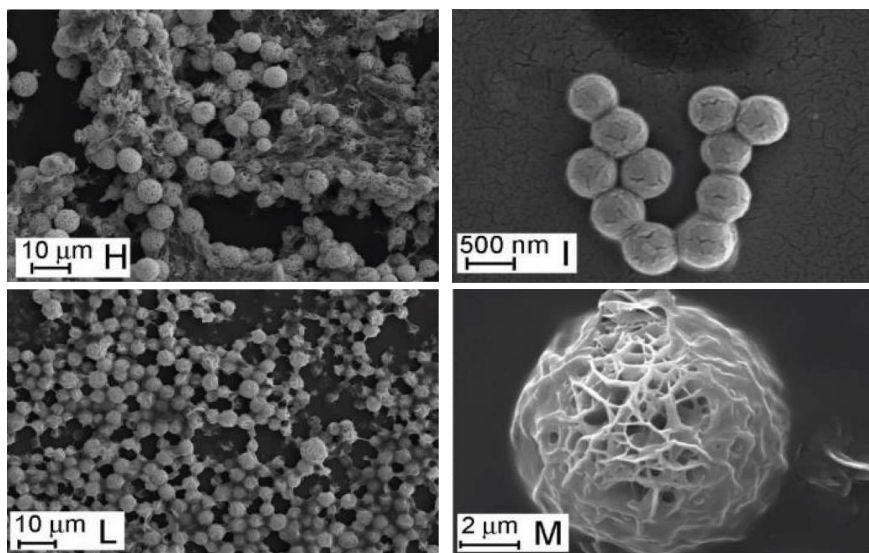


**Figure 15** SEM images of different morphologies obtained for hyaluronic acid based nanostructures. Experimental conditions:  $T = 4\text{ }^{\circ}\text{C}$ ; conc. [mg/mL] = 0.5; Solvent pair: H,  $\text{H}_2\text{O}/\text{EtOH}$ ; I,  $\text{H}_2\text{O}/\text{MeOH}$ ; L,  $\text{DMSO}/\text{MeOH}$ ; M,  $\text{H}_2\text{O}/\text{acetone}$ . Morphology: H, flowerlike; I and L, spheres and M, dandelion-like. [Adapted from ref. 70]

### I.2.2.3 Supercritical fluid technology

As may be noted, the methods discussed in the previous sections require the use of organic solvents and surfactants which are hazardous to the environment as well as to physiological systems. On the other hand, if residual solvent impurities remain in the drug-loaded PNPs, then these become toxic and may degrade the drug within the polymer matrix.<sup>19</sup> There is also a challenge to develop versatile and precise production methods for nanomedicines, which could be easily scaled up. To overcome these hurdles research efforts have been directed to develop environmentally sound methods for the production of PNPs. In this aim, supercritical fluids (SCF) have emerged as an attractive alternative due to the use of environmentally friendly technology, easy and reproducible scale up, good control of structural homogeneity and production of high purity nanomedicines.<sup>73</sup>

A SCF is a fluid that has been compressed and heated above its critical temperature ( $T_c$ ) and critical pressure ( $P_c$ ). In such conditions, its physicochemical properties are intermediate between a gas and a liquid. This is a new state of matter, in which the fluid behaves like a gas and also has the typical density of a liquid and thus its solvating properties.<sup>74</sup> Supercritical carbon dioxide ( $\text{scCO}_2$ ) is the most widely used SCF because it has mild critical conditions, is abundant, inexpensive, non-flammable, non-toxic and environmentally benign.<sup>74</sup>

SCF technology has gained significant attention in pharmaceutical research. Many recent and excellent reviews have been published on pharmaceutical particle formation, formulation, and control with a SCF. Fages *et al.* reviewed the methods to prepare particles with SCF.<sup>75</sup> The application of SCF to improve the field of drug delivery was described by Ginty *et al.*<sup>76</sup> Perrut and coworkers commented the processes that have been developed to prepare composite particles of poorly soluble active

ingredients.<sup>77</sup> Mishima *et al.* gave an overview on the formation of biodegradable particles for drug and gene delivery using SCF.<sup>78</sup>

The most common processing techniques involving supercritical fluids are rapid expansion of supercritical solutions (RESS), the gas antisolvent process (GAS), supercritical antisolvent process (SAS) and its various modifications, and the particles from gas-saturated solution (PGSS) processes.<sup>79</sup> These methods depend on the primary role played by the SCF, namely whether it is used as a solvent, a solute or an antisolvent.

There is a vast literature on the production of drug-loaded microparticles using SCF technology. Conversely, much less have been studied to prepare nanoparticles. The application of supercritical fluid technology requires a high investment for high-pressure equipment. In addition, in spite of the availability of a number of supercritical fluids, most polymers exhibit poor solubility or even non-solubility in supercritical fluids and this is main drawback of this technology.

### I.3 Characterization methods of Polymeric Nanoparticles

The use of PNPs for pharmaceutical and biomedical applications have opened a new era of diagnosis and treatment of diseases. Central to any significant advances in nanomaterial based applications is their extensive characterization, which is an important pre-requisite for preclinical development. Currently, there are no standardized methodologies or FDA regulatory protocols for the characterization of nanoparticles.<sup>80</sup> However, it is well-known that physiological interactions depend on the particle physicochemical properties. Developing a fairly accurate picture of the PNPs is essential for understanding and predicting the performance of the system in the body. A tiered approach to preclinical characterization of nanomedicines includes physicochemical characterization, sterility and pyrogenicity assessment, biodistribution and toxicity characterization (Fig. 16).<sup>81</sup> Nanoparticles are usually

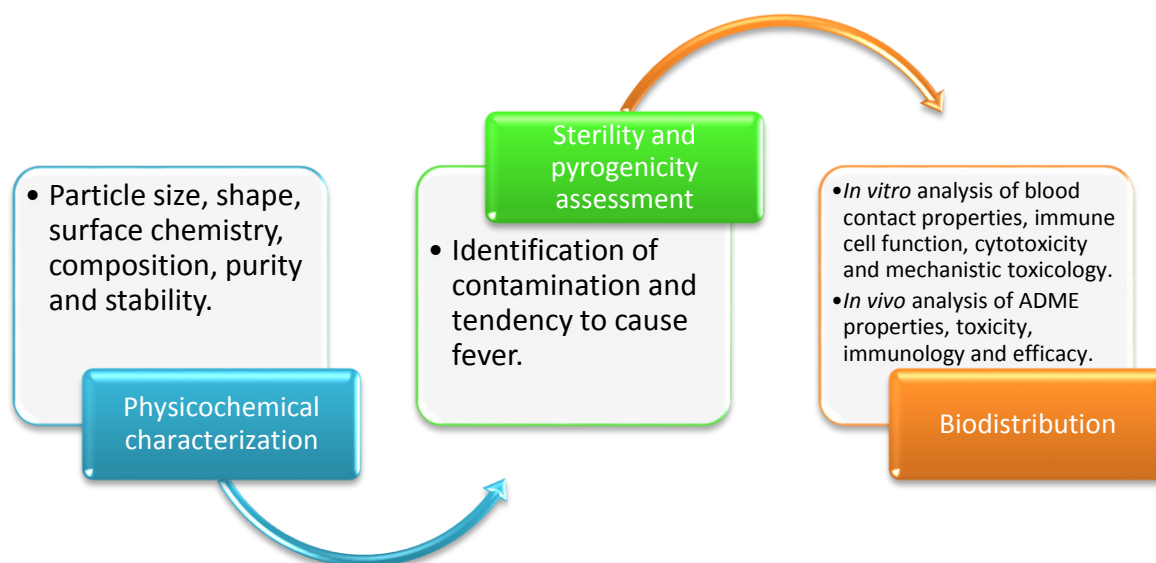


**Figure 16** A rational characterization strategy for nanoparticles.

characterized in the literature by size distribution, morphology, surface properties, stability, drug content and *in vitro* drug release. The various techniques involved in the physicochemical characterization of PNPs are summarized in table 2.<sup>80</sup> Rather than attempting to survey all characterization techniques, this thesis presents only some common characterization methods.

**Table 2** Principal techniques for evaluation of the physicochemical characteristics of PNPs.

Techniques	Physicochemical characteristics analyzed
Atomic force microscopy (AFM)	Size and size distribution
	Shape
	Structure
	Aggregation
	Surface properties (modified AFM)
Differential scanning calorimetry (DSC)	Physicochemical state and possible interactions of the drug and the polymer
Dynamic light scattering (DLS)	Hydrodynamic size distribution
Fluorescence spectroscopy	Critical association concentration (CAC) determination
	Drug content
	<i>In vitro</i> drug release
High performance liquid chromatography (HPLC)	Drug content
	<i>In vitro</i> drug release
Infrared spectroscopy (IR)	Structure and conformation of bioconjugates
	Surface chemistry analysis
Mass spectrometry (MS)	Molecular weight
	Composition
	Structure
	Surface properties (secondary ion MS)
Near-field scanning optical microscopy (NSOM)	Size and shape of nanomaterials
Nuclear magnetic resonance (NMR)	Structure
	Composition
	Purity
	Conformational change
Scanning electron microscopy (SEM)	Size and size distribution
	Shape
	Aggregation
Scanning tunneling microscopy (STM)	Size and size distribution
	Shape
	Aggregation
Transmission electron microscopy (TEM)	Size and size distribution
	Shape heterogeneity
	Aggregation
X-ray photoelectron spectroscopy (XPS)	Elemental and chemical composition at the surface
Zeta potential	Stability referring to surface charge

### I.3.1 Size, shape, surface properties and stability

The direct observation of nanoscale objects is a challenging task for conventional light microscopy because typical dimensions of nanoparticles are below the diffraction limit of visible light.<sup>82</sup> Therefore, resolution is limited to about 1  $\mu\text{m}$ . Instead, electron microscopy uses beams of accelerated electrons and electrostatic or electromagnetic lenses to control their path. Due to the much shorter wavelengths of electrons than visible light photons, images of much higher resolution are generated. Scanning electron microscopy (SEM) is a surface imaging technique in which an electron beam interacts with a sample and generates different signals, reflecting the atomic composition and surface morphology.<sup>82</sup> Among these emissions, SEM uses backscattered electrons and secondary electrons emitted from the sample to build the three-dimensional image of the analyzed sample. Once these electrons escape from the sample surface, they are typically detected by an Everhart-Thornley scintillator-photomultiplier detector.<sup>83</sup> However, many PNPs, due to their organic nature are essentially invisible to electron microscopy because they do not deflect an electron beam sufficiently.<sup>81</sup> Therefore, sample preparation requires coating with a thin layer of metal, which creates a conductive layer on the sample. This procedure inhibits surface charging, reduces thermal damage and improves the secondary electron signal required in the SEM. The size, size distribution and morphology of PNPs can be directly acquired from SEM with high resolution. The purity of the PNP sample and their degree of aggregation can also be inferred from SEM images. On the other hand, SEM possesses the disadvantage of a destructive sample preparation. In addition, one can never be sure that the observed image is truly representative of the bulk nanoparticle sample, which could lead to biased statistics of size distribution in heterogeneous samples.

Another characterization technique of PNPs is atomic force microscopy (AFM), also known as scanning probe microscopy (SPM). Since the introduction of AFM by Binnig *et al.*,<sup>84</sup> it has become an essential tool not only to study the surface morphology with nanometer resolution but also for sensitive force measurements. For example, applications beyond imaging led to deeper understanding of many biological processes down to the single molecular level<sup>85</sup> and measurements of the forces on colloidal interactions.<sup>86</sup> AFM imaging is performed by sensing the attractive/repulsive forces between a very sharp probing tip (Fig. 17A) and the sample surface.<sup>87</sup> The force is measured by attaching the probe to a pliable cantilever and monitoring the deflection of the cantilever through a laser-photodiode system which detects the difference in the photodetector output voltages (Fig. 17B).<sup>87</sup> The scanning motion is controlled by piezoelectric scanner that controls the position of the sample and moves it with respect to the tip. Several AFM imaging modes are available in which the two most widely used are contact mode and tapping mode AFM.<sup>83</sup> In the contact mode, one simply records the cantilever deflection while the sample is scanned horizontally, i.e., at constant height. In contrast, tapping mode consists of oscillating

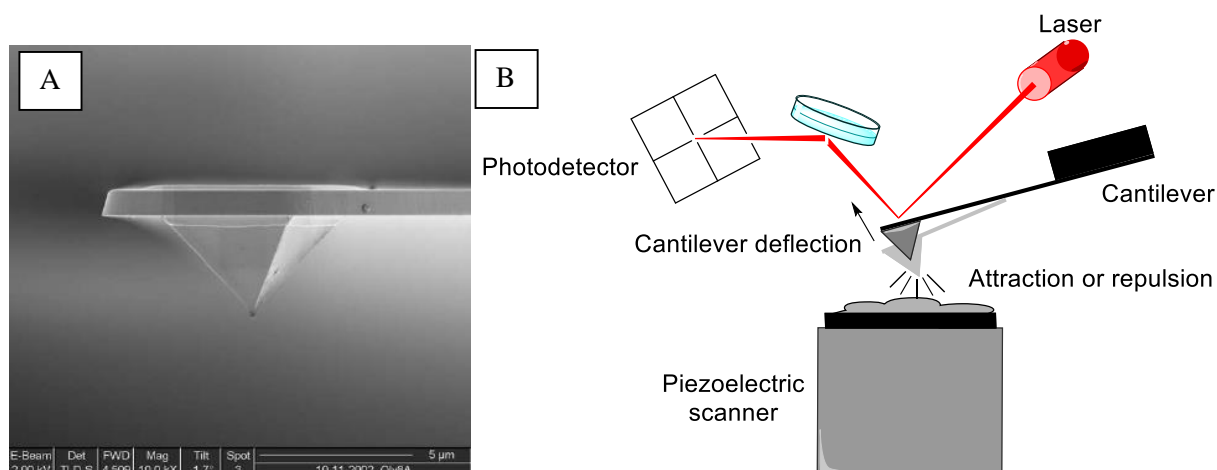


**Figure 17** Scanning electron micrographs of a cantilever tip<sup>87</sup> (A) and schematic of AFM operation (B).

the cantilever at its resonance frequency and lightly “tapping” on the surface during scanning. Similar to SEM, AFM can be used to study the size and size distribution, shape and aggregation of PNPs. Additionally, AFM requires no specific sample preparation procedure and is a relatively nondestructive technique, in other words, a large range of substrates can be studied. AFM also has the advantage to image a variety of biomaterials in aqueous fluids and is also possible to observe macromolecular motion on a surface of the same sample in real time.<sup>88</sup> The main limitation of AFM for PNP visualization is that the size of the cantilever tip is often larger than the particles being probed, which leads to overestimations of the PNP lateral dimensions.<sup>89</sup> Therefore, lateral dimensions should be used with great caution and accurate size measurements should only be taken on the height (z-axis). SEM has a larger depth of focus than AFM, but AFM is more accurate in the z dimension, not available to SEM.<sup>90</sup> An AFM equipment with comparable resolution to a SEM apparatus costs much less, requires substantially less laboratory space and is much simpler to operate. Even though SEM and AFM appear very different, it is possible to find some similarities.<sup>90</sup> Their images have comparable lateral resolution (5-100 nm) and both techniques have image artifacts.<sup>83</sup> By using this two complementary techniques, one technique will often compensate for the imaging of the other. In a work carried out by Zhang *et al.*, the surface morphology of PLA-Tween 80-10 PNPs was examined by FESEM and AFM (Fig. 18).<sup>91</sup> For both methods the PNPs showed spherical in shape and had similar particle size distribution.

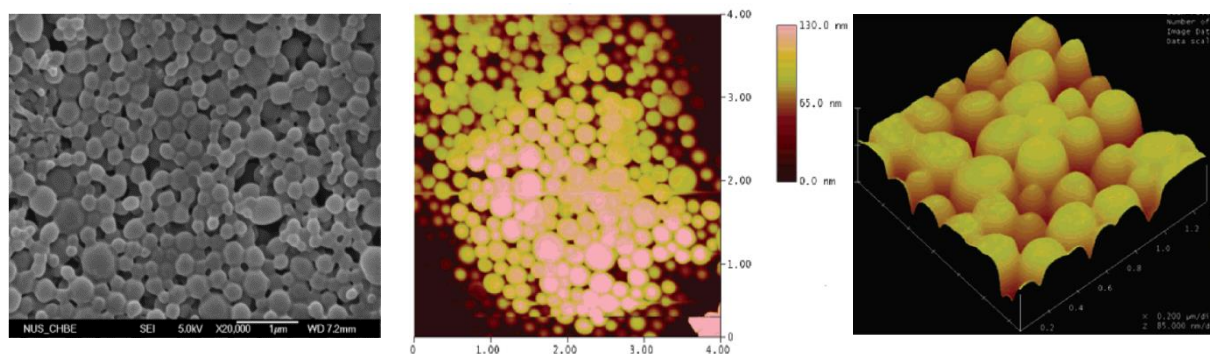


**Figure 18** FESEM image (left) and AFM images (middle (2D image) and right (zoom in 3D image)) of PLA-Tween 80-10 PNPs.

One technique that is widely used in size determination of PNPs in solution is dynamic light scattering (DLS), which is also known as photon correlation spectroscopy (PCS). In a DLS experiment, a colloidal suspension is illuminated by a monochromatic laser light that is scattered into a photon detector.<sup>92</sup> Due to the Brownian motion of the particles, the detected scattered light intensity fluctuates in time, and this is related to the particle size with the help of an autocorrelation function.<sup>93</sup> Based on the Stokes – Einstein equation the hydrodynamic diameter can be obtained. For spherical particles the relation is as follows:

$$D_h = \frac{k_B T}{3\pi\eta D_t}$$

where  $D_h$  is the hydrodynamic diameter,  $\eta$  is the relative viscosity of the solvent,  $k_B$  is the Boltzmann's constant,  $T$  is the temperature and  $D_t$  is the translational diffusion coefficient (this is what is measured by DLS). One of the major advantages of DLS is that it provides information about the whole particulate population in a short experiment duration. However, it has limited utility in determining the particle shape because DLS presumes all the particles being spherical in nature. Furthermore, as larger particles scatter more light than smaller ones, even small amounts of aggregates or dust particles could shift the particle size distribution to larger values.<sup>94</sup> Therefore, one should be cautious when interpreting size information from DLS experiments. Instead, the results should be supplemented with an imaging technique like AFM or SEM, which is helpful in resolving ambiguities associated with both techniques. For example, Sant and coworkers prepared PEG-*g*-PLA nanoparticles by the emulsification-solvent evaporation method.<sup>95</sup> The particle size reported by DLS were in the range of 178 – 192 nm. However, they observed an increase in particle size after resuspension in spite of the use of surfactant or sonication. The aggregation behavior of the PNPs was evidenced by AFM (Fig. 19).

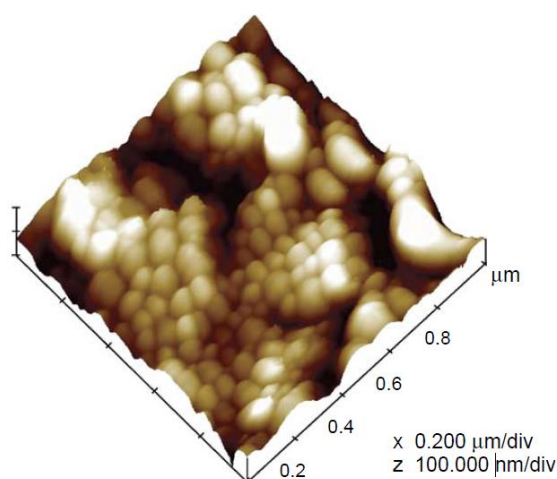


**Figure 19** Surface morphology of PEG-*g*-PLA PNPs by AFM. Scale x-axis: 0.200 μm/div.

The surface charge can determine the stability of a PNP colloidal suspension, i.e. to what degree aggregation will occur over time. Besides, it is also a key factor influencing PNP *in vivo* fate, for example in interactions with cell membranes. The particle surface charge is determined by measuring the zeta ( $\zeta$ ) potential of a suspension, which is generally done by the well-known electrophoresis method.<sup>96</sup> The basic principle involves measuring the electrophoretic mobility of charged particles under an applied electrical potential.  $\zeta$ -potential is related to the electrophoretic mobility ( $\mu$ ) by the Henry equation:

$$\mu = \frac{2\zeta\epsilon}{3\eta_0} f(kr)$$

where  $\epsilon$  is the dielectric constant,  $\eta_0$  is the medium's viscosity and  $f(kr)$  refers to Henry's function.  $\zeta$ -potential represents a measure of the stability of a colloidal suspension. Values between  $-30$  mV and  $+30$  mV indicates a condition towards instability, aggregation, coagulation or flocculation.<sup>97</sup> Thus, particle aggregation is less likely to occur for high  $\zeta$ -potential values due to electric repulsion. Ultraviolet spectroscopy can be used to determine the aggregation state by turbidity measurements.

PNPs in aqueous solutions can be stabilized by electrostatic stabilization and/or steric stabilization using surfactants. The stability and hence the  $\zeta$ -potential can be influenced by many factors such as pH, concentration, ionic strength of the solution and the nature of the surface ligands.<sup>97</sup> The uptake of PNPs usually increases with increasing the zeta potential values.<sup>98</sup> However, cationic particles are believed to be more toxic than their anionic or neutral counterparts.<sup>98</sup>

### I.3.2 Drug-polymer interactions

In order to improve drug loading efficiency and extend drug release, the nature of polymer-drug interactions as well as the polymer type and its physicochemical properties must be taken into account.

The amorphous state of pharmacologically active materials has received considerable attention<sup>99</sup> due to their higher internal energy, which leads to greater solubility and bioavailability.<sup>100</sup> However, due to physical instability, the amorphous form of a drug tends to spontaneously convert to a crystalline form, thus both the amorphous state and the crystalline state are possible. Fortunately, structural stabilization can be achieved by incorporating the drug into an amorphous polymer with concomitant formation of an amorphous solid solution.<sup>101</sup> The interactions between the two types of molecules control the solubility of these materials in each other and are accomplished by van der Waals forces and hydrogen bonds. When the drug-polymer molecular interactions are comparable to the drug-drug and the polymer-polymer interactions, the polymeric component is able to solubilize the drug material and large amounts of drug can be incorporated in the polymer matrix without drug crystallization.<sup>101</sup> On the

other hand, when the drug-polymer interactions are weaker, the drug and the polymer have a preference to interact with the molecules of their own kind, which favors drug crystallization.<sup>101</sup>

Differential scanning calorimetry (DSC) is commonly used to study the physicochemical state and possible interactions of the drug loaded in PNPs. DSC is able to detect phase transitions such as glass transition, crystallization and melting.<sup>102</sup> The glass transition temperature ( $T_g$ ) is the reversible transition in amorphous materials or in amorphous regions in semi-crystalline materials, from a hard and brittle state into a molten or rubber-like state. Polymers in their glassy state can provide mechanical strength to the polymeric nanoparticles and avoid particle aggregation. In a work carried out by Corrigan *et al.* the thermal characteristics of ketoprofen loaded PLGA nanoparticles were studied.<sup>103</sup> It has shown the absence of a melting peak from the DSC thermogram of the loaded nanoparticles (Fig. 20). This indicated that the drug was present in a non-crystalline state.

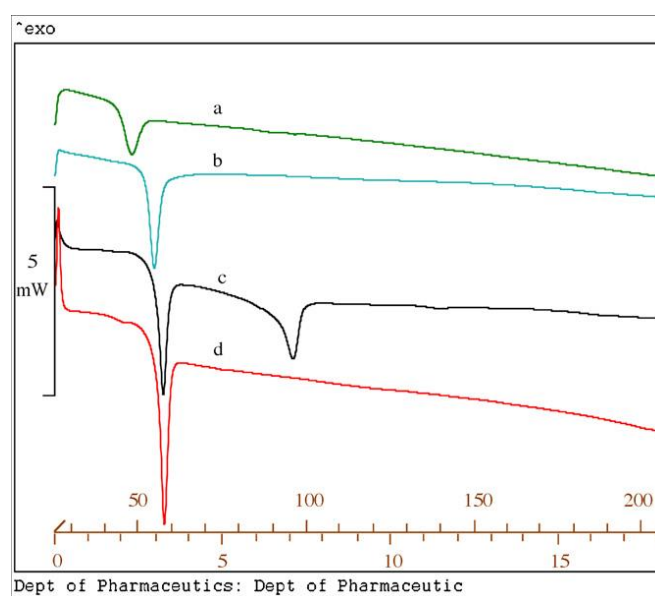


**Figure 20** DSC results of a) ketoprofen loaded PLGA nanoparticles, b) drug free PLGA nanoparticles, c) physical mixture of PLGA and ketoprofen and d) pure PLGA polymer [Adapted from ref. 103].

## I.4 Concept of this thesis

The concept of the research described in this thesis is centered on the design and synthesis of novel polymeric nanoparticle systems. The influence of the preparation method on the physicochemical properties of the PNPs was examined, as well as the effects of various parameters, such as polymer concentration of the starting solution, type of solvent and evaporation method. A small introduction is provided in each of the following chapters in order to bring the area under discussion into focus.

**Chapter 2** describes the preparation of surfactant-free polymeric nanoparticles, synthesized by chemical modification of poly(ethylene glycol) (PEG) conjugated with sucrose and a cholic acid moiety. The PNPs were prepared either by nanoprecipitation or by the emulsion-solvent evaporation technique. Physicochemical characterization was carried out by atomic force microscopy, scanning electron microscopy, fluorescence spectroscopy and dynamic light scattering.

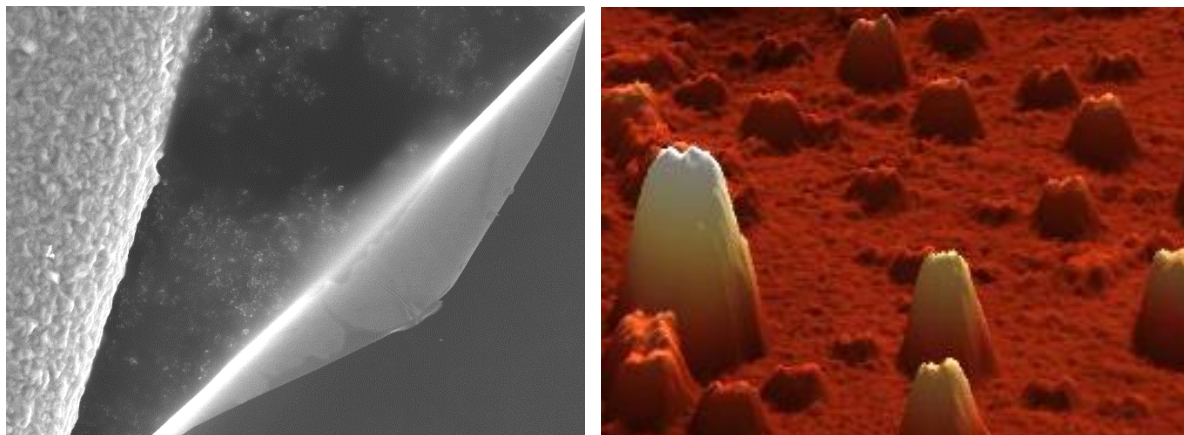
PEG-based polymers exhibit a glass transition temperature ( $T_g$ ) well below the room temperature. In addition, although PEG is FDA approved, there is some concern about safety and toxicological issues. In order to improve the PNP physicochemical properties and also their safety in biomedical applications, in **Chapter 3** PLGA-based polymer conjugates were synthesized. The PNPs were prepared either by nanoprecipitation or by the emulsion-solvent evaporation technique. The improvement of the freeze-drying process by the use of cryoprotectants was also explored. Since lyophilization is known to promote nanoparticle aggregation, particle drying under phosphorus pentoxide was explored as an alternative. The resulting PNPs were characterized by scanning electron microscopy and light scattering experiments.

To explore the synergistic properties between the different polymers, in **Chapter 4** PLGA-PEG-based polymeric nanoparticles were prepared. The conjugate polymers were prepared in a one-pot synthesis from the appropriate sucrose and cholic acid moieties. Nanoprecipitation and the emulsion-solvent evaporation method were used to formulate the respective PNPs. Physicochemical characterization was carried out by scanning electron microscopy and dynamic light scattering.

In **chapter 5** the conclusions are presented. Future strategies for further developments of a promising controlled drug delivery system are also outlined.

In **chapter 6** the experimental section is presented with the techniques that have been used to synthesize and characterize the polymeric nanoparticles prepared in this thesis.





## Chapter II

### Synthesis of PEG-based polymeric nanoparticles<sup>†</sup>

*This chapter describes the preparation of surfactant-free polymeric nanoparticles from chemical modification of PEG conjugated with sucrose and a cholic acid moiety (abbreviated as Suc-PEG-Chol). The chapter begins with an explanation of the design, as well as an introduction of the general theory in a focused manner. This is followed by a discussion of the results obtained. Initially, the synthesis of three series of polymers with different PEG chain lengths is described, followed by the confirmation of their structures by <sup>1</sup>H-NMR, <sup>13</sup>C-NMR and MALDI-TOF analysis. The following section describes the preparation of PNPs, either by nanoprecipitation or by the emulsion/solvent evaporation technique, and the self-assembling behavior, morphology and particle size distribution of the obtained PNPs by fluorescence spectroscopy, SEM, AFM and DLS. Cholic acid-PEG conjugates were also synthesized in order to study the influence of sucrose moiety on the physical properties of the PNPs. A final section summarizes the work, providing conclusions and future directions.*

<sup>†</sup> Part of this Chapter has been published in: Crucho, C.I.C.\*, Barros, M.T. *J. Mater. Chem. B*, **2014**, 2, 3946.



## II.1 Introduction

Polymer-based nanomedicine is a large and fast growing field that has gained plenty of research attention during recent decades. Different physicochemical properties exhibit by these nanocarriers (size, shape and surface properties) influence their fate in biological systems. In this regard, stability, drug release and targeting can be tailored by surface modification, highlighting the importance of well-defined chemistries.<sup>98</sup>

Surface chemistry is a key factor in bioavailability of nanoparticles as our body recognizes hydrophobic particles as foreign. The most common moiety for surface modification is the hydrophilic, non-ionic, biocompatible and FDA-approved polymer polyethylene glycol (PEG).<sup>104,105</sup> PEGylation reduces the likelihood of opsonization in the bloodstream leading to prolonged blood circulation times. Furthermore, PEG is also the most widely used polymer in delivering anticancer drugs and several PEG-conjugates have already reached late phase clinical trials.<sup>106</sup> All the modifications on PEG have been based on the replacement of the hydroxyl end group, most commonly by coupling a reactive chain-end of PEG.<sup>107</sup> In this sense, PEG has been conjugated to several biomolecules, which has been extensively reviewed (Fig. 21).<sup>107,108</sup> PEG has also been conjugated to drug molecules, such as anticancer agents. In this case, the drug is covalently linked to the polymer backbone through a physiologically labile bond to release the active molecule.

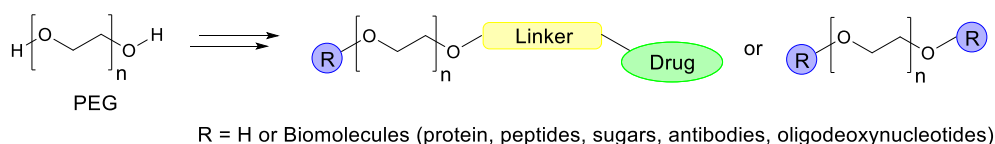


**Figure 21** Typical end-groups in polyethylene glycol modifications.

In addition to a PEG coating, most stealth PNPs also have targeting ligands, which are able to facilitate binding through specific over-expressed cell surface receptors.<sup>109</sup> Among them, lectins (carbohydrate-binding proteins) play a complex role in various biological recognition events.<sup>110</sup> Sugar-containing polymers have been developed as vehicles for therapeutics or as therapeutics themselves and some of these compounds displayed impressive gains in binding affinity or *in vivo* efficiency.<sup>111</sup> PNPs displaying saccharide moieties have been designed for liver-specific drug delivery.<sup>112</sup> Song *et al.* showed that disaccharide-modified liposomes enhanced cellular uptake into various cancer cell lines via lectins-mediated endocytosis.<sup>113</sup> In order to improve targeting efficiency and reduce side effects, introducing targeting molecules, such as sucrose into PNPs, could enhance the affinity toward cell surface lectins. Moreover, if the rate-determining step for tumor uptake is based on the enhanced permeability and retention (EPR) effect, PNPs decorated with targeting ligands are believed to be internalized easily by cells after accumulation.

An ideal drug delivery vehicle should also have a high drug-loading capacity in order to reduce the dose frequency, improving patient compliance.<sup>114</sup> Drug loading depends on the solubility of the drug molecules in the polymer, which is mainly related to intermolecular type interactions between these two molecules.<sup>114, 115</sup>

Bile acids are natural compounds with a rigid steroid cyclopentenophenanthrene structure, which has found applications in pharmacology, supramolecular chemistry and nanoscience.<sup>116</sup> Cholic acid is a unique facial amphiphilic molecule and a versatile building block in the design and synthesis of novel polymeric materials. These materials may have improved properties such as rigidity, capacity of self-assemble, biocompatibility, biodegradability and so forth.<sup>117</sup> In addition, the steroid skeleton results in the formation of a cavity, which is a suitable environment for host-guest chemistry.<sup>116</sup>

In this thesis the synthesis of PNPs based on amphiphilic polymeric conjugates composed of a cholic acid (Chol), a sucrose moiety (Suc) and a PEG polymer, to give stealth and important physicochemical properties is reported. In these PNP carriers, cholic acid will act as a drug incorporation site and the carbohydrate as targeting moiety. It is expectable that the conjugates constructed with natural building blocks – sugar and cholic acid - should be biocompatible and biodegradable, and due to their structure they will own high functionality and versatility. Combining molecular entities with distinct properties could provide novel conjugates in which the different molecular segments act cooperatively.

## II.2 Results and Discussion

### II.2.1 Synthesis and characterization of PEG-based polymer conjugates

The Suc-PEG-Chol conjugates were synthesized by covalently binding of the appropriate sucrose and cholic acid derivatives to PEG by esterification (Fig. 22). Three series of polymers with different numbers of repeating ethylene oxide units (EO) ( $n = 45, 90, 136$ ) have been synthesized. In

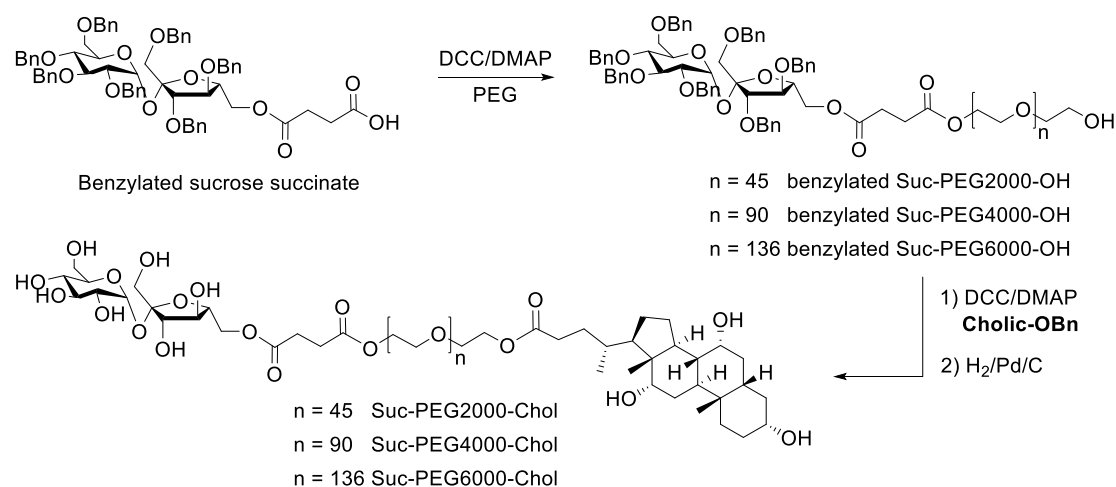


**Figure 22** Synthetic strategy for preparing the Suc-PEG-Chol polymer conjugates.

order to obtain solely a sucrose-containing linear polymer, chemoselective derivatization of sucrose was required, as well as a selective protection of the cholic acid.

### II.2.1.1 Chemoselective derivatization of 6'-hydroxyl group of sucrose

Sucrose ( $\alpha$ -D-glucopyranosyl-(1 $\rightarrow$ 2)- $\beta$ -D-fructofuranoside) is ubiquitous in the plant kingdom but the reason for this natural selection is not evident. The potential value of sucrose from a raw sugar to a chemical raw material has been the subject of considerable research due to its natural occurrence, production in large scale, low price and polyfunctional nature.<sup>118</sup> Since sucrose has eight chemically active hydroxyl groups, chemoselective derivatization is a challenging task in sucrose chemistry and also a major drawback. Only differentiation between the primary and secondary hydroxyl groups may be done conveniently by reaction with bulky reagents and a wide variety of sucrose precursors may be prepared just by varying the nature of the electrophilic reagent (Fig. 23).<sup>119</sup> In general, it is accepted that of the three primary hydroxyls, those at carbons 6 and 6' are more reactive than the neopentyl-like primary hydroxyl at carbon 1'.<sup>119</sup>

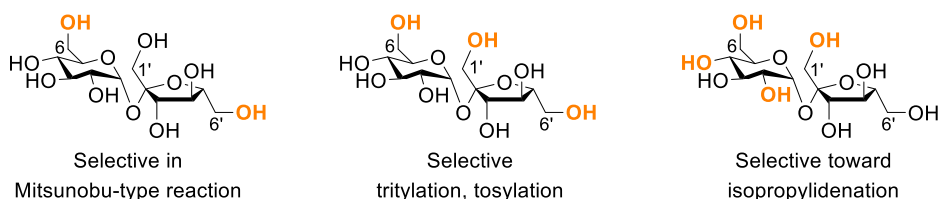
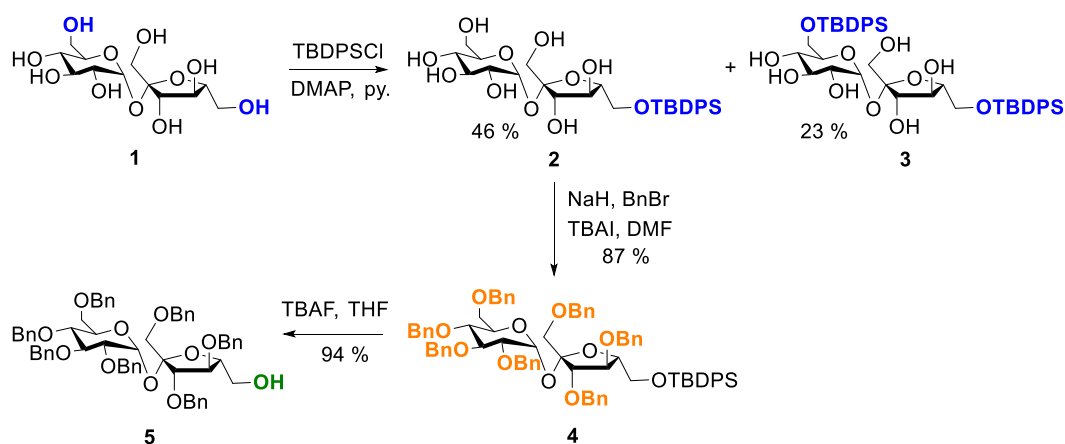


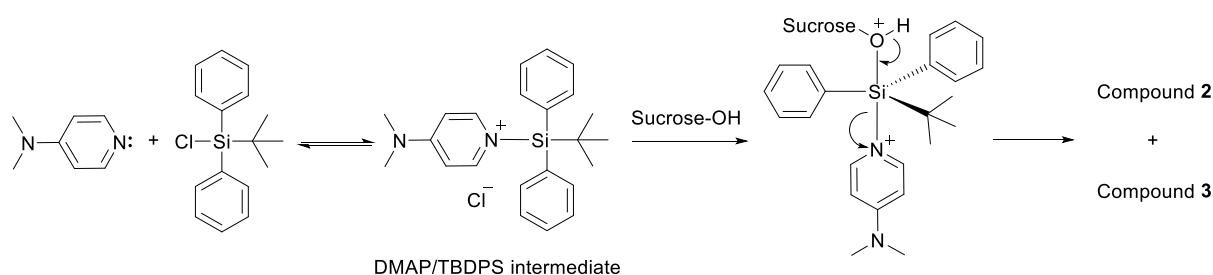
**Figure 23** Different reactivity of primary/secondary hydroxyls of sucrose.

The route to selective derivatization of the 6'-position has been developed previously.<sup>120</sup> The traditional approach includes a selective protection of the 6'-OH of sucrose with bulky ether-forming reagents, followed by benzylation and selective deprotection of the bulky ether. Hence, the target fully protected sucrose with only the 6'-hydroxyl unprotected **5** was prepared in three steps from commercially available sucrose **1** as illustrated in Scheme 1, with an overall yield of 38%. In the first



**Scheme 1** Protection/deprotection sequence from sucrose.

step, reaction of sucrose **1** with 1.0 equiv. of *tert*-butyldiphenylsilyl chloride (TBDPSCl) in dry pyridine, in the presence of a catalytic amount of DMAP, at room temperature for 2 h gave compound **2** in 46% yield. It was observed that the remainder of the product mixture contained sucrose (26 %) and 6,6'-di-*O*-*tert*-butyldiphenylsilyl-sucrose **3** (23 %) as a by-product. For the same reaction conditions, microwave irradiation (90 °C, 200 W) was applied. The reaction was complete in 10 min. attaining a similar yield of compound **3** (22 %) and the yield of **2** increased slightly (53 %). These results are consistent with the findings of Khan<sup>121</sup> and clearly show that the 6'-OH in sucrose, being essentially exocyclic, is the most reactive site towards silylation. The moderate reaction yield could be explained by the limited solubility of sucrose in pyridine. On the other hand, to explain the undesirable formation of **3**, once compound **2** is formed, the reaction proceeds more rapidly, because of the increase in its solubility, and its reactivity is only limited by the supply of the reagent. The reaction proceeds via a DMAP/TBDPS intermediate, a very reactive silylating agent (Scheme 2). In fact, in a work carried out by Corey *et al.*,<sup>122</sup> it was shown that in the absence of the catalyst the reaction was very slow with unsatisfactory yields. As is always the case in silicon chemistry, the substitution reaction proceeds via



**Scheme 2** Mechanism of the silylation of sucrose with TBDPSCl.

pentacoordinated intermediate, which is permitted due to hybridization with the vacant *d*-orbitals of silicon. The elimination takes place after the leaving group occupies the apical position. The NMR data of compound **2** showed clearly that only one silyl group was present. The <sup>1</sup>H-NMR spectrum includes the signal corresponding to the anomeric proton at 5.23 ppm and a broad singlet of the *tert*-butyl group protons at 0.97 ppm, with integral intensities equal to 1 and 9, respectively. Conversely, for the disubstituted compound **3** the *tert*-butyl groups appeared as two broad singlets at 0.93 and 0.91 ppm. For compound **2** the chemical shift in the <sup>13</sup>C-NMR spectrum for the carbon atom bearing the silyl ether (C6') was deshielded to 66.07 ppm in relation to those for the C1' and C6 (62.55 and 61.23 ppm respectively). For compound **3**, the two substituted carbon atoms C6' and C6 appeared at 65.59 and 63.14 ppm, respectively, while the signal assignable to the C1' carbon (61.88 ppm) did not change significantly compared with the corresponding carbon in compound **2**. The NMR assignments and structure determination were made by two dimensional NMR studies (HMQC, HMBC and COSY) (Fig. 24).

In the second step, the monosilylated sucrose **2** was benzylated with benzyl bromide and sodium hydride in DMF in the presence of TBAI to afford the fully protected derivative **4** in 87% yield. A small

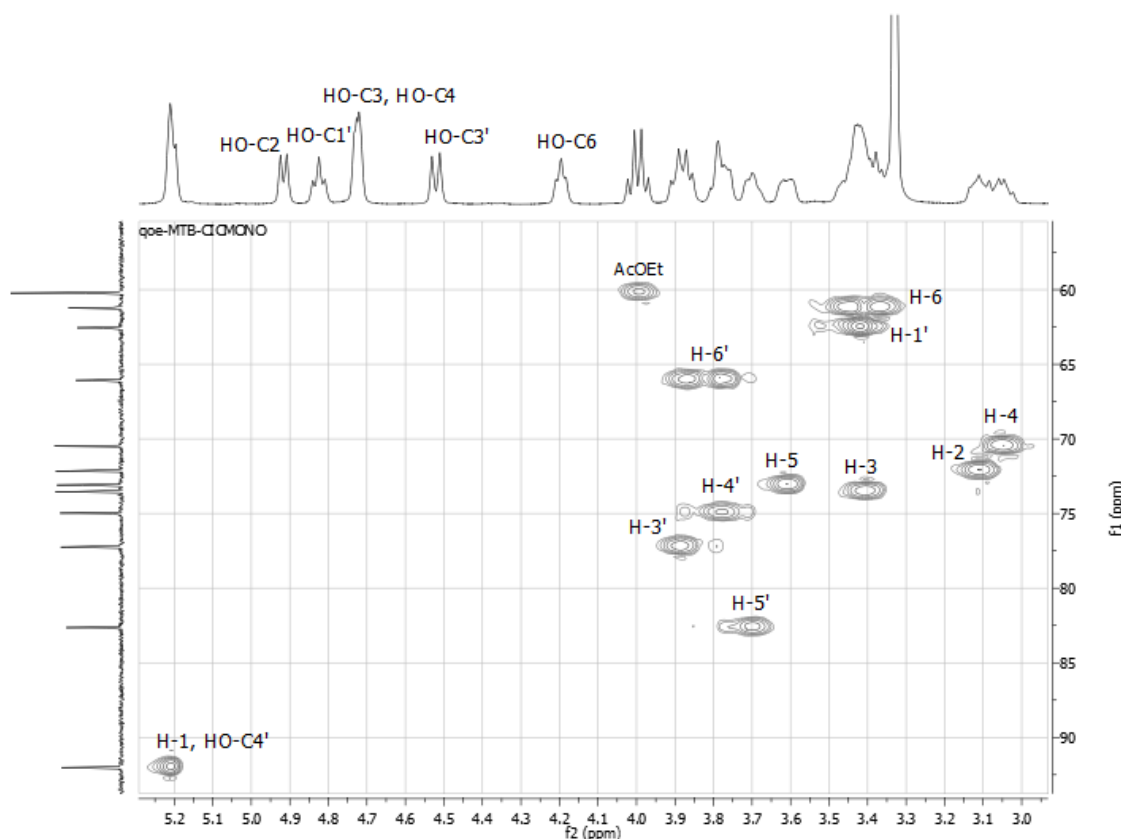
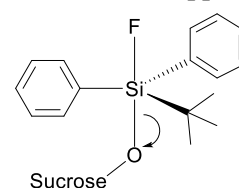


**Figure 24** HMQC spectrum expansion of 6'-*O*-*tert*-butyldiphenylsilyl-sucrose **2** in DMSO-*d*<sub>6</sub>, focused on sucrose protons.

fraction of the TBDPS protecting group is usually cleaved because it is slightly unstable under the basic conditions yielding the octabenzylated sucrose as a byproduct. The mechanism of this typical Williamson ether synthesis involves the initial deprotonation of the hydroxyl group and subsequent reaction with benzyl bromide through a S<sub>N</sub>2 pathway. The benzyl group is an electron withdrawing group and caused the <sup>13</sup>C-NMR peaks of C6 and C1' to shift downfield from 61.23 and 62.55 ppm to 68.95 and 71.34 ppm, respectively. The multiplets in <sup>1</sup>H-NMR between 4.75 and 4.30 ppm, indicated the presence of the benzylic methylene protons, whose integrated ratio with the anomeric proton supported the incorporation of seven benzyl groups. Additional NMR signals of the phenyl protons and carbon atoms of the phenyl ring were another strong evidence for a successful benzylation. The NMR assignments and structure determination were made by two dimensional NMR studies (HMQC, HMBC and COSY) (Fig. 25).

Selective deprotection of the silyl group in compound **4**, with TBAF in THF at room temperature, led to compound **5** in 94 % yield after column chromatography. The mechanism appears to involve a simple S<sub>N</sub>2 process, however, this is not the case. Akin to protection, the deprotection also proceeds through a pentacoordinated intermediate after nucleophilic attack of the small fluoride anion (Scheme 3). The driving force for a fast cleavage is the formation of strong Si-F bonds. The success of the deprotection was confirmed by <sup>1</sup>H-NMR analysis through the disappearance of the *tert*-butyl group protons at 0.92 ppm. Furthermore, in the <sup>13</sup>C-RMN



**Scheme 3** Pentacoordinate intermediate involved in the deprotection of TBDPS promoted by TBAF.

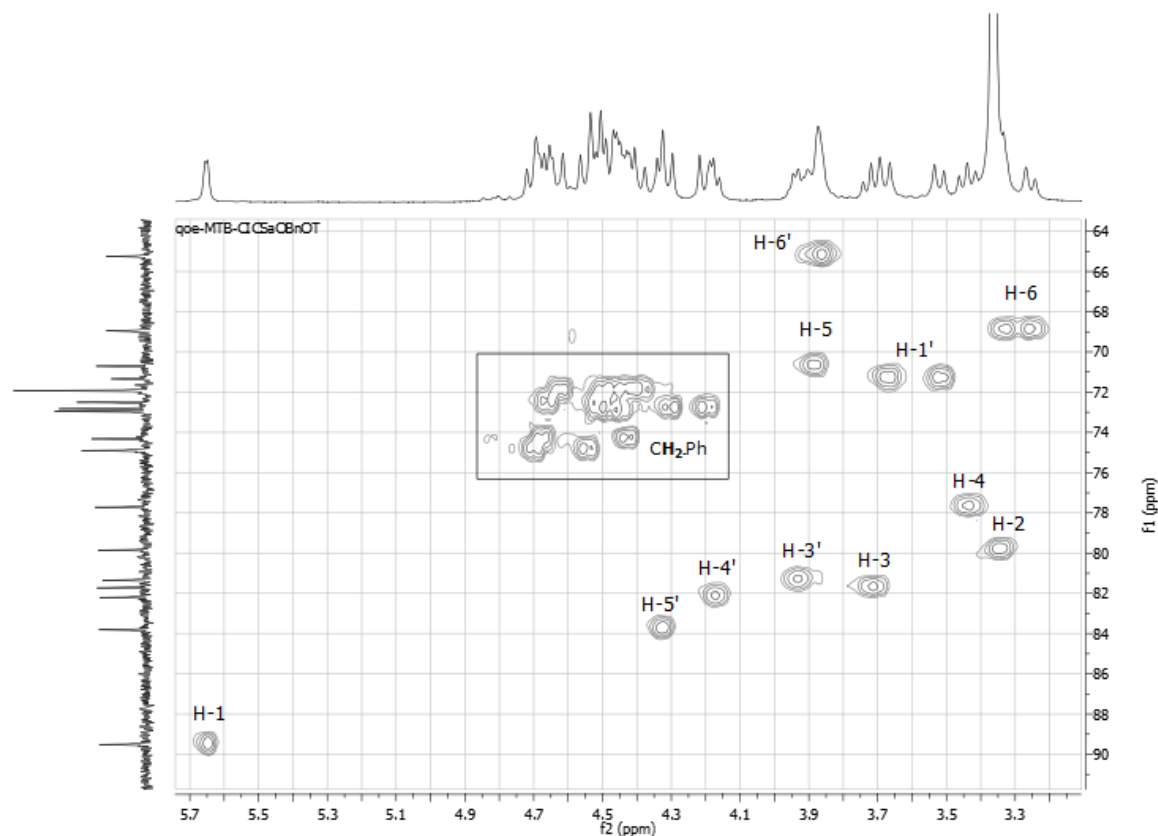
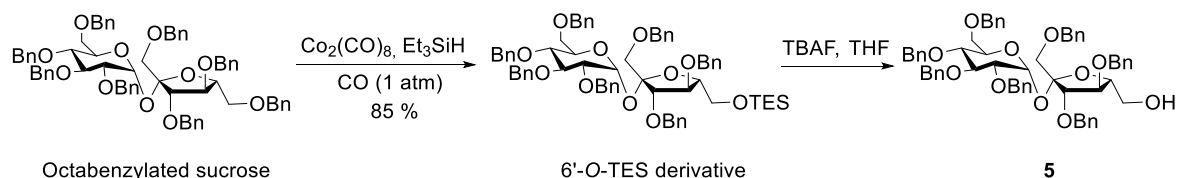


**Figure 25** HMQC spectrum expansion of 1',2,3,3',4,4',6-Hepta-*O*-benzyl-6'-*O*-*tert*-butyldiphenylsilyl sucrose **5** in DMSO-*d*<sub>6</sub>, focused on sucrose protons.

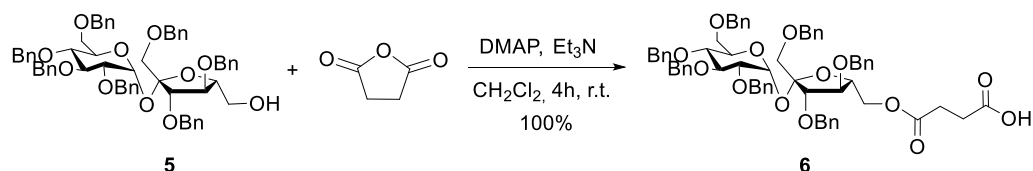
spectrum, the peak assignable to the C6' carbon was shifted upfield from 65.24 to 62.81 ppm, whereas the signals due to the carbons at other positions did not changed significantly. This data indicated that the 6'-position was deprotected in the aforementioned product **5**.

Recently, Yin *et al.* reported a highly efficient and mild method for the chemoselective de-*O*-benzylation of protected sugars by transforming terminal benzyl ethers into silyl ethers using Co<sub>2</sub>(CO)<sub>8</sub>-Et<sub>3</sub>SiH under 1 atm of CO (Scheme 4).<sup>123</sup> With this methodology, compound **5** could be prepared from fully benzylated sucrose, with an overall yield around 50 – 60 %, which is higher than the current method (38 %). The main difference between the two methodologies lies in the synthesis of the octabenzylated sucrose which is a higher yielding step (79 %)<sup>124</sup> than the sucrose monoderivatization with TBDPS.



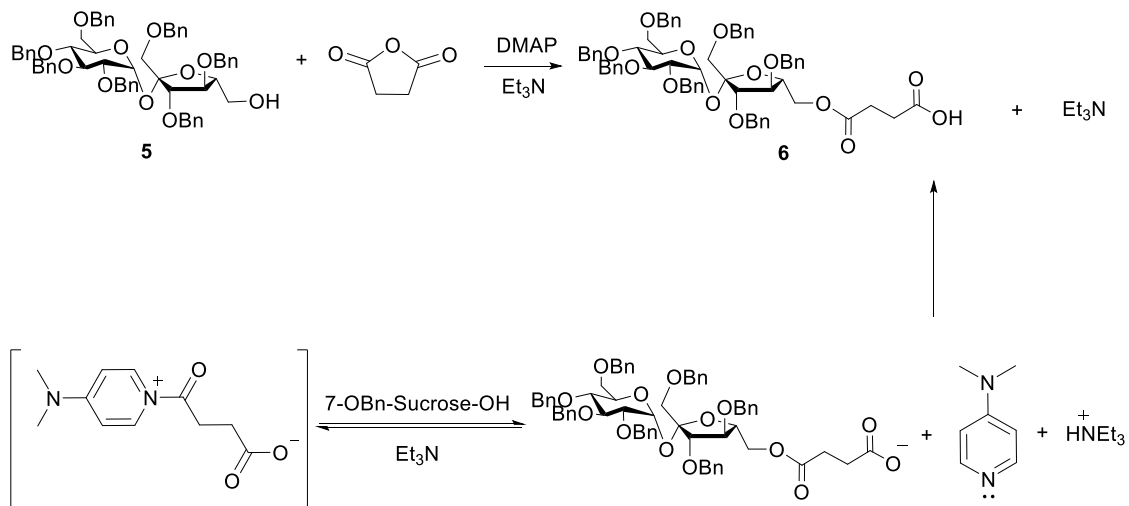
**Scheme 4** Chemoselective de-*O*-benzylation of octabenzylated sucrose proposed by Yin *et al.*

From compound **5**, the sucrose succinate derivative **6** was prepared by reaction with succinic anhydride in the presence of DMAP as catalyst and triethylamine as the auxiliary base, in quantitative yield. (Scheme 5). The excess of succinic anhydride was used to guarantee that the hydroxyl group of **5**



**Scheme 5** Synthesis of the sucrose succinate derivative 1',2,3,3',4,4',6-Hepta-*O*-benzyl-6'-*O*-succinyl-sucrose **6**.

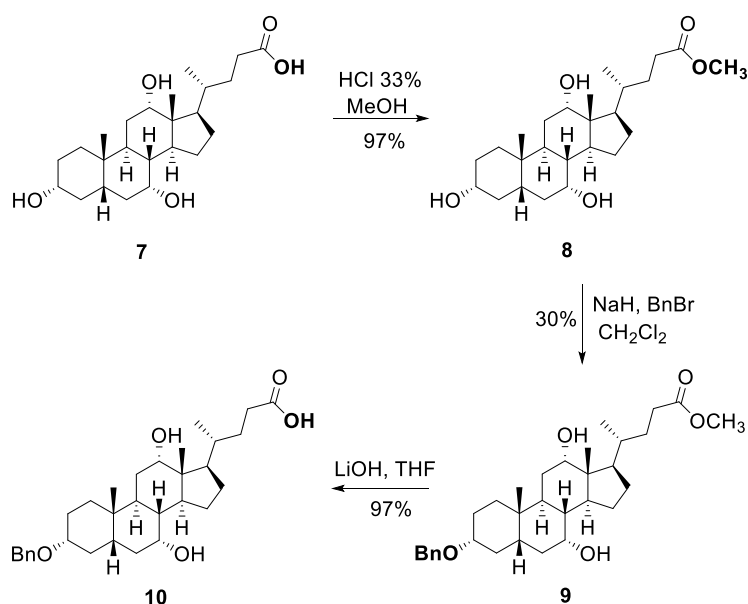
was totally reacted, avoiding a more laborious purification. The proposed mechanism involves the pre-equilibrium formation of a labile pyridinium cation by reaction of DMAP with succinic anhydride (Scheme 6). The hydroxyl group in compound **5** then reacts with the succinate catalyst to yield the ester product. In this step the triethylamine pulls away the proton from the hydroxyl group while this forms the ester linkage. Actually, in the absence of triethylamine the reaction failed to occur. This mechanism contradicts the one proposed by Xu *et al.*<sup>125</sup> in which the carboxylate counterion removes the proton from the hydroxyl group to form the ester product together with the deactivated (protonated) catalyst. In this case, the triethylamine is responsible for the regeneration of the catalyst by deprotonation of DMAP. Nevertheless, the mechanism proposed in this thesis supports the experimental results. In addition to usual sucrose signals, the <sup>1</sup>H-NMR spectrum of compound **6** revealed the succinyl protons as one multiplet centered about 2.5 ppm. Moreover, in the <sup>13</sup>C-NMR, the C6' carbon was shifted downfield from 62.81 to 64.88 ppm due to the deshielding effect of the nearby electronegative ester group. On the other hand, the carbon atoms at other positions did not changed significantly their chemical shift.



**Scheme 6** Proposed mechanism for the esterification reaction of 1',2,3,3',4,4',6-Hepta-*O*-benzyl-6'-*O*-*tert*-butyldiphenylsilyl sucrose **5** with succinic anhydride.

### II.2.1.2 Chemoselective derivatization at the 3' position of cholic acid

The synthetic route to prepare the selectively protected cholic acid derivative **10** is shown in scheme 7. The 3 $\alpha$ -OH moiety was targeted to be protected as benzyl ether due to the nucleophilic properties of this equatorial hydroxyl group. Besides, the reactivity of terminal primary OH groups of



**Scheme 7** Synthetic strategy for preparing the selectively 3 $\alpha$ -OH protected cholic acid derivative **10**.

the PEG polymer are masked due to both the high flexibility of the backbone chain and the high molecular weight, which turns it less reactive. The synthesis was started by preparing the methyl ester of cholic acid **8**, using conditions previously established.<sup>126</sup> This step was executed successfully with a yield of 97 %. Since the ester **8** has a higher solubility than cholic acid itself in organic solvents, it is preferred as a reactant in the preparation of derivatives of cholic acid. Moreover, the methyl ester also acted as a protecting group and facilitated the synthesis and purification of compound **9**. The physical characteristics such as melting point and NMR spectroscopic data, matched the results in the literature.<sup>126</sup> In the second step, treatment of methyl cholate **8** with benzyl bromide in CH<sub>2</sub>Cl<sub>2</sub>, in the presence of NaH led to the compound **9** in a lower yield (30 %). Keeping the reaction for a longer time in the presence of excess of NaH or changing to a more suitable solvent for S<sub>N</sub>2 reactions, as DMF, resulted in the formation of by-products, as supported by previous reports.<sup>127</sup> The methyl ester group was then successfully hydrolyzed under mild alkaline conditions, to afford the expected compound **10** in a good yield (97%). The observed selectivity is due to the different reactivities of the three hydroxyl groups, even though they are on same face of the steroid skeleton. For the benzylation reaction the 3 $\alpha$ -position has a higher reactivity because it is an equatorial position and hence less sterically hindered. To confirm which hydroxyls were modified, the <sup>1</sup>H-NMR spectrum of **9** was compared to that methyl cholate **8**. In methyl cholate **8**, the proton chemical shifts of 3 $\beta$ -H, 7 $\beta$ -H and 12 $\beta$ -H are seen at 3.46, 3.85 and 3.98 ppm, respectively. In compound **9**, in addition to usual benzyl protons, an upfield shift for the 3 $\beta$ -H (3.22 ppm) was observed, while 7 $\beta$ -H and 12 $\beta$ -H appeared at their original positions, thus confirming the introduction of a benzyl group only at the 3 $\alpha$ -position. The complete disappearance of the signal at 3.66 ppm for the methyl ester protons, established the formation of compound **10**. The NMR assignments and structure determination were made by two dimensional NMR studies (HMQC, HMBC and COSY) (Fig. 26).

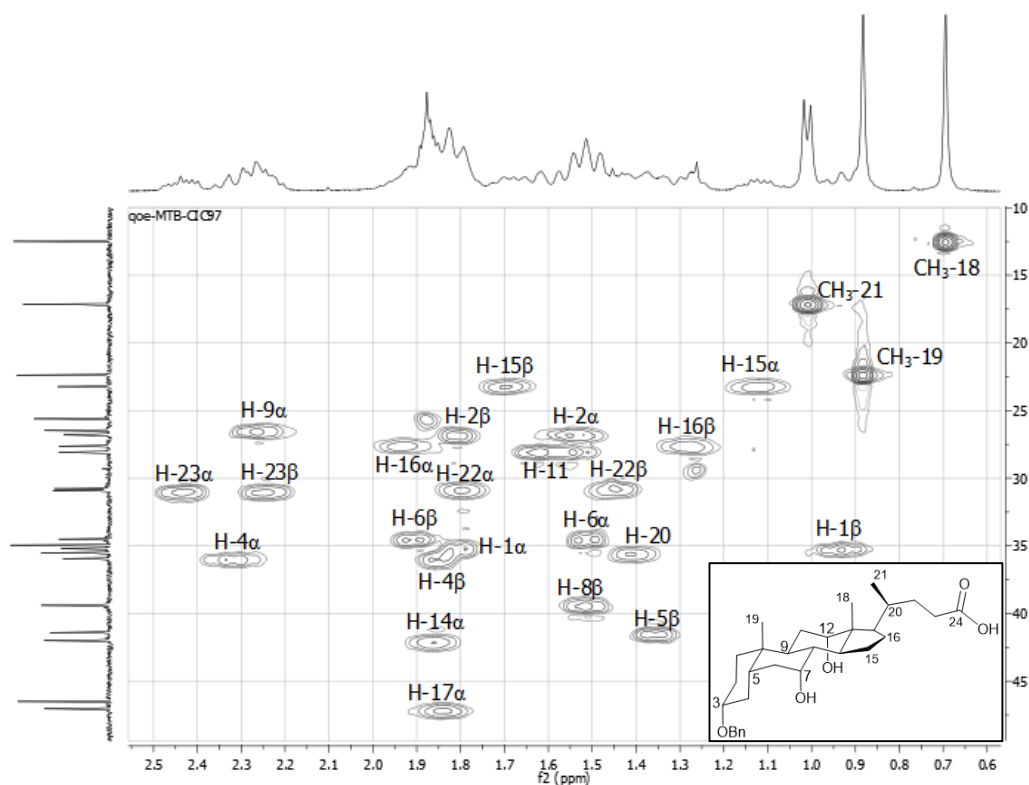
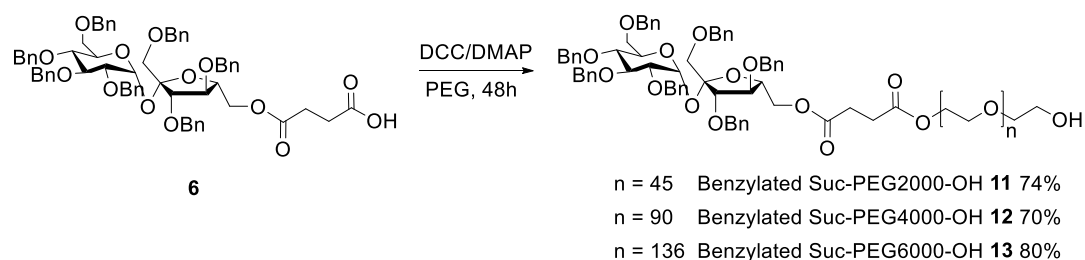


**Figure 26** HMQC spectrum expansion of 3α-*O*-benzyl, 7α, 12α-dihydroxy-5β-cholic acid **10** in CDCl<sub>3</sub>, focused on the steroid skeleton.

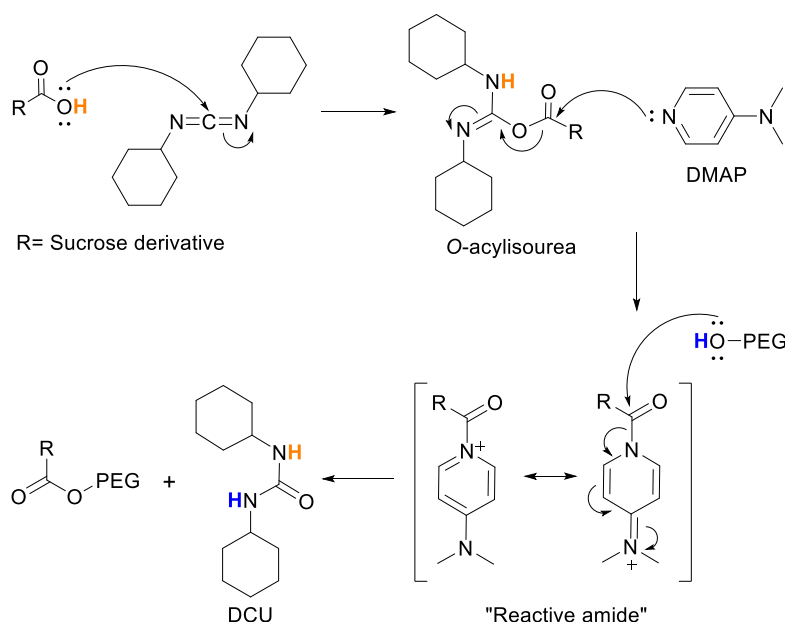
### II.2.1.3 Synthesis of Suc-PEG-Chol polymer conjugates

Upon the successful synthesis of the two protected building blocks, an efficient PEGylation was accomplished in a two-step approach. First, the PEG chains were coupled onto the carboxylic group of sucrose succinate derivative **6** by a Steglich esterification<sup>128</sup> with DCC as a coupling reagent and DMAP as a catalyst (Scheme 8). Three series of polymers with different numbers of repeating ethylene oxide units (EO) ( $n = 45, 90, 136$ ) have been synthesized. All the reactions were carried out under the same experimental conditions, starting from the same molar quantities of the reactants. Polymer conjugates **11**, **12** and **13** were obtained in moderate yields (70 – 80 %). There were, however, some problems with this procedure. Since it has proven difficult to separate the desired functionalized PEG molecules from the unreacted polymer, the molar number of **6** was 1.2-fold of the PEG molecule. No disubstituted product was formed. Though, by closely following the reaction by TLC, two major spots with similar  $R_f$  values were observed. After purifying with gradient elution flash column chromatography it was



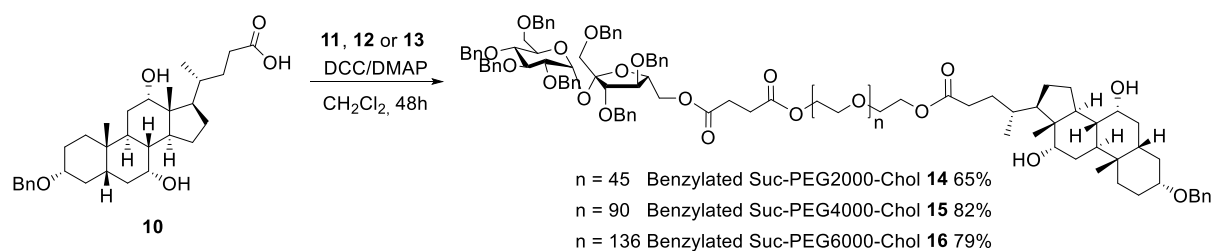
**Scheme 8** Synthesis of the benzylated Suc-PEG-OH conjugates by a Steglich esterification.

evidenced by  $^1\text{H-NMR}$  that it was the same desired compound but with different EO units. Since PEG is a synthetic polymer which shows a certain polydispersity no further attempts for separation were made. On the other hand, the purification of the PEG conjugates proved problematic, primarily because of the pronounced tendency of PEG to form complexes with the urea by-product. It is well documented that the molecular complexation of PEG and urea tends to form a kind of inclusion compound that is very stable due to hydrogen-bonding.<sup>129</sup> In synthetic organic chemistry, compounds containing the carbodiimide functionality are dehydration agents and are often used to activate carboxylic acids towards amide or ester synthesis. Additives, such as DMAP, are often used to inhibit side reactions and increase reaction yields. The reaction mechanism starts with the reaction of the carboxylic acid with DCC to form an *O*-acylisourea intermediate, which is more reactive than the free acid (Scheme 9). Then, DMAP, as a stronger nucleophile than the PEG hydroxyl group, reacts with the *O*-acylisourea leading to a reactive amide and dicyclohexylurea (DCU) by-product. DMAP acts as an acyl transfer-reagent and subsequent reaction with the alcohol provides the ester.



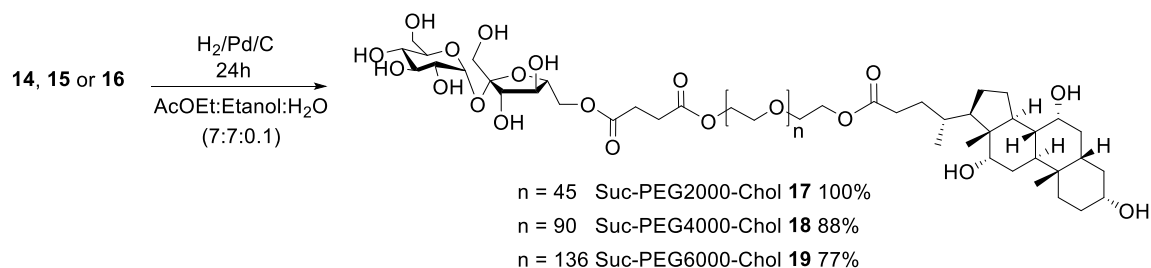
**Scheme 9** The reaction mechanism of Steglich esterification.

The next step to our target compound consisted on coupling the cholic acid derivative to the benzylated Suc-PEG-OH moiety synthesized previously (Scheme 10). To do so, the same DCC-coupling strategy was employed. The reaction followed the same experimental conditions and took place by the same mechanistic pathway. The benzylated Suc-PEG-Chol conjugates **14**, **15** and **16** were obtained in moderate yields (65 – 82 %). Although, the monitorization of the reaction by TLC and the purification step were facilitated by the formation of an unexpected purple color complex on the TLC plate upon chemical revelation with sulfuric acid. This may result from a complex between the sulfuric acid and the cholic acid moiety.



**Scheme 10** Synthesis of the benzylated Suc-PEG-Cholic conjugates by a Steglich esterification.

Subsequent debenzylation by Pd/C catalyzed hydrogenolysis in a mixture of EtOH:AcOEt:H<sub>2</sub>O (7:7:0.1), gave the desired Suc-PEG-Chol conjugates **17**, **18** and **19** in high yields (88 – 100 %) (Scheme 11). This solvent mixture is ideal to achieve the complete debenzylation of the sucrose moiety, avoiding the formation of regioisomeric mixtures. The chemical structures of the novel conjugates were confirmed by <sup>1</sup>H-NMR, <sup>13</sup>C-NMR and mass spectral data. In addition to usual sucrose and steroidal signals, the broad singlet at 3.40 ppm in the <sup>1</sup>H-NMR spectrum may be assigned to the methylene protons of the repeating EO units in PEG. Signals at 4.2 ppm were assigned to the methylene protons in PEG adjacent to the carbonyl groups. The <sup>13</sup>C-NMR spectrum showed three signals around 173.32, 171.96 and 171.87 ppm, which were attributed to carbonyl carbons, -C(=O)O<sub>Chol</sub>-PEG-, -C(=O)O<sub>Suc</sub>-PEG- and Suc-OC(=O)-, respectively. Combined with the results of the NMR spectroscopy, the MALDI-TOF analysis further confirmed the formation of the Suc-PEG-Chol conjugates. In addition, it also shows the polydispersed nature of PEG polymers (see section VI.2.5).



**Scheme 11** Synthesis of the Suc-PEG-Chol conjugates by Pd/C catalyzed hydrogenolysis.

#### II.2.1.4 Physicochemical characterization of Suc-PEG-Chol polymer conjugates

Thermal characteristics of Suc-PEG-Chol conjugates were studied by DSC. The attachment of sucrose and cholic acid moieties decreased the melting temperature ( $T_m$ ) of the corresponding PEG (Table 3). This result suggests that the addition of molecules to the ends of PEG chains reduces its crystallinity. As expected, the  $T_m$  of the polymers increased with increasing molecular weight.

In order to determine the critical association concentration (CAC), the self-aggregation behavior of Suc-PEG-Chol conjugates in aqueous media were investigated using pyrene as a fluorescence probe (Table 3). The CAC value for the Suc-PEG2000-Chol conjugate was lower than the obtained for the other conjugates, which is in agreement with the increase in the solubility of the latter polymers due to the introduction of a higher PEG chain length. Figure 27 a) depicts the fluorescence emission spectrum

**Table 3** Influence of the PEG chain length on the melting temperature ( $T_m$ ) and on the critical association concentration (CAC) of the Suc-PEG-Chol conjugates.

Polymer Conjugates	$T_m$ of PEG (°C)	$T_m$ conjugate (°C)	CAC (g/L)
Suc-PEG2000-Chol <b>17</b>	50	39	0.06
Suc-PEG4000-Chol <b>18</b>	56	49	0.13
Suc-PEG6000-Chol <b>19</b>	60	55	0.11

of pyrene obtained at a fixed excitation wavelength of 340 nm against various Suc-PEG2000-Chol concentrations. It shows an increase of fluorescence emission intensity with increasing polymer concentration, which indicated the incorporation of pyrene molecules in the hydrophobic domains of the conjugates. In addition to the monomeric peaks, a broad band appears at longer wavelengths (centered on 470 nm) due to excimer formation. Pyrene excimer reflects a high local molar concentration of pyrene where a ground state and an excited state pyrene ring are  $\sim 10$  Å from each other.<sup>130</sup> No excimer emission was observed in the absence of polymer. Figure 27 b) shows the change in overall intensity of the emission spectra as a function of polymer concentration. At a low concentration ( $c < \text{CAC}$ ) a flat region and a sigmoid change in the crossover point were observed and the CAC values were calculated. The emission spectra for all Suc-PEG-Chol conjugates were measured and the fluorescence spectroscopy data showed formation of nanoparticles.

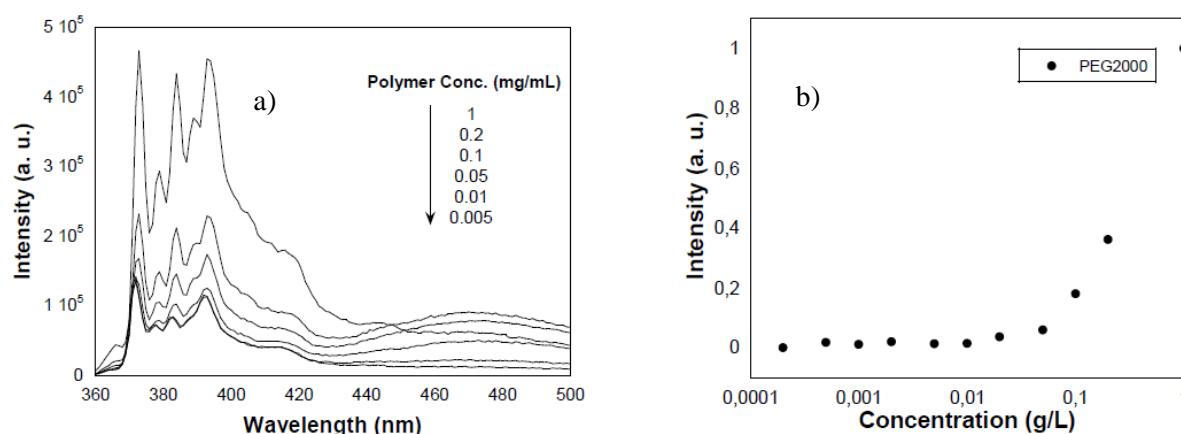


**Figure 27** a) Fluorescence emission spectra of pyrene/Suc-PEG2000-Chol against concentration of Suc-PEG2000-Chol in distilled water. b) Plots of the overall intensity of the pyrene emissions spectra vs. polymer concentrations.

The Suc-PEG-Chol polymers can self-associate in aqueous environment to form micelle like self-aggregates with a hydrophobic cholic acid core surrounded by a hydrophilic sucrose and PEG shell.  $^1\text{H}$ -NMR spectra in  $\text{D}_2\text{O}$  was employed to study these conformational states (Fig. 28). The results showed that in  $\text{D}_2\text{O}$  the complete structural resolution was observed. However, the integration between the C18 methyl protons of cholic acid and the anomeric proton of sucrose did not match with the molecular formula of the target polymer. The number of cholic acid unit determined by  $^1\text{H}$ -NMR was one third of the sucrose moiety, which indicates a hydrophobic core constituted mainly by cholic acid moieties.

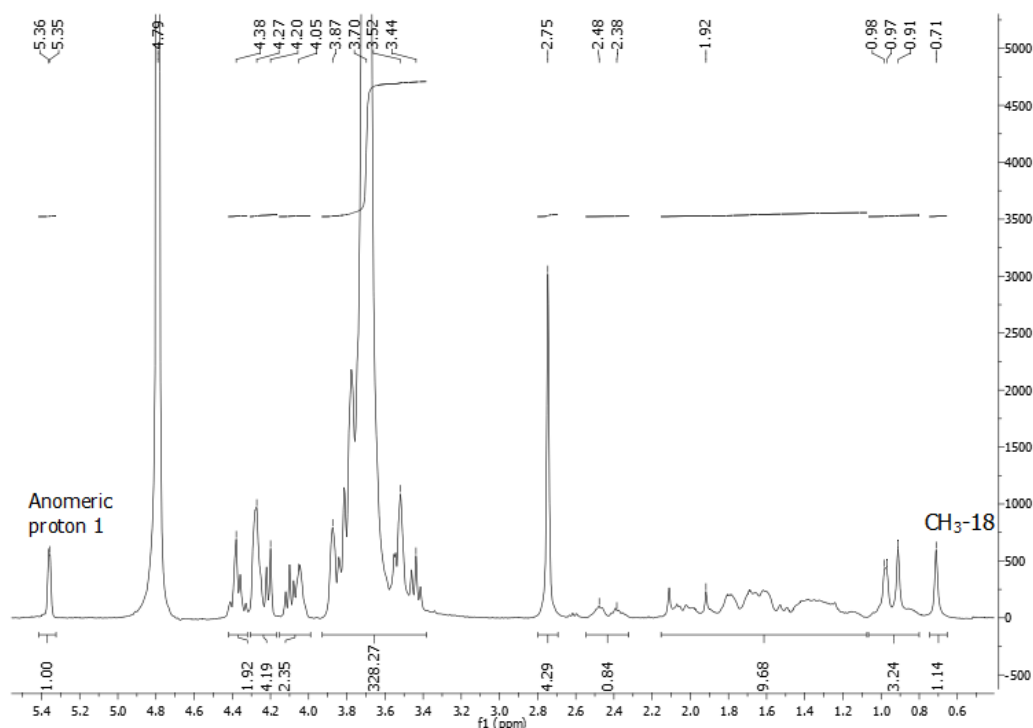
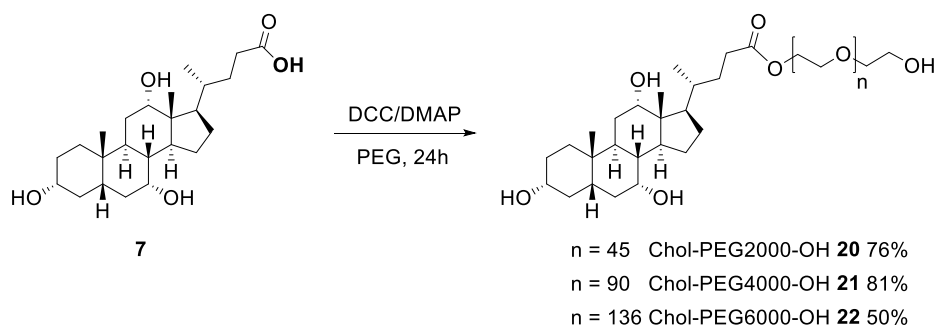


**Figure 28**  $^1\text{H}$ -NMR spectrum of Suc-PEG4000-Chol **18** in  $\text{D}_2\text{O}$ .

### II.2.1.5 Synthesis of Cholic-PEG polymer conjugates

In order to study the influence of sucrose moiety on the physicochemical properties of PNPs, Cholic-PEG polymer conjugates were prepared (Scheme 12). Steglich esterification strategy was employed as before but with a different work-up procedure. A series of washing steps to remove unwanted secondary products and non-reacting starting materials were included. The reaction followed the same experimental conditions and took place by the same mechanistic pathway. The Cholic-PEG conjugates **20**, **21** and **22** were obtained in moderate yields (50 – 81 %). The lower yield obtained for the PEG6000 derivative **22**, could be explained by its increase solubility in water due to the higher molecular weight, increasing the possibility of loss of product during the washing step. The success of the coupling reaction was confirmed by NMR spectroscopic studies. In addition to usual cholic acid signals, the  $^1\text{H}$ -NMR spectrum of the Cholic-PEG conjugates revealed the broad singlet at 3.71 ppm due to the methylene protons of the repeating EO units in PEG. Combined with the results of the NMR



**Scheme 12** Synthesis of the Cholic-PEG polymer conjugates by a Steglich esterification.

spectroscopy, the MALDI-TOF analysis further confirmed the formation of the Cholic-PEG polymer conjugates. The attachment of a cholic acid moiety slightly increased the melting temperature ( $T_m$ ) of the corresponding PEG (Table 4). This can be attributed to the increase rigidity and an easier packing of the molecules.

**Table 4** Influence of the PEG chain length on the melting temperature ( $T_m$ ) of the Cholic-PEG polymer conjugates.

<b>Polymer Conjugates</b>	<b><math>T_m</math> of PEG (°C)</b>	<b><math>T_m</math> conjugate (°C)</b>
Cholic-PEG2000 <b>20</b>	50	54
Cholic-PEG4000 <b>21</b>	56	62
Cholic-PEG6000 <b>22</b>	60	63

## II.2.2 Preparation and physicochemical characterization of PNPs

### II.2.2.1 PNPs prepared from Suc-PEG-Chol polymer conjugates

To investigate the influence of the preparation method on the physicochemical properties of Suc-PEG-Chol PNPs, these were prepared by two different methods – emulsion-solvent evaporation and nanoprecipitation.

#### II.2.2.1.1 PNPs prepared by the emulsion-solvent evaporation method

PNPs were first prepared using an o/w emulsion-solvent evaporation method. For this purpose, the polymers were dissolved in dichloromethane and emulsified in an aqueous phase having 0.5 % PVA as a stabilizer. The polymers self-assembled into PNPs after evaporation of the organic solvent by stirring at room temperature. Table 5 summarizes the size distribution characteristics and the  $\zeta$ -potential of the obtained colloidal suspensions determined by light scattering experiments. The particle size distribution of the different nanoparticulate formulations are given in Figure 29.

**Table 5** Mean particle size and  $\zeta$ -potential of the Suc-PEG-Chol PNPs prepared by o/w emulsion-solvent evaporation method with the emulsion formulated by vortex mixing.

<b>Polymer conjugates</b>	<b>Mean particle size (nm)</b>	<b>Polydispersity index (PDI)</b>	<b>Zeta potential (mV)</b>
Suc-PEG2000-Chol <b>17</b>	327	0.540	-15
Suc-PEG4000-Chol <b>18</b>	421	0.700	-9
Suc-PEG6000-Chol <b>19</b>	476	0.450	-1

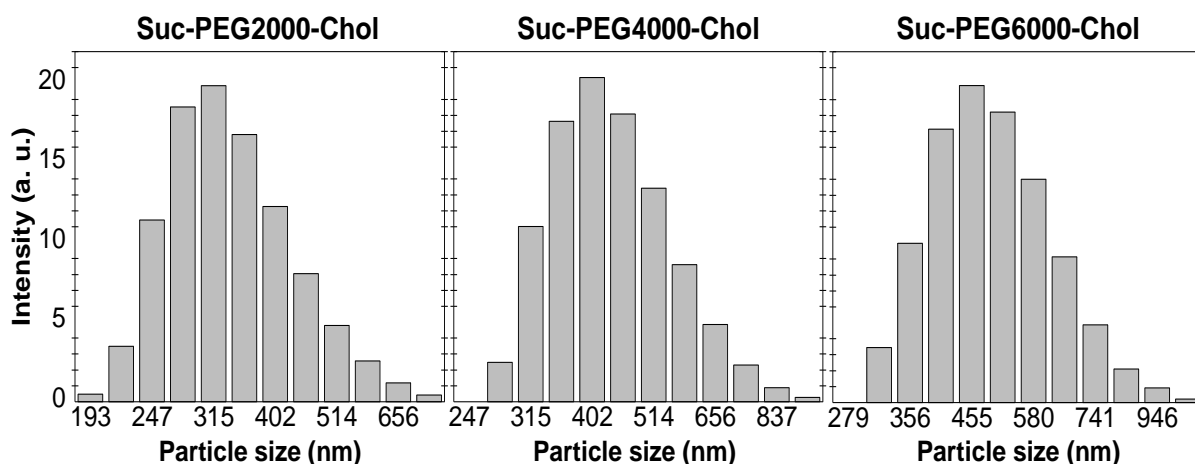


**Figure 29** Particle size distributions of Suc-PEG-Chol PNPs prepared by the emulsion-solvent evaporation method.

Freshly prepared PNPs suspensions with mean size in the range of 327 – 476 nm were obtained. Furthermore, a clear trend of increasing the particle size as their PEG content increased was observed. This could be caused by the longer PEG segments forming a thicker hydrated outer layer. The PNPs also exhibited a unimodal size distribution but with a high polydispersity value ( $> 0.300$ ). Suc-PEG-Chol PNPs showed low zeta potential values, even close to zero for the PEG6000 derivative. The greater reduction for this derivative could be explained by the possible shielding effect of the hydrophilic PEG chains as the chain length increases. On the other hand, the existence of a PVA layer at the PNP surface probably shields the surface charge of the PNPs. The emulsion-solvent evaporation method requires an additional purification step to remove process impurities. Centrifugation or ultracentrifugation, in combination with washing steps, is the most common approach to remove the excess surfactant attached on the PNP surface. Although, when centrifugation was attempted, no formation of the expected nanoparticle pellet was observed. It was found that longer centrifugation times or stronger centrifugal forces were unnecessary and did not improve separation. These findings suggest that the obtained PNPs were very stable in solution and confirm that the presence of PVA reduces the zeta potential values and hides the stability of this polymeric nanoparticulate system.

To investigate the PNP shape, the morphology was visualized by AFM as an example (Fig. 30), demonstrating that the PNPs were dispersed as individual particles with spherical shapes. The PNPs showed no aggregation in the AFM images, which could be attributed to the presence of PVA in the colloidal suspension. The mean particle size obtained by AFM for Suc-PEG4000-Chol formulation (450 nm) was slightly higher than that obtained by DLS (421 nm). This difference can be explained due to the PDI of the sample. As larger particles scatter more light than smaller ones, it was expected that the mean diameter given by DLS to be higher than those obtained by AFM, but it was not the case. Therefore, care must be taken to avoid erroneous interpretations of particle size, as the AFM image could not be representative of the whole nanoparticle population. On the other hand, the different experimental procedures between DLS and AFM may also be responsible for the observed difference

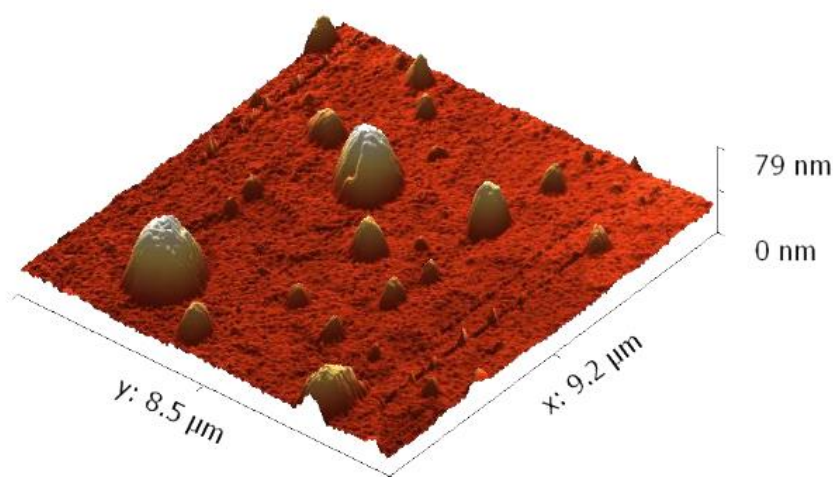


**Figure 30** AFM height image of Suc-PEG4000-Chol PNPs prepared by o/w emulsion-solvent evaporation method with the emulsion formulated by vortex mixing. The sample was prepared from a PNP solution of 0.1 mg/mL.

in the PNP diameter between these techniques.<sup>131</sup> The DLS experiments are performed under aqueous solution. However, the AFM sample preparation is carried out by depositing the PNP solution onto hydrophilic mica substrate, followed by drying. Thus, the immobilization may influence the PNP size and shape. Nevertheless, the AFM image is clearly representative of the polydispersity obtained by the emulsion-solvent evaporation method.

The particle size and size distribution strongly depend on the quality of the emulsion. The emulsion was prepared by vortex mixing, resulting in a white cloudy miniemulsion with droplet sizes above 100 nm. In order to reduce the droplet particle size, sonication was explored as an alternative to formulate the emulsion while maintaining the same experimental parameters. The ultrasound emulsification is performed under high frequency where large drops are generated by the instability of interfacial waves. The drops are subsequently broken into smaller ones through a cavitation mechanism.<sup>34</sup> Even though, a white cloudy miniemulsion was obtained as before. However, this time, the mean particle size was lower (Table 6). Though, the PDI was still very high ( $> 0.300$ ).

**Table 6** Mean particle size of the Suc-PEG-Chol PNPs prepared by o/w emulsion-solvent evaporation method with the emulsion formulated by sonication.

Polymer conjugates	Mean particle size (nm)	Polydispersity index (PDI)
Suc-PEG2000-Chol <b>17</b>	194	0.35
Suc-PEG4000-Chol <b>18</b>	205	0.40
Suc-PEG6000-Chol <b>19</b>	233	0.51

PVA is a common stabilizer used in the preparation of nanoparticles. It was found that particles formulated with this surfactant are more uniform and smaller in size.<sup>132</sup> Although, PNPs associated with larger amounts of PVA are more hydrophilic and have lower cellular uptake.<sup>133</sup> With this experimental procedure it was not possible to remove the PVA in excess. Additionally, the PNPs obtained by this method have a mean particle size and a high PDI which are not suitable for biomedical applications.

Therefore, a surfactant-free nanoprecipitation method was attempted and several experimental parameters were investigated in order to optimize the size of PNPs.

### II.2.2.1.2 PNPs prepared by nanoprecipitation

PNPs were successfully prepared by nanoprecipitation. Briefly, a solution of Suc-PEG-Chol polymer dissolved in acetone was injected into deionized water without any surfactant with moderate stirring at room temperature. Nanoparticles were immediately formed and the suspension was kept on gentle mechanical stirring until complete evaporation of the organic solvent. The physicochemical characteristics of the obtained colloidal suspensions were summarized in Table 7. The respective size distributions analyzed by DLS are shown in Fig. 31. In all cases the size distribution was monomodal with a fairly low polydispersity value ( $< 0.300$ ) which demonstrated a narrow particle size distribution. The mean particle size diameters obtained for the formulations prepared with PEG2000 and PEG4000 were similar, around 100 nm, which makes them suitable for drug delivery applications. On the other hand, PNPs prepared with the Suc-PEG6000-Chol polymer conjugate were larger, around 200 nm. As stated before, the particle size increases as their PEG content increase. The present results can be justified by the increased organic phase viscosity, which can hinder solvent diffusion, thereby producing large particles. An opposite trend, however, was observed by Shen *et al.* for PLA-PEG nanoparticles.<sup>134</sup> In terms of surface charge, zeta potential becomes less negative with increasing PEG chain length which could be explained by the possible shielding effect of the hydrophilic PEG chains.

**Table 7** Size distribution and  $\zeta$ -potential of the Suc-PEG-Chol PNPs prepared by nanoprecipitation.

Polymer conjugates	Mean particle size (nm)	Polydispersity index (PDI)	Zeta potential (mV)
Suc-PEG2000-Chol <b>17</b>	117	0.169	-26
Suc-PEG4000-Chol <b>18</b>	96	0.280	-19
Suc-PEG6000-Chol <b>19</b>	219	0.140	-12

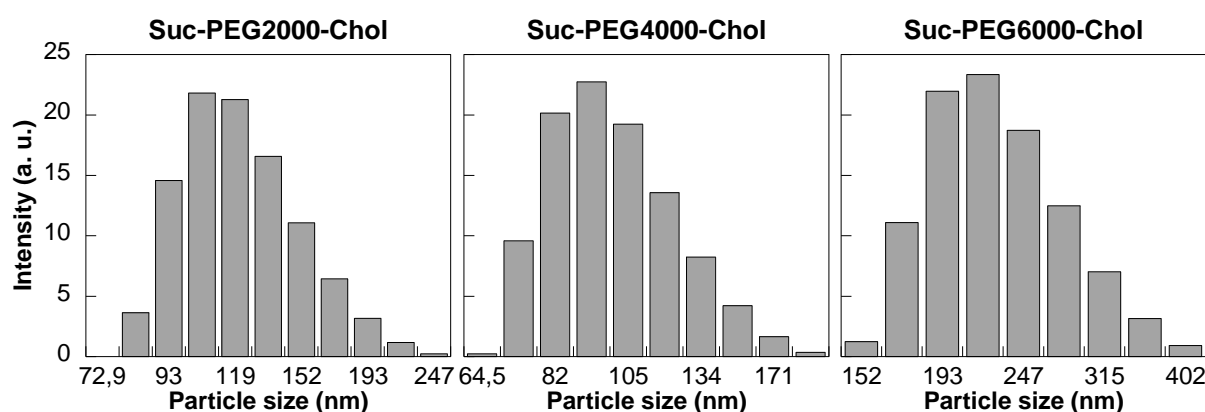


**Figure 31** Particle size distributions of Suc-PEG-Chol PNPs prepared by nanoprecipitation.

Another interesting finding was the influence of the polymer concentration on the resultant PNPs mean diameter. As shown in Figure 32a, the particle size of Suc-PEG4000-Chol and Suc-PEG6000-Chol PNPs were dependent on the organic phase concentration. On the other hand, particle size of Suc-PEG2000-Chol PNPs were scarcely affected by the polymer concentration in the studied range. Therefore, when the concentration increase, the interaction between the self-assembled nanoparticles is negligible and no aggregation occurred. Furthermore, no change on the mean diameter was observed in suspensions stored at 5 °C over one month (Fig. 32b). These findings were also in agreement with the trend of the zeta potential values in the different systems and revealed that the Suc-PEG-Chol polymers formed stable nanoparticles suspensions without aggregation. Again centrifugation

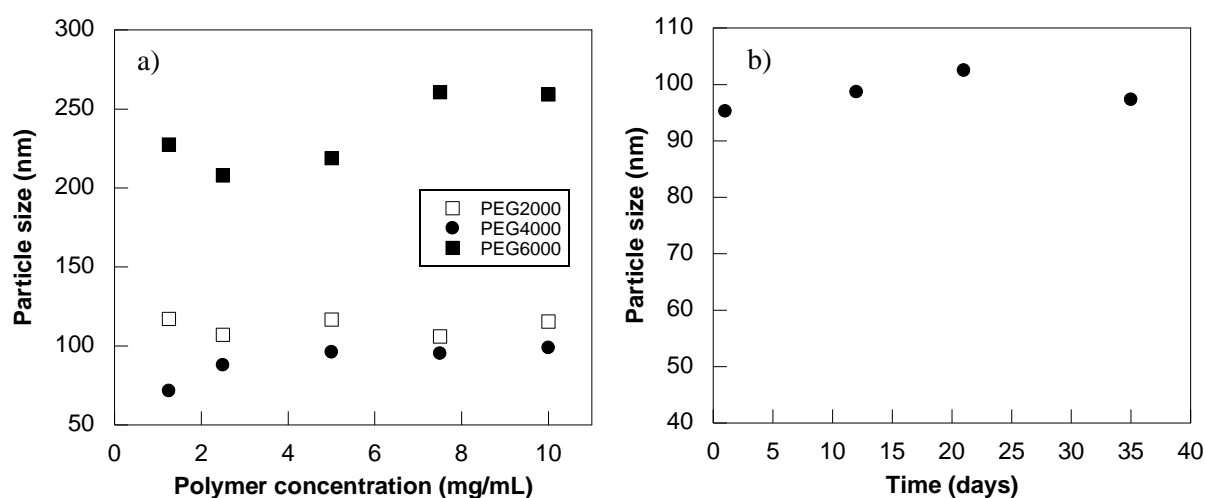


**Figure 32** a) Concentration dependent particle sizes of Suc-PEG-Chol PNPs at room temperature prepared by nanoprecipitation. b) Study on the Suc-PEG4000-Chol PNPs stability, stored at 5°C over one month.

was employed in an attempt to isolate the PNPs from the liquid phase, but without success. It was assumed, that these stable colloidal suspensions are of the size range at which the Brownian forces dominate the gravitational ones, and the particles tend to remain suspended.<sup>25</sup> On the other hand, PEG by itself is able to stabilize the colloidal system through steric interactions.

Lyophilized PNP formulations showed larger particle size when compared with freshly prepared PNPs (Table 8). Thus, lyophilization process might induce particle aggregation. Vortexing for 5 min. of a lyophilized PNP suspension in Milli Q water was able to break the aggregates and reduced the particle size to almost its original size before lyophilization. However, the polydispersity value was slightly higher.

**Table 8** Size distribution of lyophilized Suc-PEG-Chol PNPs prepared by nanoprecipitation after vortexing for 5 min.

Polymer conjugates	Mean particle size (nm)	Polydispersity index (PDI)
Suc-PEG2000-Chol <b>17</b>	108	0.35
Suc-PEG4000-Chol <b>18</b>	165	0.24
Suc-PEG6000-Chol <b>19</b>	270	0.31

Particle size distribution data by DLS was also supplemented with a visual microscopic method. AFM images of these colloidal suspensions revealed that the particles were spherical in shape. However, the average diameters determined by AFM for the three conjugates were higher than those measured by DLS. Lyophilized PNPs also exhibit the same behavior. Moreover, the degree of aggregation and the morphology was dependent on the process used for drying the water from the mica substrate during the preparation of the AFM sample. For instance, PNP suspensions prior to lyophilization and dried at 5 °C, have a roughly spherical morphology and a mean particle size of 300 nm for the PEG2000 and PEG4000 derivative and 600 nm for the PEG6000 (Fig. 33). In case of lyophilized PNPs dried at 5 °C, it was possible to find on the mica surface a “snapshot” of the aggregation process (Fig. 34). For the PEG4000

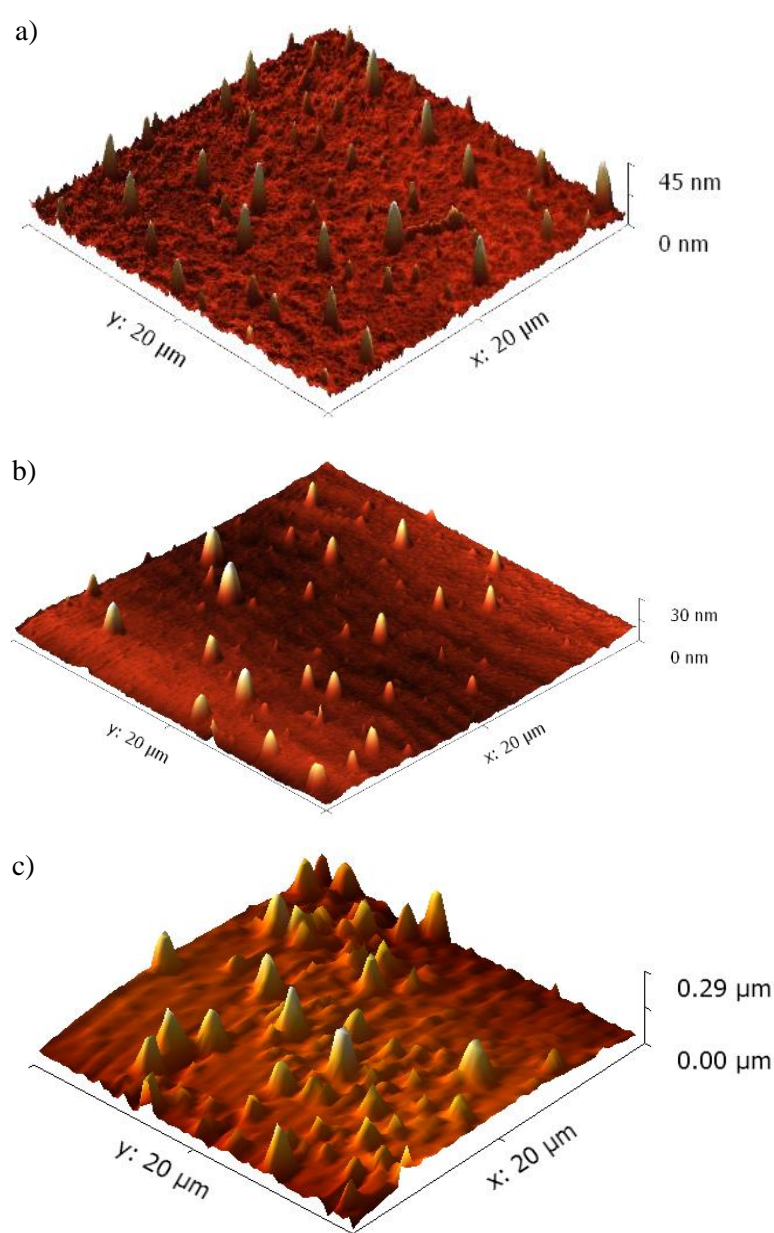


**Figure 33** AFM height image of Suc-PEG-Chol PNPs from a PNP solution of 0.1mg/mL dried at 5 °C. a) Suc-PEG2000-Chol PNPs. b) Suc-PEG4000-Chol PNPs. c) Suc-PEG6000-Chol PNPs.

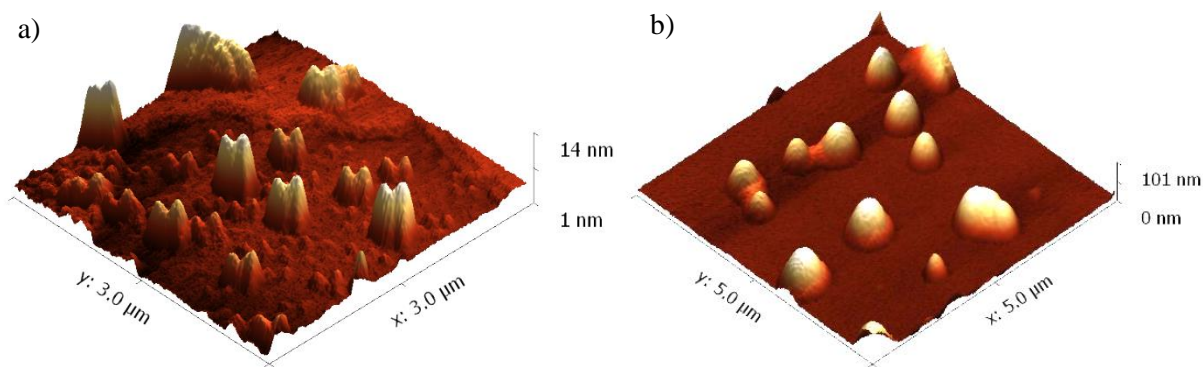


**Figure 34** AFM height image of lyophilized Suc-PEG-Chol PNPs from a PNP solution of 0.1mg/mL dried at 5 °C. a) Suc-PEG4000-Chol PNPs. b) Suc-PEG6000-Chol PNPs.

formulation the average PNP diameter was 112 nm which indicates that no aggregation occurred during the lyophilization process even without any cryoprotectant.

In a different approach, a lyophilized Suc-PEG2000-Chol PNP suspension was dropped on a freshly cleaved mica substrate and the mica was rapidly frozen. Then the mica wafer was lyophilized to remove the water. AFM images revealed an average nanoparticle diameter of 202 nm with regular spherical shape (Fig. 35).

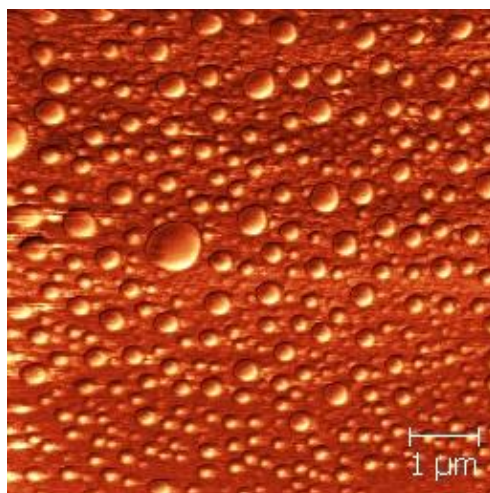


**Figure 35** AFM phase image of lyophilized Suc-PEG2000-Chol nanoparticles from a PNP solution of 0.1mg/mL dried by freeze-drying.

The aggregation behavior was more pronounced when the samples were dried under phosphorus pentoxide. Two particles populations were observed, the first one with diameter around 1.6 μm and the second one around 230 nm. (Fig. 36). Regarding the Suc-PEG4000-Chol PNPs, besides the formation of large aggregates, it was possible to observe the formation of nanometric crystallites of PEG (Fig. 37). From these results we noticed some influence from the water evaporation entailed in the AFM sample preparation on the size of the PNPs. In fact, the aggregation may be caused by the hydrophilicity of the mica substrate which could have traces of water even after evaporation, causing nanoparticle coalescence.<sup>135</sup>

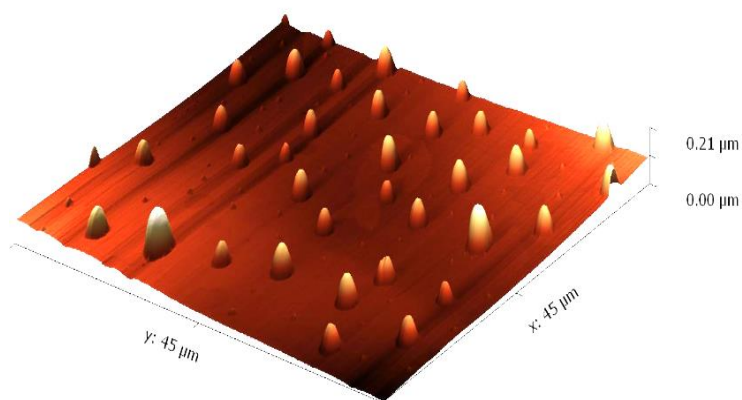


**Figure 36** AFM phase image of lyophilized Suc-PEG2000-Chol nanoparticles from a PNP solution of 0.1mg/mL dried under phosphorus pentoxide.

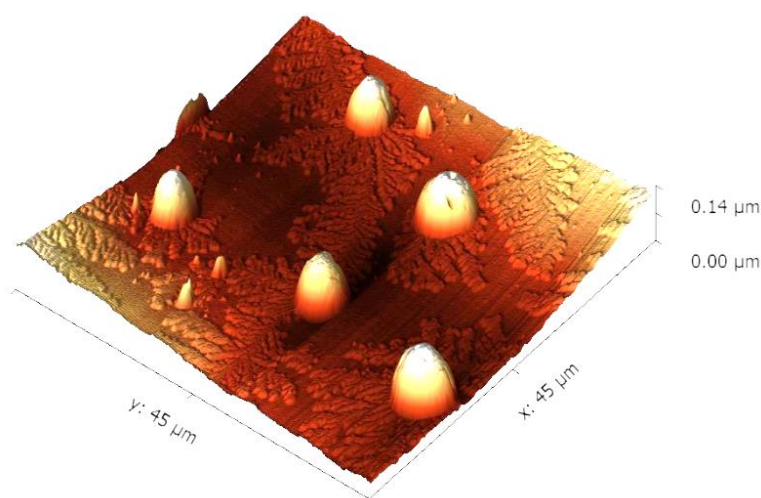


**Figure 37** AFM phase image of lyophilized Suc-PEG4000-Chol nanoparticles from a PNP solution of 0.1mg/mL dried under phosphorus pentoxide. Visualization of nanometric crystallites of PEG.

SEM was also used to study the PNP surface morphology with higher resolution as shown in Figure 38. The size of lyophilized Suc-PEG4000-Chol PNPs found from the SEM images tallies with that detected by DLS previous to lyophilization (Fig. 38a). It was not possible to examine the PEG2000 conjugate by SEM due to its low melting point. In fact, the SEM observations were also very tricky. The PNPs formed as a thin film and behind that film it was possible to see the PNPs (Fig. 38b).

#### II.2.2.2 PNPs prepared from Cholic-PEG polymer conjugates

In order to study the influence of the sucrose moiety on the physicochemical properties of the PNPs, it was tried to prepare PNPs from Cholic-PEG polymer conjugates. As the best results were obtained with the nanoprecipitation method, the same experimental parameters were applied to Cholic-PEG polymer conjugates. Although, the polymers without the sucrose moiety, were very insoluble in acetone. Consequently, upon the addition of the organic solution to the aqueous phase, occurred the precipitation of polymer aggregates, larger than colloidal size. Even after filtering out insoluble

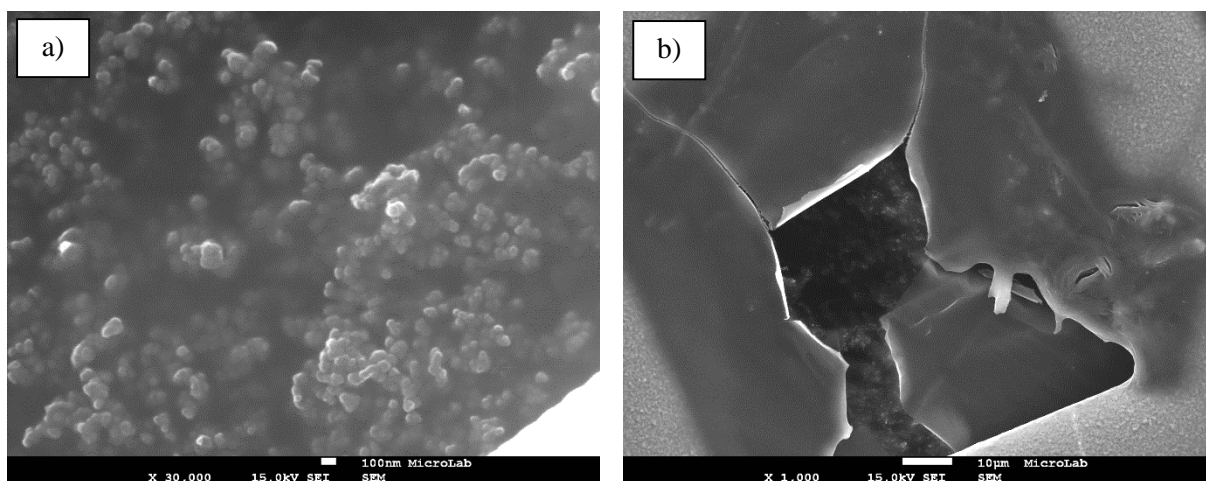


**Figure 38** SEM image of a) Suc-PEG4000-Chol PNPs and b) Suc-PEG6000-Chol PNPs.

impurities, it was not possible to obtain an accurate measurement by DLS. Acetonitrile and THF when used as the polymer solvent, also failed to produce stable PNPs. On the other hand, PNPs were successfully prepared by the o/w emulsion-solvent evaporation method, since the Cholic-PEG polymer conjugates were soluble in dichloromethane. Sonication were used to prepare the emulsions in the presence of 0.5% PVA. Table 8 summarizes the size distribution characteristics of the obtained colloidal suspensions and Figure 39 shows the respective particle size distribution. The average PNP diameter was around 550 nm for the formulations prepared with PEG2000 and PEG4000. As opposed to what was previously observed the particle size decreased as their PEG content increase and so, the average PNP diameter for Cholic-PEG6000 conjugate was 320 nm. This could be related to the more amphiphilic nature of the polymers without the sucrose moiety, reducing the interfacial tension between the aqueous and the organic phases. The PNPs also exhibited a unimodal size distribution but with a high polydispersity value ( $> 0.300$ ).

AFM phase imaging was utilized to characterize the surface changes of Cholic-PEG PNPs. In addition to a roughly spherical morphology, the PNPs seem to be constituted by a nucleus surrounded by PEG chains (Fig. 40). Apparently, the formation of internal cavities was favored by the facial characteristics of the cholic acid molecule. The average diameter of the PNPs was 162 nm. Presumably, the smaller “hollow-core” micelles were not detected by DLS.

**Table 9** Mean particle size of the Cholic-PEG PNPs prepared by o/w emulsion-solvent evaporation method with the emulsion formulated by sonication.

Polymer conjugates	Mean particle size (nm)	Polydispersity index (PDI)
Cholic-PEG2000 <b>20</b>	533	0.36
Cholic-PEG4000 <b>21</b>	547	0.77
Cholic-PEG6000 <b>22</b>	320	0.66

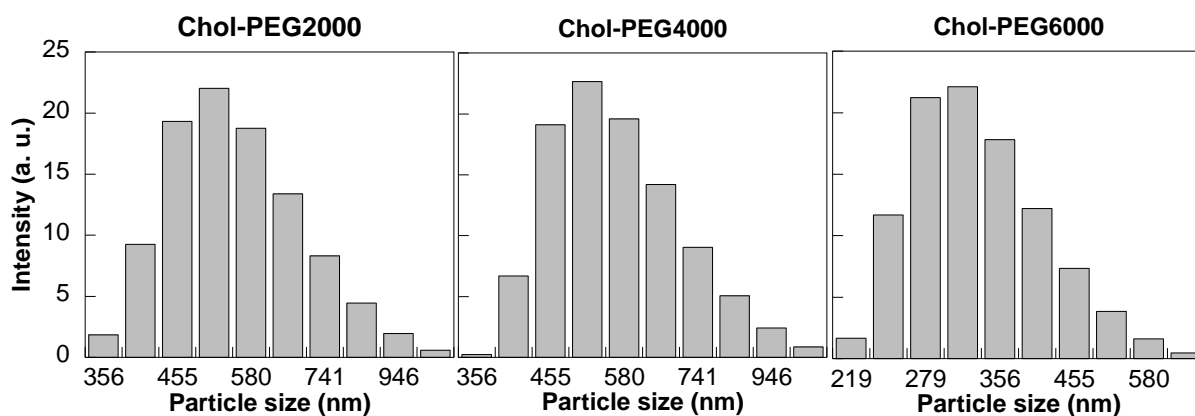


**Figure 39** Particle size distributions of Cholic-PEG conjugates PNPs prepared by the emulsion-solvent evaporation method.

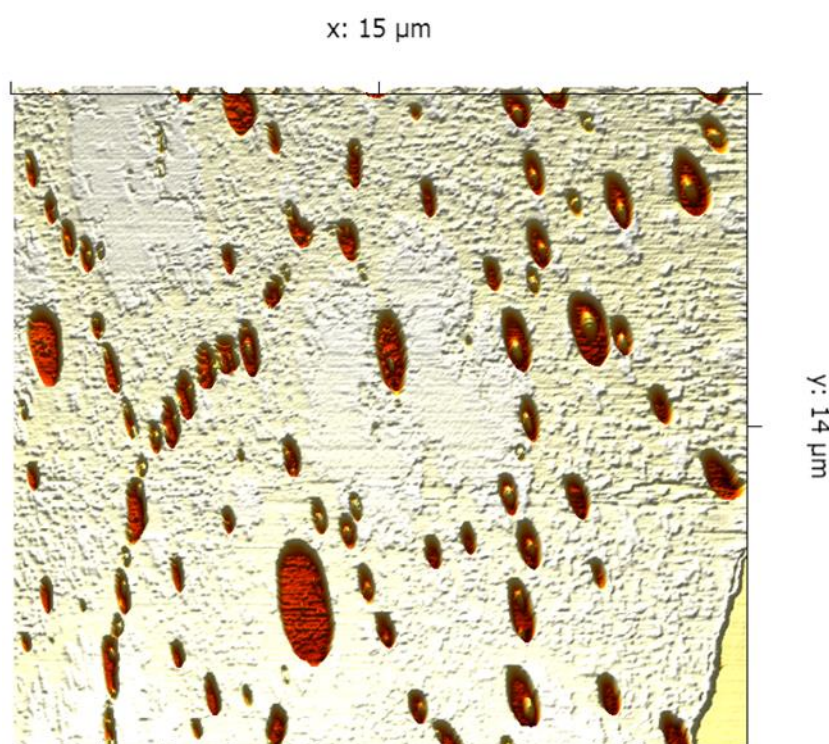


**Figure 40** AFM phase image of lyophilized Chol-PEG2000 nanoparticles from a PNP solution of 0.1mg/mL prepared by the emulsion-solvent evaporation method.

## II.3 Conclusion

The present study demonstrated the synthesis and self-aggregation behavior of Suc-PEG-Chol conjugate polymers in an aqueous milieu prepared from different PEG chain length. The polymers were successfully synthesized by covalent binding of the appropriate sucrose and cholic acid derivatives to PEG by a Steglich esterification. The main difficulties were the purification of the conjugates by column chromatography due to the formation of stable complexes between the PEG chains and the urea by-product. By applying two different methods: nanoprecipitation and emulsion-solvent evaporation, PNPs

**Table 10** Physicochemical characteristics of the Suc-PEG-Chol PNPs obtained by nanoprecipitation and emulsion-solvent evaporation technique.

Polymer conjugates	Nanoprecipitation			Emulsion-solvent evaporation (vortex)			Emulsion-solvent evaporation (sonication)	
	Particle size (nm)	PDI	$\zeta$ -potential	Particle size (nm)	PDI	$\zeta$ -potential	Particle size (nm)	PDI
Suc-PEG2000-Chol <b>17</b>	117	0.169	-26	327	0.540	-15	194	0.35
Suc-PEG4000-Chol <b>18</b>	96	0.280	-19	421	0.700	-9	205	0.40
Suc-PEG6000-Chol <b>19</b>	219	0.140	-12	476	0.450	-1	233	0.51

were successfully synthesized (Table 10). The PNPs prepared by nanoprecipitation were smaller in size and with a low polydispersity index than those prepared by the emulsion-solvent evaporation method. When the emulsion was formulated by sonication smaller particles were obtained, in contrast to that obtained by vortex mixing. However, it is known, that longer exposure times to sonication can produce surfactant degradation by radicals which form during the thermal decomposition of water. The utilization of PVA as colloidal stabilizer resulted in  $\zeta$ -potential close to zero, while the surfactant-free nanoprecipitation method resulted in negative  $\zeta$ -potentials, with the Suc-PEG2000-Chol **17** formulation having the highest value, which indicates a stable colloidal suspension. From this results and due to the difficulty in generating a monodisperse emulsion, the nanoprecipitation technique proved to be the best method to prepare PNPs with a narrow particle size distribution. Nevertheless, as the purification step by centrifugation failed for this type of PNPs, the dialysis method could be an attractive alternative. Surfactants are not necessary for the preparation of PEGylated PNPs, as PEG is able to stabilize the colloidal system through steric interactions. Although, surfactants do improve the resuspension of particles after lyophilization and it is well known that production of non-aggregated nanoparticles is just the first step for drug delivery. Alternatively, vitamin E TPGS could also function as an effective stabilizer for synthesizing PNPs. It is amphipathic, less hydrophilic than PVA and have the ability to enhance absorption through the intestinal wall.<sup>136</sup>

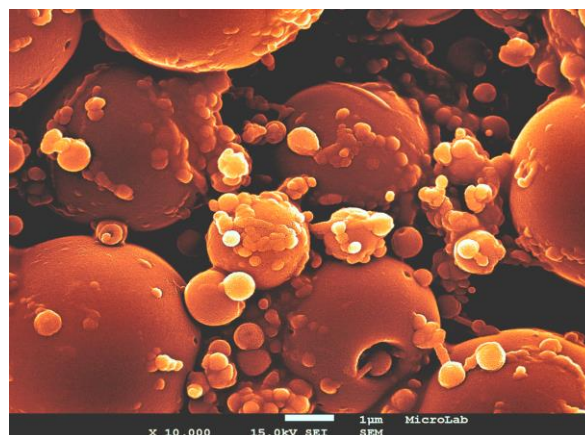
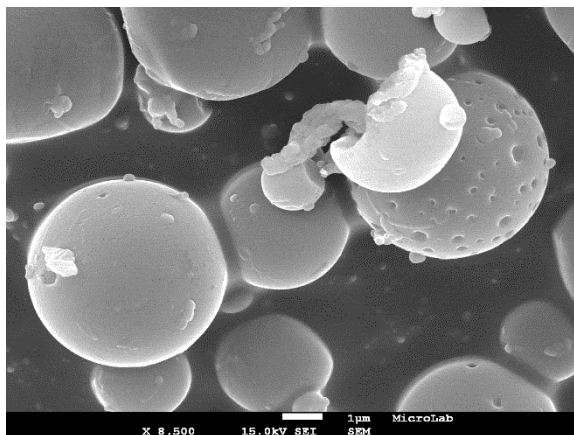
AFM and SEM experiments showed that the PNP formulations were of spherical shape. Although, the necessary care should be taken in order to avoid erroneous interpretation of particle size. It was shown, that the information taken from AFM, strongly depends on the sample preparation. Samples were prepared by drying the colloidal suspension on the mica substrate and it was evidenced that removing the water by freeze-drying promoted lower coalescence. Thus, AFM, SEM and DLS should be used as complementary techniques and are important tools to characterize nanoparticles.

The sucrose moiety on the polymer conjugate influenced not only their solubility in organic solvents but also the particle morphology obtained by the emulsion-solvent evaporation method. AFM phase images showed a type of micellar particles for the Cholic-PEG polymer conjugates, which were

different from the nanospheres obtained with the Suc-PEG-Chol ones. In addition, the sucrose moiety was also responsible for the observed negative  $\zeta$ -potentials.

Some problems were encountered in the PNP purification step, due to colloidal stability offered by PEG. On the other hand, although well tolerated clinically, PEG is non-biodegradable in the main-chain. Even if lower molecular weight PEG polymers exhibit renal elimination, following endocytotic capture there is inevitably a risk of lysosomal accumulation.<sup>137</sup> Increasing preclinical evidence that certain PEG-protein conjugates induce (albeit transient) intracellular vacuolation in animal models, is raising awareness of the potential advantage of biodegradable polymers in respect of potential safety benefit.<sup>137</sup> Moreover, PEG-based polymers have a glass transition temperature ( $T_g$ ) well below room temperature, which means they are in a molten or rubber-like state and do not provide mechanical strength to the PNPs. With this in mind, changing the polymer backbone could improve not only the physicochemical characteristics of the PNPs but also their safety in biomedical applications.





## Chapter III

### Synthesis of PLGA-based polymeric nanoparticles

---

*This chapter describes the preparation of polymeric nanoparticles from chemical modification of PLGA conjugated with sucrose and a cholic acid moiety (abbreviated as Suc-PLGA-Chol). The first part of this Chapter presents why PLGA has been chosen to design nanoparticles as drug delivery systems in various biomedical applications and focuses on the understanding of specific characteristics exploited by PLGA nanoparticles. In the second part the synthesis and physicochemical properties of the polymers are discussed. The PNPs were prepared either by nanoprecipitation or by the emulsion-solvent evaporation technique and characterized by dynamic light scattering and scanning electron microscopy. The improvement of the freeze-drying process by the use of cryoprotectants was also studied. Drying of the PNPs under phosphorus pentoxide was explored as an alternative to lyophilization.*



## III.1 Introduction

Biodegradability has been the major consideration in the development of biomedical materials due to problems associated with long-term biocompatibility. Biomaterials should perform their function with an appropriate host response and degrade after accomplishing their tasks.<sup>138</sup> Biodegradable polymers are largely used in medical application where they undergo degradation by chemical hydrolysis and are able to be excreted or resorbed without removal or surgical revision.<sup>138</sup> These polymers are attractive materials for numerous biomedical applications, such as drug delivery devices, scaffolds for tissue regeneration, artificial skin, and orthopedic implants, among others.<sup>139</sup>

Over the past few decades, there has been a considerable interest in the development of biodegradable drug carriers, given that they are considered to be highly suitable for human applications.<sup>17a,19</sup> An ever-growing number of biodegradable polymers, both synthetic and natural, have been used to formulate biodegradable PNPs. Among all, synthetic polymers possess several inherent advantages since their structures can be manipulated to produce specifically designed carriers to suit particular applications. PLGA is one of the most attractive biodegradable synthetic polymer due to its safety profile, which made it one of the most successful commercialized nanocarrier for controlled delivery (Fig. 41).<sup>140</sup> In addition to being biocompatible and biodegradable, it has tunable mechanical properties and is approved by Food and Drug Administration (FDA) and European Medicine Agency (EMA).

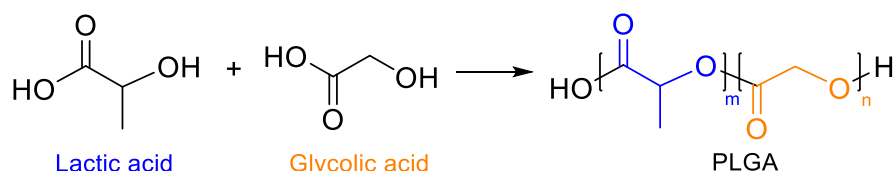


**Figure 41** Chemical structure of poly(D,L-lactic-co-glycolic acid) and its monomers.

In order to design a better controlled drug delivery vehicle, it is necessary to understand the physicochemical properties of PLGA, which are known to depend on the polymer molecular weight and the copolymer ratio. In general, the polymer can be made in highly crystalline form or completely amorphous due to disordered polymer chains. PLGA copolymer prepared from poly(L-lactic acid) (PLLA) and poly(glycolic acid) (PGA) are crystalline copolymers. On the other hand, copolymers from poly(D,L-lactic acid) (PDLLA) and PGA are amorphous in nature.<sup>141</sup> Unlike pure PLA and PGA, PLGA can be dissolved by a wide range of common solvents, including chlorinated solvents, tetrahydrofuran, acetone or ethyl acetate.<sup>142</sup> It can be processed into almost any shape and size, and can encapsulate biomolecules of virtually any size.<sup>142</sup> PLGA degrades in the body by hydrolysis of its ester linkages to produce the biodegradable and biocompatible lactic and glycolic acids. These monomers are metabolized in the body *via* the Krebs cycle, providing a minimal systemic toxicity associated with the use of PLGA.<sup>141</sup> The degradation rate can be adjusted by the PGA/PLA ratio in the polymer backbone.

As PLA is more hydrophobic than PGA due to the presence of methyl side groups, PLA-rich PLGA copolymers are less hydrophilic, absorb less water and subsequently degrade more slowly.<sup>143</sup> The glass transition temperature ( $T_g$ ) of PLGA is reported to be above the physiological temperature, and, hence, PLGA is glassy in nature, providing it a fairly rigid chain structure to be formulated as a drug delivery system. It has been further reported that the  $T_g$  of PLGA decreases with reducing the PLA content and the molecular weight.<sup>143</sup>

Despite fine qualities, one of the major drawbacks of using PLGA nanoparticles relates to the poor drug loading (around 1%).<sup>140</sup> However, PLGA-based nanoparticles often present high encapsulation efficiencies. A second important drawback consists in the rapid initial or burst release which is often attributed to the drug fraction adsorbed or weakly bound to the large surface area of the nanoparticles and this phenomenon is common for most PLGA-based PNPs.<sup>103</sup>

PLGA nanocarriers have shown promising pharmacokinetic at both cellular and whole-body levels due to tumor localization, taking advantage of the well-documented EPR effect.<sup>144</sup> The active targeting is usually achieved by the chemical attachment of a targeting component, such as a sugar moiety. Carbohydrate-functionalized nanoparticles constitute a good bio-mimetic model to intervene in carbohydrate-mediated biological processes.<sup>145</sup>

In this chapter, the first preparation of sucrose functionalized PLGA PNPs is described. In addition, a cholic acid moiety will also be incorporated in the polymer structure in order to improve the drug loading capacity.

## III.2 Results and Discussion

### III.2.1 Synthesis and characterization of PLGA-based polymer conjugates

The synthesis of Suc-PLGA-Chol polymer conjugates was accomplished by covalent binding of the appropriate sucrose and cholic acid derivatives to PLGA by esterification. Figure 42 shows a synthetic scheme of sucrose and cholic acid-derivatized PLGA polymers. Uncapped PLGA polymer has two functional groups, a hydroxyl group and a carboxylic acid group at its terminal ends. The synthesis of the Suc-PLGA-OH conjugate **23** proceeded by one-pot method. In the first step, the carboxylic acid terminal end of PLGA was first activated with NHS by using DCC (Scheme 13). The obtained PLGA-NHS did not require separation before the addition of sucrose monoderivative **5** in  $\text{CH}_2\text{Cl}_2$ . The benzylated sucrose-derivatized PLGA polymers were obtained in high yield (94 %). In the succeeding step, the hydroxyl terminal group of Suc-PLGA-OH **23** was coupled in anhydrous  $\text{CH}_2\text{Cl}_2$  with cholic

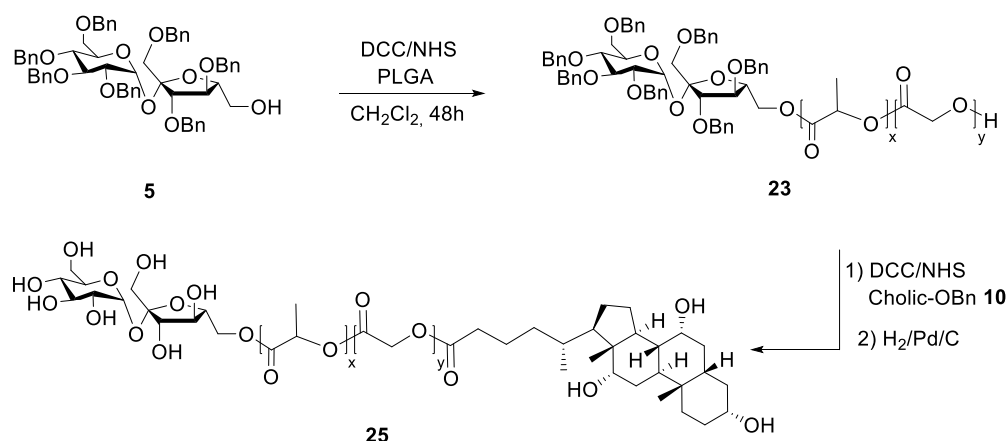
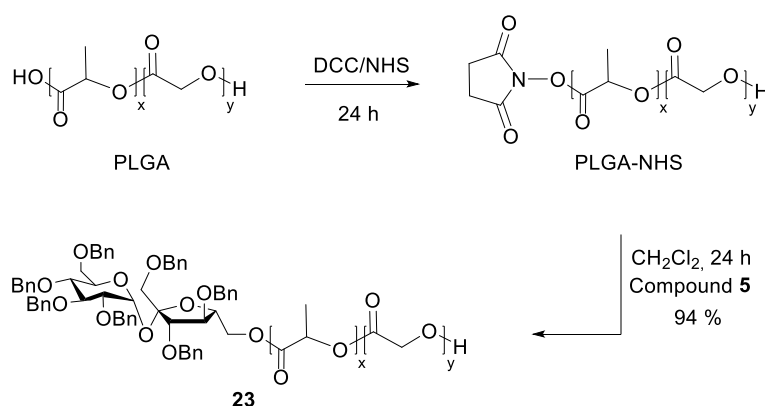
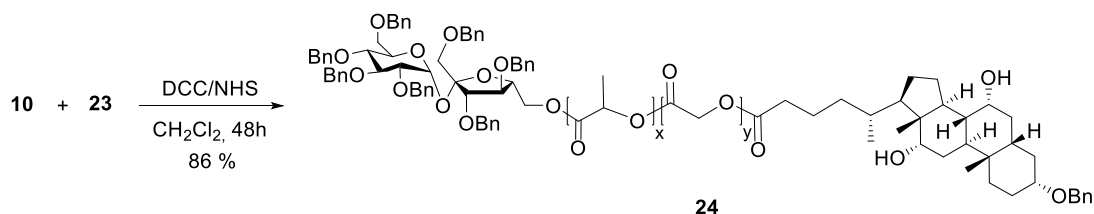


**Figure 42** Synthetic strategy for preparing the Suc-PLGA-Chol polymer conjugate.



**Scheme 13** Synthesis of the benzylated Suc-PLGA-OH conjugates by esterification reaction through a PLGA-NHS intermediate.

acid derivative **10**, of which the carboxylic acid group was pre-activated by the same DCC-coupling strategy previously employed (Scheme 14). This procedure led to benzylated Suc-PLGA-Chol conjugate **24** in high yield (86 %). The reactions took place by the same mechanistic pathway exemplified before for the DCC/DMAP coupling reaction but in this case, the hydroxyl group of NHS makes a nucleophilic attack on *O*-acylisourea, giving urea derivative and the succinimidyl ester intermediate. The NHS was chosen due to the formation of a less hydrolysis-sensitive compound. In the last step, debenzoylation by Pd/C catalyzed hydrogenolysis in a solvent mixture of EtOH:AcOEt:H<sub>2</sub>O (7:7:0.1) and CH<sub>2</sub>Cl<sub>2</sub> to dissolve the polymer, gave the desired Suc-PLGA-Chol conjugate **25** in quantitative yield. To verify the structure of the conjugates, NMR technique was used. A typical <sup>1</sup>H-NMR spectrum of benzylated Suc-PLGA-OH is shown in Fig. 43. The characteristic peaks appearing at 5.36 – 5.15 and 1.68 – 1.46 ppm are assigned to the methine proton and to the methyl protons of the lactide units, respectively. The peak



**Scheme 14** Synthesis of the benzylated Suc-PLGA-Chol conjugates by esterification reaction.

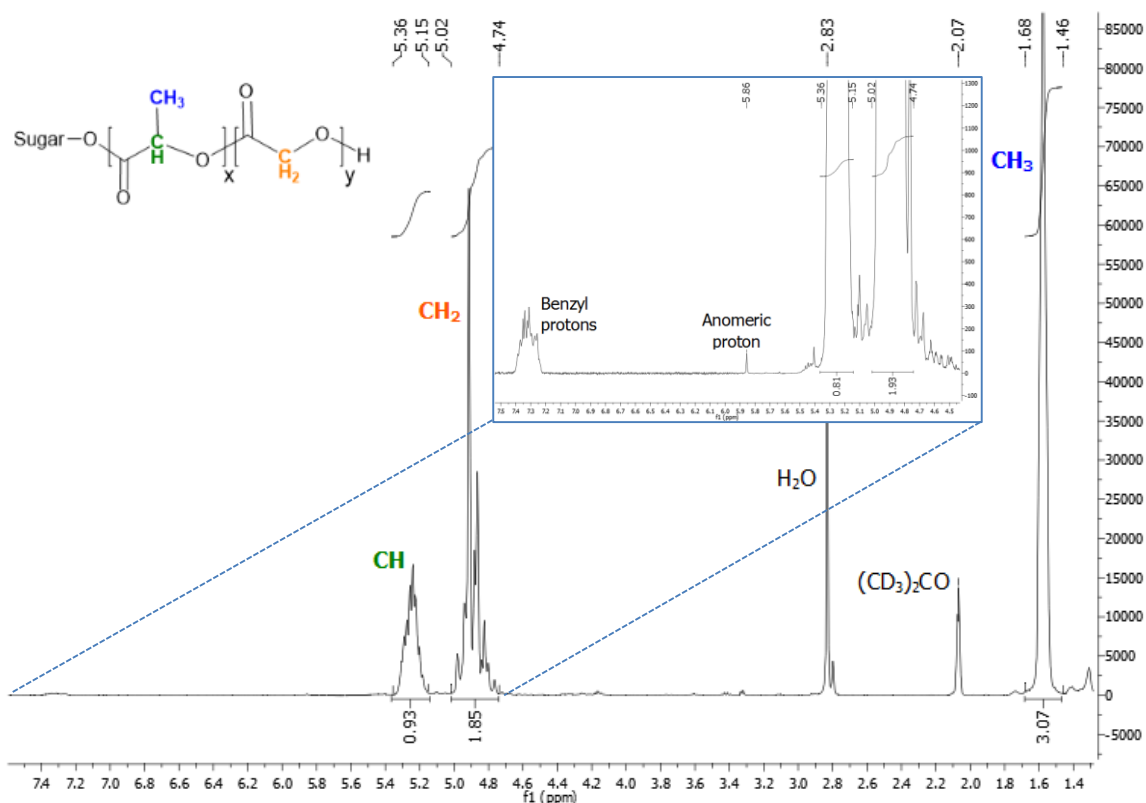


**Figure 43**  $^1\text{H}$ -NMR spectrum of benzylated Suc-PLGA-OH **23**.

corresponding to the methylene protons of the glycolide units, appeared at 5.02 – 4.74 ppm. Due to the lack of resolution it was not possible to determine the amount of conjugated sucrose in thus obtained polymer by comparing the peak areas of the methyl and methylene groups present in PLGA with the sucrose protons. Although, it was possible to find the benzyl protons and the sucrose anomeric proton (5.86 ppm) in the benzylated Suc-PLGA-OH  $^1\text{H}$ -NMR spectrum (Fig. 43 inset). In addition to usual PLGA signals, the peak at 0.75 ppm in the  $^1\text{H}$ -NMR spectrum of benzylated Suc-PLGA-Chol conjugate **24** may be assigned to the methyl protons of the cholic acid moiety (Fig. 44 inset). Due to its inherent low sensitivity, through  $^{13}\text{C}$ -NMR spectroscopy it was only possible to detect the signals corresponding to PLGA. These results confirm successful conjugation of sucrose and cholic acid to PLGA copolymer.

The thermal characteristics of PLGA conjugates were compared to free PLGA. The obtained glass transition temperatures ( $T_g$ ) are listed in Table 11. Benzylated Suc-PLGA-OH **23** had a  $T_g$  lower than pure PLGA polymer due to the introduction of the benzylated sucrose moiety, which contributed to less hydrogen bonding. On the other hand, the introduction of cholic acid resulted in an increase in  $T_g$  slightly above the  $T_g$  of PLGA. The incorporation of cholic acid moieties within a polymer provide rigidity and restricts rotational motion within the polymer chains.<sup>146</sup> Upon the removal of the benzyl groups, the obtained  $T_g$  was similar to that of pure PLGA. All the polymers displayed a  $T_g$  without any evidence of melting, suggesting that they are amorphous within this temperature range.

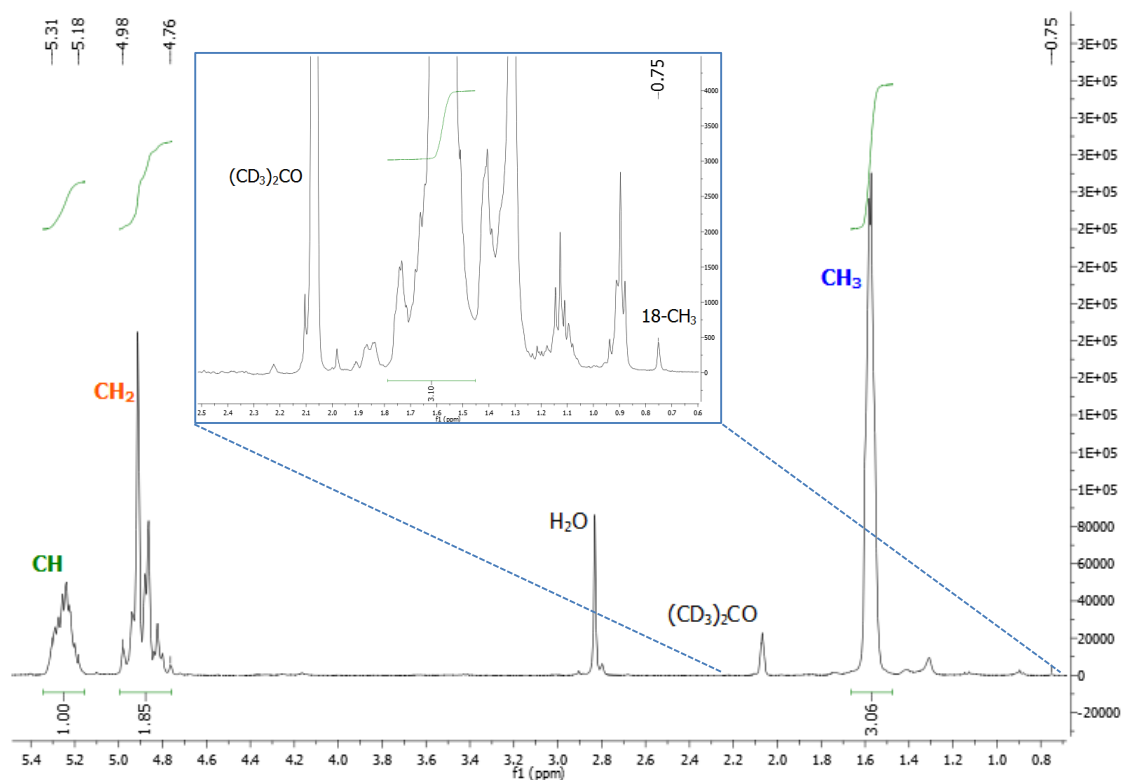


**Figure 44**  $^1\text{H}$ -NMR spectrum of benzylated Suc-PLGA-Chol **24**.

**Table 11** Glass transition temperatures ( $T_g$ ) of PLGA and PLGA-based conjugates.

Polymer	$T_g$ ( $^{\circ}\text{C}$ )
PLGA	41.89
Benzylated Suc-PLGA-OH <b>23</b>	35.60
Benzylated Suc-PLGA-Chol <b>24</b>	44.07
Suc-PLGA-Chol <b>25</b>	42.01

## III.2.2 Preparation and physicochemical characterization of PNPs

Suc-PLGA-Chol PNPs were prepared by two different methods, namely the emulsion-solvent evaporation and the nanoprecipitation technique. Their influence on the physicochemical properties of the obtained PNPs was also evaluated in order to select the more suitable method for further studies.

### III.2.2.1 PNPs prepared by the emulsion-solvent evaporation method

The o/w emulsion-solvent evaporation method was successfully applied for the preparation of PLGA and Suc-PLGA-Chol PNPs. In detail, the polymers were fully dissolved in dichloromethane yielding a clear solution. The organic phase was then added into an aqueous phase containing the

emulsifier at a given concentration and a vortex was used to disperse the emulsion. The solution was allowed to stir overnight to evaporate the organic solvent. The PNPs were obtained after centrifugation and several washes were done to remove the emulsifier. The mean particle size and size distribution characteristics of the obtained colloidal suspensions determined by light scattering experiments are shown in Table 12 and Fig. 45. Under the same experimental conditions, the particle size increased from 370 nm (PLGA PNPs) to 488 nm (Suc-PLGA-Chol PNPs). A similar trend was observed in the literature for galactose decorated PLGA PNPs.<sup>147</sup> As described previously for PEG-based PNPs formulated by the emulsion-solvent evaporation method, the obtained mean particle size was not suitable for drug delivery applications. In addition the PDI was also very high, especially for PLGA PNPs.

**Table 12** Mean particle size and polydispersity index (PDI) of PLGA and Suc-PLGA-Chol PNPs prepared by o/w emulsion-solvent evaporation method with the emulsion formulated by vortex mixing.

Polymer	Mean particle size (nm)	Polydispersity index (PDI)
PLGA	370	1.39
Suc-PLGA-Chol <b>25</b>	488	0.52

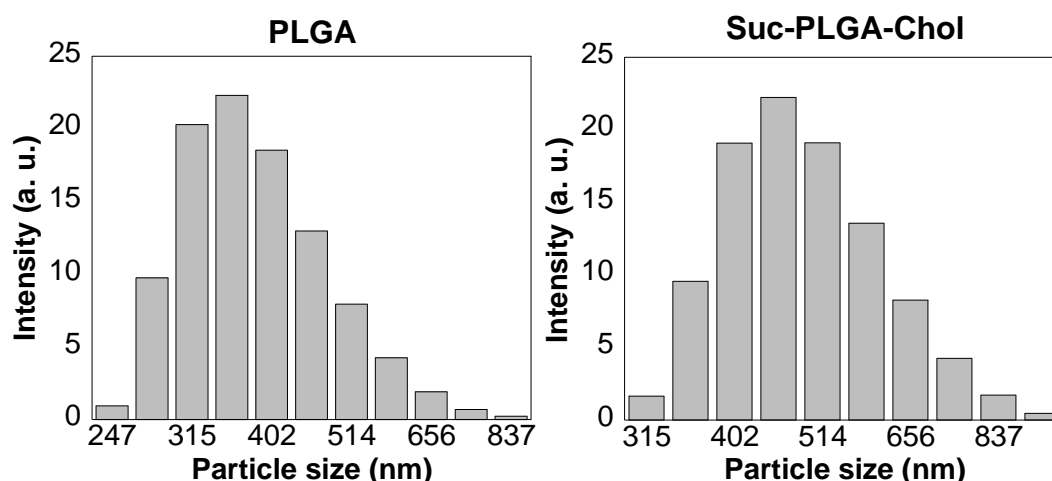


**Figure 45** Particle size distributions of PLGA and Suc-PLGA-Chol PNPs prepared by the emulsion-solvent evaporation.

The lyophilized PLGA and Suc-PLGA-Chol PNPs were investigated by SEM. A typical micrograph is shown in Fig. 46 for PLGA PNPs. As shown in the figure, the most prominent property of the particles is their almost perfect spherical shape. Although, the SEM diameter is notably larger than the size determined by DLS before freeze-drying. Suc-PLGA-Chol PNPs also exhibited the same behavior (Fig. 47) but their shape clearly indicates that the morphology is somewhat more complex than suggested by the DLS measurements. The difference between two values could be related to changes in particle properties during freeze-drying and contrasting of the sample for SEM. On the other hand, it must be remembered that these PNPs presented a high PDI, which indicates a less homogeneous size distribution, so differences between the results of the two methods will be inevitable.

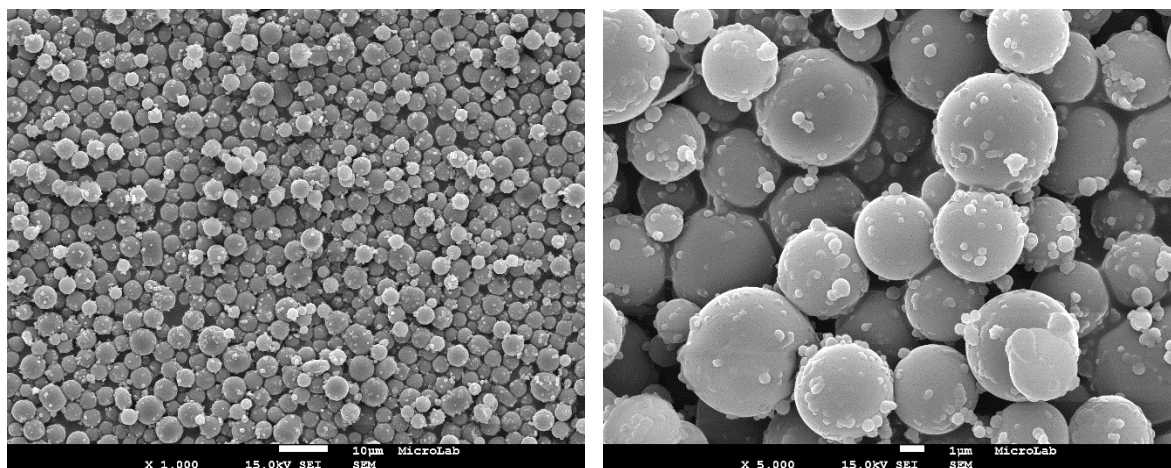


**Figure 46** SEM micrographs of lyophilized PLGA PNPs prepared by the emulsion solvent evaporation method.

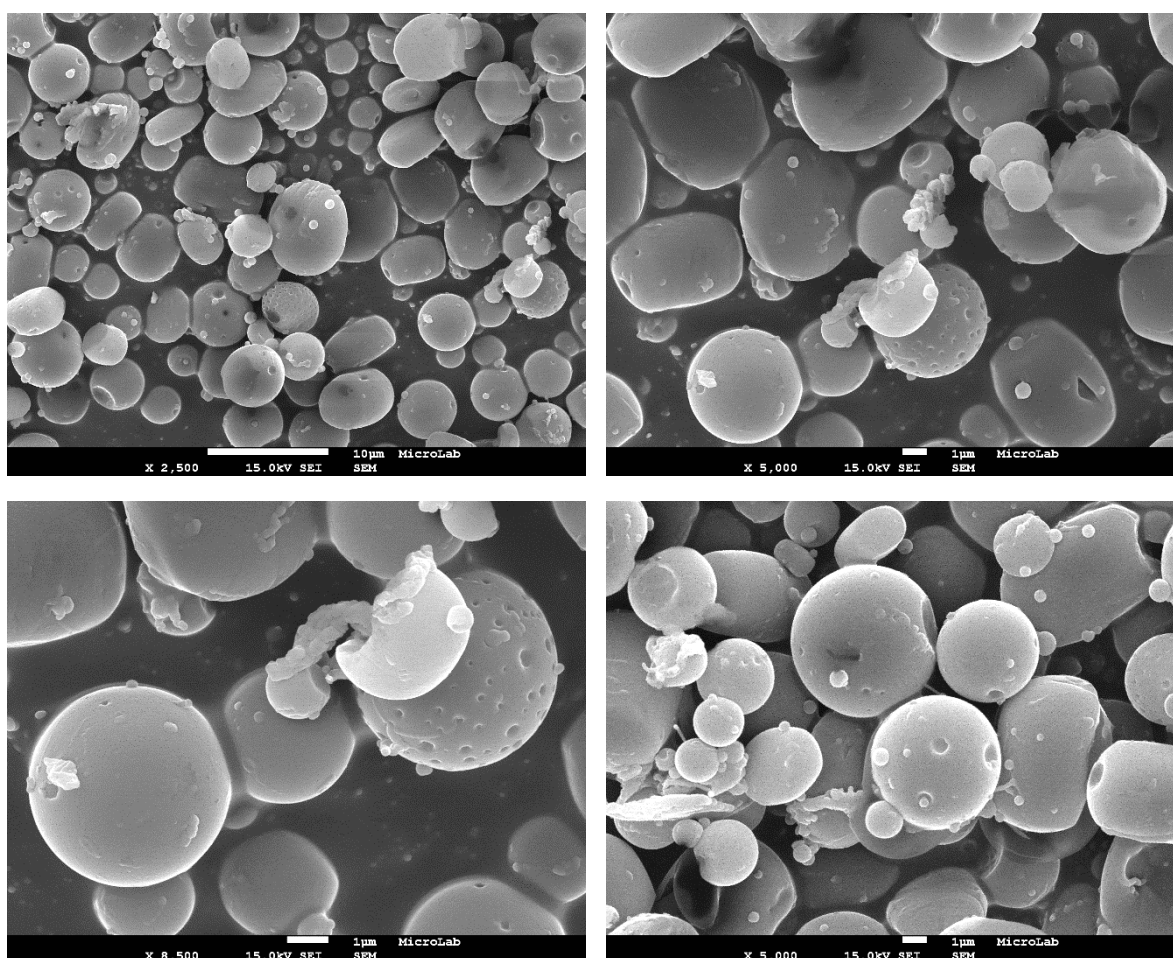


**Figure 47** SEM micrographs of lyophilized Suc-PLGA-Chol PNPs prepared by the emulsion solvent evaporation method.

### III.2.2.2 PNPs prepared by nanoprecipitation

PLGA and Suc-PLGA-Chol PNPs were prepared by nanoprecipitation as follows: the polymers were dissolved in the organic solvent and a clear solution was obtained. The organic phase was then added drop wise into a stirring aqueous solution without surfactant. After evaporation of the organic

solvent, the PNPs were collected by centrifugation and then freeze-dried. The size and size distribution were determined by DLS before freeze-drying.

As a starting point for controlling the nanoparticle size distribution, the effect of the organic solvent used in polymer solution was studied. Generally, the miscibility of the organic solvent in water can influence the mean particle size of PNPs, since the difference in solubility parameters between solvents is minimized with increasing miscibility. To evaluate the relationship between PNP size and solvent miscibility with water, three organic solvents (acetone, acetonitrile, tetrahydrofuran) were used for the preparation of Suc-PLGA-Chol PNPs and a dependence of their size on the solubility parameters was observed. As shown in Fig. 48, the mean particle size distribution of Suc-PLGA-Chol PNPs decreased with an increase of water miscibility, while maintaining all other experimental parameters constant. Smaller particles were obtained using the most water miscible solvent (acetone), which could be related to a more efficient solvent diffusion and faster polymer dispersion into water. In addition, a similar trend was observed for the polydispersity index. Under this light, acetone was chosen as the organic phase solvent.

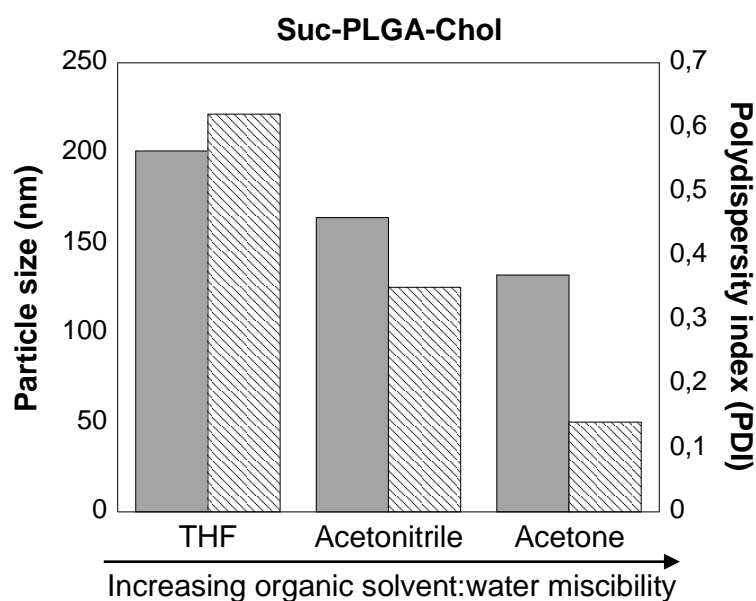


**Figure 48** Effect of varying the organic solvent in the particle size (grey bar) and PDI (striped bar) of Suc-PLGA-Chol PNPs obtained by nanoprecipitation.

In addition to the solvent effect, the influence of the evaporation rate on the mean particle size of PLGA and Suc-PLGA-Chol PNPs was also investigated. The results obtained for the mean particle size and particle size distribution (Table 13, Fig. 49) showed that evaporation under reduce-pressure resulted in the smallest particle size, suggesting that increasing the evaporation rate reduces the likelihood of PNP coalescence. The PNP size measurements demonstrated a homogeneous population characterized by a narrow size distribution, except for PLGA PNPs which exhibited a high PDI.

**Table 13** Effect of evaporation method in the mean particle size and PDI of PLGA and Suc-PLGA-Chol PNPs obtained by nanoprecipitation.

Polymer	Particle size (nm)	PDI	Particle size (nm)	PDI
	(vacuum evaporation)		(Atm. pressure evaporation)	
PLGA	96	0.47	132	0.13
Suc-PLGA-Chol <b>25</b>	132	0.14	203	0.20

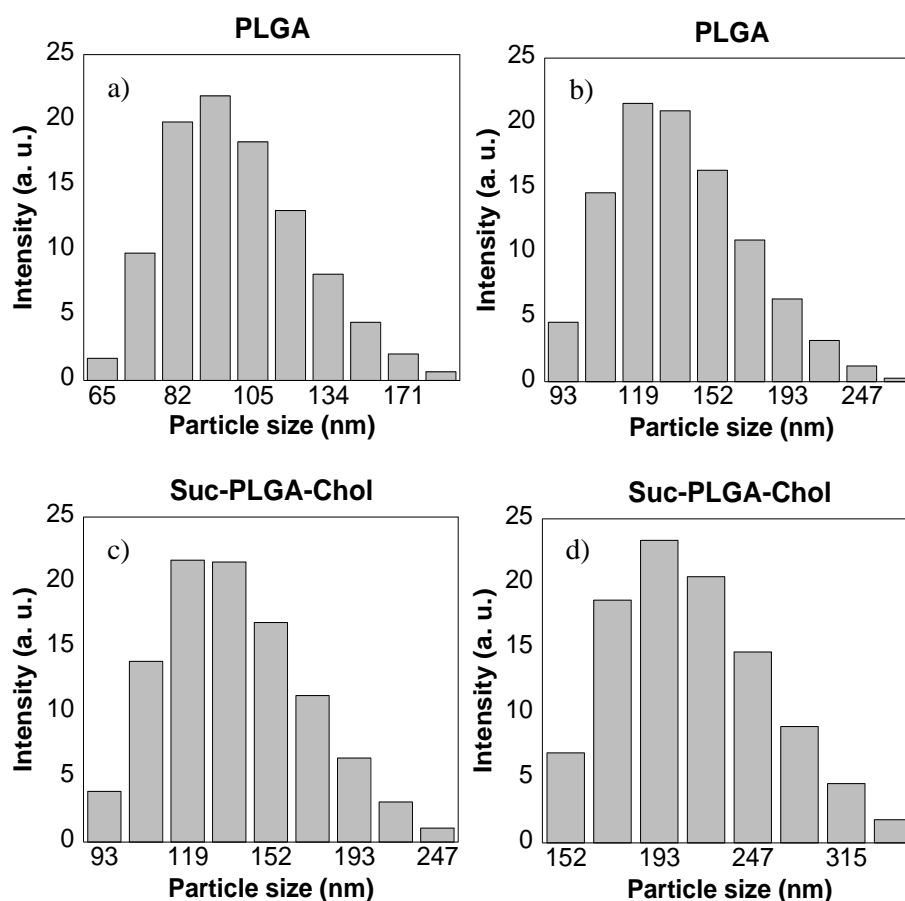


**Figure 49** Influence of the evaporation rate on the particle size distribution of PLGA and Suc-PLGA-Chol PNPs. Solvent evaporation method: a) and c) evaporation under reduce-pressure; b) and d) Atm. pressure evaporation.

The effect of initial polymer concentration on the PNP size distribution was also studied. It was evidenced (Fig. 50) that the mean particle size increased with increasing polymer concentration. This result is attributed to the increase in organic phase viscosity that leads to slower solvent diffusion and, consequently, to the formation of larger droplets during phase mixing. Following this, the stability of PLGA and Suc-PLGA-Chol PNP suspensions was investigated by  $\zeta$ -potential measurements. It was observed that both polymers yielded PNPs with negative  $\zeta$ -potential. PLGA PNPs had a negative surface charge of  $-12$  mV which can be attributed to the presence of end carboxyl groups of the polymer on the PNP surface. For Suc-PLGA-Chol PNPs the negative surface charge decreased to  $-28$  mV, thus

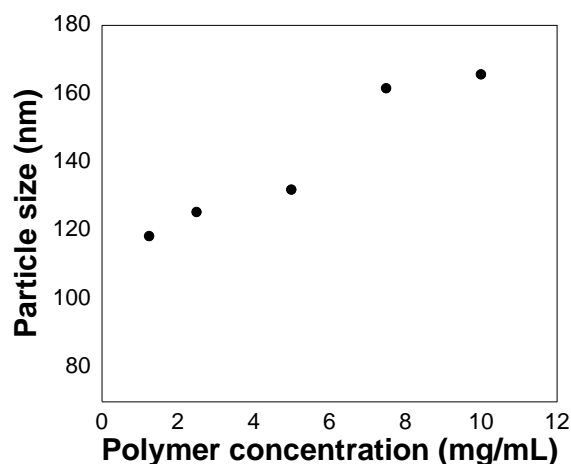


**Figure 50** Correlation of PNP mean particle size with Suc-PLGA-Chol polymer concentration obtained by nanoprecipitation. All the samples were brought to the same concentration before analyzed by DLS.

increasing the stability of the colloidal suspension. This may be attributed to the presence of hydroxyl groups from the sucrose moiety on the PNP surface. Experimental results reported in the literature showed contradictory results in which the conjugation of a galactose moiety to PLGA did not change significantly the  $\zeta$ -potential of free PLGA.<sup>147</sup>

The morphology of lyophilized PLGA and Suc-PLGA-Chol PNPs was investigated with SEM. With respect to the morphological properties of PLGA PNPs, SEM images showed that the particles were virtually perfect spheres (Fig. 51). However, the mean particle size (240 nm) was higher than the size determined with DLS before freeze-drying (96 nm). SEM micrographs also exhibited aggregates and coalescence of small nanoparticles. Lyophilized Suc-PLGA-Chol PNPs also exhibited the same behavior with a mean particle size of 260 nm (Fig. 52). This phenomenon of aggregation between PNPs observed in the SEM micrographs can be attributed to the growth by coalescence of PNPs resulting in larger particles. The DLS measurements before lyophilization showed a clean decay of the autocorrelation function and a low PDI, which indicates that the presence of aggregates in the suspensions was negligible. Thus, the aggregates seen in SEM could be attributed to the post-synthesis processing.

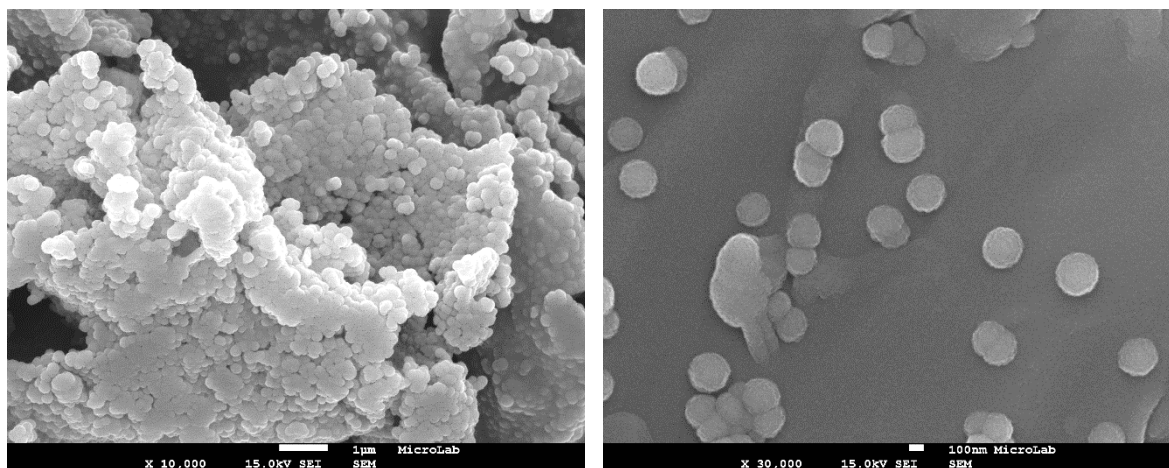


**Figure 51** SEM micrographs of lyophilized PLGA PNPs prepared by nanoprecipitation.

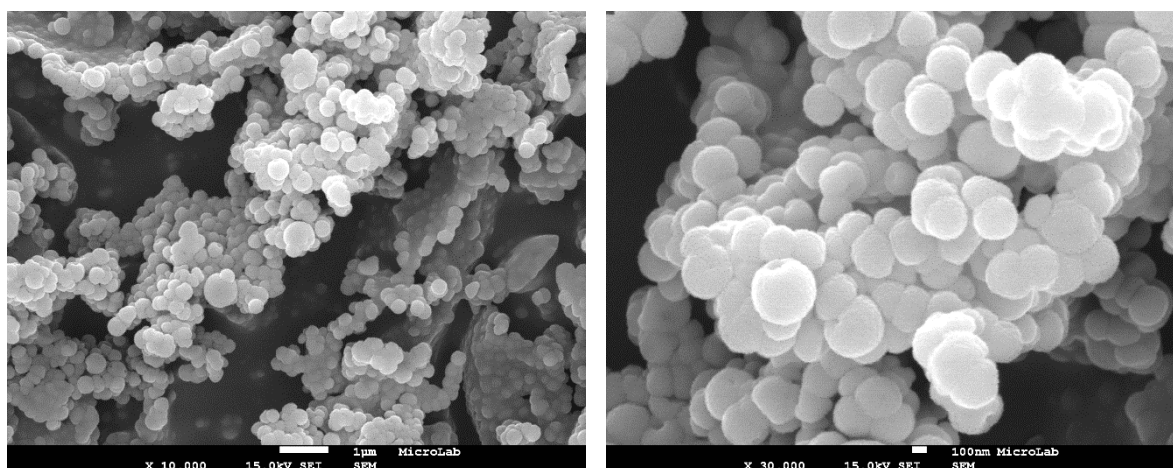


**Figure 52** SEM micrographs of lyophilized Suc-PLGA-Chol PNPs prepared by nanoprecipitation.

For Suc-PLGA-Chol polymer conjugates the effect of rhodamine b loading on resulting PNP size distributions were studied. The size distribution increases from approximately 130 nm to 167 nm and PDI of the particle preparations increased from 0.14 to 0.30 for PNPs loaded with 0.25 % rhodamine b. The formation of spherical particles were evidenced by SEM micrographs (Fig. 53). Though, as before the mean particle size was higher (400 nm) than the size measured by DLS previously to freeze-drying.

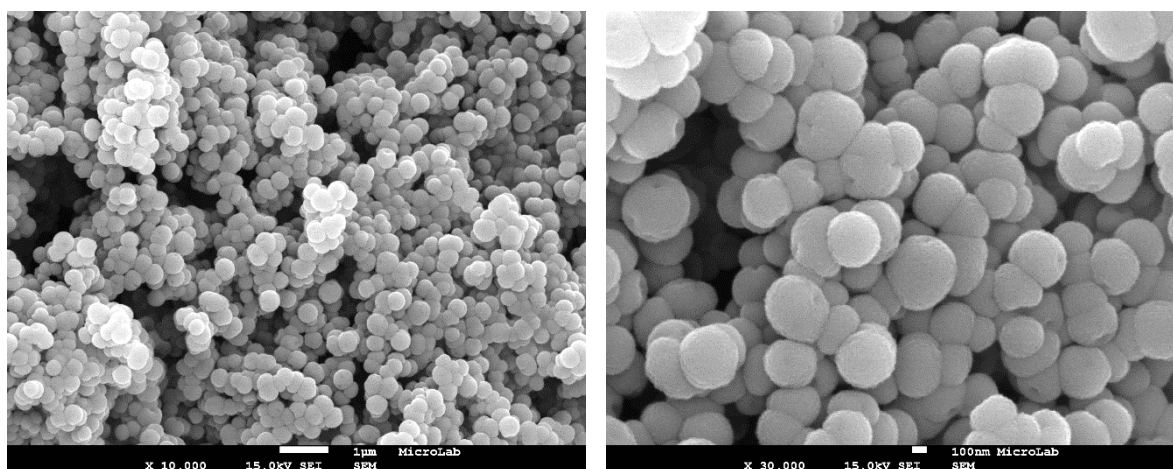


**Figure 53** SEM micrographs of lyophilized Suc-PLGA-Chol PNPs prepared by nanoprecipitation loaded with 0.25% rhodamine b.

As discussed above, during freeze-drying the concentration of the nanoparticles increases during time, which may induce aggregation and sometimes irreversible fusion of nanoparticles. In addition, the water crystallization induces a mechanical stress, which can change the nanoparticle morphological properties. Thus, it was hypothesized that the use of cryoprotectants could prevent particle aggregation and other morphological modifications during freeze-drying. Fonte *et al.* showed that glucose promoted less aggregation for PLGA PNPs.<sup>148</sup> Therefore, glucose was added to PLGA and Suc-PLGA-Chol PNP formulations before freeze-drying. For a cryoprotectant concentration of 10 % (w/w), the visualization by SEM of isolated particles was considerably difficult as the particles were embedded in the solid

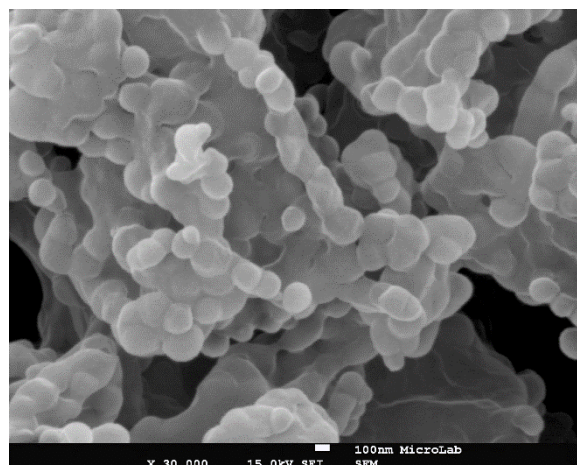


**Figure 54** SEM micrographs of lyophilized PLGA PNPs prepared by nanoprecipitation. The sample was freeze-dried in the presence of 10% (w/w) glucose as a cryoprotector.

matrix of the cryoprotectant. The results obtained from SEM analysis for the PLGA PNPs showed spherical particles with a mean diameter of 186 nm, which was still higher than the size measured by DLS previously to freeze-drying (Fig. 54).

Drying under vacuum over phosphorus pentoxide was also attempted as an alternative to lyophilization. Nevertheless, Suc-PLGA-Chol PNPs also showed the same aggregation behavior as previously mentioned with a mean particle size of 300 nm (Fig. 55). Therefore, it was evidenced that centrifugation step could also be responsible for the increase in particle size due to aggregation upon pelleting. However, purification by centrifugation is crucial to properly visualize the particles with SEM, as skipping the centrifugation step resulted in PNPs embedded in polymer matrix (similarly to what was observed for samples with cryoprotectant). Though, roughly spherical particles with a mean particle size ~124 nm were detected, which is in agreement with the size determined by DLS before freeze-drying (130 nm) (Fig. 56). Therefore, it was demonstrated that centrifugation step may affect the particle size of the PNPs. Contradictory conclusions have been obtained throughout the literature, where the aggregation behavior is mainly attributed to lyophilization. For all the PNP formulations, reconstitution of the lyophilized cakes was very hard to accomplish.

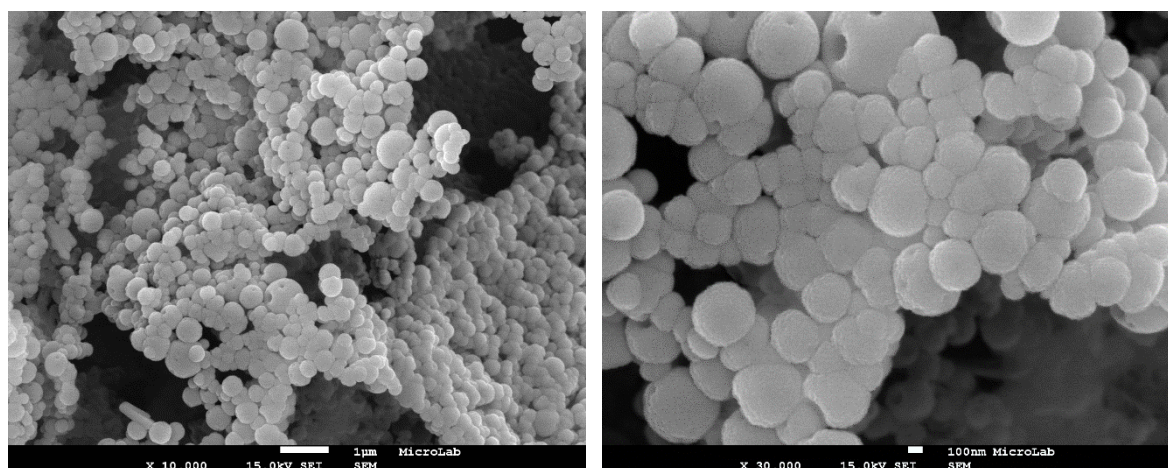


**Figure 55** SEM micrographs of lyophilized Suc-PLGA-Chol PNPs prepared by nanoprecipitation and dried under vacuum over phosphorus pentoxide as an alternative to freeze-drying.

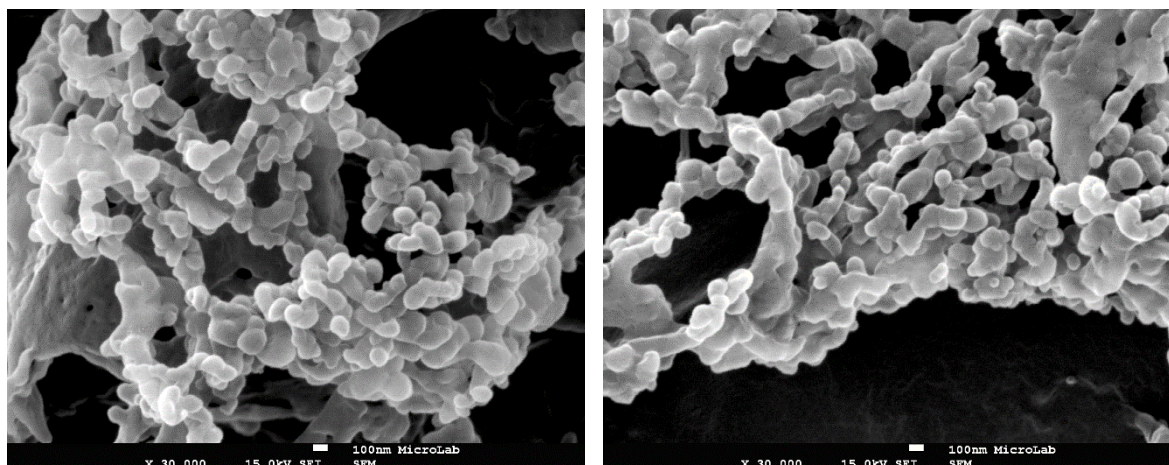


**Figure 56** SEM micrographs of lyophilized Suc-PLGA-Chol PNPs prepared by nanoprecipitation without purification by centrifugation.

### III.3 Conclusion

Sucrose- and cholic acid- modified PLGA PNPs were successfully prepared. The conjugates were synthesized by covalently binding of the appropriate sucrose and cholic acid derivatives to PLGA by esterification reaction. Due to the targeting function of sucrose, the PNPs are expected to enhance cellular uptake after tumor accumulation promoted by the EPR effect.

In order to select the adequate method which satisfies specific objectives in the nanoparticle design, the emulsion-solvent evaporation and nanoprecipitation techniques were chosen for preparing the PNPs. The influence of several processing parameters on particle size was investigated. It was concluded that the size of the PNPs could be adjust by modifying the organic solvent, evaporation method and concentration of the polymer in the organic phase. The smallest particle sizes were obtained using acetone and reduced-pressure evaporation method. (Table 14).  $\zeta$ -potential values were satisfactory and evidenced the importance of sucrose moiety on the polymeric system, which is responsible for the increase in the negative surface charge providing colloidal stability. On the other hand, it also indicated that the sucrose moiety is mainly present on the surface of PNPs, as designed.

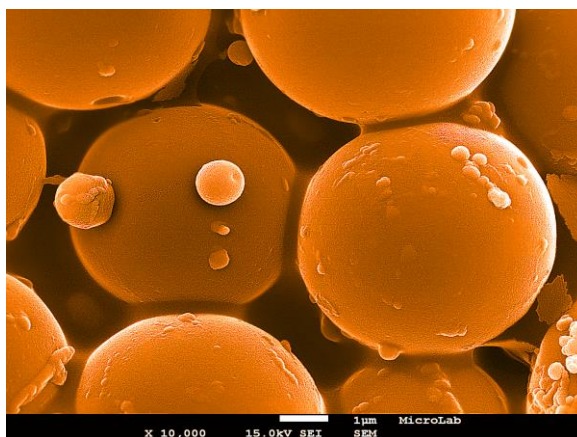
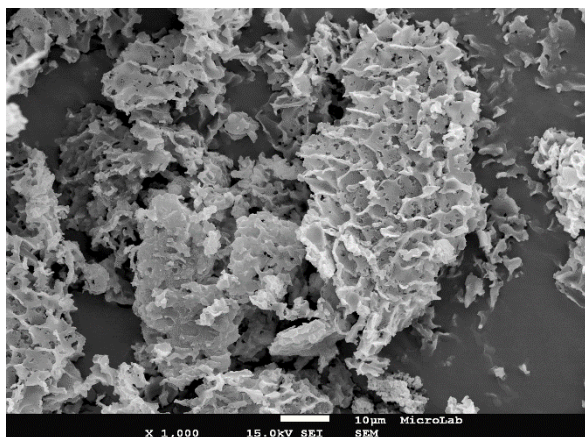
**Table 14** Physicochemical characteristics of the PLGA and Suc-PLGA-Chol PNPs obtained by nanoprecipitation and emulsion-solvent evaporation technique.

Polymer	Nanoprecipitation			Emulsion-solvent evaporation	
	Particle size (nm)	PDI	$\zeta$ -potential	Particle size (nm)	PDI
PLGA	96	0.47	-12	370	1.39
Suc-PLGA-Chol	132	0.14	-28	488	0.52

PNPs prepared by nanoprecipitation generally do not require surfactant. Though, its absence can cause PNP aggregation. For example, in SEM micrographs of PNPs prepared by the emulsion-solvent evaporation technique, the particles maintained their individuality, while for the nanoprecipitation method they formed agglomerates.

After PNP preparation, the processing conditions, such as centrifugation and freeze-drying, have shown to influence the particle size. Particularly, centrifugation can substantially increase particle size. As an alternative, the aggregation behavior can be avoided by low-speed ultrafiltration.

Aggregate formation resulting from nanoprecipitation highlights the limitations of this method. Regarding PLGA-based PNPs, the principal concern is the hydrolytic instability of the polymer in aqueous solutions. Thus, lyophilization, is a usual procedure to improve PLGA PNP stability during storage and maintain their physicochemical characteristics. As freeze-drying may also result in changes of PNP characteristics, different excipients, such as trehalose, sucrose, glucose, may be used as cryoprotecting agents, with the right formulation to protect PNPs and prevent their aggregation during freeze-drying.



## Chapter IV

### Synthesis of PLGA-PEG-based polymeric nanoparticles

*This chapter describes the preparation of polymeric nanoparticles from sucrose and cholic-functionalized PLGA-co-PEG diblock copolymers (abbreviated as Suc-PLGA-co-PEG-Chol). The chapter begins with nanomedicine's Fantastic Voyage through the advantage of PLGA block copolymers, focused on PEGylated polymers. This is followed by a discussion of the results obtained. The polymer was prepared by one-pot synthesis from the conjugation of the appropriate sucrose and cholic acid derivatives to PLGA-co-PEG by esterification. The preparation of PNPs was accomplished by nanoprecipitation. The first objective was to optimized PNP formulation by studying the influence of process variables on the mean particle size. In the second part the morphology, size distribution and surface charge of the PNPs were investigated by dynamic light scattering and scanning electron microscopy.*



## IV.1 Introduction

In the 1966 science fiction movie *Fantastic Voyage*, a team of surgeons board a submarine, which was then miniaturized down to microscopic size and inject it into a patient's bloodstream on a mission to destroy a life-threatening cerebral blood clot.<sup>149</sup> The crew had just one hour to save the life of the soviet scientist while avoiding our immune system. In real science, nanomedicine's *Fantastic Voyage* through drug delivery technologies is using nanoparticles as intravenous "submarines" to deliver drugs to specific parts of the body, at the right time and for the correct duration.<sup>4</sup>

Multifunctional nanoparticles are paid much attention for their site-specific targeting capacity and controlled release of therapeutic and diagnostic agents. A greater flexibility in the design of the polymeric matrix can lead to improved drug safety and efficacy and newer biophysicochemical properties. Recent developments in the biomaterial field have been focused in the use of biodegradable PNPs for drug delivery applications.<sup>139</sup> One of the most promising polymers has been PLGA due to its biocompatibility and resorbability through natural pathways.<sup>140</sup> Several innovative products made from this polymer are in clinical use today, such as PLGA-based nanoparticles, liposomes, microspheres and so on.<sup>140</sup> Despite its fine qualities, using PLGA PNPs for *in vivo* applications still remains an open challenge due to poor stability in water and rapid opsonization.<sup>150</sup> The need for better drug delivery formulations has resulted in the development of several types of PLGA block copolymers, because their physicochemical properties can be tuned by the type and molecular weight of the constitutive blocks.<sup>151</sup> One important strategy is to conjugate PLGA with PEG, producing diblock (PLGA-PEG) or triblock copolymers (PLGA-PEG-PLGA or PEG-PLGA-PEG), that have been used for preparing nanoparticles with well controlled surface properties.<sup>151</sup> This novel improvement in PLGA-based materials is attributed to PEG due to its stealth properties, where steric repulsions inhibits the fast recognition by the immune system, increasing blood circulation time.<sup>152</sup> For example, in model studies with mice, the liver had cleared only 30% of optimized formulation of PLGA-PEG nanoparticles. On the other hand, 66% of nanospheres made of PLGA were cleared in only 5 min.<sup>153</sup> Therefore, when designing PNPs for targeting applications, it is not only necessary to adjust the size, but also to prevent the opsonization phenomenon. PLGA-PEG block copolymers are known to undergo self-assembly into PNPs with a PLGA hydrophobic core and a PEG hydrophilic corona shell, reducing opsonization whilst maintaining the qualities of PLGA.

PLGA-PEG nanoparticles are well-established in the literature as nanocarriers for nanomedicine applications. Their drug-loading capacity and improvement of the circulation time are an important hallmark, which made this polymeric material highly attractive. Although, many efforts have still to be performed to improve not only the physicochemical properties, but also the distribution into tumor tissues, with the help of new and more specific targeting moieties.<sup>151</sup>

On these premises, the idea here was to develop an amphiphilic PLGA-PEG copolymer conjugated to a sucrose moiety as the targeting and stabilizing ligand and cholic acid as a site for drug incorporation. To prepare the sucrose and cholic acid conjugates a one-pot synthetic strategy was applied. It is believed that not every polymer chain needs to have the same targeting moieties. The important thing is to have enough targeting moieties on the PNP surface to trigger endocytosis after extravasation into the tumor.

## IV.2 Results and Discussion

### IV.2.1 One-pot synthesis of PLGA-*co*-PEG-based polymer conjugates

The Suc-PLGA-*co*-PEG-Chol polymer conjugates were synthesized by covalently binding of the appropriate sucrose and cholic acid derivatives to PLGA-*co*-PEG by esterification. Figure 57 shows a synthetic scheme of sucrose and cholic acid-derivatized PLGA-*co*-PEG polymers. The two conjugation steps can be accomplished in one pot. The pendant hydroxyl functional groups of PLGA-*co*-PEG were conjugated *via* an ester linkage to the carboxyl groups in sucrose **5** and cholic acid **10** derivatives, which were pre-activated by using NHS and DCC. This procedure led to a mixture of benzylated Suc-PLGA-*co*-PEG-Chol conjugates. In the succeeding step, debenzylation by Pd/C catalyzed hydrogenolysis in a solvent mixture of EtOH:AcOEt:H<sub>2</sub>O (7:7:0.1) and CH<sub>2</sub>Cl<sub>2</sub> to dissolve the polymer, gave the desired Suc-PLGA-*co*-PEG-Chol conjugates **27** in quantitative yield. The reactions took place by the same mechanistic pathway exemplified before for the DCC/NHS coupling reaction. Suc-PLGA-*co*-PEG-Chol **27** polymer conjugates were characterized by NMR spectroscopy as depicted in Fig. 58. A typical PLGA-*co*-PEG diblock copolymer <sup>1</sup>H-NMR spectrum was obtained with a characteristic peak in a multiplet at 5.1 – 5.4 ppm corresponding to the tertiary PLA proton, and another multiplet at 1.5 – 1.7 ppm for the pendant methyl group of the PLA chain. Furthermore, the integration ratio of those two characteristic peaks was 3:1, which is also a characteristic feature for the protons of

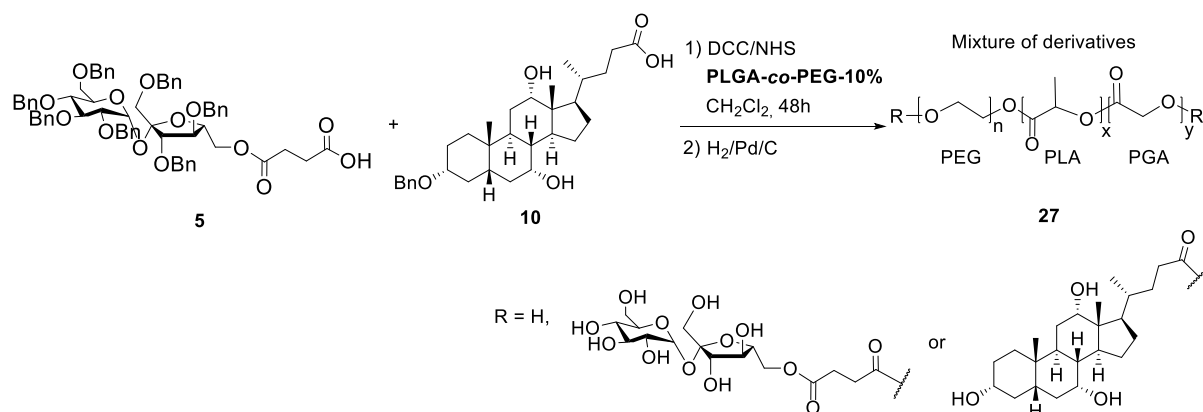


**Figure 57** Synthetic strategy for preparing the Suc-PLGA-*co*-PEG-Chol polymer conjugates.

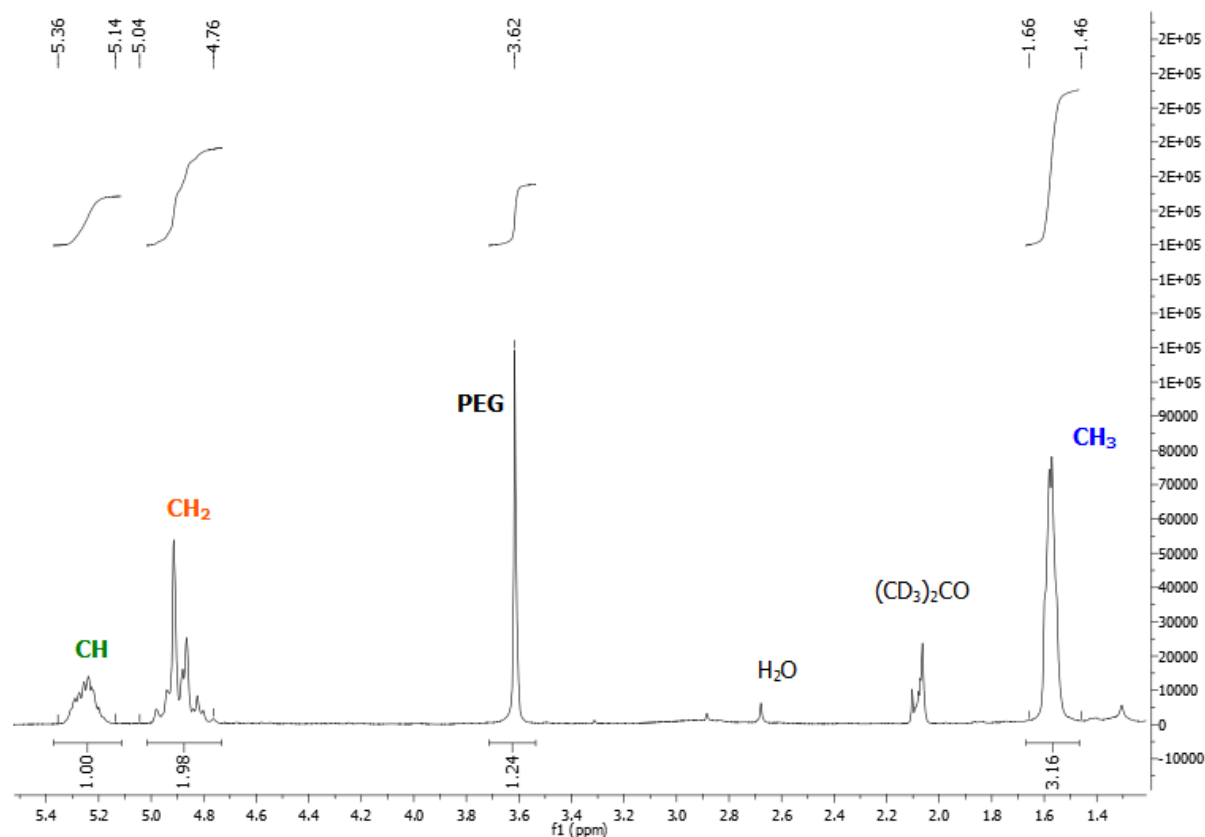


**Figure 58**  $^1\text{H}$ -NMR spectrum of Suc-PLGA-*co*-PEG-Chol **27** polymer conjugates.

PLA homopolymer. The peak corresponding to the methylene protons of the PGA units appeared at 4.76 – 5.04 ppm. While an additional peak could be seen at around 3.6 ppm corresponding to the protons of the repeating units in the PEG chain. Due to the lack of resolution, it was not possible to determine the amount of conjugated sucrose and cholic acid in thus obtained polymers by comparing the peak areas of the characteristic PLGA-*co*-PEG protons with the sucrose anomeric proton and the methyl protons of the cholic acid moiety. As before, the  $^{13}\text{C}$ -NMR spectra only shows the signals corresponding to PLGA-*co*-PEG diblock copolymer as the experiment is less sensitive than  $^1\text{H}$ -NMR spectroscopy.

The glass transition temperature ( $T_g$ ) of Suc-PLGA-*co*-PEG-Chol **27** polymer conjugates (29.83 °C) was slightly higher to that of pure PLGA-*co*-PEG diblock copolymer (26.81 °C), which indicates a small decrease in the flexibility of the polymer chain, probably due to the introduction of the cholic acid moiety.<sup>146</sup> The polymer displayed a  $T_g$  without any evidence of melting, suggesting that it is likely to be amorphous within this temperature range. As expected, the  $T_g$  of pure PLGA decreases with the introduction of PEG in the polymer structure. The decrease in  $T_g$  can be explained by the increased movement of the polymer chains, because the use of a plasticizer, like PEG, reduces the intermolecular forces.

## IV.2.2 Preparation and physicochemical characterization of PNPs

Colloidal suspensions of PNPs with a low polydispersity could be easily and reproducibly prepared from the synthesized PLGA-*co*-PEG derivatives by the previously described nanoprecipitation method. To improve the versatility of this technique, the influence of the solvent nature on the nanoparticle size was explored. Previous studies have suggested that the miscibility of the organic solvent in water can influence the PNP size for a given solvent: water system. Therefore, acetone, acetonitrile and THF were explored as organic solvents. As shown in Fig. 59, the sizes of Suc-PLGA-*co*-PEG-Chol PNPs and the water-miscibility of the three organic solvents used in this study were not correlated, despite contradictory reports found in the literature.<sup>151</sup> Nevertheless, the mechanisms mastering the self-assembling of amphiphilic polymer chains can be quite complex. Freshly prepared PNPs with THF as solvent, showed larger hydrodynamic diameter (136 nm) than the PNPs prepared with acetone (127 nm) and acetonitrile (117 nm). In addition, a similar trend was observed for the polydispersity index. Hence, acetonitrile was selected as the organic solvent as it produced PNPs of smaller size.

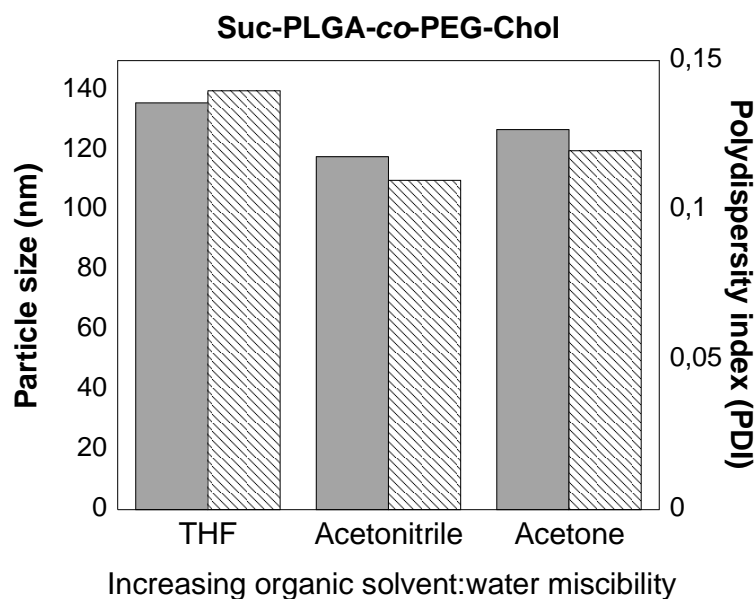


**Figure 59** Effect of varying the organic solvent in the particle size (grey bar) and PDI (striped bar) of Suc-PLGA-*co*-PEG-Chol PNPs obtained by nanoprecipitation.

The results of the physicochemical characteristics of the prepared PNPs are shown in Table 15 and Figure 60. For comparison, unsubstituted PLGA-*co*-PEG PNPs were also included as controls. Particle size distribution determined by DLS showed the unimodal distribution ( $PDI < 0.3$ ) with a size range of 110-130 nm for both PNP sets. As can be seen, the size of Suc-PLGA-*co*-PEG-Chol PNPs was slightly smaller than that of the control. This decrease in particle size was a first indication of the attachment of sucrose and cholic acid moieties to the polymer backbone. Differences on the surface of the PNPs can be estimated by measuring the surface charge. In the case of PLGA-*co*-PEG PNPs, these particles were negatively charge ( $\zeta$ -potential in the range of  $-15$  mV). For Suc-PLGA-*co*-PEG-Chol

PNPs the negative surface charge decreased to -46 mV, which combined with the low PDI was in favor of the stability and homogeneity of the colloidal suspensions. This trend is in agreement with the previous studies describing reductions in the  $\zeta$ -potential. This difference in the surface charge of the PNPs is the second evidence of the presence of sucrose and cholic acid moieties in the polymer backbone.

**Table 15** Size distribution and  $\zeta$ -potential of the PLGA-*co*-PEG and Suc-PLGA-*co*-PEG-Chol PNPs prepared by nanoprecipitation.

Polymer conjugates	Mean particle size (nm)	Polydispersity index (PDI)	Zeta potential (mV)
PLGA- <i>co</i> -PEG	125	0.120	-15
Suc-PLGA- <i>co</i> -PEG-Chol <b>27</b>	118	0.110	-46

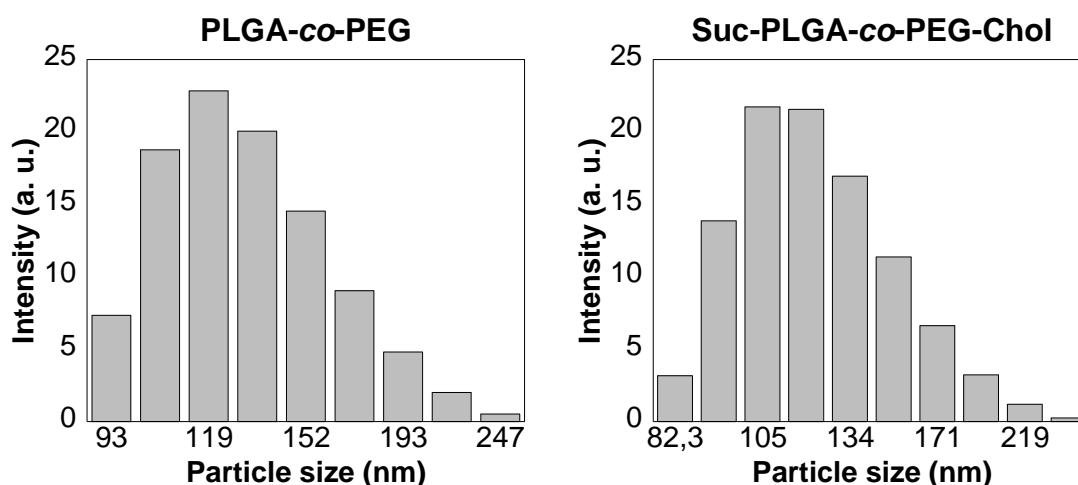


**Figure 60** Particle size distributions of PLGA-*co*-PEG and Suc-PLGA-*co*-PEG-Chol PNPs prepared by nanoprecipitation.

As shown in Fig. 61, the polymer concentration of the organic phase used during the nanoprecipitation process influenced the mean particle size of the PNPs. The increase in polymer concentration leads to a gradual increase in PNP diameters. This trend can be explained based on the

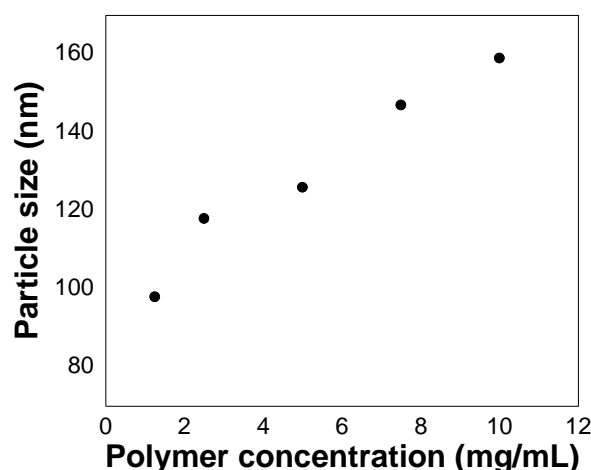


**Figure 61** Correlation of PNP mean particle size with Suc-PLGA-*co*-PEG-Chol polymer concentration, obtained by nanoprecipitation. All the samples were brought to the same concentration before measured by DLS.

viscosity of the dispersed phase. Commonly, an increase in the viscosity hinders solvent diffusion to the aqueous phase.

Particle size distribution data determined by DLS was also supplemented with a visual method such as SEM. SEM observations demonstrated that Suc-PLGA-*co*-PEG-Chol PNPs were regularly spherical with smooth surface (Figure 62). The particles were agglomerated, which was certainly caused by the centrifugation process. However, PLGA-*co*-PEG PNPs were hardly observed by SEM (Figure 63). The particles formed a film, similar to that observed previously for PEG-based PNPs.

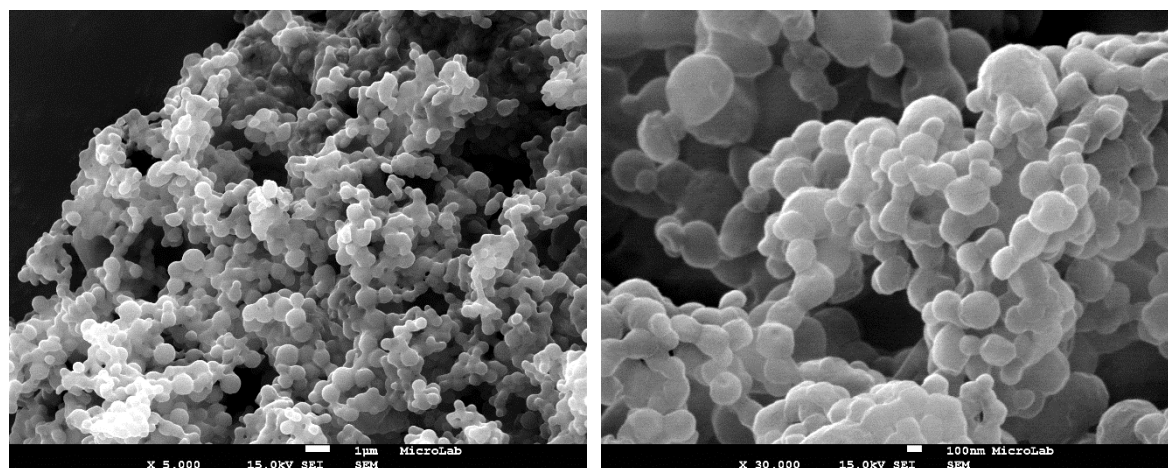


**Figure 62** SEM micrographs of lyophilized Suc-PLGA-*co*-PEG-Chol PNPs prepared by nanoprecipitation.

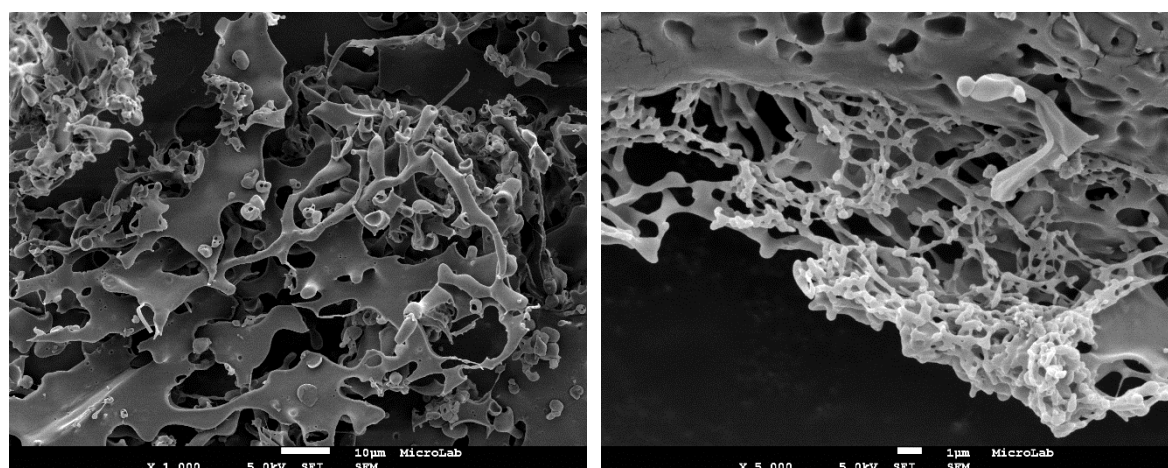


**Figure 63** SEM micrographs of lyophilized PLGA-*co*-PEG PNPs prepared by nanoprecipitation.

## IV.3 Conclusion

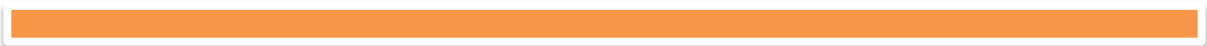
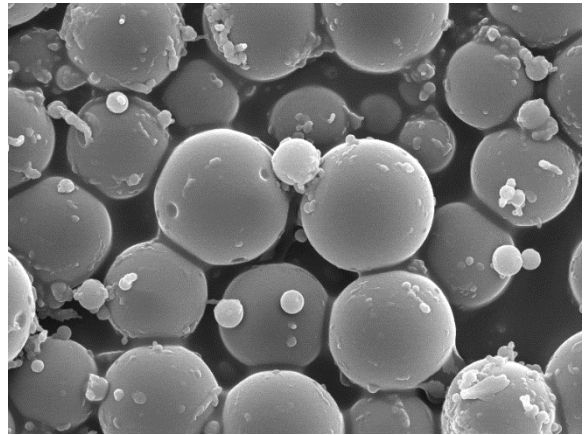
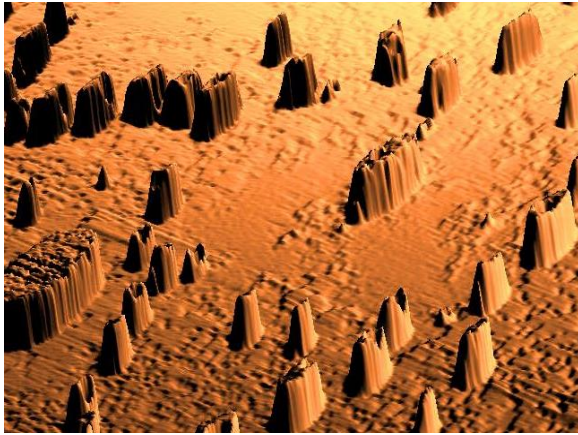
Sucrose and cholic acid modified PLGA-*co*-PEG PNPs were successfully prepared. The polymer conjugates were synthesized by covalently binding of the appropriate sucrose and cholic acid derivatives to PLGA-*co*-PEG by esterification. A one-pot synthesis strategy was applied to improve the efficiency of the coupling reaction. A PEGylated PLGA polymer was used in order to obtain a coating

that might prevent opsonization and recognition by the mononuclear phagocyte system. Due to interesting self-assembling properties, the amphiphilic nature of this diblock copolymer were used for the preparation of multifunctional nanoparticles.

From this study it may be concluded that stable colloidal suspensions with a very narrow size distribution can be prepared by nanoprecipitation. The mean diameter of freshly prepared PNPs was around 120 nm, which is suitable for drug delivery applications. In addition, the high  $\zeta$ -potential helps the formulations repel each other, which ensures long-term stability and avoids particle aggregation in solution.

It is expected that the outer PEG layer will provide an excellent stealth shield for the PNPs, while simultaneously the small size will permit the PNPs to reach tissues. These preliminary results are encouraging and must be considered as the basis for further extensive exploration of the potential of these PNPs for targeted drug delivery strategies.





# Chapter V

## Conclusions and Future Perspectives

---



Nanoparticles have a rich history filled with a wide variety of applications. Together with their applications, there are many challenges associated with nanoparticles and perhaps one of the most important challenges is the transition from lab-scale proof of concept research to reproducible with precisely physicochemical properties and high-yielding production of useful nanomaterials. This is a key point which is usually not addressed in the literature. Moreover, some nanomaterials will never reach clinical trials. This could be overcome, to some extent, if the regulatory requirements for clinical trials and the key features that make a polymer suitable for biological application (biodegradable, stable, non-cytotoxic and well characterized) were taken into account. In addition, the designed polymer must be cost-effective to produce as a nanomedicine.

Nanomedicine offers a great opportunity for improvement of current therapies and development of new treatment options for diseases previously thought difficult or impossible to treat. Although the research on pharmaceutical nanoparticles has been extensive during recent years and many nanomedicines are already in the market, a breakthrough of products to the market has not occurred so far.

Several methods have been extensively applied to fabricate PNPs. However, the size-distribution is usually very broad and mean particle size is not suitable for drug delivery applications. A new class of PNPs bearing a sucrose and a cholic acid moiety was synthesized in the present study from three different pre-formed polymers. The main focus of this thesis was in the physicochemical characterization of the nanoparticles and their dependence on the processes parameters. PNPs were successfully prepared by the nanoprecipitation technique, which proved to be the best preparation method. It offered the advantages of simple and gentle formulation under room temperature without the use of stabilizers or harsh formulation processes. In PNPs prepared by emulsion-solvent evaporation technique both the size and PDI values were higher. The PNPs developed in this thesis by nanoprecipitation, had a small and appropriate size around 100 nm, a low PDI and a high negative surface charge, which ensures long-term stability and avoids particle aggregation. It is worth noting that, despite the polymer used to formulate the PNPs, under the same experimental formulation conditions, these have nearly the same size.

Polymer conjugates	Nanoprecipitation		
	Particle size (nm)	PDI	$\zeta$ -potential
Suc-PEG2000-Chol <b>17</b>	117	0.169	-26
Suc-PEG4000-Chol <b>18</b>	96	0.280	-19
Suc-PEG6000-Chol <b>19</b>	219	0.140	-12
Suc-PLGA-Chol <b>25</b>	132	0.140	-28
Suc-PLGA-co-PEG-Chol <b>27</b>	117	0.110	-46

Applying different characterization methods, notably AFM, SEM, and DSC, changes in the physicochemical characteristics of the PNPs influenced by the preparation process were detected. More detailed information was found in AFM and SEM images, which demonstrated that all these PNPs were regularly spherical.

Throughout this thesis, the results implied that PLGA-based PNPs conjugated with sucrose and cholic acid moieties, could be a promising drug carrier. Future works are required to investigate the cellular uptake of the obtained PNPs *in vitro* and *in vivo*. Nevertheless, this study opens the possibility to incorporate sucrose moieties in polymeric structures and benefit not only from the targeting function but also from the interesting properties sucrose provides to PNPs physical properties. In addition, the presence of reactive functional groups in sucrose and cholic acid offers great opportunity for chemical modification which affords the possibility for incorporating additional therapeutic and diagnostic moieties.

When designing PNPs for targeting applications, it is not only necessary to adjust the size, but also to prevent the opsonization phenomenon. In this thesis, this was accomplished by the use of PLGA-*co*-PEG diblock copolymers in which the PEG moiety provided the stealth behavior. However, it is known that although well tolerated clinically, PEG is non-biodegradable in the main-chain.

Polysaccharides are nowadays recognized for having high potential in the development of long-circulating systems. In addition, sugars have a very attractive biocompatibility, biodegradability and non-toxicity. Furthermore, surface tailoring of PNPs with living polymerization techniques allows access to complex polymeric matrices. Among these, reversible addition-fragmentation chain transfer (RAFT) polymerization, has proven to be a versatile tool for generating several functional polymers, from which well-defined particles can be obtained.

Glycosylated nanoparticles and their binding ability may allow for novel applications in carbohydrate-ligand mediated targeted drug delivery. In addition, glyconanoconjugates will emerge as good glycomimetic models in carbohydrate-mediated biological processes, with greatly improved binding properties and thus promising for biomedical applications. In addition, tumors are characterized by highly glycosylated cell surfaces. Therefore, carbohydrate polymer conjugates may become an essential aspect of nanoparticle design, enhancing both targeting and diagnostics.

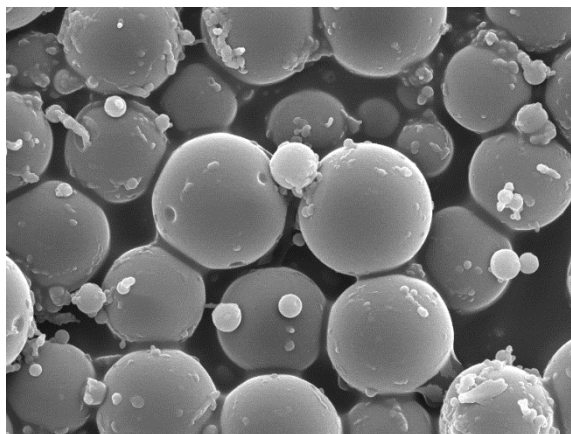
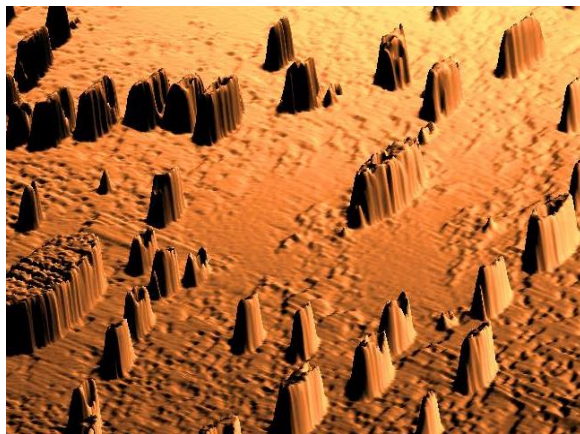
A deep understanding on how the material properties affect the PNPs behavior *in vitro* and *in vivo* will undoubtedly promote the rapid expansion of new applications of nanomedicine for innovative treatment strategies. During this investigation, much attention was paid to the inherent relationship between the molecular structure and the physicochemical characteristics of the PNPs. For instance, the molecular structure of the polymer will regulate the polymer self-assemble, rendering different physicochemical properties and a hydrophilic surface need to be considered upfront.

The combination of nanotechnology and polymers will be enormously useful in near-term medical applications, generating materials with unique properties. Stimuli-responsive PNPs may exhibit synergistic properties due to the combination of a polymeric matrix and a stimulus ingredient. In multi-

responsive systems the conjugation of polymers with different properties could form novel conjugates having the combined properties of its individual components, in which the different molecular segments act cooperatively.

Finally, as Robert Langer said in 2003 in a publication entitled "*Where a pill won't reach*", we will still be looking for a day when any drug can be administered at the right time, at the right dose, for the correct duration, anywhere in the body with specificity and efficiency. Maybe the future still holds implantable microchips that deliver drugs in preprogrammed doses and that connect with computers in physician's offices.





---

# Chapter VI

## Experimental Part

---

*The first half of this chapter describes the materials and reagents used in this research and the synthetic methods. The equipment is listed along with the model and type of apparatus used. The second half of the chapter covers the techniques that have been used to synthesize and characterize the polymeric nanoparticles produced.*



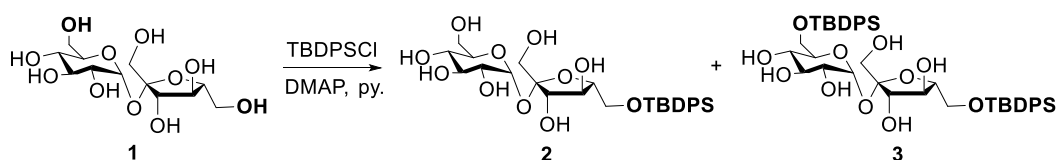
## VI.1 Materials and Instruments

All chemicals were purchased from the Aldrich Chemical Company and used without further purification. PEG2000, PEG4000 and PEG6000 were supplied from Aldrich and dried over  $P_2O_5$  in vacuum to remove the residual water. PLGA with a weight-average molecular weight of 40 000-75 000, whose copolymer ratio of lactide to glycolide is 75:25 was purchased from Sigma Aldrich. PLGA-*co*-PEG 10%-diblock (Mw ~ 600000) was purchased from Resormer. All solvents were distilled prior to use from an appropriate drying agent by standard procedures.<sup>154</sup>  $CH_2Cl_2$  was freshly distilled from CaH. DMF was dried overnight over BaO followed by decantation and vacuum distillation. THF was refluxed over sodium wire and benzophenone until it acquired a violet colour and pyridine was distilled twice from KOH. Anhydrous  $Na_2SO_4$  was used to dry organic extracts. Organic solvents were evaporated using a rotary evaporator under reduced pressure at 40°C. Unless otherwise noted, all non-aqueous reactions were carried out under dry argon atmosphere. Reactions were monitored by analytical thin layer chromatography (TLC) on commercially available precoated aluminium plates (Merck Kieselgel 60 F<sub>254</sub>) and compounds were detected by using a UV lamp ( $\lambda_{max} = 254$  nm) and/or staining with a solution of concentrated  $H_2SO_4/MeOH$  2:8 or with a solution of phosphomolybdic acid (5 g) in EtOH (95 mL) and subsequent heating. Flash Chromatography columns were prepared with silica gel from Macherey-Nagel (Kieselgel 60 M). Infrared spectra were recorded using a Perkin Elmer Spectrum FT-IR spectrophotometer in the range of 4000 – 500  $cm^{-1}$  using KBr and NaCl discs. Transmittance maxima ( $\nu_{max}$ ) are reported in wave-numbers ( $cm^{-1}$ ) and classified as strong (s), medium (m) or broad (br). Optical rotations were measured on an Optical Activity AA-1000 polarimeter at 589 nm and values are given in units of  $10^{-1}deg.cm^3.g^{-1}$  at 20 °C. Melting points were measured on an Electrothermal capillary melting point apparatus or by DSC on a Setaram DSC 131 scanning calorimeter equipped with a thermal analysis data system. Hydrogenation reactions were performed in a Parr Shaker apparatus. Elemental analyses were performed on Thermo Finnigan-CE Flash EA 1112 CHNS series analyzer. Mass spectra were measured by matrix-assisted laser desorption ionization time-of-flight (MALDI-TOF) on a Bruker Autoflex with  $\alpha$ -cyano-4-hydroxycinnamic acid (4-HCCA) matrix. Differential scanning calorimetry (DSC) measurements were carried out on a Setaram DSC 131 scanning calorimeter equipped with a thermal analysis data system. Samples of 10 mg were placed in aluminum pans and sealed. The probes were heated from -130 °C to 100 °C at a rate of 10 °C/min under nitrogen atmosphere.  $^1H$  NMR resonance ( $\delta^H$ ) and  $^{13}C$  NMR ( $\delta^C$ ) spectra were recorded on a Bruker AMX-400 instrument operating at 400 MHz for  $^1H$  nuclei and 100 MHz for  $^{13}C$  nuclei.  $CDCl_3$  (99.50 % isotopic purity),  $DMSO-d_6$  (99.80 % isotopic purity) and  $D_2O$  (99.9 % isotopic purity) were purchased from Aldrich. Chemical shifts ( $\delta$ ) are reported in parts per million (ppm), using TMS as internal standard. Signals were recorded in terms of chemical shifts and are expressed in ppm ( $\delta$ ), multiplicity, coupling constants (in Hz), integration, and assignments in that order. Coupling constants ( $J$ ) are reported in Hertz (Hz).

## VI.2 Synthesis and characterization of polymer conjugates

### VI.2.1 Chemoselective derivatization of the 6' position of the sucrose

#### VI.2.1.1 6'-*O*-*tert*-butyldiphenylsilyl-sucrose (2)



To a solution of sucrose **1** (5.0 g, 15 mmol, 1.0 eq) in dry pyridine (80 mL) was added *tert*-butyldiphenylsilyl chloride (3.8 mL, 15 mmol, 1.0 eq) and a catalytic amount of DMAP (98 mg, 0.75 mmol, 0.05 eq). The reaction mixture was then left to stir at room temperature for 2 hours until the less polar 6,6'-di-*O*-*tert*-butyldiphenylsilyl-sucrose **3** appeared (*R<sub>f</sub>* 0.49, ethyl acetate/acetone/water 10:10:1). The solvent was evaporated to yield a viscous residue, which was purified by column chromatography with ethyl acetate/acetone/water (gradient from 100:100:1 to 10:10:1) to afford **2** as a white solid foam. Recrystallization from ethyl acetate resulted in the formation of white needles of **2** (4.0 g, 6.91 mmol, 46 %). 6,6'-di-*O*-*tert*-butyldiphenylsilyl-sucrose **3** was obtained as a byproduct (2.8 g, 3.45 mmol, 23 %) along with the starting material **1** recovered (1.3 g, 3.9 mmol, 26 %).

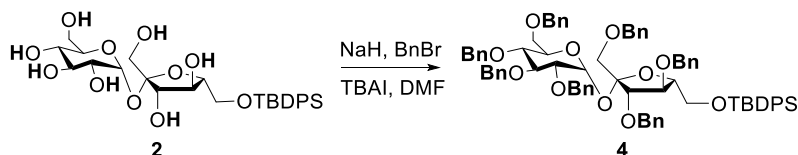
#### 6'-*O*-*tert*-butyldiphenylsilyl-sucrose (2)

**R<sub>f</sub>** 0.37 (ethyl acetate/acetone/water 10:10:1). **[α]<sub>D</sub><sup>20</sup>** + 44.4 (*c* 1, MeOH) (lit.<sup>121</sup> **[α]<sub>D</sub><sup>20</sup>** + 44.0 (*c* 1, MeOH)). **m.p.** 193 - 194 °C (AcOEt) (lit.<sup>121</sup> 192 - 195 °C). **FT-IR** (KBr) **ν<sub>max</sub>** (cm<sup>-1</sup>): 3355 (br, O-H), 3054 (m, C-H<sub>arom</sub>), 2930 (s, C-H<sub>stad</sub>), 2817 (s, C-H<sub>stad</sub>), 1428 (s, Si-C<sub>6</sub>H<sub>5</sub>), 1265 (m, Si-C), 1113 (m, Si-C<sub>6</sub>H<sub>5</sub>), 1061 (m, C-O-C), 1035 (m, C-O), 738 (s, C-H<sub>arom</sub>), 705 (s, C=C<sub>arom</sub>). **<sup>1</sup>H NMR** (DMSO-*d*<sub>6</sub>): δ 7.71 - 7.59 (m, 4H, Ph-**H**), 7.47 - 7.36 (m, 6H, Ph-**H**), 5.26 - 5.20 (m, 2H, H-1, **HO-C<sub>4'</sub>**), 4.95 (d, *J* = 6.6 Hz, 1H, **HO-C<sub>2</sub>**), 4.85 (t, *J* = 6.2 Hz, 1H, **HO-C<sub>1'</sub>**), 4.76 - 4.68 (m, 2H, **HO-C<sub>3</sub>**, **HO-C<sub>4</sub>**), 4.52 (d, *J* = 8.1 Hz, 1H, **HO-C<sub>3'</sub>**), 4.20 (t, *J* = 5.2 Hz, 1H, **HO-C<sub>6</sub>**), 3.91 - 3.86 (m, 2H, H-3', H-6'<sub>a</sub>), 3.81 - 3.76 (m, 2H, H-4', H-6'<sub>b</sub>), 3.70 - 3.66 (m, 1H, H-5'), 3.65 - 3.56 (m, 1H, H-5), 3.51 - 3.32 (m + DMSO-*d*<sub>6</sub>, 5H, H-3, H-6, H-1'), 3.16 - 3.01 (m, 2H, H-2, H-4), 0.97 (s, 9H, -C(CH<sub>3</sub>)<sub>3</sub>). **<sup>13</sup>C NMR** (DMSO-*d*<sub>6</sub>): δ 135.59 (C-H<sub>meta</sub>(Ph)), 135.55 (C-H<sub>meta</sub>(Ph)), 133.67 (C(Ph)), 133.65 (C(Ph)), 130.19 (C-H<sub>para</sub>(Ph)), 130.17 (C-H<sub>para</sub>(Ph)), 128.31 (C-H<sub>ortho</sub>(Ph)), 128.28 (C-H<sub>ortho</sub>(Ph)), 104.89 (C2'), 92.02 (C1), 82.64 (C5'), 77.24 (C3'), 74.98 (C4'), 73.53 (C3), 73.09 (C5), 72.15 (C2), 70.49 (C4), 66.07 (C6'), 62.55 (C-1'), 61.23 (C-6), 27.18 (-C(CH<sub>3</sub>)<sub>3</sub>), 19.32 (-C(CH<sub>3</sub>)<sub>3</sub>).

### 6,6'-di-*O-tert*-butyldiphenylsilyl-sucrose (3)

**Rf** 0.49 (ethyl acetate/acetone/water 10:10:1).  $[\alpha]_D^{20} + 28$  (*c* 1, MeOH) (lit.<sup>121</sup>  $[\alpha]_D^{20} + 26$  (*c* 1, MeOH)). **m.p.** 210 - 212 °C (AcOEt) (lit.<sup>121</sup> 212 - 213 °C). **FT-IR** (KBr)  $\nu_{\max}$  (cm<sup>-1</sup>): 3398 (br, O-H), 3054 (m, C-H<sub>arom</sub>), 2928 (s, C-H<sub>stad</sub>), 2884 (s, C-H<sub>stad</sub>), 1426 (s, Si-C<sub>6</sub>H<sub>5</sub>), 1265 (m, Si-C), 1112 (m, Si-C<sub>6</sub>H<sub>5</sub>), 1063 (m, C-O-C), 1043 (m, C-O), 739 (s, C-H<sub>arom</sub>), 705 (s, C=C<sub>arom</sub>). **<sup>1</sup>H NMR** (DMSO-*d*<sub>6</sub>):  $\delta$  7.68 – 7.53 (m, 8H, Ph-H), 7.44 – 7.25 (m, 12H, Ph-H), 5.32 (d, *J* = 3.4 Hz, 1H, H-1), 5.16 (d, *J* = 5.8 Hz, 1H, HO-C<sub>4'</sub>), 5.06 (d, *J* = 6.6 Hz, 1H, HO-C<sub>2</sub>), 4.89 – 4.79 (m, 3H, HO-C<sub>1'</sub>, HO-C<sub>3</sub>, HO-C<sub>4</sub>), 4.52 (d, *J* = 8.2 Hz, 1H, HO-C<sub>3'</sub>), 3.95 (t, *J* = 7.9 Hz, 1H, H-3'), 3.87 – 3.62 (m, 7H, H-5, H-6, H-4', H-5', H-6'), 3.56 – 3.43 (m, 3H, H-3, H-1'), 3.40 – 3.33 (m + DMSO-*d*<sub>6</sub>, H-4), 3.20 – 3.15 (m, 1H, H-2), 0.93 (s, 9H, -C(CH<sub>3</sub>)<sub>3</sub>), 0.91 (s, 9H, -C(CH<sub>3</sub>)<sub>3</sub>). **<sup>13</sup>C NMR** (DMSO-*d*<sub>6</sub>):  $\delta$  135.12 (C-H<sub>meta</sub>(Ph)), 135.07 (C-H<sub>meta</sub>(Ph)), 135.05 (C-H<sub>meta</sub>(Ph)), 135.00 (C-H<sub>meta</sub>(Ph)), 133.41 (C(Ph)), 133.11 (C(Ph)), 133.02 (C(Ph)), 129.63 (C-H<sub>para</sub>(Ph)), 129.62 (C-H<sub>para</sub>(Ph)), 129.56 (C-H<sub>para</sub>(Ph)), 129.53 (C-H<sub>para</sub>(Ph)), 127.77 (C-H<sub>ortho</sub>(Ph)), 127.73 (C-H<sub>ortho</sub>(Ph)), 127.67 (C-H<sub>ortho</sub>(Ph)), 127.64 (C-H<sub>ortho</sub>(Ph)), 104.85 (C2'), 92.08 (C1), 82.20 (C5'), 76.91 (C3'), 74.94 (C4'), 73.07 (C3), 72.58 (C5), 71.76 (C2), 69.43 (C4), 65.59 (C6'), 63.14 (C-6), 61.88 (C-1'), 26.63 (-C(CH<sub>3</sub>)<sub>3</sub>), 26.55 (-C(CH<sub>3</sub>)<sub>3</sub>), 18.86 (-C(CH<sub>3</sub>)<sub>3</sub>), 18.78 (-C(CH<sub>3</sub>)<sub>3</sub>).

### VI. 2.1.2 1',2,3,3',4,4',6-Hepta-*O*-benzyl-6'-*O-tert*-butyldiphenylsilyl sucrose (4)



6'-*O-tert*-butyldiphenylsilyl-sucrose **2** (2.5 g, 4.2 mmol, 1.0 eq) was dissolved in dry DMF (20 mL) together with a catalytic amount of TBAI (78 mg, 0.21 mmol, 0.05 eq). The solution was cooled to 0 °C and NaH (1.9 g, 47 mmol, 60 wt. % dispersion in mineral oil, 11.2 eq) was added carefully over which time a grey gel was formed and the reaction ceased to stir. The reaction mixture was diluted with an additional portion of DMF (5 mL) and after stirring for 15 min. benzyl bromide (7.35 mL, 58.8 mmol, 14 eq) was added dropwise. The temperature was allowed to rise to r.t.. After stirring for 3 h, ice was added to the cooled suspension, followed by extractions with ethyl ether (2 x 50 mL). The organic extracts were dried (Na<sub>2</sub>SO<sub>4</sub>) and the solvent evaporated to yield a yellowish oil. Purification by column chromatography (hexane/ethyl acetate 5:1) afforded **4** (4.43 g, 3.65 mmol, 87 %) as a colorless oil. **Rf** 0.39 (hexane/ethyl acetate 5:1).  $[\alpha]_D^{20} + 31.6$  (*c* 1, CHCl<sub>3</sub>) (lit.<sup>120</sup>  $[\alpha]_D^{20} + 30.9$  (*c* 0.9, CHCl<sub>3</sub>)). **FT-IR** (NaCl)  $\nu_{\max}$  (cm<sup>-1</sup>): 2929 (s, C-H<sub>stad</sub>), 2858 (s, C-H<sub>stad</sub>), 1642 (m, C=C-H), 1454 (s, Si-C<sub>6</sub>H<sub>5</sub>), 1362 (m, C-H<sub>stad</sub>), 1265 (m, Si-C), 1091 (m, C-O-C), 1027 (m, C-O), 909 (s, C-H<sub>arom</sub>), 740 (s, C=C<sub>arom</sub>). **<sup>1</sup>H NMR** (DMSO-*d*<sub>6</sub>):  $\delta$  7.65 – 7.55 (m, 4H, Ph-H), 7.41 – 7.08 (m, 41H, Ph-H), 5.65 (d, *J* = 2.8 Hz, 1H, H-1), 4.76 – 4.27 (m, 14H, H-5', CH<sub>2</sub>-Ph), 4.25 – 4.14 (m, 2H, H-4', CH<sub>2</sub>-Ph), 3.97 – 3.83 (m, 4H, H-5, H-

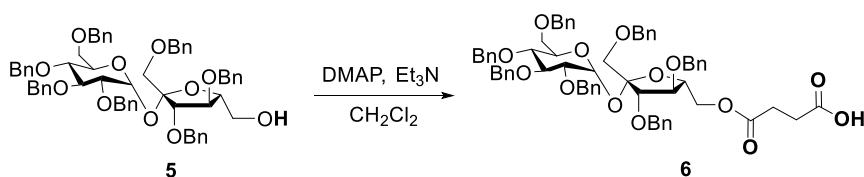
6', H-3'), 3.74 – 3.64 (m, 2H, H-3, H-1'a), 3.52 (d,  $J = 10.9$  Hz, 1H, H-1'b), 3.45 (t,  $J = 9.5$  Hz, 1H, H-4), 3.40 – 3.30 (m + DMSO- $d_6$ , 2H, H-2, H-6a), 3.26 (d,  $J = 10.4$  Hz, 1H, H-6b), 0.97 (s, 9H, -C(CH<sub>3</sub>)<sub>3</sub>). <sup>13</sup>C NMR (DMSO- $d_6$ ):  $\delta$  139.22 (C(Ph)), 138.90 (C(Ph)), 138.73 (C(Ph)), 138.61 (C(Ph)), 138.54 (C(Ph)), 138.49 (C(Ph)), 138.44 (C(Ph)), 135.56 (C-H<sub>meta</sub>(Ph)<sub>TBDPS</sub>), 135.48 (C-H<sub>meta</sub>(Ph)<sub>TBDPS</sub>), 133.29 (C(Ph)<sub>TBDPS</sub>), 133.10 (C(Ph)<sub>TBDPS</sub>), 130.31 (C-H<sub>para</sub>(Ph)<sub>TBDPS</sub>), 130.26 (C-H<sub>para</sub>(Ph)<sub>TBDPS</sub>), 128.71 (C-H(Ph)), 128.63 (C-H(Ph)), 128.58 (C-H(Ph)), 128.32 (C-H(Ph)), 128.27 (C-H(Ph)), 128.17 (C-H(Ph)), 128.15 (C-H(Ph)), 128.02 (C-H(Ph)), 127.92 (C-H(Ph)), 127.89 (C-H(Ph)), 127.81 (C-H(Ph)), 104.65 (C2'), 89.51 (C1), 83.81 (C5'), 82.20 (C4'), 81.72 (C3), 81.35 (C3'), 79.85 (C2), 77.72 (C4), 74.90 (CH<sub>2</sub>-Ph), 74.32 (CH<sub>2</sub>-Ph), 72.96 (CH<sub>2</sub>-Ph), 72.83 (CH<sub>2</sub>-Ph), 72.51 (CH<sub>2</sub>-Ph), 71.92 (CH<sub>2</sub>-Ph), 71.34 (C1'), 70.71 (C5), 68.95 (C6), 65.24 (C6'), 27.07 (-C(CH<sub>3</sub>)<sub>3</sub>), 19.22 (-C(CH<sub>3</sub>)<sub>3</sub>).

### VI. 2.1.3 1',2,3,3',4,4',6-Hepta-*O*-benzyl-sucrose (**5**)



To a solution of **4** (5.1 g, 4.25 mmol, 1.0 eq) in THF (50 mL) was added TBAF (5.5 mL, 5.5 mmol, 1.3 eq). The reaction was stirred at r.t. overnight. The evaporation of the solvent gave a yellowish residue that was purified by column chromatography (hexane/ethyl acetate 3:1), to yield **5** (3.89 g, 3.99 mmol, 94 %) as a colorless oil. **R<sub>f</sub>** 0.38 (hexane/ethyl acetate 3:1).  $[\alpha]_D^{20} + 53.6$  ( $c$  1, CHCl<sub>3</sub>) (lit.<sup>120</sup>  $[\alpha]_D^{20} + 46.12$  ( $c$  1.34, CHCl<sub>3</sub>)). **FT-IR** (NaCl)  $\nu_{\max}$  (cm<sup>-1</sup>): 3063 (m, C-H<sub>arom</sub>), 3030 (m, C-H<sub>arom</sub>), 2918 (s, C-H<sub>stad</sub>), 2865 (s, C-H<sub>stad</sub>), 1496 (m, C=C-H), 1453 (m, C=C-H), 1362 (m, C-H<sub>stad</sub>), 1091 (m, C-O-C), 1027 (m, C-O), 910 (s, C-H<sub>arom</sub>), 736 (s, C-H<sub>arom</sub>), 698 (s, C=C<sub>arom</sub>). <sup>1</sup>H NMR (DMSO- $d_6$ ):  $\delta$  7.39 – 7.11 (m, 35H, Ph-H), 5.67 (d,  $J = 2.9$  Hz, 1H, H-1), 4.82 – 4.35 (m, 14H, CH<sub>2</sub>-Ph), 4.31 (d,  $J = 7.2$  Hz, 1H, H-5'), 4.06 (t,  $J = 7.2$  Hz, 1H, H-4'), 4.01 – 3.94 (m, 1H, H-5), 3.85 – 3.74 (m, 2H, H-3, H-3'), 3.70 – 3.56 (m, 3H, H-1'a, H-6'), 3.55 – 3.25 (m + DMSO- $d_6$ , 5H, H-2, H-4, H-6, H-1'b). <sup>13</sup>C NMR (DMSO- $d_6$ ):  $\delta$  139.24 (C(Ph)), 138.88 (C(Ph)), 138.80 (C(Ph)), 138.75 (C(Ph)), 138.65 (C(Ph)), 138.44 (C(Ph)), 128.73 (C-H(Ph)), 128.67 (C-H(Ph)), 128.63 (C-H(Ph)), 128.61 (C-H(Ph)), 128.56 (C-H(Ph)), 128.15 (C-H(Ph)), 128.12 (C-H(Ph)), 128.10 (C-H(Ph)), 128.03 (C-H(Ph)), 128.01 (C-H(Ph)), 127.96 (C-H(Ph)), 127.92 (C-H(Ph)), 127.88 (C-H(Ph)), 127.80 (C-H(Ph)), 104.25 (C2'), 89.37 (C1), 83.65 (C5'), 82.02 (C4'), 81.83 (C3), 81.66 (C3'), 79.75 (C2), 77.80 (C4), 74.86 (CH<sub>2</sub>-Ph), 74.37 (CH<sub>2</sub>-Ph), 72.93 (CH<sub>2</sub>-Ph), 72.81 (CH<sub>2</sub>-Ph), 72.29 (CH<sub>2</sub>-Ph), 71.95 (CH<sub>2</sub>-Ph), 71.85 (CH<sub>2</sub>-Ph), 71.57 (C1'), 70.63 (C5), 68.93 (C6), 62.81 (C6').

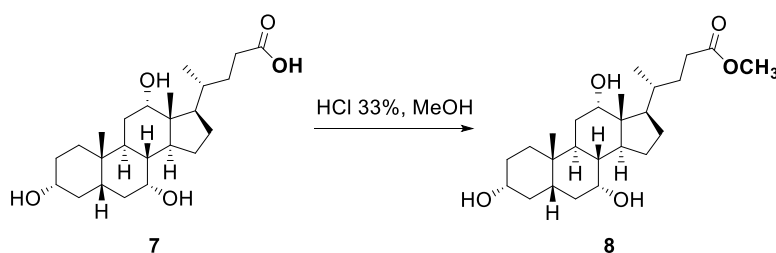
#### VI. 2.1.4 1',2,3,3',4,4',6-Hepta-*O*-benzyl-6'-*O*-succinyl-sucrose (**6**)



To a solution of **5** (3.35 g, 3.44 mmol, 1 eq) in dry CH<sub>2</sub>Cl<sub>2</sub> (60 mL) were added succinic anhydride (0.70 g, 6.88 mmol, 2 eq), DMAP (0.43 g, 3.44 mmol, 1 eq) and triethylamine (0.30 mL). The mixture was kept for 4 h at r.t. until all the starting material had been consumed. The reaction mixture was diluted with CH<sub>2</sub>Cl<sub>2</sub> (100 mL), washed successively with HCl 0.1 M (6 x 10 mL), brine (3 x 10 mL) and H<sub>2</sub>O (2 x 10 mL). The organic layer was dried with anhydrous Na<sub>2</sub>SO<sub>4</sub> and concentrated to yield **6** (3.67 g, 3.4 mmol, 100 %) as a very viscous colorless oil. **R<sub>f</sub>** 0.39 (hexane/ethyl acetate 3:2). [ $\alpha$ ]<sub>D</sub><sup>20</sup> + 26.4 (*c* 1, CHCl<sub>3</sub>). **<sup>1</sup>H NMR** (DMSO-*d*<sub>6</sub>):  $\delta$  7.41-7.20 (m, 33H Ph), 7.18-7.10 (m, 2H Ph), 5.69 (d, *J* = 4.0 Hz, 1H, H-1), 4.96 (d, *J* = 10.9 Hz, 1H, CH<sub>2</sub>-Ph), 4.85 (d, *J* = 10.9 Hz, 1H, CH<sub>2</sub>-Ph), 4.80 (d, *J* = 10.9 Hz, 1H, CH<sub>2</sub>-Ph), 4.70 – 4.30 (m, 14H, H-5', H-6', CH<sub>2</sub>-Ph), 4.21 – 4.13 (m, 1H, H-4'), 4.11 – 4.04 (m, 2H, H-5, H-3'), 3.97 (t, *J* = 8.0 Hz, 1H, H-3), 3.76 (d, *J* = 10.9 Hz, 1H, H-1'<sub>a</sub>), 3.66 (t, *J* = 9.6 Hz, 1H, H-4), 3.60 – 3.48 (m, 3H, H-2, H-6<sub>a</sub>, H-1'<sub>b</sub>), 3.46 – 3.38 (m, 1H, H-6<sub>b</sub>), 2.59 – 2.45 (m, 4H, CH<sub>2</sub>CH<sub>2</sub>COOH). **<sup>13</sup>C NMR** (DMSO-*d*<sub>6</sub>):  $\delta$  174.89 (COOH), 171.95 (C(=O)O), 138.92 (C(Ph)), 138.27 (C(Ph)), 138.00 (C(Ph)), 137.94 (C(Ph)), 137.74 (C(Ph)), 137.70 (C(Ph)), 128.41 (C-H(Ph)), 128.35 (C-H(Ph)), 128.30 (C-H(Ph)), 128.13 (C-H(Ph)), 128.09 (C-H(Ph)), 127.97 (C-H(Ph)), 127.83 (C-H(Ph)), 127.72 (C-H(Ph)), 127.66 (C-H(Ph)), 127.56 (C-H(Ph)), 127.51 (C-H(Ph)), 104.51 (C2'), 89.97 (C1), 83.99 (C5'), 81.82 (C3), 81.47 (C4'), 79.56 (C2), 77.99 (C3'), 77.55 (C4), 75.60 (CH<sub>2</sub>-Ph), 74.99 (CH<sub>2</sub>-Ph), 73.49 (CH<sub>2</sub>-Ph), 73.36 (CH<sub>2</sub>-Ph), 73.17 (CH<sub>2</sub>-Ph), 72.85 (CH<sub>2</sub>-Ph), 72.25 (CH<sub>2</sub>-Ph), 71.00 (C1'), 70.34 (C5), 68.25 (C6), 64.88 (C6'), 29.26 (CH<sub>2</sub>COOH), 28.82 (CH<sub>2</sub>CH<sub>2</sub>COOH). **Analysis calculated for C<sub>65</sub>H<sub>68</sub>O<sub>14</sub>**: C 72.74, H 6.39 **Found**: C 72.85, H 6.46.

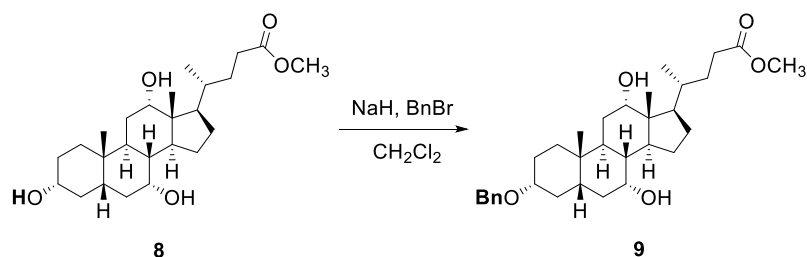
### VI. 2.2 Chemoselective derivatization at the 3' position of cholic acid

#### VI. 2.2.1 Methyl 3 $\alpha$ ,7 $\alpha$ ,12 $\alpha$ -trihydroxy-5 $\beta$ -cholan-24-ate (**8**)



A solution of commercial available cholic acid **7** (14 g, 33.5 mmol) in MeOH (65 mL) was acidified with hydrochloric acid 33% (0.5 mL). The mixture was refluxed for 20 min. and after cooling, the solvent was concentrated to 40 mL in a rotary evaporator and then cooled to 5 °C. The resulting crystals were separated from the mother liquor and rinsed with cold MeOH to give **8** (13.74 g, 32.5 mmol, 97 %) as white needles. **R<sub>f</sub>** 0.33 (chloroform/methanol 9:1).  $[\alpha]_D^{20} + 26$  (*c* 1, CHCl<sub>3</sub>). **m.p.** 153 - 154 °C (lit.<sup>126</sup> 154 - 155 °C). <sup>1</sup>H NMR (CDCl<sub>3</sub>): δ 4.02-3.93 (m, 1H, H-12β), 3.90-3.80 (m, 1H, H-7β), 3.67 (s, 3H, OCH<sub>3</sub>), 3.52-3.39 (m, 1H, H-3β), 2.45-2.31 (m, 1H, H-23α), 2.30-2.13 (m, 3H, H-4α, H-9α, H-23β), 2.00-1.85 (m, 3H, H-6β, H-14α, H-16α), 1.84-1.73 (m, 4H, H-1α, H-4β, H-17α, H-22α), 1.72-1.63 (m, 2H, H-2β, H-15β), 1.62-1.47 (m, 4H, H-6α, H-8β, H-11), 1.47-1.33 (m, 4H, H-2α, H-5β, H-20, H-22β), 1.33-1.23 (m, 1H, H-16β), 1.18-1.05 (m, 1H, H-15α), 1.03-0.93 (m, 1H, H-1β), 0.99 (d, *J* = 5.6 Hz, 3H, 21-CH<sub>3</sub>), 0.89 (s, 3H, 19-CH<sub>3</sub>), 0.68 (s, 3H, 18-CH<sub>3</sub>). <sup>13</sup>C NMR (CDCl<sub>3</sub>): δ 174.84 (C(=O)O), 73.09 (C12), 71.96 (C3), 68.47 (C7), 51.51 (C25), 47.01 (C17), 46.43 (C13), 41.66 (C14), 41.47 (C5), 39.49 (C8), 39.46 (C4), 35.31 (C1), 35.29 (C20), 34.76 (C10), 34.63 (C6), 31.11 (C23), 30.92 (C22), 30.33 (C2), 28.16 (C11), 27.51 (C16), 26.38 (C9), 23.22 (C15), 22.46 (C19), 17.31 (C21), 12.48 (C18).

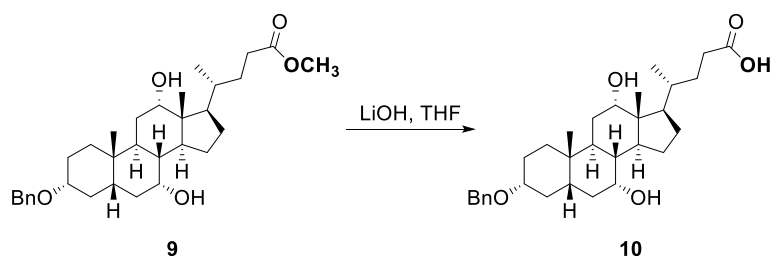
#### VI. 2.2.2 Methyl 3α-O-benzyl, 7α, 12α-dihydroxy-5β-cholan-24-oate (**9**)



To a solution of **8** (2 g, 4.74 mmol, 1 eq) in dry CH<sub>2</sub>Cl<sub>2</sub> (15 mL) at 0 °C, was added NaH (0.375 g, 9.48 mmol, 2 eq) under argon flush. The mixture was stirred for 30 min. and then BnBr (1.13 mL, 9.48 mmol, 2 eq) was added dropwise. The temperature was allowed to rise to r.t.. After 12 h the reaction was quenched by adding crushed ice. The mixture was extracted with CH<sub>2</sub>Cl<sub>2</sub> (2 x 50 mL) and the combined organic extracts were washed with brine (2 x 20 mL), dried (Na<sub>2</sub>SO<sub>4</sub>) and concentrated. The residue obtained was purified by column chromatography (ethyl acetate/hexane 1:1 to 2:1) to yield pure **9** (0.72 g, 1.4 mmol, 30%) as a colorless oil that foamed under vacuum. **R<sub>f</sub>** 0.68 (ethyl acetate/hexane 2:1).  $[\alpha]_D^{20} + 34$  (*c* 1, CHCl<sub>3</sub>). **m.p.** 49.2 °C. <sup>1</sup>H NMR (CDCl<sub>3</sub>): δ 7.39 - 7.29 (m, 4H, Ph-H), 7.28 - 7.22 (m, 1H, Ph-H<sub>para</sub>), 4.60-4.50 (m, 2H, CH<sub>2</sub>-Ph), 4.01-3.94 (m, 1H, H-12β), 3.88-3.79 (m, 1H, H-7β), 3.66 (s, 3H, OCH<sub>3</sub>), 3.28-3.17 (m, 1H, H-3β), 2.43-2.32 (m, 1H, H-23α), 2.30-2.13 (m, 3H, H-4α, H-9α, H-23β), 2.01-1.73 (m, 8H, H-1α, H-2β, H-4β, H-6β, H-14α, H-16α, H-17α, H-22α), 1.71-1.47 (m + H<sub>2</sub>O, 5H, H-6α, H-8β, H-11, H-15β), 1.46-1.22 (m, 5H, H-2α, H-5β, H-20, H-16β, H-22β), 1.21-1.07 (m, 1H, H-15α), 1.02-0.90 (m, 1H, H-1β), 0.98 (d, *J* = 5.8 Hz, 3H, 21-CH<sub>3</sub>), 0.89 (s, 3H, 19-CH<sub>3</sub>), 0.69 (s, 3H, 18-CH<sub>3</sub>). <sup>13</sup>C NMR (CDCl<sub>3</sub>): δ 174.72 (C(=O)O), 139.20 (C(Ph)), 128.31 (C-H<sub>meta</sub>(Ph)), 127.57 (C-

$H_{ortho}(\text{Ph})$ ), 127.31 ( $\text{C-H}_{para}(\text{Ph})$ ), 78.65 (C3), 72.86 (C12), 69.71 ( $\text{CH}_2\text{-Ph}$ ), 68.27 (C7), 51.51 (C25), 47.10 (C17), 46.52 (C13), 42.02 (C14), 41.44 (C5), 39.65 (C8), 36.26 (C4), 35.22 (C1), 35.12 (C20), 35.02 (C10), 34.61 (C6), 31.04 (C23), 30.88 (C22), 28.42 (C11), 27.39 (C16), 27.27 (C2), 26.75 (C9), 23.19 (C15), 22.64 (C19), 17.32 (C21), 12.59 (C18). **Analysis calculated for  $\text{C}_{32}\text{H}_{48}\text{O}_5$ :** C 74.96, H 9.44. **Found:** C 74.81, H 9.58.

### VI. 2.2.3 $3\alpha$ -O-benzyl, $7\alpha$ , $12\alpha$ -dihydroxy- $5\beta$ -cholic acid (**10**)



To a solution of **9** (0.75 g, 1.46 mmol) in THF (25 mL) was added a solution of 0.5 N aqueous lithium hydroxide (12 mL). The reaction mixture was stirred at r.t. until all the starting material had been consumed (6 h). The solution was then acidified with HCl 10% and it was extracted with  $\text{CH}_2\text{Cl}_2$  (2 x 50 mL). The combined organic layers were washed with brine (3 x 10 mL) followed by  $\text{H}_2\text{O}$  (2 x 10 mL), dried ( $\text{Na}_2\text{SO}_4$ ), and concentrated in vacuum to give **10** (0.726 g, 1.46 mmol, 97 %) as a colorless oil that foamed under vacuum. **R<sub>f</sub>** 0.40 (ethyl acetate/hexane 2:1).  $[\alpha]_D^{20} + 37.7$  ( $c$  1,  $\text{CHCl}_3$ ). **m.p.** 64.2 °C.  **$^1\text{H NMR}$**  ( $\text{CDCl}_3$ ):  $\delta$  7.38 - 7.32 (m, 4H, Ph-H), 7.31 - 7.26 (m, 1H, Ph- $H_{para}$ ), 4.58 (s, 2H,  $\text{CH}_2\text{-Ph}$ ), 4.01-3.94 (m, 1H, H-12 $\beta$ ), 3.82-3.72 (m + THF, 1H, H-7 $\beta$ ), 3.33-3.21 (m, 1H, H-3 $\beta$ ), 2.50-2.38 (m, 1H, H-23 $\alpha$ ), 2.36-2.18 (m, 3H, H-4 $\alpha$ , H-9 $\alpha$ , H-23 $\beta$ ), 1.98-1.76 (m, 8H, H-2 $\beta$ , H-4 $\beta$ , H-6 $\beta$ , H-14 $\alpha$ , H-16 $\alpha$ , H-17 $\alpha$ , H-22 $\alpha$ ), 1.73-1.34 (m, 9H, H-2 $\alpha$ , H-5 $\beta$ , H-6 $\alpha$ , H-8 $\beta$ , H-11, H-15 $\beta$ , H-20, H-22 $\beta$ ), 1.30-1.22 (m, 1H, H-16 $\beta$ ), 1.19-1.06 (m, 1H, H-15 $\alpha$ ), 1.05-0.91 (m, 1H, H-1 $\beta$ ), 1.01 (d,  $J$  = 6.1 Hz, 3H, 21- $\text{CH}_3$ ), 0.88 (s, 3H, 19- $\text{CH}_3$ ), 0.69 (s, 3H, 18- $\text{CH}_3$ ).  **$^{13}\text{C NMR}$**  ( $\text{CDCl}_3$ ):  $\delta$  178.35 ( $\text{C(=O)OH}$ ), 138.70 (C(Ph)), 128.34 (C- $H_{meta}(\text{Ph})$ ), 127.71 (C- $H_{ortho}(\text{Ph})$ ), 127.49 (C- $H_{para}(\text{Ph})$ ), 78.98 (C3), 73.09 (C12), 69.79 ( $\text{CH}_2\text{-Ph}$ ), 68.35 (C7), 47.04 (C17), 46.50 (C13), 42.00 (C14), 41.41 (C5), 39.39 (C8), 35.95 (C4), 35.52 (C20), 35.20 (C1), 34.94 (C10), 34.50 (C6), 30.91 (C23), 30.77 (C22), 28.08 (C11), 27.63 (C16), 26.80 (C2), 26.47 (C9), 23.22 (C15), 22.37 (C19), 17.14 (C21), 12.48 (C18). **Analysis calculated for  $\text{C}_{31}\text{H}_{46}\text{O}_5$ :** C 74.66, H 9.30. **Found:** C 74.69, H 9.29.

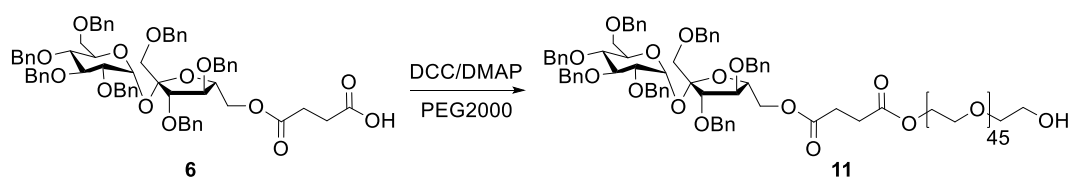
### VI.2.3 General procedure 1 for DCC-mediated coupling reactions

To an ice-cold solution of  $\text{CH}_2\text{Cl}_2$  containing the carboxylic acid component (1.2 eq or 2.0 eq) were added DMAP (1.2 eq or 2.0 eq) and DCC (2.4 eq or 4.0 eq). The mixture was stirred for 20 min. and

then the appropriate PEG compound (1.0 eq) was added. The ice bath was removed and the reaction mixture was stirred for 48 h at r.t.. After cooling overnight in a refrigerator (4 °C) the suspension was filtered through a plug of celite and concentrated. The crude product material was purified by column chromatography using a step gradient of MeOH (1-10 %) in CHCl<sub>3</sub>. Compounds were visualized with phosphomolybdic acid by TLC analysis (CHCl<sub>3</sub>:MeOH 9:1).

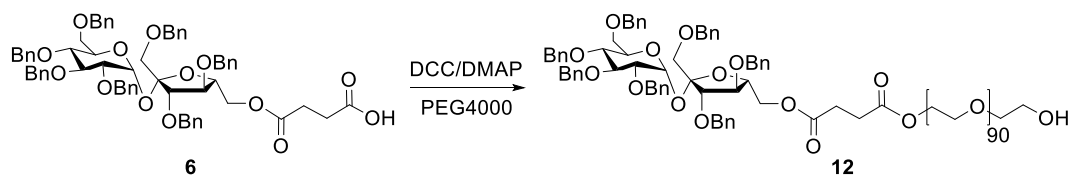
## VI.2.4 Synthesis of PEG-based conjugates

### VI.2.4.1 Benzylated Suc-PEG2000-OH (11)



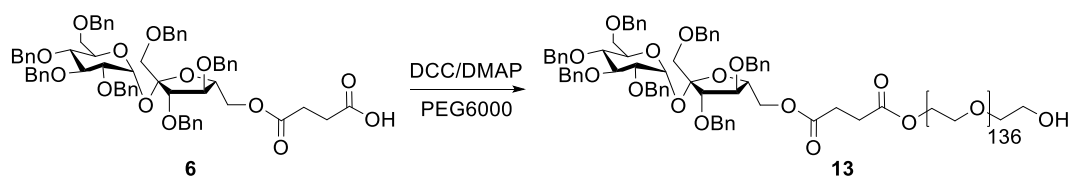
According to the general method **1**, compound **6** (0.64 g, 0.6 mmol) dissolved in dry CH<sub>2</sub>Cl<sub>2</sub> (20 mL), DMAP (73 mg, 0.6 mmol), DCC (0.25 g, 1.2 mmol) and PEG2000 (1 g, 0.5 mmol) were reacted for 48 h. Purification by column chromatography (CHCl<sub>3</sub>:MeOH 1-10 %) afforded product **11** (1.12 g, 0.37 mmol, 74 %) as a white waxy solid. **R<sub>f</sub>** 0.46 and 0.58 (CHCl<sub>3</sub>:MeOH 9:1). [ $\alpha$ ]<sub>D</sub><sup>20</sup> + 16.0 (*c* 0.5, CHCl<sub>3</sub>). <sup>1</sup>H NMR (CDCl<sub>3</sub>):  $\delta$  7.33-7.18 (m, 33H, Ph-H), 7.14-7.09 (m, 2H, Ph-H), 5.63 (d, *J* = 3.5 Hz, 1H, H-1), 4.91 (d, *J* = 10.9 Hz, 1H, CH<sub>2</sub>-Ph), 4.80 (d, *J* = 10.9 Hz, 1H, CH<sub>2</sub>-Ph), 4.76 (d, *J* = 10.9 Hz, 1H, CH<sub>2</sub>-Ph), 4.66 – 4.25 (m, 14H, H-5', H-6', CH<sub>2</sub>-Ph), 4.23 – 4.16 (m, 2H, -C(=O)OCH<sub>2</sub>CH<sub>2</sub>O-), 4.13 – 4.04 (m, 3H, H-5, H-3', H-4'), 3.95 (t, *J* = 9.3 Hz, 1H, H-3), 3.64 (m and Brs, H-4, PEG backbone), 3.55 – 3.40 (m, 5H, H-2, H-6, H-1'), 2.60 – 2.52 (m, 4H, -CH<sub>2</sub>CH<sub>2</sub>COO-PEG). <sup>13</sup>C NMR (CDCl<sub>3</sub>):  $\delta$  172.17 (C(=O)O-PEG), 171.99 (C(=O)O), 138.83 (C(Ph)), 138.46 (C(Ph)), 138.24 (C(Ph)), 138.04 (C(Ph)), 138.01 (C(Ph)), 137.89 (C(Ph)), 137.75 (C(Ph)), 128.33 (C-H(Ph)), 128.29 (C-H(Ph)), 128.27 (C-H(Ph)), 128.25 (C-H(Ph)), 128.23 (C-H(Ph)), 127.91 (C-H(Ph)), 127.89 (C-H(Ph)), 127.88 (C-H(Ph)), 127.85 (C-H(Ph)), 127.77 (C-H(Ph)), 127.69 (C-H(Ph)), 127.63 (C-H(Ph)), 127.56 (C-H(Ph)), 127.50 (C-H(Ph)), 127.46 (C-H(Ph)), 104.59 (C2'), 90.08 (C1), 83.68 (C5'), 81.99 (C4'), 81.86 (C3), 79.66 (C2), 78.23 (C3'), 77.59 (C4), 75.51 (CH<sub>2</sub>-Ph), 74.82 (CH<sub>2</sub>-Ph), 73.32 (CH<sub>2</sub>-Ph), 72.82 (CH<sub>2</sub>-Ph), 72.58 (CH<sub>2</sub>-Ph), 72.55 (CH<sub>2</sub>-Ph), 72.47 (CH<sub>2</sub>-Ph), 70.88 (C1'), 70.55 (PEG backbone), 70.23 (C5), 69.00 (PEG backbone), 68.39 (C6), 65.53 (C6'), 63.73 (-C(=O)OCH<sub>2</sub>CH<sub>2</sub>O-), 61.66 (PEG backbone), 28.77 (-CH<sub>2</sub>CH<sub>2</sub>-).

### VI.2.4.2 Benzylated Suc-PEG4000-OH (12)



According to the general method **1**, compound **6** (0.64 g, 0.6 mmol) dissolved in dry  $\text{CH}_2\text{Cl}_2$  (20 mL), DMAP (73 mg, 0.6 mmol), DCC (0.25 g, 1.2 mmol) and PEG4000 (2 g, 0.5 mmol) were reacted for 48 h. Purification by column chromatography ( $\text{CHCl}_3$ :MeOH 1-10 %) afforded product **12** (1.77 g, 0.35 mmol, 70 %) as a white waxy solid. **R<sub>f</sub>** 0.42 ( $\text{CHCl}_3$ :MeOH 9:1).  $[\alpha]_{\text{D}}^{20} + 16.8$  (c 0.5,  $\text{CHCl}_3$ ). **<sup>1</sup>H NMR** ( $\text{CDCl}_3$ ):  $\delta$  7.39-7.20 (m, 33H, Ph-H), 7.17-7.11 (m, 2H, Ph-H), 5.66 (d,  $J = 3.4$  Hz, 1H, H-1), 4.93 (d,  $J = 10.9$  Hz, 1H,  $\text{CH}_2$ -Ph), 4.82 (d,  $J = 10.9$  Hz, 1H,  $\text{CH}_2$ -Ph), 4.79 (d,  $J = 10.9$  Hz, 1H,  $\text{CH}_2$ -Ph), 4.72 – 4.28 (m, 14H, H-5', H-6',  $\text{CH}_2$ -Ph), 4.26 – 4.17 (m, 2H,  $-\text{C}(=\text{O})\text{OCH}_2\text{CH}_2\text{O}-$ ), 4.15 – 4.06 (m, 3H, H-5, H-3', H-4'), 3.97 (t,  $J = 9.4$  Hz, 1H, H-3), 3.66 (m and Brs, PEG backbone, H-2, H-4, H-6, H-1'), 2.66 – 2.52 (m, 4H,  $-\text{CH}_2\text{CH}_2\text{COO-PEG}$ ). **<sup>13</sup>C NMR** ( $\text{CDCl}_3$ ):  $\delta$  172.15 ( $\text{C}(=\text{O})\text{O-PEG}$ ), 171.97 ( $\text{C}(=\text{O})\text{O}$ ), 138.89 (C(Ph)), 138.30 (C(Ph)), 138.10 (C(Ph)), 138.07 (C(Ph)), 137.95 (C(Ph)), 137.81 (C(Ph)), 128.37 (C-H(Ph)), 128.34 (C-H(Ph)), 128.31 (C-H(Ph)), 128.30 (C-H(Ph)), 128.28 (C-H(Ph)), 127.95 (C-H(Ph)), 127.93 (C-H(Ph)), 127.92 (C-H(Ph)), 127.89 (C-H(Ph)), 127.81 (C-H(Ph)), 127.73 (C-H(Ph)), 127.67 (C-H(Ph)), 127.61 (C-H(Ph)), 127.54 (C-H(Ph)), 127.50 (C-H(Ph)), 104.65 (C2'), 90.09 (C1), 83.74 (C5'), 82.01 (C4'), 81.87 (C3), 79.69 (C2), 78.23 (C3'), 77.60 (C4), 75.50 ( $\text{CH}_2$ -Ph), 74.83 ( $\text{CH}_2$ -Ph), 73.33 ( $\text{CH}_2$ -Ph), 72.82 ( $\text{CH}_2$ -Ph), 72.55 ( $\text{CH}_2$ -Ph), 72.48 ( $\text{CH}_2$ -Ph), 72.47 ( $\text{CH}_2$ -Ph), 70.53 (PEG backbone), 70.28 (C5), 69.00 (PEG backbone), 68.39 (C6), 65.53 (C6'), 63.73 ( $-\text{C}(=\text{O})\text{OCH}_2\text{CH}_2\text{O}-$ ), 61.69 (PEG backbone), 28.77 ( $-\text{CH}_2\text{CH}_2-$ ).

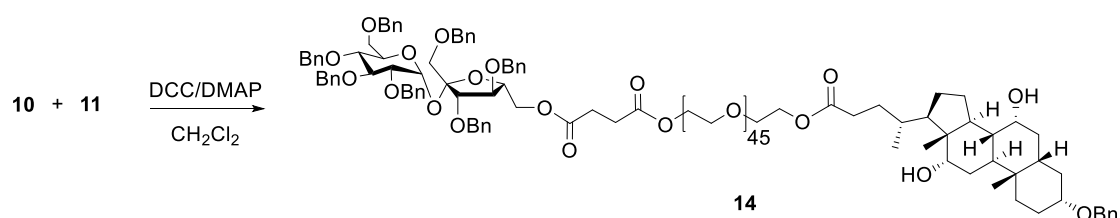
#### VI.2.4.3 Benzylated Suc-PEG6000-OH (**13**)



According to the general method **1**, compound **6** (0.64 g, 0.6 mmol) dissolved in dry  $\text{CH}_2\text{Cl}_2$  (20 mL), DMAP (73 mg, 0.6 mmol), DCC (0.25 g, 1.2 mmol) and PEG6000 (3 g, 0.5 mmol) were reacted for 48 h. Purification by column chromatography ( $\text{CHCl}_3$ :MeOH 1-10 %) afforded product **13** (2.8 g, 0.4 mmol, 80 %) as a white waxy solid. **R<sub>f</sub>** 0.42 ( $\text{CHCl}_3$ :MeOH 9:1).  $[\alpha]_{\text{D}}^{20} + 4.8$  (c 0.5,  $\text{CHCl}_3$ ). **<sup>1</sup>H NMR** ( $\text{CDCl}_3$ ):  $\delta$  7.37-7.18 (m, 33H, Ph-H), 7.16-7.09 (m, 2H, Ph-H), 5.67 – 5.62 (m, 1H, H-1), 4.92 (d,  $J = 11.0$  Hz, 1H,  $\text{CH}_2$ -Ph), 4.81 (d,  $J = 11.9$  Hz, 1H,  $\text{CH}_2$ -Ph), 4.77 (d,  $J = 11.1$  Hz, 1H,  $\text{CH}_2$ -Ph), 4.70 – 4.28 (m, 14H, H-5', H-6',  $\text{CH}_2$ -Ph), 4.27 – 4.17 (m, 2H,  $-\text{C}(=\text{O})\text{OCH}_2\text{CH}_2\text{O}-$ ), 4.15 – 4.04 (m, 3H, H-

5, H-3', H-4'), 3.95 (t,  $J = 9.2$  Hz, 1H, H-3), 3.65 (m and Brs, PEG backbone, H-2, H-4, H-6, H-1'), 2.63 – 2.54 (m, 4H,  $-\text{CH}_2\text{CH}_2\text{COO-PEG}$ ).  $^{13}\text{C}$  NMR ( $\text{CDCl}_3$ ):  $\delta$  167.44 (C(=O)O-PEG), 167.22 (C(=O)O), 134.12 (C(Ph)), 133.74 (C(Ph)), 133.43 (C(Ph)), 133.32 (C(Ph)), 133.30 (C(Ph)), 133.17 (C(Ph)), 133.03 (C(Ph)), 127.88 (C-H(Ph)), 123.60 (C-H(Ph)), 123.53 (C-H(Ph)), 123.52 (C-H(Ph)), 123.51 (C-H(Ph)), 123.50 (C-H(Ph)), 123.16 (C-H(Ph)), 123.14 (C-H(Ph)), 123.13 (C-H(Ph)), 123.00 (C-H(Ph)), 122.96 (C-H(Ph)), 122.90 (C-H(Ph)), 122.82 (C-H(Ph)), 122.76 (C-H(Ph)), 104.62 (C2'), 90.86 (C1), 83.73 (C5'), 82.00 (C4'), 81.83 (C3), 79.66 (C2), 78.22 (C3'), 77.58 (C4), 75.48 (CH<sub>2</sub>-Ph), 74.82 (CH<sub>2</sub>-Ph), 73.32 (CH<sub>2</sub>-Ph), 72.81 (CH<sub>2</sub>-Ph), 72.53 (CH<sub>2</sub>-Ph), 72.47 (CH<sub>2</sub>-Ph), 72.44 (CH<sub>2</sub>-Ph), 70.52 (PEG backbone), 70.26 (C5), 69.03 (PEG backbone), 68.34 (C6), 65.52 (C6'), 63.71 (C(=O)OCH<sub>2</sub>CH<sub>2</sub>O-), 61.68 (PEG backbone), 28.76 ( $-\text{CH}_2\text{CH}_2-$ ).

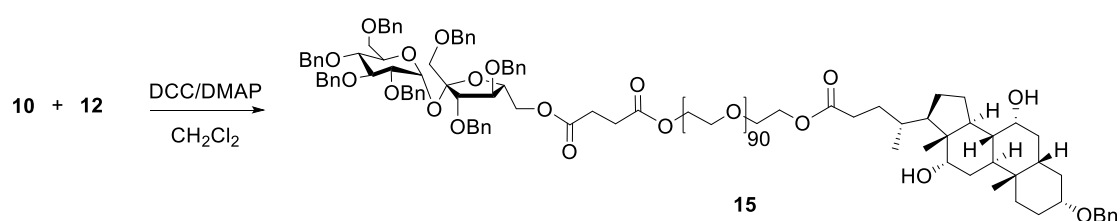
#### VI.2.4.4 Benzylated Suc-PEG2000-Chol (14)



According to the general method **1**, compound **10** (0.34 g, 0.68 mmol) dissolved in dry  $\text{CH}_2\text{Cl}_2$  (20 mL), DMAP (82 mg, 0.68 mmol), DCC (0.29 g, 1.36 mmol) and benzylated Suc-PEG2000-OH **11** (1.03 g, 0.34 mmol) were reacted for 48 h. Purification by column chromatography ( $\text{CHCl}_3$ :MeOH 1-10 %) afforded product **14** (0.77 g, 0.22 mmol, 65 %) as a white waxy solid. A single purple spot was visualized by staining with a solution of concentrated  $\text{H}_2\text{SO}_4$ /MeOH 2:8 by TLC analysis. **R<sub>f</sub>** 0.56 ( $\text{CHCl}_3$ :MeOH 9:1).  $^1\text{H}$  NMR ( $\text{CDCl}_3$ ):  $\delta$  7.35-7.18 (m, 38H, Ph-H), 7.15-7.08 (m, 2H, Ph-H), 5.63 (d,  $J = 3.5$  Hz, 1H, H-1), 4.91 (d,  $J = 10.9$  Hz, 1H, CH<sub>2</sub>-Ph), 4.80 (d,  $J = 10.9$  Hz, 1H, CH<sub>2</sub>-Ph), 4.76 (d,  $J = 10.9$  Hz, 1H, CH<sub>2</sub>-Ph), 4.66 – 4.26 (m, 14H, H-5', H-6', CH<sub>2</sub>-Ph), 4.26 – 4.24 (m, 4H,  $-\text{C}(=\text{O})\text{OCH}_2\text{CH}_2\text{O}-$ ), 4.13 – 4.03 (m, 3H, H-5, H-3', H-4'), 3.98 – 3.91 (m, 2H, H-3, H-12 $\beta_{\text{chol}}$ ), 3.85 – 3.78 (m, 1H, H-7 $\beta_{\text{chol}}$ ), 3.74 (Brs, PEG backbone), 3.55 – 3.41 (m, 6H, H-2, H-4, H-6, H-1'), 3.26 – 3.17 (m, 1H, H-3 $\beta_{\text{chol}}$ ), 2.61 – 2.51 (m, 4H,  $-\text{CH}_2\text{CH}_2-$ ), 2.45 – 2.34 (m, 1H, H-23 $\alpha_{\text{chol}}$ ), 2.33 – 2.16 (m, 3H, H-4 $\alpha_{\text{chol}}$ , H-9 $\alpha_{\text{chol}}$ , H-23 $\beta_{\text{chol}}$ ), 2.01 – 1.46 (m, 13H, H-1 $\alpha_{\text{chol}}$ , H-2 $\beta_{\text{chol}}$ , H-4 $\beta_{\text{chol}}$ , H-6 $\text{chol}$ , H-8 $\beta_{\text{chol}}$ , H-11 $\text{chol}$ , H-14 $\alpha_{\text{chol}}$ , H-15 $\beta_{\text{chol}}$ , H-16 $\alpha_{\text{chol}}$ , H-17 $\alpha_{\text{chol}}$ , H-22 $\alpha_{\text{chol}}$ ), 1.45 – 1.24 (m, 5H, H-2 $\alpha_{\text{chol}}$ , H-5 $\beta_{\text{chol}}$ , H-16 $\beta_{\text{chol}}$ , H-20 $\text{chol}$ , H-22 $\beta_{\text{chol}}$ ), 1.20-1.06 (m, 1H, H-15 $\alpha$ ), 1.01-0.92 (m, 1H, H-1 $\beta_{\text{chol}}$ ), 0.97 (d,  $J = 6.2$  Hz, 3H, 21-CH<sub>3 $\text{chol}$</sub> ), 0.88 (s, 3H, 19-CH<sub>3 $\text{chol}$</sub> ), 0.68 (s, 3H, 18-CH<sub>3 $\text{chol}$</sub> ).  $^{13}\text{C}$  NMR ( $\text{CDCl}_3$ ):  $\delta$  174.16 (C24 $\text{chol}$ ), 172.17 (C(=O)O-PEG), 171.99 (C(=O)O), 139.21 (C(Ph)), 138.86 (C(Ph)), 138.49 (C(Ph)), 138.26 (C(Ph)), 138.07 (C(Ph)), 138.04 (C(Ph)), 137.92 (C(Ph)), 137.78 (C(Ph)), 128.34 (C-H(Ph)), 128.30 (C-H(Ph)), 128.27 (C-H(Ph)), 128.26 (C-H(Ph)), 128.24 (C-H(Ph)), 127.92 (C-H(Ph)), 127.90 (C-H(Ph)), 127.88 (C-H(Ph)), 127.86 (C-H(Ph)), 127.78 (C-H(Ph)), 127.70 (C-H(Ph)), 127.64 (C-H(Ph)), 127.57 (C-H(Ph)), 127.49

(C-H(Ph)), 127.25 (C-H(Ph)), 104.61 (C2'), 90.09 (C1), 83.70 (C5'), 82.02 (C4'), 81.88 (C3), 79.69 (C2), 78.61 (C3<sub>chol</sub>), 78.25 (C3'), 77.62 (C4), 75.51 (CH<sub>2</sub>-Ph), 74.82 (CH<sub>2</sub>-Ph), 73.34 (CH<sub>2</sub>-Ph), 72.83 (CH<sub>2</sub>-Ph), 72.75 (C12<sub>chol</sub>), 72.56 (CH<sub>2</sub>-Ph), 72.48 (CH<sub>2</sub>-Ph), 70.94 (C1'), 70.54 (PEG backbone), 69.64 (CH<sub>2</sub>-Ph<sub>chol</sub>), 69.17 (PEG backbone), 69.02 (PEG backbone), 68.42 (C6), 68.18 (C7<sub>chol</sub>), 65.54 (C6'), 63.75 (-C(=O)OCH<sub>2</sub>CH<sub>2</sub>O-), 63.40 ((-C<sub>chol</sub>(=O)OCH<sub>2</sub>CH<sub>2</sub>O-), 47.05 (C17<sub>chol</sub>), 46.49 (C13<sub>chol</sub>), 41.99 (C14<sub>chol</sub>), 41.42 (C5<sub>chol</sub>), 39.65 (C8<sub>chol</sub>), 36.21 (C4<sub>chol</sub>), 35.19 (C1<sub>chol</sub>), 35.08 (C20<sub>chol</sub>), 34.99 (C10<sub>chol</sub>), 34.56 (C6<sub>chol</sub>), 31.10 (C23<sub>chol</sub>), 30.76 (C22<sub>chol</sub>), 28.79 (-CH<sub>2</sub>CH<sub>2</sub>-), 28.43 (C11<sub>chol</sub>), 27.38 (C16<sub>chol</sub>), 27.23 (C2<sub>chol</sub>), 26.73 (C9<sub>chol</sub>), 23.12 (C15<sub>chol</sub>), 22.62 (C19<sub>chol</sub>), 17.30 (C21<sub>chol</sub>), 12.57 (C18<sub>chol</sub>).

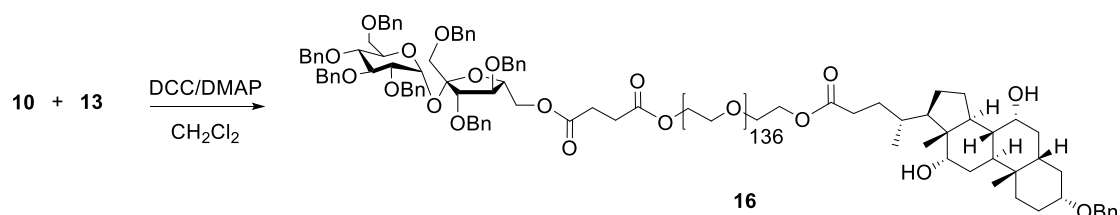
#### VI.2.4.5 Benzylated Suc-PEG4000-Chol (15)



According to the general method 1, compound **10** (0.34 g, 0.68 mmol) dissolved in dry CH<sub>2</sub>Cl<sub>2</sub> (15 mL), DMAP (82 mg, 0.68 mmol), DCC (0.29 g, 1.36 mmol) and benzylated Suc-PEG4000-OH **12** (1.7 g, 0.34 mmol) were reacted for 48 h. Purification by column chromatography (CHCl<sub>3</sub>:MeOH 1-10 %) afforded product **15** (1.53 g, 0.28 mmol, 82 %) as a white waxy solid. A single purple spot was visualized by staining with a solution of concentrated H<sub>2</sub>SO<sub>4</sub>/MeOH 2:8 by TLC analysis. **R<sub>f</sub>** 0.40 (CHCl<sub>3</sub>:MeOH 9:1). [α]<sub>D</sub><sup>20</sup> +21.2 (c 0.5, CHCl<sub>3</sub>). <sup>1</sup>H NMR (CDCl<sub>3</sub>): δ 7.37-7.17 (m, 38H, Ph-H), 7.15-7.09 (m, 2H, Ph-H), 5.64 (d, *J* = 3.5 Hz, 1H, H-1), 4.92 (d, *J* = 10.9 Hz, 1H, CH<sub>2</sub>-Ph), 4.81 (d, *J* = 10.9 Hz, 1H, CH<sub>2</sub>-Ph), 4.80 (d, *J* = 10.9 Hz, 1H, CH<sub>2</sub>-Ph), 4.69 – 4.26 (m, 14H, H-5', H-6', CH<sub>2</sub>-Ph), 4.25 – 4.16 (m, 4H, -C(=O)OCH<sub>2</sub>CH<sub>2</sub>O-), 4.14 – 4.04 (m, 3H, H-5, H-3', H-4'), 3.99 – 3.91 (m, 2H, H-3, H-12β<sub>chol</sub>), 3.86 – 3.79 (m, 1H, H-7β<sub>chol</sub>), 3.78 – 3.39 (m and Brs, PEG backbone, H-2, H-4, H-6, H-1'), 3.27 – 3.17 (m, 1H, H-3β<sub>chol</sub>), 2.63 – 2.52 (m, 4H, -CH<sub>2</sub>CH<sub>2</sub>-), 2.45 – 2.35 (m, 1H, H-23α<sub>chol</sub>), 2.34 – 2.11 (m + H<sub>2</sub>O, 3H, H-4α<sub>chol</sub>, H-9α<sub>chol</sub>, H-23β<sub>chol</sub>), 2.01 – 1.73 (m, 8H, H-1α<sub>chol</sub>, H-2β<sub>chol</sub>, H-4β<sub>chol</sub>, H-6β<sub>chol</sub>, H-14α<sub>chol</sub>, H-16α<sub>chol</sub>, H-17α<sub>chol</sub>, H-22α<sub>chol</sub>), 1.71 – 1.24 (m, 10H, H-2α<sub>chol</sub>, H-5β<sub>chol</sub>, H-6α<sub>chol</sub>, H-8β<sub>chol</sub>, H-11<sub>chol</sub>, H-15β<sub>chol</sub>, H-16β<sub>chol</sub>, H-20<sub>chol</sub>, H-22β<sub>chol</sub>), 1.20-1.06 (m, 1H, H-15α<sub>chol</sub>), 0.99-0.91 (m, 1H, H-1β<sub>chol</sub>), 0.98 (d, *J* = 6.1 Hz, 3H, 21-CH<sub>3</sub><sub>chol</sub>), 0.89 (s, 3H, 19-CH<sub>3</sub><sub>chol</sub>), 0.69 (s, 3H, 18-CH<sub>3</sub><sub>chol</sub>). <sup>13</sup>C NMR (CDCl<sub>3</sub>): δ 174.12 (C24<sub>chol</sub>), 172.12 (C(=O)O-PEG), 171.94 (C(=O)O), 139.14 (C(Ph)), 138.79 (C(Ph)), 138.41 (C(Ph)), 138.20 (C(Ph)), 138.00 (C(Ph)), 137.97 (C(Ph)), 137.85 (C(Ph)), 137.71 (C(Ph)), 128.28 (C-H(Ph)), 128.25 (C-H(Ph)), 128.21 (C-H(Ph)), 128.19 (C-H(Ph)), 127.87 (C-H(Ph)), 127.85 (C-H(Ph)), 127.84 (C-H(Ph)), 127.81 (C-H(Ph)), 127.73 (C-H(Ph)), 127.65 (C-H(Ph)), 127.59 (C-H(Ph)), 127.52 (C-H(Ph)), 127.44 (C-H(Ph)), 127.41 (C-H(Ph)), 127.20 (C-H(Ph)), 104.55 (C2'), 90.04 (C1), 83.63 (C5'), 81.95 (C4'), 81.82 (C3), 79.62 (C2), 78.57 (C3<sub>chol</sub>), 78.18 (C3'), 77.55 (C4), 75.46 (CH<sub>2</sub>-Ph),

74.77 ( $\text{CH}_2\text{-Ph}$ ), 73.28 ( $\text{CH}_2\text{-Ph}$ ), 72.77 ( $\text{CH}_2\text{-Ph}$ ), 72.69 ( $\text{C}_{12\text{chol}}$ ), 72.50 ( $\text{CH}_2\text{-Ph}$ ), 72.42 ( $\text{CH}_2\text{-Ph}$ ), 70.88 ( $\text{C}_{1'}$ ), 70.48 (PEG backbone), 69.58 ( $\text{CH}_2\text{-Ph}_{\text{chol}}$ ), 69.11 (PEG backbone), 68.96 (PEG backbone), 68.33 ( $\text{C}_6$ ), 68.11 ( $\text{C}_{7\text{chol}}$ ), 65.48 ( $\text{C}_6'$ ), 63.69 ( $-\text{C}(=\text{O})\text{OCH}_2\text{CH}_2\text{O}-$ ), 63.34 ( $(-\text{C}_{\text{chol}}(=\text{O})\text{OCH}_2\text{CH}_2\text{O}-)$ ), 46.97 ( $\text{C}_{17\text{chol}}$ ), 46.42 ( $\text{C}_{13\text{chol}}$ ), 41.91 ( $\text{C}_{14\text{chol}}$ ), 41.36 ( $\text{C}_{5\text{chol}}$ ), 39.57 ( $\text{C}_{8\text{chol}}$ ), 36.14 ( $\text{C}_{4\text{chol}}$ ), 35.13 ( $\text{C}_{1\text{chol}}$ ), 35.03 ( $\text{C}_{20\text{chol}}$ ), 34.93 ( $\text{C}_{10\text{chol}}$ ), 34.51 ( $\text{C}_{6\text{chol}}$ ), 31.03 ( $\text{C}_{23\text{chol}}$ ), 30.69 ( $\text{C}_{22\text{chol}}$ ), 28.73 ( $-\text{CH}_2\text{CH}_2-$ ), 28.36 ( $\text{C}_{11\text{chol}}$ ), 27.33 ( $\text{C}_{16\text{chol}}$ ), 27.16 ( $\text{C}_{2\text{chol}}$ ), 26.65 ( $\text{C}_{9\text{chol}}$ ), 23.07 ( $\text{C}_{15\text{chol}}$ ), 22.57 ( $\text{C}_{19\text{chol}}$ ), 17.24 ( $\text{C}_{21\text{chol}}$ ), 12.51 ( $\text{C}_{18\text{chol}}$ ).

#### VI.2.4.6 Benzylated Suc-PEG6000-Chol (16)



According to the general method 1, compound **10** (0.34 g, 0.68 mmol) dissolved in dry  $\text{CH}_2\text{Cl}_2$  (20 mL), DMAP (82 mg, 0.68 mmol), DCC (0.29 g, 1.36 mmol) and benzylated Suc-PEG6000-OH **13** (2.4 g, 0.34 mmol) were reacted for 48 h. Purification by column chromatography ( $\text{CHCl}_3\text{:MeOH}$  1-10 %) afforded product **16** (1.97 g, 0.27 mmol, 77 %) as a white waxy solid. A single purple spot was visualized by staining with a solution of concentrated  $\text{H}_2\text{SO}_4\text{/MeOH}$  2:8 by TLC analysis. **R<sub>f</sub>** 0.40 ( $\text{CHCl}_3\text{:MeOH}$  9:1). **<sup>1</sup>H NMR** ( $\text{CDCl}_3$ ):  $\delta$  7.39-7.20 (m, 38H, Ph-H), 7.16-7.08 (m, 2H, Ph-H), 5.68 – 5.63 (m, 1H, H-1), 4.92 (d,  $J$  = 10.9 Hz, 1H,  $\text{CH}_2\text{-Ph}$ ), 4.81 (d,  $J$  = 10.9 Hz, 1H,  $\text{CH}_2\text{-Ph}$ ), 4.80 (d,  $J$  = 11.0 Hz, 1H,  $\text{CH}_2\text{-Ph}$ ), 4.68 – 4.28 (m, 14H, H-5', H-6',  $\text{CH}_2\text{-Ph}$ ), 4.27 – 4.15 (m, 4H,  $-\text{C}(=\text{O})\text{OCH}_2\text{CH}_2\text{O}-$ ), 4.15 – 4.03 (m, 3H, H-5, H-3', H-4'), 4.00 – 3.90 (m, 2H, H-3, H-12 $\beta_{\text{chol}}$ ), 3.87 – 3.79 (m, 1H, H-7 $\beta_{\text{chol}}$ ), 3.78 – 3.39 (m and Brs, PEG backbone, H-2, H-4, H-6, H-1'), 3.28 – 3.20 (m, 1H, H-3 $\beta_{\text{chol}}$ ), 2.71 – 2.46 (m, 4H,  $-\text{CH}_2\text{CH}_2-$ ), 2.44 – 2.36 (m, 1H, H-23 $\alpha_{\text{chol}}$ ), 2.35 – 2.15 (m +  $\text{H}_2\text{O}$ , 3H, H-4 $\alpha_{\text{chol}}$ , H-9 $\alpha_{\text{chol}}$ , H-23 $\beta_{\text{chol}}$ ), 2.01 – 1.74 (m, 8H, H-1 $\alpha_{\text{chol}}$ , H-2 $\beta_{\text{chol}}$ , H-4 $\beta_{\text{chol}}$ , H-6 $\beta_{\text{chol}}$ , H-14 $\alpha_{\text{chol}}$ , H-16 $\alpha_{\text{chol}}$ , H-17 $\alpha_{\text{chol}}$ , H-22 $\alpha_{\text{chol}}$ ), 1.71 – 1.23 (m, 10H, H-2 $\alpha_{\text{chol}}$ , H-5 $\beta_{\text{chol}}$ , H-6 $\alpha_{\text{chol}}$ , H-8 $\beta_{\text{chol}}$ , H-11 $\text{chol}$ , H-15 $\beta_{\text{chol}}$ , H-16 $\beta_{\text{chol}}$ , H-20 $\text{chol}$ , H-22 $\beta_{\text{chol}}$ ), 1.22-1.04 (m, 1H, H-15 $\alpha_{\text{chol}}$ ), 0.99-0.91 (m, 1H, H-1 $\beta_{\text{chol}}$ ), 0.99 (d,  $J$  = 5.9 Hz, 3H, 21- $\text{CH}_3_{\text{chol}}$ ), 0.90 (s, 3H, 19- $\text{CH}_3_{\text{chol}}$ ), 0.70 (s, 3H, 18- $\text{CH}_3_{\text{chol}}$ ). **<sup>13</sup>C NMR** ( $\text{CDCl}_3$ ):  $\delta$  174.14 ( $\text{C}_{24\text{chol}}$ ), 172.15 ( $\text{C}(=\text{O})\text{O-PEG}$ ), 171.97 ( $\text{C}(=\text{O})\text{O}$ ), 139.17 ( $\text{C}(\text{Ph})$ ), 138.83 ( $\text{C}(\text{Ph})$ ), 138.45 ( $\text{C}(\text{Ph})$ ), 138.23 ( $\text{C}(\text{Ph})$ ), 138.04 ( $\text{C}(\text{Ph})$ ), 138.01 ( $\text{C}(\text{Ph})$ ), 137.89 ( $\text{C}(\text{Ph})$ ), 137.75 ( $\text{C}(\text{Ph})$ ), 137.11 ( $\text{C-H}(\text{Ph})$ ), 131.82 ( $\text{C-H}(\text{Ph})$ ), 128.31 ( $\text{C-H}(\text{Ph})$ ), 128.28 ( $\text{C-H}(\text{Ph})$ ), 127.24 ( $\text{C-H}(\text{Ph})$ ), 128.22 ( $\text{C-H}(\text{Ph})$ ), 127.89 ( $\text{C-H}(\text{Ph})$ ), 127.86 ( $\text{C-H}(\text{Ph})$ ), 127.84 ( $\text{C-H}(\text{Ph})$ ), 127.76 ( $\text{C-H}(\text{Ph})$ ), 127.68 ( $\text{C-H}(\text{Ph})$ ), 127.62 ( $\text{C-H}(\text{Ph})$ ), 127.55 ( $\text{C-H}(\text{Ph})$ ), 127.48 ( $\text{C-H}(\text{Ph})$ ), 127.23 ( $\text{C-H}(\text{Ph})$ ), 104.58 ( $\text{C}_2'$ ), 90.07 ( $\text{C}_1$ ), 83.67 ( $\text{C}_5'$ ), 81.85 ( $\text{C}_4'$ ), 81.82 ( $\text{C}_3$ ), 79.66 ( $\text{C}_2$ ), 78.59 ( $\text{C}_{3\text{chol}}$ ), 78.22 ( $\text{C}_3'$ ), 77.59 ( $\text{C}_4$ ), 75.48 ( $\text{CH}_2\text{-Ph}$ ), 74.80 ( $\text{CH}_2\text{-Ph}$ ), 73.31 ( $\text{CH}_2\text{-Ph}$ ), 72.81 ( $\text{CH}_2\text{-Ph}$ ), 72.68 ( $\text{C}_{12\text{chol}}$ ), 72.54 ( $\text{CH}_2\text{-Ph}$ ), 72.46 ( $\text{CH}_2\text{-Ph}$ ), 70.90 ( $\text{C}_{1'}$ ), 70.51 (PEG backbone), 69.62

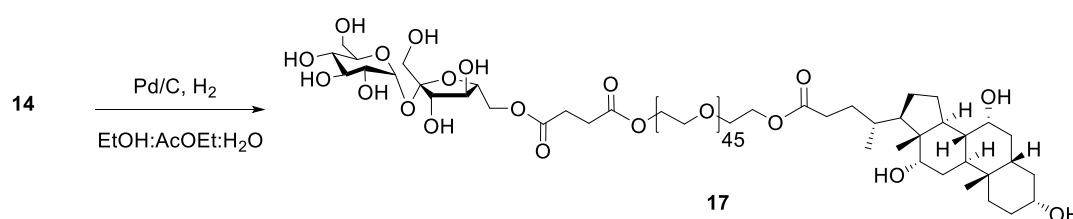
(CH<sub>2</sub>-Ph<sub>chol</sub>), 69.14 (PEG backbone), 68.99 (PEG backbone), 68.41 (C6), 68.17 (C7<sub>chol</sub>), 65.51 (C6'), 63.72 (-C(=O)OCH<sub>2</sub>CH<sub>2</sub>O-), 63.37 ((-C<sub>chol</sub>(=O)OCH<sub>2</sub>CH<sub>2</sub>O-), 47.01 (C17<sub>chol</sub>), 46.46 (C13<sub>chol</sub>), 41.96 (C14<sub>chol</sub>), 41.40 (C5<sub>chol</sub>), 39.62 (C8<sub>chol</sub>), 36.19 (C4<sub>chol</sub>), 35.13 (C1<sub>chol</sub>), 34.96 (C20<sub>chol</sub>), 34.93 (C10<sub>chol</sub>), 34.54 (C6<sub>chol</sub>), 31.06 (C23<sub>chol</sub>), 30.73 (C22<sub>chol</sub>), 28.77 (-CH<sub>2</sub>CH<sub>2</sub>-), 28.39 (C11<sub>chol</sub>), 27.35 (C16<sub>chol</sub>), 27.19 (C2<sub>chol</sub>), 26.69 (C9<sub>chol</sub>), 23.10 (C15<sub>chol</sub>), 22.60 (C19<sub>chol</sub>), 17.27 (C21<sub>chol</sub>), 12.54 (C18<sub>chol</sub>).

## VI.2.4 General procedure 2 for hydrogenation reactions

A Parr hydrogenation flask was charged with a solution of the benzylated compound in EtOH:AcOEt:H<sub>2</sub>O (7:7:0.1) and Pd-charcoal activated hydrogenation catalyst (Pd 10% wt). This mixture was hydrogenated at 40 bar for 24 h. The suspension was filtered through a plug of celite and the residue washed with MeOH. The mixture was then concentrated under reduced pressure.

## VI.2.5 Deprotection of PEG-based conjugates

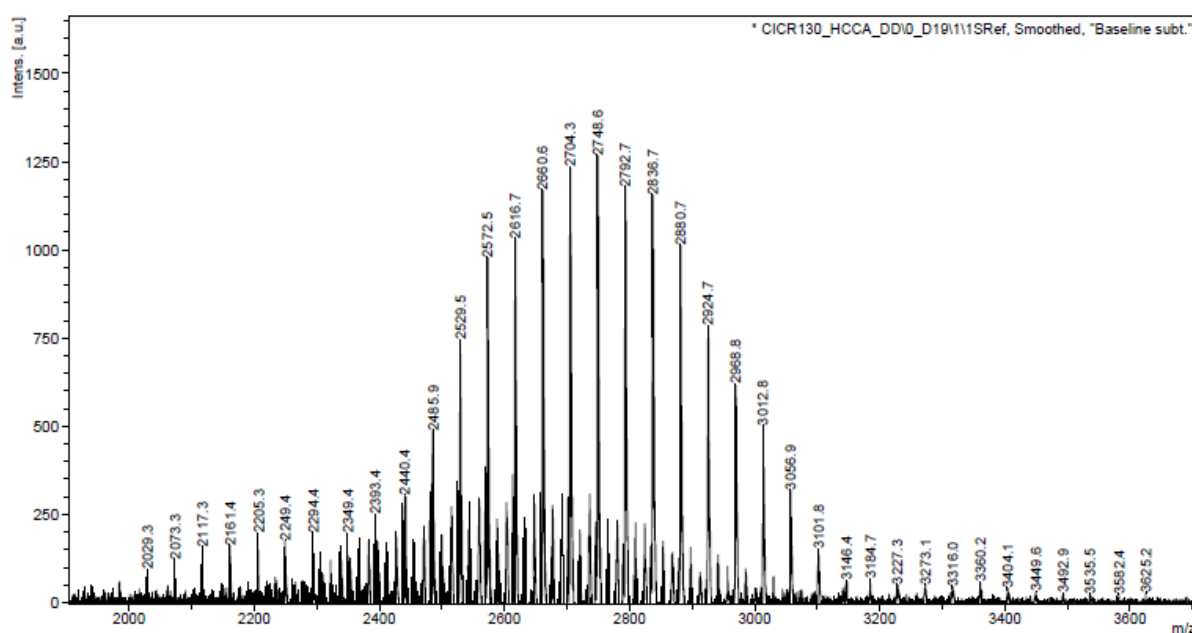
### VI.2.5.1 Suc-PEG2000-Chol (17)



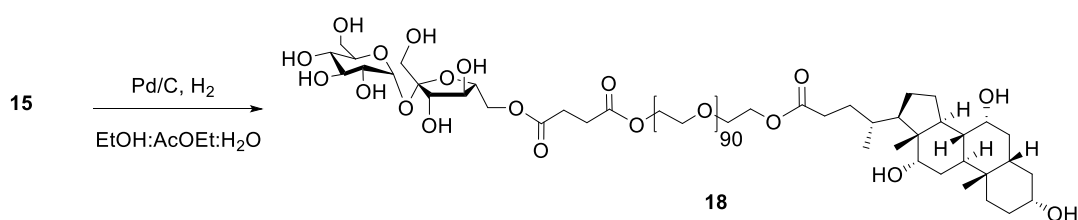
According to the general method 2, benzylated Suc-PEG2000-Chol **14** (0.76 g, 0.22 mmol) dissolved in EtOH:AcOEt:H<sub>2</sub>O (7:7:0.1) (30 mL) and Pd/C 10% (0.20 g) were reacted for 24 h. Pure **17** (0.62 g, 0.22 mmol, 100 %) was obtained as a white waxy solid. **m.p.** 38.60 °C. <sup>1</sup>H NMR (DMSO-*d*<sub>6</sub>): δ 5.6 (d, *J* = 8.0 Hz, 1H, -OH), 5.40 – 5.33 (m, 1H, -OH), 5.1 (d, *J* = 3.6 Hz, 1H, H-1), 5.08 – 5.01 (m, 1H, -OH), 4.91 – 4.61 (m, 3H, -OH), 4.39 – 4.27 (m, 2H, H-6'<sub>a</sub>, -OH), 4.15 – 4.06 (m, 6H, H-6'<sub>b</sub>, -C(=O)OCH<sub>2</sub>CH<sub>2</sub>O), 3.99 (d, *J* = 3.2 Hz, 1H, -OH), 3.92 – 3.85 (m, 1H, H-3'), 3.83 – 3.73 (m, 2H, H-4', H-12β<sub>chol</sub>), 3.72 – 3.64 (m, 2H, H-5, H-5'), 3.63 – 3.24 (m and Brs, H-3, H-6, H-1', H-7β<sub>chol</sub>, PEG backbone), 3.21 – 3.12 (m, 2H, H-2, H-3β<sub>chol</sub>), 3.08 (t, *J* = 9.3 Hz, 1H, H-4), 2.57 – 2.54 (m, 4H, -CH<sub>2</sub>CH<sub>2</sub>-), 2.36 – 2.26 (m, 1H, H-23α<sub>chol</sub>), 2.26 – 2.07 (m, 3H, H-4α<sub>chol</sub>, H-9α<sub>chol</sub>, H-23β<sub>chol</sub>), 2.02 – 1.92 (m, 1H, H-14α<sub>chol</sub>), 1.83 – 1.55 (m, 6H, H-1α<sub>chol</sub>, H-6β<sub>chol</sub>, H-15β<sub>chol</sub>, H-16α<sub>chol</sub>, H-17α<sub>chol</sub>, H-22α<sub>chol</sub>), 1.53 – 0.95 (m, 12H, H-2α<sub>chol</sub>, H-4β<sub>chol</sub>, H-5β<sub>chol</sub>, H-6α<sub>chol</sub>, H-8β<sub>chol</sub>, H-11<sub>chol</sub>, H-15α<sub>chol</sub>, H-16β<sub>chol</sub>, H-20<sub>chol</sub>, H-22β<sub>chol</sub>), 0.93 – 0.74 (m, 1H, H-1β<sub>chol</sub>), 0.91 (d, *J* = 6.3 Hz, 3H, 21-CH<sub>3chol</sub>), 0.79 (s, 3H, 19-CH<sub>3chol</sub>), 0.57 (s, 3H, 18-CH<sub>3chol</sub>). <sup>13</sup>C NMR (DMSO-*d*<sub>6</sub>): δ 173.32 (C24<sub>chol</sub>), 171.96 (-C(=O)O-PEG),

171.87 (-C(=O)O), 104.25 (C2'), 91.74 (C1), 79.17 (C5'), 76.39 (C3'), 74.73 (C4'), 72.84 (C3), 72.78 (C5), 71.62 (C2), 70.97 (C12<sub>chol</sub>), 70.42 (C3<sub>chol</sub>), 70.03 (C4), 69.77 (PEG backbone), 68.33 (-C(=O)OCH<sub>2</sub>CH<sub>2</sub>O-), 68.21 (-C(=O)OCH<sub>2</sub>CH<sub>2</sub>O-), 66.22 (C7<sub>chol</sub>), 65.93 (C6'), 63.47 (PEG backbone), 63.04 (PEG backbone), 61.64 (C-1'), 60.72 (C-6), 46.08 (C17<sub>chol</sub>), 45.76 (C13<sub>chol</sub>), 41.51 (C5<sub>chol</sub>), 41.36 (C14<sub>chol</sub>), 39.75 (C4<sub>chol</sub>)\*, 39.47 (C8<sub>chol</sub>)\*, 35.30 (C1<sub>chol</sub>), 35.00 (C20<sub>chol</sub>), 34.86 (C6<sub>chol</sub>), 34.37 (C10<sub>chol</sub>), 30.70 (C22<sub>chol</sub>), 30.65 (C23<sub>chol</sub>), 30.40 (C2<sub>chol</sub>), 28.51 (C11<sub>chol</sub>), 28.45 (-CH<sub>2</sub>CH<sub>2</sub>-), 27.25 (C16<sub>chol</sub>), 26.19 (C9<sub>chol</sub>), 22.80 (C15<sub>chol</sub>), 22.61 (C19<sub>chol</sub>), 16.86 (C21<sub>chol</sub>), 12.30 (C18<sub>chol</sub>). \*DEPT

#### MALDI-TOF:



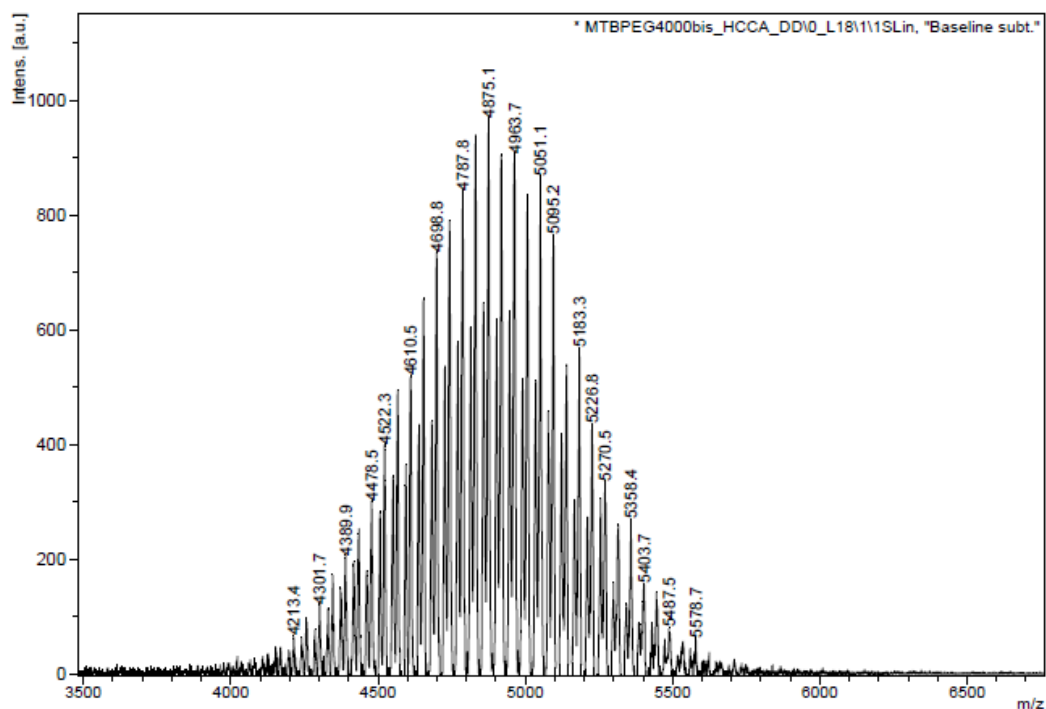
#### VI.2.5.2 Suc-PEG4000-Chol (18)



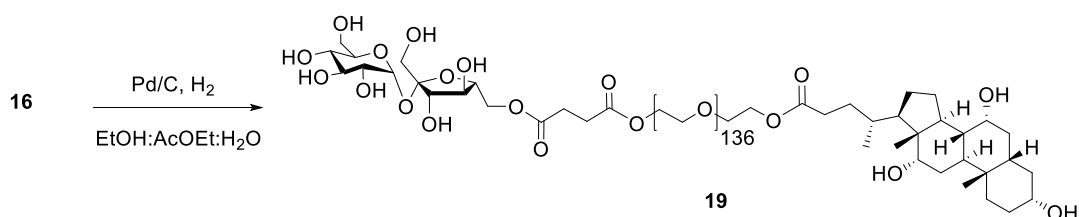
According to the general method **2**, benzylated Suc-PEG4000-Cholic **15** (0.90 g, 0.16 mmol) dissolved in EtOH:AcOEt:H<sub>2</sub>O (7:7:0.1) (30 mL) and Pd/C 10% (0.25 g) were reacted for 24 h. Pure **18** (0.67 g, 0.14 mmol, 88 %) was obtained as a white waxy solid.  $[\alpha]_D^{20} +11.2$  (c 0.5, CHCl<sub>3</sub>). **m.p.** 47.58 °C. **<sup>1</sup>H NMR** (DMSO-*d*<sub>6</sub>): δ 5.60 (d, *J* = 8.0 Hz, 1H, -OH), 5.45 – 5.35 (m, 1H, -OH), 5.13 (d, *J* = 3.6 Hz, 1H, H-1), 5.10 – 5.01 (m, 1H, -OH), 4.91 – 4.63 (m, 3H, -OH), 4.39 – 4.28 (m, 2H, H-6'<sub>a</sub>, -OH), 4.20 – 4.06 (m, 6H, H-6'<sub>b</sub>, -C(=O)OCH<sub>2</sub>CH<sub>2</sub>O), 3.95 – 3.86 (m, 1H, H-3'), 3.85 – 3.76 (m, 2H, H-4', H-12<sub>chol</sub>), 3.75 – 3.24 (m and Brs, H-3, H-5, H-6, H-1', H-5'H-7<sub>chol</sub>, PEG backbone), 3.22 – 3.14 (m, 2H, H-2,

H-3<sub>chol</sub>), 3.13 – 3.03 (m, 1H, H-4), 2.60 – 2.54 (m, 4H, -CH<sub>2</sub>CH<sub>2</sub>-), 2.38 – 2.27 (m, 1H, H-23<sub>αchol</sub>), 2.25 – 2.09 (m, 3H, H-4<sub>αchol</sub>, H-9<sub>αchol</sub>, H-23<sub>βchol</sub>), 2.05 – 1.93 (m, 1H, H-14<sub>αchol</sub>), 1.85 – 1.57 (m, 6H, H-1<sub>αchol</sub>, H-6<sub>βchol</sub>, H-15<sub>βchol</sub>, H-16<sub>αchol</sub>, H-17<sub>αchol</sub>, H-22<sub>αchol</sub>), 1.52 – 0.97 (m, 12H, H-2<sub>αchol</sub>, H-4<sub>βchol</sub>, H-5<sub>βchol</sub>, H-6<sub>αchol</sub>, H-8<sub>βchol</sub>, H-11<sub>chol</sub>, H-15<sub>αchol</sub>, H-16<sub>βchol</sub>, H-20<sub>chol</sub>, H-22<sub>βchol</sub>), 0.91 – 0.76 (m, 1H, H-1<sub>βchol</sub>), 0.92 (d, *J* = 6.3 Hz, 3H, 21-CH<sub>3chol</sub>), 0.76 (s, 3H, 19-CH<sub>3chol</sub>), 0.59 (s, 3H, 18-CH<sub>3chol</sub>). <sup>13</sup>C NMR (DMSO-*d*<sub>6</sub>): δ 173.36 (C24<sub>chol</sub>), 172.00 (C(=O)O-PEG), 171.90 (C(=O)O), 104.24 (C2'), 91.76 (C1), 79.19 (C5'), 76.42 (C3'), 74.76 (C4'), 72.87 (C3), 72.79 (C5), 71.64 (C2), 71.02 (C12<sub>chol</sub>), 70.42 (C3<sub>chol</sub>), 70.05 (C4), 69.80 (PEG backbone), 68.35 (-C(=O)OCH<sub>2</sub>CH<sub>2</sub>O-), 68.23 (-C(=O)OCH<sub>2</sub>CH<sub>2</sub>O-), 66.26 (C7<sub>chol</sub>), 65.95 (C6'), 63.50 (PEG backbone), 63.07 (PEG backbone), 61.68 (C-1'), 60.75 (C-6), 46.11 (C17<sub>chol</sub>), 45.79 (C13<sub>chol</sub>), 41.38 (C5<sub>chol</sub>), 41.06 (C14<sub>chol</sub>), 35.30 (C1<sub>chol</sub>), 35.00 (C20<sub>chol</sub>), 34.86 (C6<sub>chol</sub>), 34.40 (C10<sub>chol</sub>), 30.72 (C22<sub>chol</sub>), 30.65 (C23<sub>chol</sub>), 30.40 (C2<sub>chol</sub>), 28.56 (C11<sub>chol</sub>), 28.48 (-CH<sub>2</sub>CH<sub>2</sub>-), 27.27 (C16<sub>chol</sub>), 26.19 (C9<sub>chol</sub>), 22.79 (C15<sub>chol</sub>), 22.63 (C19<sub>chol</sub>), 16.89 (C21<sub>chol</sub>), 12.32 (C18<sub>chol</sub>).

#### MALDI-TOF:

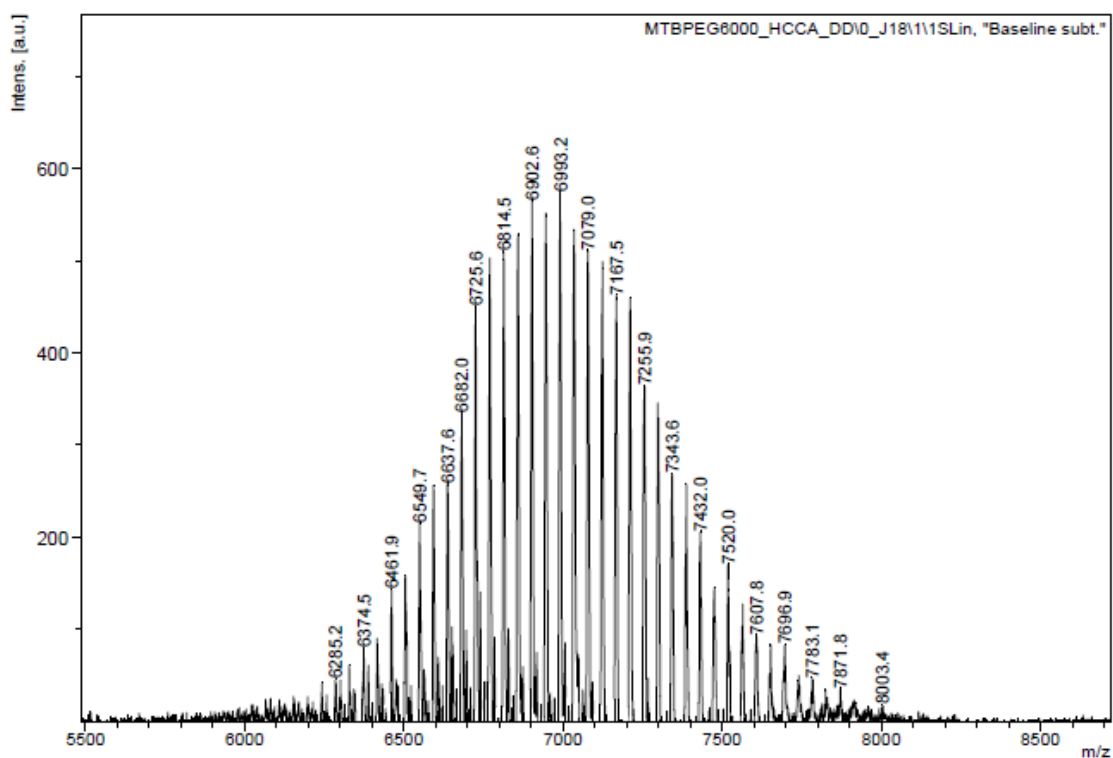


#### VI.2.5.3 Suc-PEG6000-Chol (19)



According to the general method **2**, benzylated Suc-PEG6000-Chol **16** (1.92 g, 0.26 mmol) dissolved in EtOH:AcOEt:H<sub>2</sub>O (7:7:0.1) (60 mL) and Pd/C 10% (0.5 g) were reacted for 24 h. Pure **19** (1.63 g, 0.24 mmol, 94 %) was obtained as a white waxy solid. **m.p.** 54.93 °C. <sup>1</sup>H NMR (DMSO-*d*<sub>6</sub>): δ 5.77 (d, *J* = 7.5 Hz, 1H, -OH), 5.43 – 5.35 (m, 1H, -OH), 5.10 – 5.08 (m, 1H, H-1), 5.03 (d, *J* = 5.8 Hz, 1H, -OH), 4.89 – 4.53 (m, 3H, -OH), 4.51 – 4.25 (m, 2H, H-6'<sub>a</sub>, -OH), 4.18 – 4.05 (m, 6H, H-6'<sub>b</sub>, -C(=O)OCH<sub>2</sub>CH<sub>2</sub>O), 4.03 – 3.95 (m, 1H, -OH), 3.94 – 3.84 (m, 1H, H-3'), 3.83 – 3.66 (m, 2H, H-4', H-12β<sub>chol</sub>), 3.65 – 3.25 (m and Brs, H-3, H-5, H-6, H-1', H-5'H-7β<sub>chol</sub>, PEG backbone), 3.22 – 3.12 (m, 2H, H-2, H-3β<sub>chol</sub>), 3.12 – 3.04 (m, 1H, H-4), 2.62 – 2.42 (m, 4H, -CH<sub>2</sub>CH<sub>2</sub>-), 2.36 – 2.25 (m, 1H, H-23α<sub>chol</sub>), 2.25 – 2.05 (m, 3H, H-4α<sub>chol</sub>, H-9α<sub>chol</sub>, H-23β<sub>chol</sub>), 2.02 – 1.90 (m, 1H, H-14α<sub>chol</sub>), 1.83 – 1.56 (m, 6H, H-1α<sub>chol</sub>, H-6β<sub>chol</sub>, H-15β<sub>chol</sub>, H-16α<sub>chol</sub>, H-17α<sub>chol</sub>, H-22α<sub>chol</sub>), 1.55 – 0.96 (m, 12H, H-2α<sub>chol</sub>, H-4β<sub>chol</sub>, H-5β<sub>chol</sub>, H-6α<sub>chol</sub>, H-8β<sub>chol</sub>, H-11<sub>chol</sub>, H-15α<sub>chol</sub>, H-16β<sub>chol</sub>, H-20<sub>chol</sub>, H-22β<sub>chol</sub>), 0.89 – 0.84 (m, 1H, H-1β<sub>chol</sub>), 0.91 (d, *J* = 6.5 Hz, 3H, 21-CH<sub>3chol</sub>), 0.79 (s, 3H, 19-CH<sub>3chol</sub>), 0.57 (s, 3H, 18-CH<sub>3chol</sub>). <sup>13</sup>C NMR (DMSO-*d*<sub>6</sub>): δ 173.26 (C24<sub>chol</sub>), 171.99 (C(=O)O-PEG), 171.90 (C(=O)O), 104.30 (C2'), 91.79 (C1), 79.17 (C5'), 76.51 (C3'), 74.75 (C4'), 72.85 (C3), 72.81 (C5), 71.99 (C2), 71.95 (C12<sub>chol</sub>), 71.68 (C3<sub>chol</sub>), 70.01 (C4), 69.80 (PEG backbone), 68.35 (-C(=O)OCH<sub>2</sub>CH<sub>2</sub>O-), 68.23 (-C(=O)OCH<sub>2</sub>CH<sub>2</sub>O-), 66.26 (C7<sub>chol</sub>), 65.97 (C6'), 63.49 (PEG backbone), 63.07 (PEG backbone), 61.63 (C-1'), 60.69 (C-6), 46.13 (C17<sub>chol</sub>), 45.78 (C13<sub>chol</sub>), 41.53 (C5<sub>chol</sub>), 40.13 (C14<sub>chol</sub>), 35.25 (C1<sub>chol</sub>), 35.02 (C20<sub>chol</sub>), 34.88 (C6<sub>chol</sub>), 34.39 (C10<sub>chol</sub>), 30.72 (C22<sub>chol</sub>), 30.68 (C23<sub>chol</sub>), 30.40 (C2<sub>chol</sub>), 28.54 (C11<sub>chol</sub>), 28.47 (-CH<sub>2</sub>CH<sub>2</sub>-), 27.28 (C16<sub>chol</sub>), 26.22 (C9<sub>chol</sub>), 22.82 (C15<sub>chol</sub>), 22.63 (C19<sub>chol</sub>), 16.88 (C21<sub>chol</sub>), 12.32 (C18<sub>chol</sub>).

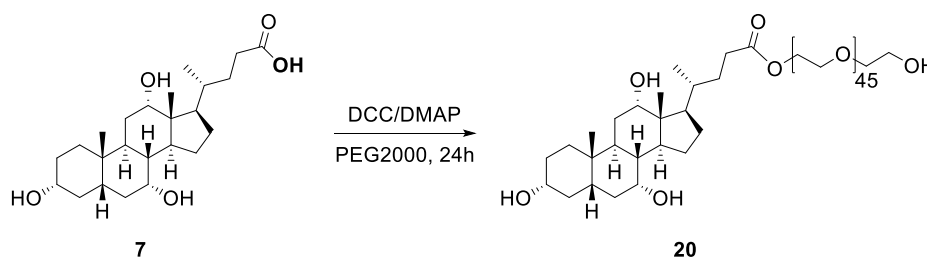
#### MALDI-TOF:



## VI.2.6 General procedure 3 for the synthesis of Cholic-PEG conjugates

To a suspension of cholic acid **7** (0.2 g, 0.5 mmol, 1 eq) in anhydrous THF (20 mL) were added DMAP (61 mg, 0.5 mmol, 1 eq) and the appropriate PEG compound (0.5 mmol, 1.0 eq). The resulting mixture was heated up to 30 °C to aid dissolution. Then, DCC (0.21 g, 1 mmol, 2 eq) was added and the reaction was stirred for 24 h at 30 °C. TLC analysis (CHCl<sub>3</sub>:MeOH 9:1) revealed total consumption of cholic acid but PEG was still present in the reaction mixture. The solvent was evaporated. The residue was dissolved in CH<sub>2</sub>Cl<sub>2</sub> (100 mL), washed with HCl 10 % (3 x 10 mL), a saturated solution of NaHCO<sub>3</sub> (3 x 10 mL) and brine (2 x 10 mL). The whole organic layer was dried over anhydrous Na<sub>2</sub>SO<sub>4</sub>. The residue was purified by column chromatography using a step gradient of MeOH (1-10 %) in CHCl<sub>3</sub>. Compounds were visualized with phosphomolybdic acid by TLC analysis (CHCl<sub>3</sub>:MeOH 9:1).

### VI.2.6.1 Cholic-PEG2000 (**20**)



According to the general method **3**, cholic acid **7**, DMAP, DCC and PEG2000 (1.0 g, 0.5 mmol, 1eq) dissolved in dry THF (20 mL), were reacted for 24 h at 30 °C. Purification by column chromatography (CHCl<sub>3</sub>:MeOH 1-10 %) afforded product **20** (0.91 g, 0.38 mmol, 76 %) as a white waxy solid. **R<sub>f</sub>** 0.53 (CHCl<sub>3</sub>:MeOH 9:1). **m.p.** 53.55 °C. **T<sub>c</sub>** 15.02 °C. **<sup>1</sup>H NMR** (DMSO-*d*<sub>6</sub>): δ 4.31 (d, *J* = 4.3 Hz, 1H, C3-OH), 4.09 (d, *J* = 3.4 Hz, 1H, C12-OH), 3.99 (d, *J* = 3.3 Hz, 1H, C7-OH), 3.81 – 3.74 (m, 1H, H-12β), 3.71 – 3.68 (m, 1H, PEG-OH), 3.65 – 3.60 (m, 1H, H-7β), 3.59 – 3.46 (m and Brs, PEG backbone), 3.42 (t, *J* = 4.9 Hz, 2H, PEG backbone), 3.26 – 3.14 (m, 1H, H-3β), 2.36 – 2.10 (m, 4H, H-4α, H-9α, H-23αβ), 2.05 – 1.93 (m, 1H, H-14α), 1.85 – 1.51 (m, 6H, H-1α, H-2α, H-6β, H-15β, H-16α, H-17α, H-20, H-22α), 1.50 – 0.93 (m, 12H, H-2α, H-4β, H-5β, H-6α, H-8β, H-11, H-15α, H-16β, H-20, H-22β), 0.93 – 0.74 (m, 1H, H-1β), 0.90 (d, *J* = 6.1 Hz, 3H, 21-CH<sub>3</sub>), 0.82 (s, 3H, 19-CH<sub>3</sub>), 0.59 (s, 3H, 18-CH<sub>3</sub>). **<sup>13</sup>C NMR** (DMSO-*d*<sub>6</sub>): δ 170.12 (C24), 72.32 (PEG backbone), 70.95 (C12), 70.41 (C3), 70.16 (PEG backbone), 69.76 (PEG backbone), 66.21 (C7), 60.19 (-OCH<sub>2</sub>CH<sub>2</sub>OH), 46.03 (C17), 45.69 (C13), 41.50 (C5), 41.33 (C14), 39.75 (C4)\*, 39.54 (C8)\*, 35.28 (C1), 35.04 (C20), 34.86 (C6), 34.36 (C10), 30.14 (C22), 30.36 (C23), 30.31 (C2), 28.54 (C11), 27.22 (C16), 26.20 (C9), 22.75 (C15), 22.60 (C19), 17.07 (C21), 12.29 (C18). \*DEPT

Amostra Cholic-PEG2000 com DHB+Na

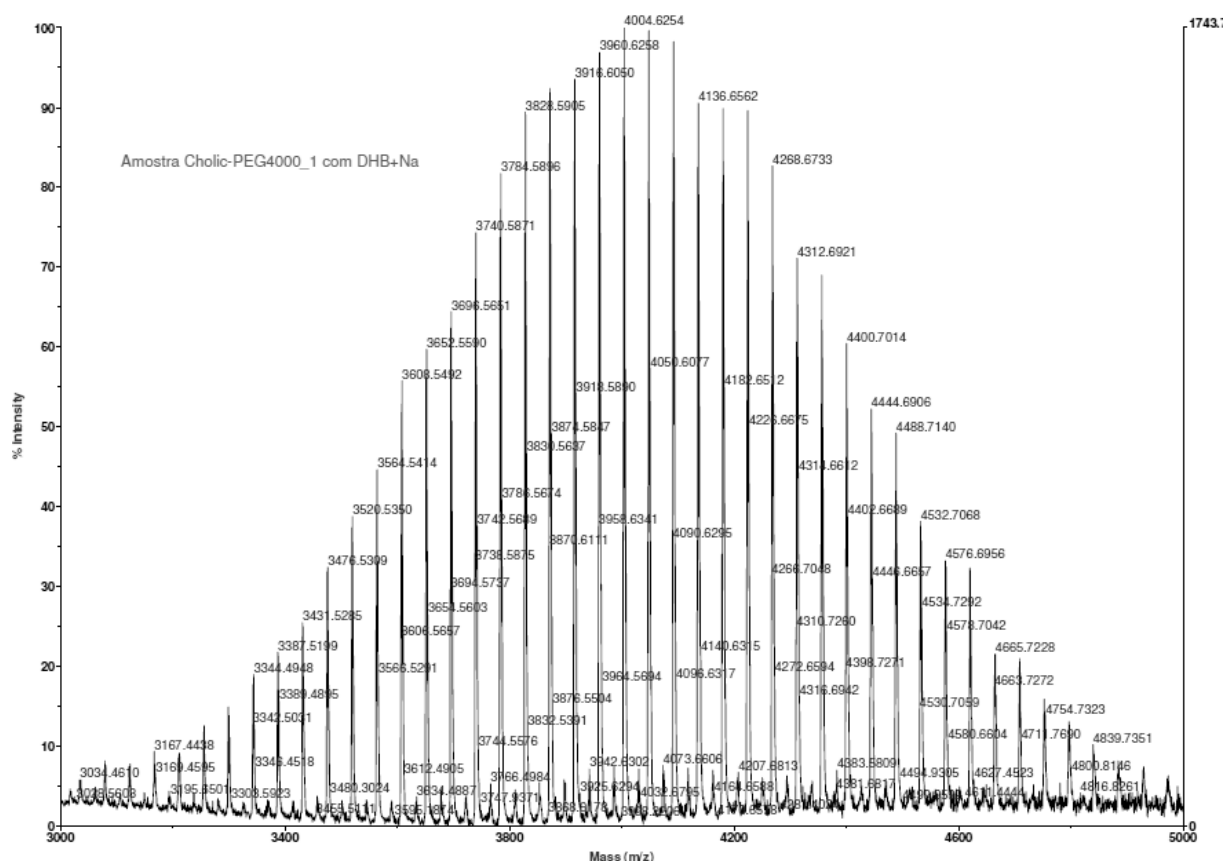
m/z	% Intensity (approx)
1027.8940	10
1053.7835	5
1097.9107	5
1167.8910	5
1314.0015	5
1353.9497	5
1362.0235	10
1404.0686	15
1434.1010	10
1450.0890	15
1494.1114	20
1538.1413	30
1540.1441	10
1552.0997	10
1577.0641	15
1582.1737	40
1584.1542	10
1596.1711	10
1624.1912	50
1628.1869	10
1670.2164	65
1672.2104	25
1689.2424	10
1714.2413	75
1716.2418	35
1722.2727	10
1758.2736	85
1760.2727	45
1794.6910	10
1802.2986	90
1844.3218	100
1844.3193	50
1873.3760	10
1884.3490	10
1892.3446	55
1935.3761	95
1957.3096	10
1979.4037	95
1989.4169	25
2005.4369	10
2023.4246	90
2067.4498	85
2071.3782	10
2111.4757	75
2113.4821	20
2155.5030	65
2157.5087	15
2190.5312	55
2209.4210	10
2209.5393	15
2243.5558	45
2287.5633	35
2289.5806	10
2331.5956	30
2377.6458	10
2419.6544	15
2429.5955	10
2463.6882	15
2507.6885	10
2551.7139	10
2553.7963	10
2683.7402	10
2867.0121	10
3431	100

Chemical reaction scheme showing the synthesis of compound 21 from compound 7. Compound 7 is a steroid with a carboxylic acid side chain. It reacts with PEG4000 in the presence of DCC/DMAP for 24 hours to form compound 21, where the carboxylic acid is esterified with a PEG chain of approximately 90 units.

108

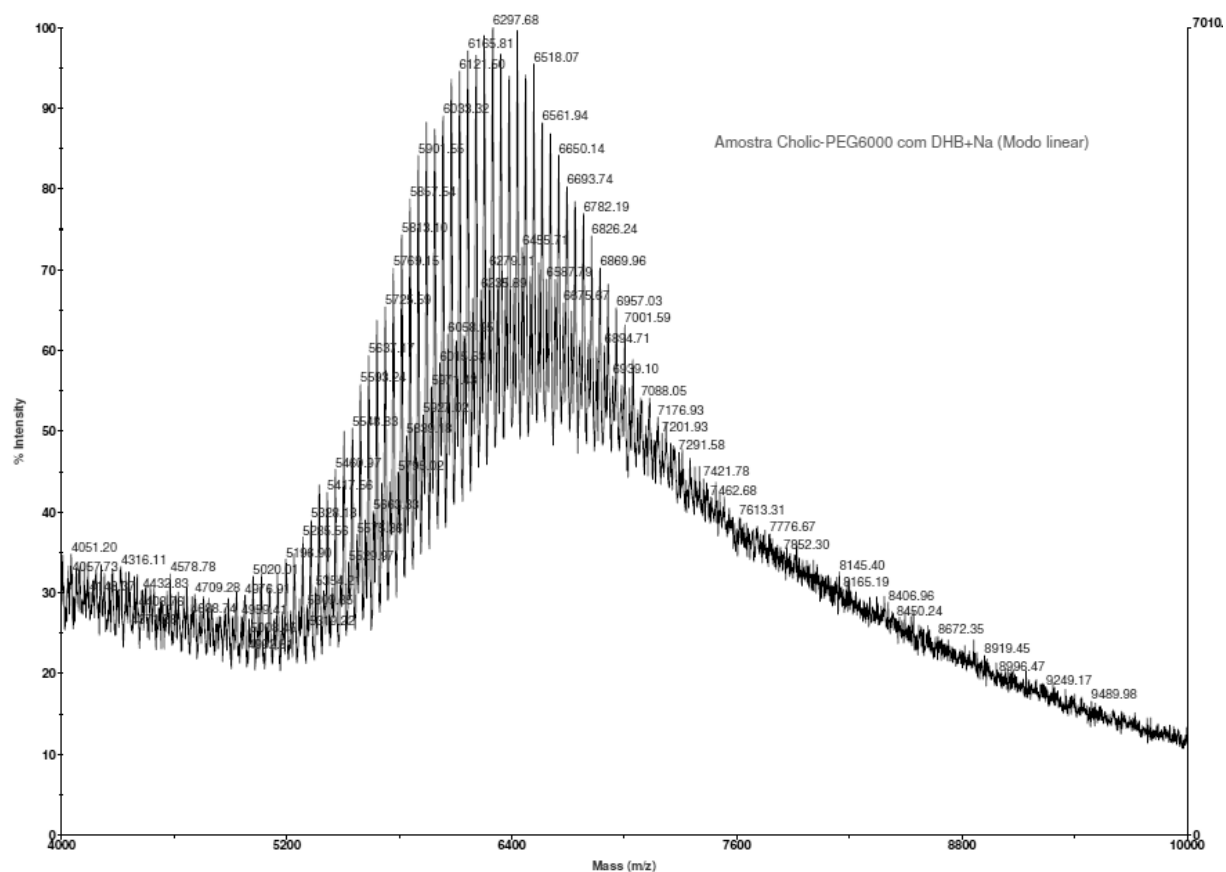
18-CH<sub>3</sub>). <sup>13</sup>C NMR (DMSO-*d*<sub>6</sub>): δ 170.12 (C24), 72.32 (PEG backbone), 70.95 (C12), 70.41 (C3), 70.16 (PEG backbone), 69.76 (PEG backbone), 66.21 (C7), 60.19 (-OCH<sub>2</sub>CH<sub>2</sub>OH), 46.03 (C17), 45.69 (C13), 41.50 (C5), 41.33 (C14), 39.75 (C4)\*, 39.54 (C8)\*, 35.28 (C1), 35.04 (C20), 34.86 (C6), 34.36 (C10), 30.14 (C22), 30.36 (C23), 30.31 (C2), 28.54 (C11), 27.22 (C16), 26.20 (C9), 22.75 (C15), 22.60 (C19), 17.07 (C21), 12.29 (C18). \*DEPT

#### MALDI-TOF:



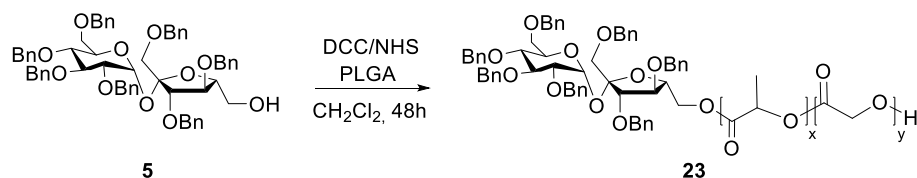
4.3 Hz, 1H, C3-OH), 4.09 (d,  $J = 3.4$  Hz, 1H, C12-OH), 3.99 (d,  $J = 3.3$  Hz, 1H, C7-OH), 3.81 – 3.75 (m, 1H, H-12 $\beta$ ), 3.71 – 3.68 (m, 1H, PEG-OH), 3.65 – 3.46 (m and Brs, H-7 $\beta$ , PEG backbone), 3.44 – 3.38 (m, 2H, PEG backbone), 3.25 – 3.14 (m, 1H, H-3 $\beta$ ), 2.36 – 2.10 (m, 4H, H-4 $\alpha$ , H-9 $\alpha$ , H-23 $\alpha\beta$ ), 2.05 – 1.92 (m, 1H, H-14 $\alpha$ ), 1.85 – 1.51 (m, 6H, H-1 $\alpha$ , H-2 $\alpha$ , H-6 $\beta$ , H-15 $\beta$ , H-16 $\alpha$ , H-17 $\alpha$ , H-20, H-22 $\alpha$ ), 1.50 – 0.94 (m, 12H, H-2 $\alpha$ , H-4 $\beta$ , H-5 $\beta$ , H-6 $\alpha$ , H-8 $\beta$ , H-11, H-15 $\alpha$ , H-16 $\beta$ , H-20, H-22 $\beta$ ), 0.93 – 0.82 (m, 1H, H-1 $\beta$ ), 0.90 (d,  $J = 6.1$  Hz, 3H, 21-CH<sub>3</sub>), 0.82 (s, 3H, 19-CH<sub>3</sub>), 0.59 (s, 3H, 18-CH<sub>3</sub>). <sup>13</sup>C NMR (DMSO-*d*<sub>6</sub>):  $\delta$  170.12 (C24), 72.32 (PEG backbone), 70.95 (C12), 70.41 (C3), 70.19 (PEG backbone), 69.76 (PEG backbone), 66.20 (C7), 60.18 (-OCH<sub>2</sub>CH<sub>2</sub>OH), 46.03 (C17), 45.69 (C13), 41.50 (C5), 41.32 (C14), 39.75 (C4)\*, 39.54 (C8)\*, 35.28 (C1), 35.04 (C20), 34.86 (C6), 34.36 (C10), 30.14 (C22), 30.36 (C23), 30.31 (C2), 28.54 (C11), 27.22 (C16), 26.19 (C9), 22.75 (C15), 22.59 (C19), 17.07 (C21), 12.29 (C18). \*DEPT

#### MALDI-TOF:



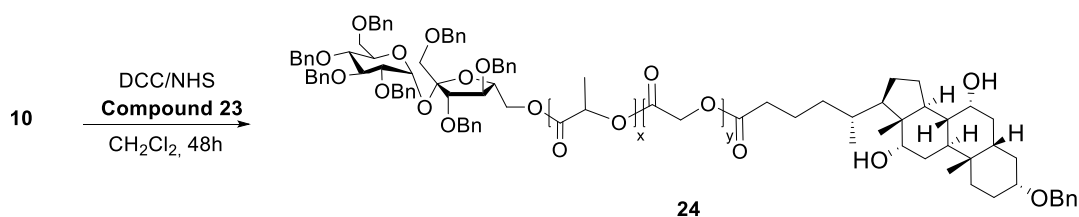
## VI.2.7 Synthesis of PLGA-based conjugates

### VI.2.7.1 Benzylated Suc-PLGA-OH (23)



PLGA 75:25 (0.5 g, 0.009 mmol based on the average molecular weight, 1 eq) was dissolved in dry  $\text{CH}_2\text{Cl}_2$  (10 mL) and the polymer solution was cooled down to 0 °C. DCC (8.5 mg, 0.04 mmol, 4 eq) and NHS (4.0 mg, 0.04 mmol, 4 eq) were added and the mixture was allowed to react for 24 h (activation reaction of the carboxylic acid end group in PLGA). Compound **5** (27 mg, 0.027 mmol, 3 eq) dissolved in dry  $\text{CH}_2\text{Cl}_2$  (1 mL) was added into the polymer solution under magnetic stirring and the reaction was kept for 24 h. The conjugate was purified by precipitation from ice-cold diethyl ether. The collected gel mass was washed with an excess amount of ether and dried under vacuum to yield product **23** (0.5 g, 0.0086 mmol, 94 %) as a white polymeric foam.  $T_g$  35.60 °C.  $^1\text{H NMR}$  ( $(\text{CD}_3)_2\text{CO}$ ):  $\delta$  5.36 – 5.15 (m, 1H,  $\text{CH}_{(\text{lactic acid})}$ ), 5.02 – 4.74 (m, 2H,  $\text{CH}_{2(\text{glycolic acid})}$ ), 1.68 – 1.46 (m, 3H,  $\text{CH}_{3(\text{lactic acid})}$ ).  $^{13}\text{C NMR}$  ( $(\text{CD}_3)_2\text{CO}$ ):  $\delta$  170.32 ( $\text{C}=\text{O}_{(\text{glycolic acid})}$ ), 170.16 ( $\text{C}=\text{O}_{(\text{glycolic acid})}$ ), 170.07 ( $\text{C}=\text{O}_{(\text{glycolic acid})}$ ), 167.63 ( $\text{C}=\text{O}_{(\text{lactic acid})}$ ), 167.56 ( $\text{C}=\text{O}_{(\text{lactic acid})}$ ), 167.47 ( $\text{C}=\text{O}_{(\text{lactic acid})}$ ), 69.95 ( $\text{CH}_{(\text{lactic acid})}$ ), 69.80 ( $\text{CH}_{(\text{lactic acid})}$ ), 61.58 ( $\text{CH}_{2(\text{glycolic acid})}$ ), 61.51 ( $\text{CH}_{2(\text{glycolic acid})}$ ), 61.46 ( $\text{CH}_{2(\text{glycolic acid})}$ ), 17.12 ( $\text{CH}_{3(\text{lactic acid})}$ ), 17.06 ( $\text{CH}_{3(\text{lactic acid})}$ ).

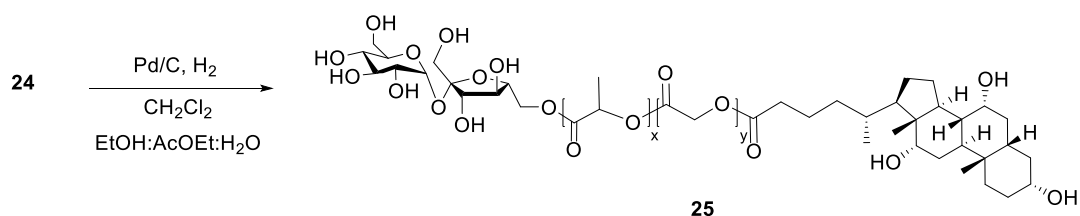
### VI.2.7.2 Benzylated Suc-PLGA-Chol (24)



Compound **10** (18 mg, 0.036 mmol, 5 eq) was dissolved in  $\text{CH}_2\text{Cl}_2$  (5 mL) and the solution was cooled down to 0 °C. DCC (17 mg, 0.07 mmol, 10 eq) and NHS (8.0 mg, 0.07 mmol, 10 eq) were added and the mixture was allowed to react for 20 min. Afterwards, a solution of compound **23** (0.39 g, 0.007 mmol, 1 eq) in dry  $\text{CH}_2\text{Cl}_2$  (10 mL) was added under magnetic stirring and the reaction was kept for 24 h at room temperature. The product was precipitated from ice-cold diethyl ether. The collected gel mass was washed with an excess amount of ether and dried under vacuum to yield product **24** (0.36 g, 0.006 mmol, 86 %) as a white polymeric foam.  $T_g$  44.07 °C.  $^1\text{H NMR}$  ( $(\text{CD}_3)_2\text{CO}$ ):  $\delta$  5.31 – 5.18 (m, 1H,

CH<sub>(lactic acid)</sub>), 4.98 – 4.76 (m, 2H, CH<sub>2(glycolic acid)</sub>), 1.66 – 1.51 (m, 3H, CH<sub>3(lactic acid)</sub>). <sup>13</sup>C NMR ((CD<sub>3</sub>)<sub>2</sub>CO): δ 170.24 (C=O<sub>(glycolic acid)</sub>), 167.54 (C=O<sub>(lactic acid)</sub>), 167.47 (C=O<sub>(lactic acid)</sub>), 69.87 (CH<sub>(lactic acid)</sub>), 69.72 (CH<sub>(lactic acid)</sub>), 61.50 (CH<sub>2(glycolic acid)</sub>), 61.42 (CH<sub>2(glycolic acid)</sub>), 17.04 (CH<sub>3(lactic acid)</sub>), 16.98 (CH<sub>3(lactic acid)</sub>)).

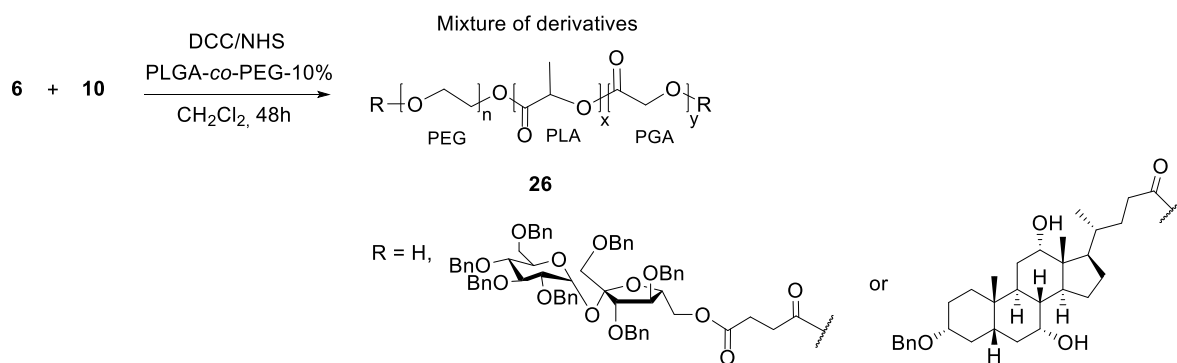
### VI.2.7.3 Suc-PLGA-Chol (25)



A Parr hydrogenation flask was charged with a solution of compound **24** (0.32 g, 0.005 mmol) in a mixture of CH<sub>2</sub>Cl<sub>2</sub> (5 mL) and EtOH:AcOEt:H<sub>2</sub>O (7:7:0.1) (5 mL). Then Pd/C 10% (0.5 g) was added and the mixture was hydrogenated at 40 bar for 24 h. The suspension was filtered through a plug of celite and the residue washed with MeOH. The mixture was then concentrated under reduced pressure. Pure **25** was obtained as a white polymeric foam in quantitative yield. *T<sub>g</sub>* 42.01 °C. <sup>1</sup>H NMR ((CD<sub>3</sub>)<sub>2</sub>CO): δ 5.32 – 5.12 (m, 1H, CH<sub>(lactic acid)</sub>), 5.01 – 4.70 (m, 2H, CH<sub>2(glycolic acid)</sub>), 1.69 – 1.38 (m, 3H, CH<sub>3(lactic acid)</sub>). <sup>13</sup>C NMR ((CD<sub>3</sub>)<sub>2</sub>CO): δ 170.24 – 169.99 (C=O<sub>(glycolic acid)</sub>), 167.54 (C=O<sub>(lactic acid)</sub>), 167.47 (C=O<sub>(lactic acid)</sub>), 167.38 (C=O<sub>(lactic acid)</sub>), 69.93 (CH<sub>(lactic acid)</sub>), 69.86 (CH<sub>(lactic acid)</sub>), 69.72 (CH<sub>(lactic acid)</sub>), 61.50 (CH<sub>2(glycolic acid)</sub>), 61.42 (CH<sub>2(glycolic acid)</sub>), 61.38 (CH<sub>2(glycolic acid)</sub>), 17.03 (CH<sub>3(lactic acid)</sub>), 16.97 (CH<sub>3(lactic acid)</sub>)).

## VI.2.8 Synthesis of PLGA-PEG based conjugates

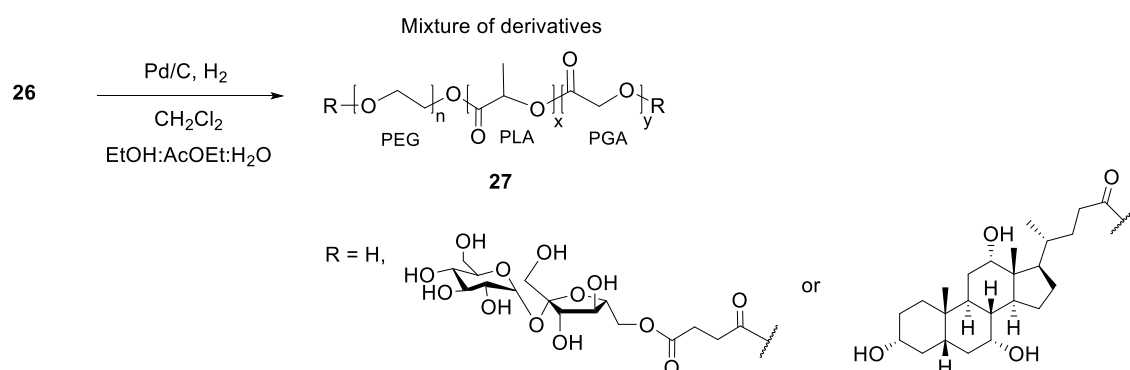
### VI.2.8.1 One-pot synthesis of benzylated Suc/Chol-PLGA-PEG-Chol/Suc (26)



Sucrose and cholic-functionalized copolymer PLGA-co-PEG was synthesized by conjugation of 1',2,3,3',4,4',6-Hepta-*O*-benzyl-6'-*O*-succinyl-sucrose **6** (86 mg, 0.08 mmol, 4 eq) and 3α-*O*-benzyl,

7 $\alpha$ , 12 $\alpha$ -dihydroxy-5 $\beta$ -cholic acid **10** (40 mg, 0.08 mmol, 4 eq) to PLGA-*co*-PEG-10% diblock (1.0 g, 0.02 mmol, 1 eq). The coupling reaction was performed in CH<sub>2</sub>Cl<sub>2</sub> (20 mL) in the presence of DCC (75 mg, 0.32 mmol, 16 eq) and NHS (35 mg, 0.32 mmol, 16 eq) under magnetic stirring for 48 h at room temperature. The product was precipitated from ice-cold diethyl ether. The collected gel mass was washed with an excess amount of ether and dried under vacuum to yield PLGA-*co*-PEG-10% conjugates as a mixture of sucrose and cholic acid derivatives **26** (0.9 g).

#### VI.2.8.2 Benzyl deprotection of Suc/Chol-PLGA-PEG-Chol/Suc **26** (**27**)



A solution of the protected polymer conjugate **26** (0.9 g) in a mixture of CH<sub>2</sub>Cl<sub>2</sub> (20 mL) and EtOH:AcOEt:H<sub>2</sub>O (7:7:0.1) (15 mL), previously deaerated (argon purged), was treated with Pd/C 10% (0.1 g). The mixture was hydrogenated at 40 bar for 18 h. The suspension was filtered through a plug of celite and the residue washed with MeOH. The mixture was then concentrated under reduced pressure to yield PLGA-*co*-PEG-10% conjugates as a mixture of sucrose and cholic acid derivatives **27** in quantitative yield. *T<sub>g</sub>* 29.83 °C. <sup>1</sup>H NMR ((CD<sub>3</sub>)<sub>2</sub>CO): δ 5.36 – 5.14 (m, 1H, CH<sub>(lactic acid)</sub>), 5.04 – 4.76 (m, 2H, CH<sub>2(glycolic acid)</sub>), 3.62 (Brs, PEG backbone), 1.66 – 1.46 (m, 3H, CH<sub>3(lactic acid)</sub>). <sup>13</sup>C NMR ((CD<sub>3</sub>)<sub>2</sub>CO): δ 170.23 (C=O<sub>(glycolic acid)</sub>), 170.07 (C=O<sub>(glycolic acid)</sub>), 169.98 (C=O<sub>(glycolic acid)</sub>), 167.53 (C=O<sub>(lactic acid)</sub>), 167.47 (C=O<sub>(lactic acid)</sub>), 167.38 (C=O<sub>(lactic acid)</sub>), 71.15 (PEG backbone), 69.86 (CH<sub>(lactic acid)</sub>), 69.72 (CH<sub>(lactic acid)</sub>), 61.49 (CH<sub>2(glycolic acid)</sub>), 61.42 (CH<sub>2(glycolic acid)</sub>), 17.03 (CH<sub>3(lactic acid)</sub>), 16.97 (CH<sub>3(lactic acid)</sub>).

#### VI.2.9 Measurement of fluorescence spectroscopy (pyrene)

The self-aggregation behavior and critical aggregation concentration (CAC) of the polymer conjugates in aqueous environment were investigated by photophysical methods using pyrene as fluorescence probe. Pyrene emission fluorescence spectra were obtained by using a spectrofluorophotometer (SPEX Fluorolog Spectrofluorimeter). All emission spectra were collected with 2 nm slit bandwidth for excitation and 1 nm for emission, with correction files. The excitation

wavelength was 340 nm. The samples were prepared as follows: a known amount of pyrene dissolved in acetone was added to a series of 4 mL vials and the acetone was then evaporated overnight in a vacuum excicator. The pyrene concentration was then adjust to give a final concentration of  $6.0 \times 10^{-7}$  M in 3 mL of polymer solutions concentrations from 1 mg/mL to  $1 \times 10^{-4}$  mg/mL. The resulting solutions were left overnight at room temperature to equilibrate the pyrene and the polymeric nanoparticles.

## **VI.3 Preparation of polymeric nanoparticles**

### **VI.3.1 Emulsion-solvent evaporation method**

Polymeric nanoparticles were prepared using an o/w emulsion solvent evaporation method. In detail, 20 mg of polymer conjugate was dissolved in 2 mL of  $\text{CH}_2\text{Cl}_2$ . The polymer solution was added to 4 mL of an aqueous solution containing 0.5 % w/v PVA as a stabilizer. Emulsions were prepared by mixing the oil and water phases for 6 min. at 2500 rpm with a vortex mixer or by sonication using a ultrasonic bath at an output of 120 W. The resulting PNP suspension was allowed to stir uncovered for 16 h at room temperature to completely evaporate the organic solvent. PNPs were purified by centrifugation (10 min., 5000 rpm). The PNPs were re-suspended, washed three times with deionized water, and collected likewise. Then the obtained PNP suspension was frozen in liquid nitrogen and freeze-dried at  $-55^\circ\text{C}$  and 0.5 kPa. The powdered PNPs were stored at  $4^\circ\text{C}$  until used. Millipore water was used to prepare nanoparticle suspensions.

### **VI.3.2 Nanoprecipitation method**

The nanoprecipitation method was employed for the formation of PNPs. Briefly, accurately weighed 20 mg of the polymer conjugate was dissolved in 2 mL of an organic solvent that is miscible with water. The organic phase was added drop-wise into 4 mL of an aqueous phase under moderate magnetic stirring (360 rpm). The organic solvent was removed by stirring uncovered for 16 h at room temperature or rapidly eliminated by evaporation under reduced pressure. Finally, the particles were isolated by centrifugation for 15 min. at 5000 rpm. Dry particles were collected by freeze drying or by drying under vacuum over phosphorus pentoxide. The dry powder was stored at  $4^\circ\text{C}$  until used. Millipore water was used to prepare nanoparticle solutions. To formulate PNPs loaded with rhodamine b, the model drug (1 mg) was added in the organic phase, followed by the same sequence as above.

## **VI.4 Characterization of polymeric nanoparticles**

### **VI.4.1 Particle size and zeta potential**

The mean particle size and particle size distribution were measured by dynamic light scattering (DLS) using a laser light scattering instrument (SZ-100 nanopartica, Horiba) at 90° scattering angle. Refractive index was 1.330 and temperature was kept at 25 °C during measuring process. The intensity-weighted mean value was recorded as the average of three measurements.

$\zeta$ -potential values of the PNPs were determined by laser doppler electrophoresis technique (SZ-100 nanopartica, Horiba). The Smoluchowski approximation was applied. For each sample the mean value of three determinations was established.

### **VI.4.2 Surface morphology – scanning electron microscopy (SEM) and atomic force microscopy (AFM)**

Morphological evaluation of prepared PNPs was performed using atomic force microscopy (AFM) and scanning electron microscope (SEM). AFM images were taken by vibrating mode in air on a TT-AFM instrument from AFM Workshop. A drop of aqueous nanoparticles solution (0.1 mg/mL) was deposited onto freshly cleaved mica lamella and dried. SEM experiments were conducted by depositing the freeze-dried PNPs on a metal stub, in which a thin film of a conducting metal was sputtered. Samples were imaged with JEOL Field Emission Scanning Electron Microscope JSM-7001F. For each sample, the mean diameter was calculated based on the measurements of 100 randomly chosen particles.



# Chapter VII

## References

---



- <sup>1</sup> Lane, N. J. *Nanopart. Res.* **2001**, 3, 95.
- <sup>2</sup> Ochekepe, N. A., Olorunfemi, P. O., Ngwuluka, N. C. *Trop. J. Pharm. Res.*, **2009**, 8, 265.
- <sup>3</sup> Leucuta, S. E. *Curr. Clin. Pharmacol.* **2010**, 5, 257.
- <sup>4</sup> Wagner, V., Dullaart, A., Bock, A.-K., Zweck, A. *Nature Biotechnol.* **2006**, 24, 1211.
- <sup>5</sup> Strebhardt, K., Ullrich, A. *Nat. Rev. Cancer*, **2008**, 8, 473.
- <sup>6</sup> Langer, R. *Nature*, **1998**, 392, 5.
- <sup>7</sup> Singh, S. J. *Nanosci. Nanotechnol.* **2010**, 10, 7906.
- <sup>8</sup> Nahar, M., Murugesan, S., Asthana, A., Mishra, D., Rajkumar, V., Saraf, S., Jain, N. K. *Crit. Rev. Ther. Drug Carrier Syst.*, **2006**, 23, 259.
- <sup>9</sup> a) Rao, J. P., Geckeler, K. E. *Prog. Polym. Sci.*, **2011**, 36, 887; b) Pinto Reis, C., Neufeld, R. J., Ribeiro, A. J., Veiga, F. *Nanomed. Nanotechnol. Biol. Med.*, **2006**, 2, 8; c) Patel, T., Zhou, J., Piepmeier, J. M., Saltzman, W. M. *Adv. Drug Delivery Rev.*, **2012**, 64, 701.
- <sup>10</sup> Jiang, W., Kim, B. Y. S., Rutka, J. T., Chan, W. C. W. *Nat. Nanotechnol.*, **2008**, 3, 14.
- <sup>11</sup> Iversen, T.-G., Skotland, T., Sandvig, K. *Nano Today*, **2011**, 6, 176.
- <sup>12</sup> a) Paiphansiri, U., Tangboriboonrat, P., Landfester, K. *Macromol. Biosci.* **2006**, 6, 33; b) Lambert, G., Fattal, E., Pinto-Alphandary, H., Gulik, A., Couvreur, P. *Pharm. Res.* **2000**, 17, 707.
- <sup>13</sup> Zhong, Y.; Meng, F., Deng, C., Zhong, Z. *Biomacromol.* **2014**, 15, 1955.
- <sup>14</sup> Shokeen, M., Pressly, E. D., Hagooley, A., Zheleznyak, A., Ramos, N., Fiamengo, A. L., Welch, M. J., Hawker, C. J., Anderson, C. J. *ACS Nano*, **2011**, 5, 738.
- <sup>15</sup> Webster, R., Elliott, V., Parker, B. K., Walker, D., Hankin, M., Taupin, P. PEG and PEG conjugates toxicity: towards an understanding of the toxicity of PEG and its relevance to PEGylated biologicals, F. M. Veronese, ed., *PEGylated Protein Drugs: Basic Science and Clinical Applications*, Birkhäuser Basel, Switzerland, **2009**, pp. 127-146.
- <sup>16</sup> Toub, N., Malvy, C., Fattal, E., Couvreur, P. *Biomed. Pharmacother.*, **2006**, 60, 607.
- <sup>17</sup> a) Kumari, A., Yadav, S. K., Yadav, S. C. *Colloids Surf. B: Biointerfaces*, **2010**, 75, 1; b) Mansour, H. M., Sohn, M., Al-Ghananeem, A., Deluca, P. P. *Int. J. Mol. Sci.* **2010**, 11, 3298; c) Joshi, J. R., Patel, R. P. *Int. J. Curr. Pharm. Res.* **2012**, 4, 74.
- <sup>18</sup> Allouche, J. Synthesis of Organic and Bioorganic Nanoparticles: An overview of the preparation methods, Brayner, R., Fiévet, F., Coradin, T., ed., *Nanomaterials: A Danger or a Promise? A Chemical and Biological Perspective*, Springer London, **2013**, pp.27-74.
- <sup>19</sup> Soppimath, K. S., Aminabhavi, T. M., Kulkarni, A. R., Rudzinski, W. E., *J. Control. Rel.* **2001**, 70, 1.
- <sup>20</sup> Mason, T. G., Wilking, J. N., Chang, C. B., Graves, S. M. *J. Phys.: Condens. Matter* **2006**, 18, R635.
- <sup>21</sup> McClements, D. J., *Soft Matter* **2012**, 8, 1719.
- <sup>22</sup> Vanderhoff, J. W., El Asser, M. S., *US Patent* **1979**, 4,177,177.
- <sup>23</sup> Gurny, R., Peppas, N. A., Harrington, D. D., Banker, G. S. *Drug Dev. Ind. Pharm.*, **1981**, 7, 1.
- <sup>24</sup> Vauthier, C., Bouchemal, K. *Pharm. Res.*, **2009**, 5, 1025.
- <sup>25</sup> Abdelwahed, W., Degobert, G., Stainmesse, S., Fessi, H. *Adv. Drug Del. Rev.*, **2006**, 58, 1688.
- <sup>26</sup> Zambaux, M. F., Bonneaux, F., Gref, R., Maincent, P., Dellacherie, E., Alonso, M. J., Labrude, P., Vigneron, C. *J. Control. Rel.* **1998**, 50, 31.
- <sup>27</sup> Bilati, U., Allemann, E., Doelker, E. *Pharm. Dev. Technol.*, **2003**, 8, 1.
- <sup>28</sup> Mainardes, R. M., Evangelista, R.C. *J. Microencapsul.*, **2005**, 22, 13.
- <sup>29</sup> Manchanda, R., Fernandez-Fernandez, A., Nagesetti, A., McGoron, A. J. *Colloids Surf., B*, **2010**, 75, 260.
- <sup>30</sup> Budhian, A., Siegel, S. J., Winey, K. I. *Int. J. Pharm.*, **2007**, 336, 367.
- <sup>31</sup> Ashjari, M., Khoee, S., Mahdavian, A. R. *Colloids Surf., A*, **2012**, 408, 87.
- <sup>32</sup> Khoee, S., Sattari, A., Atyabi, F. *Mater. Sci. Eng., C*, **2012**, 32, 1078.
- <sup>33</sup> Wachsmann, P., Moulari, B., Béduneau, A., Pellequer, Y., Lamprecht, A. *J. Control. Rel.*, **2013**, 172, 62.
- <sup>34</sup> Barba, A. A., Dalmoro, A., d'Amore, M., Vascello, C., Lamberti, G. *J. Mater. Sci.*, **2014**, 49, 5160.
- <sup>35</sup> Leroux J. C., Allémann, E., Doelker, E., Gurny, R. *Eur. J. Pharm. Biopharm.*, **1995**, 41, 14.
- <sup>36</sup> Moinard-Chécot, D., Chevalier, Y., Briançon, S., Beney, L., E., Fessi, J. *Colloid Interface Sci.*, **2008**, 317, 458.
- <sup>37</sup> Guinebrière, S., Briançon, S., Lieto, J., Mayer, C., Fessi, H. *Drug Dev. Res.*, **2002**, 57, 18.
- <sup>38</sup> Quintanar-Guerrero, D., Fessi, H., Alléman, E., Doelker, E., *Int. J. Pharm.*, **1996**, 143, 133.
- <sup>39</sup> Trimaille, T., Pichot, C., Elaïssari, A., Briançon, S., Delair, T. *Colloid Polym. Sci.*, **2003**, 281, 1184.
- <sup>40</sup> Surassmo, S., Min, S.-G., Bejrapha, P., Choi, M.-J. *Food Res. In.*, **2010**, 43, 8.
- <sup>41</sup> Colombo, A. P., Briançon, S., Lieto, J., Fessi, H., *Drug Dev. Ind. Pharm.*, **2001**, 27, 1063.
- <sup>42</sup> Sahana, D. K., Mittal, G., Bhardwaj, V., Kumar, M. N. V. R. *J. Pharm. Sci.*, **2008**, 97, 1530.
- <sup>43</sup> Jain, A. K., Swarnakar, N. K., Godugu, C., Singh, R. P., Jain, S. *Biomaterials*, **2011**, 32, 503.
- <sup>44</sup> Hallouard, F., Briançon, Anton, N., Li, X., Vandamme, T., Fessi, H., *J. Pharm. Sci.*, **2013**, 102, 4150.
- <sup>45</sup> Musazzi, U. M., Youm, I., Murowchick, J. B., Ezoulin, M. J., Youn, B.-B. C., *Colloids Surf., B*, **2014**, 118, 234.

- <sup>46</sup> Mora-Huertas, C. E., Fessi, H., Elaissari, A., *Adv. Colloid Interface Sci.*, **2011**, 163, 90.
- <sup>47</sup> Song, K. C., Lee, H. S., Choung, I. Y., Cho, K. I., Ahn, Y., Choi, E. J. *Colloids Surf., A*, **2006**, 276, 162.
- <sup>48</sup> Kwon, H.-Y., Lee, J.-Y., Choi, S.-W., Jang, Y., Kim, J.-H. *Colloids Surf., A*, **2001**, 182, 123.
- <sup>49</sup> Quintanar-Guerrero, D., Alléman, E., Doelker, E., Fessi, H., *Colloid Polym. Sci.*, **1997**, 275, 640.
- <sup>50</sup> Ibrahim, H., Bindchaedler, C., Doelker, E., Buri, P., Gurny, R., *Int. J. Pharm.*, **1992**, 87, 239.
- <sup>51</sup> Ganachaud, F., Katz, J. L., *ChemPhysChem*, **2005**, 6, 209.
- <sup>52</sup> Konan, Y. N., Gurny, R., Alléman, E., *Int. J. Pharm.*, **2002**, 233, 239.
- <sup>53</sup> Alléman, E., Gurny, R., Doelker, E., *Int. J. Pharm.*, **1992**, 87, 247.
- <sup>54</sup> Zweers, M. L. T., Grijpma, D. W., Engbers, G. H. M., Feijen, J., *J. Biomed. Mater. Res. B Appl. Biomater.* **2003**, 66, 559.
- <sup>55</sup> Song, X., Zhao, Y., Wu, W., Bi, Y., Cai, Z., Chen, Q., Li, Y., Hou, S., *Int. J. Pharm.* **2008**, 350, 320.
- <sup>56</sup> Fessi, H., Puisieux, F., Devissaguet, J. P., Ammoury, N., Benita, S., *Int. J. Pharm.*, **1989**, 55, R1.
- <sup>57</sup> Sternling, C. V., Scriven, L. E., *AIChE Journal*, **1959**, 5, 514.
- <sup>58</sup> a) Murakami, H., Kobayashi, M., Takeuchi, H., Kawashima, Y., *Int. J. Pharm.*, **1999**, 187, 143; b) Chang, J., Jallouli, Y., Kroubi, M., Yuan, X.-b., Feng, W., Kang, C.-s., Pu, P.-y., Betbeder, D., *Int. J. Pharm.*, **2009**, 379, 285; c) Thioune, O., Fessi, H., Devissaguet, J. P., Puisieux, F., *Int. J. Pharm.*, **1997**, 146, 233.
- <sup>59</sup> Chorny, M., Fishbein, I., Danenberg, H. D., Golomb, G., *J. Control. Release* **2002**, 83, 389.
- <sup>60</sup> Chancón, M., Berges, L., Molpeceres, J., Aberturas, M. R., Guzman, M., *Int. J. Pharm.*, **1996**, 141, 81.
- <sup>61</sup> Simsek, S., Eroglu, H., Kurum, B., Ulubayram, K., *J. Microencapsul.*, **2013**, 30, 10.
- <sup>62</sup> Dong, Y., Feng, S.-S., *Biomaterials*, **2004**, 25, 2843.
- <sup>63</sup> Özcan, I., Segura-Sánchez, F., Bouchemal, K., Sezak, M., Özer, Ö., Güneri, T., Ponchel, G., *Int. J. Nanomed.*, **2010**, 5, 1103.
- <sup>64</sup> Asadi, H., Rostamizadeh, K., Salari, D., Hamidi, M., *J. Microencapsul.*, **2011**, 28, 406.
- <sup>65</sup> Bukhari, A., Idris, A., Atta, M., *Malaysian J. Fund. Appl. Sci.*, **2014**, 10, 28.
- <sup>66</sup> a) Xie, H., Smith, J. W., *J. Nanobiotechnology*, **2010**, 8, 18; b) Karnil, R., Gu, P., Basto, P., Cannizzaro, C., Dean, L., Kyei-Manu, W., Langer, R., Farokhzad, O. C., *Nano Lett.*, **2008**, 8, 2906.
- <sup>67</sup> a) Schubert, S., Tekin, E., Smith, P. J., *Soft Matter*, **2008**, 4, 703; b) Schubert, S., Delaney, J. T., Schubert, U. S., *Soft Matter*, **2011**, 7, 158.
- <sup>68</sup> a) Leo, E., Brina, B., Forni, F., Vandelli, M.A., *Int. J. Pharm.*, **2004**, 278, 133; b) Peltonen, L., Aitta, J., Hyvönen, S., Karjalainen, M., and Hirvonen, J., *AAPS Pharm. Sci. Tech.*, **2004**, 5, 115.
- <sup>69</sup> Jeon, H. J., Jeong, Y. I., Jang, M. K., Park, Y. H., Nah, J. W., *Int. J. Pharm.*, **2000**, 207, 99.
- <sup>70</sup> Chronopoulou, L., Fratoddi, I., Palocci, C., Venditti, I., Russo, M. V., *Langmuir*, **2009**, 25, 11940.
- <sup>71</sup> Akagi, T., Kaneko, T., Kida, T., Akashi, M., *J. Control. Rel.*, **2005**, 108, 226.
- <sup>72</sup> Jeong, Y.-I., Cho, C.-S., Kim, S.-H., Ko, K.-S., Kim, S.-I., Shim, Y.-H., Nah, J.-W., *J. Appl. Polym. Sci.*, **2001**, 80, 2228.
- <sup>73</sup> Elizondo, E., Veciana, J., Ventosa, N., *Nanomedicine*, **2012**, 7, 1391.
- <sup>74</sup> Sanli, D., Bozbag, S. E., Erkey, C., *J. Mater. Sci.*, **2012**, 47, 2995.
- <sup>75</sup> Fages, J., Lochard, H., Letourneau, J.-J., Sauceau, M., Rodier, E., *Powder Technol.*, **2004**, 141, 219.
- <sup>76</sup> Ginty, P. J., Whitaker, M. J., Shakesheff, K. M., Howdle, S. M., *Mater. Today*, **2005**, 8, 42.
- <sup>77</sup> Perrut, M., Leboeuf, J. J., *Int. J. Pharm.*, **2005**, 288, 11.
- <sup>78</sup> Mishima, K., *Adv. Drug Deliv. Rev.*, **2008**, 60, 411.
- <sup>79</sup> Yeo, S.-D., Kiran, E., *J. Supercrit. Fluids*, **2005**, 34, 287.
- <sup>80</sup> Lin, P.-C., Lin, S., Wang, P. C., Sridhar, R., *Biotechnol. Adv.*, **2014**, 32, 711.
- <sup>81</sup> Hall, J. B., Dobrovolskaia, M. A., Patri, A. K., McNeil, S. E., *Nanomedicine*, **2007**, 2, 789.
- <sup>82</sup> Herrera, J., Sakulchaicharoen, N., Microscopic and Spectroscopic Characterization of Nanoparticles, Pathak, Y., Thassu, D., ed., *Nanoparticulate Drug Delivery Systems (NPDDS) – II: Formulation and Characterization*, Informa Healthcare, New York **2009**, pp. 237 – 249.
- <sup>83</sup> Russel, P., Batchelor, D., “SEM and AFM: Complementary Techniques for Surface Investigations”, *Microscopy and Analysis*. John Wiley & Sons, Ltd. July **2001**, pp. 9 – 12.
- <sup>84</sup> Binnig, G., Quate, C. F., Gerber, Ch., *Phys. Rev. Lett.*, **1986**, 56, 930.
- <sup>85</sup> Dufrêne, Y. F., *J. Bacteriol.*, **2002**, 184, 5205.
- <sup>86</sup> a) Ducker, W. A., Senden, T. J., Pahley, R. M., *Nature*, **1991**, 353, 239; b) Hodgesm C. S., Cleaver, J. A. S., Ghadiri, M., Jones, R., Pollock, H. M., *Langmuir*, **2002**, 18, 5741.
- <sup>87</sup> Drelich, J., Tormoen, G. W., Beach, E. R., *J. Colloid Interface Sci.*, **2004**, 280, 484.
- <sup>88</sup> Gu, X., Nguyen, T., Oudina, M., Martin, D., Kidah, B., Jasmin, J., Rezig, A., Sung, L., Byrd, E., Martin, J. W., *J. Coat. Technol. Res.*, **2005**, 2, 547.
- <sup>89</sup> Tiede, K., Boxall, A. B. A., Tear, S. P., Lewis, J., David, H., Hassellöv, M., *Food Addit. Contam. Part A*, **2008**, 25, 795.
- <sup>90</sup> Kaminskyl, S. G. W., Dahms, T. E. S., *Micron*, **2008**, 39, 349.
- <sup>91</sup> Zhang, Z., Feng, S.-S., *Biomacromol.*, **2006**, 7, 1139.

- <sup>92</sup> Kaszuba, M., McKnight, D., Connah, M. T., McNeil-Watson, F. K., Nobbmann, U., *J. Nanopart. Res.*, **2008**, *10*, 823.
- <sup>93</sup> Lim, J., Yeap, S. P., Che, H. X., Low, S.C., *Nanoscale Res. Lett.*, **2013**, *8*, 381.
- <sup>94</sup> Filipe, V., Hawe, A., Jiskoot, W., *Pharmaceut. Res.*, **2010**, *27*, 796.
- <sup>95</sup> Sant, S., Nadeau, V., Hildgen, P., *J. Control. Rel.*, **2005**, *107*, 203.
- <sup>96</sup> Tantra, R., Schulze, P., Quincey, P., *Particuology*, **2010**, *8*, 279.
- <sup>97</sup> Sapsford, K. E., Tyner, K. M., Dair, B. J., Deschamps, J. R., Medintz, I. L., *Anal. Chem.*, **2011**, *83*, 4453.
- <sup>98</sup> Elsabahy M., Wooley, K. L. *Chem. Soc. Rev.*, **2012**, *41*, 2545.
- <sup>99</sup> Hancock, B. C., Parks, M., *Pharm. Res.*, **2000**, *17*, 397.
- <sup>100</sup> Yu, L., *Adv. Drug Deliv. Rev.*, **2001**, *48*, 27.
- <sup>101</sup> Raula, J., Eerikäinen, H., Lähde, A., Kauppinen, E. I., Aerosol flow reactor method for the synthesis of multicomponent drug nano- and microparticles, Thassu, D., Deleers, M., Pathak, Y. V., ed., *Nanoparticulate Drug Delivery Systems*, CRC Press, March **2007**, pp.111-128.
- <sup>102</sup> Kerč, J., Srčič, S., *Thermochimica Acta*, **1995**, *248*, 81.
- <sup>103</sup> Corrigan, O. I., Li, X., *Eur. J. Pharm. Sci.*, **2009**, *37*, 477.
- <sup>104</sup> Kolate, A., Baradia, D., Patil, S., Vhora, I., Kore, G. *J. Control. Rel.*, **2014**, doi:10.1016/j.jconrel.2014.06.046
- <sup>105</sup> Owens III, D. E., Peppas, N. A. *Int. J. Pharm.*, **2006**, *307*, 93.
- <sup>106</sup> Banerjee, S. S., Aher, N., Patil, R., Khandare, J. *J. Drug Deliv.*, **2012**, *2012*, 1.
- <sup>107</sup> Joralemon, M. J., McRae, S., Emrick, T. *Chem. Commun.*, **2010**, *46*, 1377.
- <sup>108</sup> Elvira, C., Gallardo, A., Roman, J. S., Cifuentes, A. *Molecules*, **2005**, *10*, 114.
- <sup>109</sup> Kamaly, N., Xiao, Z., Valencia, P. M., Radovic-Moreno, A. F., Farokhzad, O. C. *Chem. Soc. Rev.*, **2012**, *41*, 29711.
- <sup>110</sup> Spain, S. G., Cameron, N. R., *Polym. Chem.*, **2011**, *2*, 60.
- <sup>111</sup> Deniaud, D., Julienne, K., Gouin, S. G. *Org. Biomol. Chem.*, **2011**, *9*, 966.
- <sup>112</sup> a) Kim, I.-S., Kim, S.-H. *Int. J. Pharm.*, **2003**, *257*, 195; b) Kim, I.-S., Kim, S.-H., Cho, C.-S. *Macromol. Rapid Commun.*, **2000**, *21*, 1272.
- <sup>113</sup> Song, C. K., Jung, S. H., Kim, D.-D., Jeong, K.-S., Shin, B. C., Seong, H. *Int. J. Pharm.*, **2009**, *380*, 161.
- <sup>114</sup> Panyam, J., Williams, D., Dash, A., Leslie-Pelecky, D., Labhasetwar, V. *J. Pharm. Sci.*, **2004**, *7*, 1804.
- <sup>115</sup> Govender, T., Riley, T., Ehtezazi, T., Garnett, M. C., Stolnik, S., Illum, L., Davis, S. S., *Int. J. Pharm.*, **2000**, *199*, 95.
- <sup>116</sup> Virtanen, E., Kolehmainen, E. *Eur. J. Org. Chem.*, **2004**, 3385.
- <sup>117</sup> Hao, J.-Q., Li, H., Woo, H.-G. *J. Appl. Polym. Sci.*, **2009**, *112*, 2976.
- <sup>118</sup> Petrova, K. T., Correia-da-Silva, P., Crucho, C. I. C., Barros, M. T., *Curr. Org. Chem.*, **2014**, *18*, 1788.
- <sup>119</sup> Jarosk, S., Mach, M., *Eur. J. Org. Chem.*, **2002**, 769.
- <sup>120</sup> Barros, M. T., Petrova, K. T., Ramos, A. M. *J. Org. Chem.*, **2004**, *69*, 7772.
- <sup>121</sup> Karl, H., Lee, C. K., Khan, R. *Carbohydr. Res.*, **1982**, *101*, 31.
- <sup>122</sup> Corey, E. J., Venkateswarlu, A. *J. Am. Chem. Soc.*, **1972**, *94*, 6190.
- <sup>123</sup> Yin, Z.-J., Wang, B., Li, Y.-B., Xiang-Bao, M., Zhong-Jun, L., *Org. Lett.*, **2010**, *12*, 536.
- <sup>124</sup> Yamanoi, T., Misawa, N., Matsuda, S., Watanabe, M., *Carbohydr. Res.*, **2008**, *343*, 1366.
- <sup>125</sup> Xu, S., Held, I., Kempf, B., Mayr, H., Steglich, W., Zipse, H., *Chem. Eur. J.*, **2005**, *11*, 4751.
- <sup>126</sup> Gouin, S., Zhu, X. X., *Steroids*, **1996**, *61*, 664.
- <sup>127</sup> Wess, G., Kramer, W., Bartmann, W., Enhnsen, A., Glombik, H., Müllner, S., Bock, K., Dries, A., Kleine, H., Schmitt, W., *Tetrahedron Lett.*, **1992**, *33*, 195.
- <sup>128</sup> Neises, B., Steglich, W., *Angew. Chem. Int. Ed. Engl.*, **1978**, *17*, 522.
- <sup>129</sup> a) Bogdanov, B. G., Michailov, M., Uzov, C. V., Gavrilova, G. G., *J. Polym. Sci. B*, **1994**, *32*, 387-394; b) Chenite, A., Brisse, F., *Macromolecules*, **1991**, *24*, 2221.
- <sup>130</sup> Bains, G., Patal, A. B., Narayanaswami, V., *Molecules*, **2011**, *16*, 7909.
- <sup>131</sup> Zanetti-Ramos, B. G., Fritzen-Garcia, M. B., de Oliveira, C. S., Pasa, A. A., Soldi, V., Borsali, R., Creczynski-Pasa, T. B., *Mater. Sci. Eng., C*, **2009**, *29*, 630.
- <sup>132</sup> Panyam, J., Labhasetwar, V., *Adv. Drug Deliv. Rev.*, **2003**, *55*, 329.
- <sup>133</sup> Sahoo, S. K., Panyam, J., Prabha, S., Labhasetwar, V., *J. Control. Rel.*, **2002**, *8*, 105.
- <sup>134</sup> Sheng, Y., Yuan, Y., Liu, C., Tao, X., Shan, X., Xu, F., *J. Mater. Sci.: Mater. Med.*, **2009**, *20*, 1881.
- <sup>135</sup> Rao, A., Schoenenberger, M., Gnecco, E., Glatzel, TH., Meyer, E., Brändlin, D., Scandella, L., *J. Phys. : Conf. Ser.*, **2007**, *61*, 971.
- <sup>136</sup> Mu, L., Feng, S. S., *J. Control. Rel.*, **2002**, *8*, 129.
- <sup>137</sup> Duncan, R., *Curr. Opin. Biotechnol.*, **2011**, *22*, 492.
- <sup>138</sup> Ulery, B. D., Nair, L. S., Laurencin, C. T., *J. Polym. Sci. Part B: Polym. Phys.*, **2011**, *49*, 832.
- <sup>139</sup> Suggs, L. J., Moore, S. A., Mikos, A. G., Synthetic Biodegradable Polymers for Medical Applications, Mark, J. E., ed., *Physical Properties of Polymers Handbook*, Springer Science, **2007**, pp. 939 – 951.
- <sup>140</sup> Danhier, F., Ansorena, E., Silva, J. M., Coco, R., Breton, A. L., Préat, V., *J. Control. Rel.*, **2012**, *161*, 505.

- 
- <sup>141</sup> Bala, I., Hariharan, S., Kumar, M. N. V. R., *Crit. Rev. Ther. Drug*, **2004**, 21, 387.
- <sup>142</sup> Gentile, P., Chione, V., Carmagnola, I., Hatton, P. V., *Int. J. Mol. Sci.*, **2014**, 15, 3640.
- <sup>143</sup> Makadia, H. K., Siegel, S. J., *Polymers*, **2011**, 3, 1377.
- <sup>144</sup> Stevanović, M., Uskoković, D., *Curr. Nanosci.*, **2009**, 5, 1.
- <sup>145</sup> Abeylath, S. C., Turos, E., *Carbohydr. Polym.*, **2007**, 70, 32.
- <sup>146</sup> Davis, A. P., *Molecules*, **2007**, 12, 2106.
- <sup>147</sup> Peça, I. N., Petrova, K. T., Cardoso, M. M., Barros, M. T., *Reac. Funct. Polym.*, **2012**, 72, 729.
- <sup>148</sup> Fonte, P., Soares, S., Costa, A., Andrade, J. C., Seabra, V., Reis, S., Sarmento, B. *Biomatter*, **2012**, 2, 329.
- <sup>149</sup> Sailor, M. J., Park, J.-H., *Adv. Mater.* **2012**, 24, 3779.
- <sup>150</sup> Avgoustakis, K., *Curr. Drug Deliv.* **2004**, 1, 321.
- <sup>151</sup> Locatelli, E., Franchini, M. C., *J. Nanopart. Res.* **2012**, 14, 1316.
- <sup>152</sup> Betancourt, T., Byrne, J. D., Sunaryo, N., Crowder, S. W., Kadapakkam M., Patel, S., Casciato, S., Brannon-Peppas, L., *J. Biomed. Mater. Res. A*, **2009**, 91, 263.
- <sup>153</sup> a) Gref. R., Minamitake, Y., Peracchia, M. T., Trubetskoy, V., Torchilin, V., Langer, R. *Science*, **1994**, 263, 1600; b) Gref. R., Domb, A., Quellec, P., Blunk, T., Müller, R. H., Verbavatz, J. M., *Adv. Drug Del. Rev.*, **1995**, 16, 215.
- <sup>154</sup> Perrin, D. D., Armaredo, W. L. F., *Purification of Laboratory Chemicals*, Pergamon Press Ltd., New York, **1980**.